Engineering of multi-functional conductive thin films using graphene materials and their composites

A thesis submitted in fulfilment of the requirement for the degree of

Doctor of Philosophy

Engineering

by **Faisal Khalid Alotaibi**

School of Chemical Engineering

Faculty of Engineering, Computer and Mathematical Sciences

The University of Adelaide, Australia

July 2019

Table of Contents

Declaration

I certify that this work contains no material which has been accepted for the award of any other degree or diploma in my name, in any university or other tertiary institution and, to the best of my knowledge and belief, contains no material previously published or written by another person, except where due reference has been made in the text. In addition, I certify that no part of this work will, in the future, be used in a submission in my name, for any other degree or diploma in any university or other tertiary institution without the prior approval of the University of Adelaide and where applicable, any partner institution responsible for the joint-award of this degree.

I acknowledge that copyright of published works contained within this thesis resides with the copyright holder(s) of those works.

I also give permission for the digital version of my thesis to be made available on the web, via the University's digital research repository, the Library Search and also through web search engines, unless permission has been granted by the University to restrict access for a period of time.

I acknowledge the support I have received for my research through the provision of an Australian Government Research Training Program Scholarship.

Name: Faisal Alotaibi

Signed **Date 20-03-2019**

Acknowledgments

Firstly, I want to show my sincere gratitude to my primary supervisor Prof. Dusan Losic for his unlimited aid and support during my Ph.D research, for his patience, enthusiasm inspiration, and knowledge. His was very helpful whenever I need a research advice or support for writing papers. I could not have imagined having a better advisor and mentor for my Ph.D study.

In addition to my prime supervisor, I would like to thank my co-supervisor Dr. Tran Thanh Tung for his support, patient guidance, encouragement and advice he has provided throughout my time as PhD student. I have been extremely lucky to have him as co-supervisor who cared so much about my work, and who responded to my questions and queries so promptly.

I am also expressing my thankfulness to lab members especially to Dr. Md Julker Nine, Dr Shervin Kabiri, Dr. Diana N.H. Tran, Ramesh Karunagaran, who, in many ways, provide technical, and scientific support and made my Ph.D. program enjoyable and easier to overcome every obstacle.

I like to thank the University of Adelaide for providing me the opportunity to pursue my study. The support extended by the Adelaide Microscopy team including Ken Neubauer, Animesh Basak, and Ashley Slattery are very much appreciated. The assistance of the School of Chemical Engineering office staffs provided with all my administration related work, chemical ordering etc. I also like to extend a special thanks to Jason Peak in the Chemical Engineering workshop for attending all my inquiries without hesitation and helping me with

the equipment installations. I am so grateful for the staff of Adelaide Graduate Centre for providing me with appropriate information whenever I approached them.

Special thanks to King Abdullah Scholarship Program and Saudi cultural mission in Australia for this opportunity that allowed me do my higher degree studies and for their support during my studies.

I would also like to thank the entire students and researchers of the Losic research group providing an enjoyable and more pleasant place to work. Every event we celebrated together including visit to Barossa valley, Mouth Lofty, Bowling and BBQs, soccer that gives me fantastic memories.

Last but not the least, I would like to thank my family: my parents “Dlayel and Khalid” and my two beautiful daughters “Leen and Hala” and my great six siblings “Abdurrahman, Abdullah, Aliyah, Sarah, Reem, May, Salma” for their continued support and encouragement.

Abstract

Graphene was successfully exfoliated in 2004 by A. Geim and K. Novoselov by using the mechanical scotch-tape technique and these inventors have awarded the Nobel Prize in 2010. Since then graphene has attracted enormous research interests due to its unique electrical, mechanical and optical properties which has potential applications across many sectors. The aim of this Ph.D, project is to explore the use of different graphene derivatives such as pristine graphene (pG), reduced graphene oxide (rGO) and graphene oxide (GO) and their composites for development of their inks and fabrication of highly conductive films that can be used for a broad range of applications such solar cells, supercapacitor electrodes, sensors, electromagnetic shielding etc.

The first concept developed and explored in this thesis was to demonstrate a new method based on scanning atmospheric plasma for an ultrafast reduction of graphene oxide (P-rGO) and preparation of highly conductive graphene films and patterns. Outcomes of this study are development of a simple cold plasma approach for scalable preparation of graphene film based on atmospheric pressure plasma jets (APPJs). The atmospheric plasma provides not only high electron densities (>1013 cm^3) and high energetic electrons (>20 eV), but also highly reactive gas species and radicals that react with the oxygen functional groups on GO films causing their ionization reduction and removal. This reduction process happens over very short time (~1 min), being able to covert nonconductive thin or thick GO films into rGO films throughout all layers (not only the top surface) on different substrates (glass, plastic and textile) with various shapes (circles, squares, lines, arrays, etc.) from micron to millimetre size patterns.

The second concept explored in this thesis was to develop a new method to engineer graphene surfaces with continuous gradual change of multiple functions including structural, chemical, wettability, charge, surface energy, electrical and thermal conductivity at a large scale (cm) that are not achieved before. The developed fabrication protocol is based on conversion of GO films by non-uniform exposure of atmospheric pressure plasma beam (to gradually remove GO oxygen functional groups across the surface, thus to create rGO. The method is simple, low-cost, scalable, applicable on different surfaces (metals, plastic, textile, glass, curved, flexible) with the ability to create multifunctional surface gradients at a large scale, and used for solving many fundamental and engineering problems that cannot be addressed with the homogenous surfaces.

The third topic explored in this Ph.D project was to develop of a facile method to improve both the stability and performance of silver nanowire (AgNW) film (conductivity and transparency)**.** The AgNWs inks were synthesis and combined with pristine graphene (pG) inks with the goals to prove that the pG sheets can provide a barrier shielding to protect against AgNW oxidation and improving the connections between wires and stability of the films. The fabrication of these composite films was successfully demonstrated on wide range of substrates including glass, plastic, textile, and paper. A surface resistance of 18.23 Ω/sq and an optical transparency of 89% were obtained on the glass substrates, 50 Ω/sq and 88% transparency for poly(ethylene terephthalate) (PET), and 0.35 Ω/sq resistance on the textile substrate. The APPJ treatment was further used to enhance the performance of the film (i.e., glass), resulting in a significant reduction of 30.6% in sheet resistance (15.20 Ω/sq) and an improvement of transparency to 91%. The stability of AgNW/pG film under environmental conditions and higher temperatures was significantly improved due to the graphene acting as an oxidation barrier and dissipating heat. The test showed a minor sheet resistance increases

after 30 days and further thermal stability to temperature up to 300 °C. In comparison, the control (AgNW film) showed a sharp sheet resistance increase after 8−10 days only and thermally stable until 150 °C as a result of Ag oxidation.

Lastly, the thesis presented the development of a new method for the fabrication of highly conductive and transparent ultrathin nitrogen (N) doped graphene films from graphene inks by combining a microwave treatment, ultrasonic nebulizer coating and thermal annealing. This method involving in situ N-doping offers a promising environmentally-friendly, low-cost and scalable manufacture of high-quality conductive N-doped graphene films. The starting GO solution was mixed with poly(ionic liquids) (PIL) and treated with microwave (Mw) irradiation to prepare Mw-rGO@PIL inks, which is a gentle reduction of PIL attached rGO to not only mediate microwave irradiation and prevent disorder of the graphitic structure, but also repair the lattice defects and introduce nitrogen into the graphitic structure. The prepared films displayed a surface resistance of$\sim 1.45\times10^{7}$ Ω/sq at a transparency of∼87%. A further thermal treatment was conducted to improve the conductivity of the prepared films by annealing at a high temperature (900 °C), which allowed complete reduction of oxygen containing groups, enhanced graphitization, and reordering of the basal graphene plane and N-doping of the carbon lattice (pyrolytic PIL). The resulting thin films significantly reduced the surface resistance in the range of 1.5×10^{3} to 6.2×10^{3} Ω/sq at a transparency ranging from 68 to 82%, respectively.

By means of using physical strategies including cold plasma and microwave for treatment of advanced materials (graphene and AgNWs), the thin graphene-based films fabrication methods developed during this PhD research will provide considerable contribution to the field of high performing conductive films required for conventional electronic devices such

as new wearable electronics, flexible displays, solar cells, supercapacitors, energy generations, sensors, electrothermal heaters, electromagnetic shielding and so on.

List of publications

Journal papers

1. **Faisal Alotaibi**, Tran T. Tung, Md J. Nine, S. Kabiri, Mahmoud Moussa, Diana N. H. Tran, Dusan Losic, Scanning atmospheric plasma for ultrafast reduction of graphene oxide and fabrication of highly conductive graphene films and patterns, *Carbon*, 127 (2018) 113-
2. **Faisal. Alotaibi,** T. T. Tung, Md J. Nine, C. J Coghlan. D. Losic, Silver Nanowires with Graphene Oxidation Barriers for Stable and High Performance Transparent Conductive Films, ACS Applied Nano Materials, 2018 ACS Appl. Nano Mater. 2018, 1, 5, 2249-2260
3. **Faisal Alotaibi,** Tran T. Tung, Md J. Nine,Dusan Losic , Graphene based Multifunctionally Graded Surfaces (MFGS), Advanced Materials DOI: 10.1002 (submitted)
4. T. T. Tung**, Faisal Alotaibi**, Md J. Nine, Rifat Silva, Diana N. H. Tran, Dusan Losic, Engineering of highly conductive and ultra-thin nitrogen-doped graphene films by ultrasonic spraying, Chemical Engineering Journal, 338 (2018) 764-773.
5. Md J. Nine, Tran Thanh Tung**, Faisal Alotaibi**, Diana N. H. Tran, Dusan Losic, Facile Adhesion-Tuning of Superhydrophobic Surfaces between "Lotus" and "Petal" Effect and Their Influence on Icing and Deicing Properties, *ACS Applied Materials & Interfaces*, 9 (9) (2017) 8393–8402.
6. Tran Thanh Tung, Jeongha Yoo, **Faisal Alotaibi,** Md J. Nine, Ramesh Karunagaran, Melinda Krebsz, Giang T Nguyen, Diana NH Tran, Jean-Francois Feller, Dusan

Losic, Graphene oxide-assisted liquid phase exfoliation of graphite into graphene for highly conductive film and electromechanical sensors, *ACS Applied Materials & Interfaces*, 8 (25) (2016) 16521-16532.

Conference papers and proceedings:

1. **Faisal. Alotaibi**, T.T. Tung , M. Krebsz ,G. Nguyen, D. Losic , Graphene-based composite with conductive polymer for application in electronics, ICONN 2015, 5th International conference on Nanoscience and Nanotechnology, Feb 8-12, 2015, Canberra, Australia.
2. D. Losic, D.N.H. Tran, T. Tung, C. Cambell, Md. J. Nine, M. Abdalisk, S. Kabiri, **F. Alotaibi**, P. Lay Yap, Engineering of graphene 3-dimensional composites for emerging applications, 2018 International Symposium of Advanced Composite Technology, 2-3 August 2018, Adelaide
3. Dusan Losic, D.N.H. Tran, T. Tung, Md. J. Nine, C.J. Coghlan, M. Abdalisk, S. Kabiri, **F. Alotaibi,** P. Lay Yap, From graphene production to innovative engineering of new materials and products for emerging applications, Grapchina 2018, International Graphene Innovation conference, Sept 19-21, 2018, Xian, China

List of Figures

Chapter 1

Chapter 2

Chapter 3

Chapter 4

Chapter 5

Chapter 1

Introduction

This introductory chapter provides an overall overview of the conductive coatings materials and backgrounds followed by a short summary on graphene derivatives, properties, and their use, which are supported for the aims and objectives of this PhD research program. The thesis contents will be provided in the individual chapters (5) that will be summarized with final concluding chapter.

Blank Page

1.1 Introduction

Typically conductive coatings are used to cover less conductive dielectric substrates than the coating. In particular, applying sensitive coating involves a fine-tuned technique which does not change the electrical, optical and mechanical properties [1,2]. In the past, the use of conductive nanomaterials for example conductive nanomaterials based on carbon has opened up new ways for electronic and optoelectronic applications. Furthermore, it is important to search for conductive nanomaterials with the scalable methods and best properties like flexibility, mechanical and chemical stability, transparency and cost-effective [2-8].

In addition, the world market size of conductive materials was projected at USD 434.7 million in 2016 and is expected to hit USD 3.4 trillion by 2025 at a CAGR of 25.7 %, according to Grand View Research, Inc **Figure 1.1** report in September 2017.

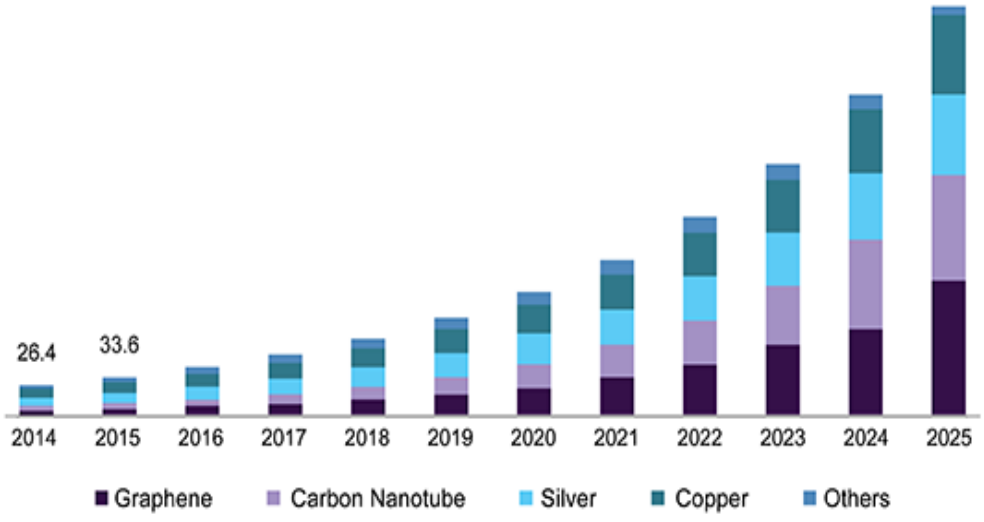

Figure 1.1 Growing conductive materials demand and market value 2014-2025 ($ Million) by Grand View Research, Inc 2017 with permission.

The purpose of functional coatings is to improve material propitiates, many conventional conductive coating materials were associated with limitation or drawbacks. For example, Indium tin oxide (ITO) has been commonly used as electrodes. ITO does not have properties to be used as a flexible transparent electrode. This is because of its film brittleness and low infrared transmittance [9-12]. The perception of that ITO is sufficient for many applications has begun to change due to the shortages of indium tin oxide today and increasing its cost. Moreover, many forms of conductive polymers, such as poly(3,4-ethylenedioxythiophene) :poly(styrenesulfonate) and poly(3-hexylthiophene-2,5-diyl):[6,6]-phenyl-C61-butyric acid methyl ester have been proposed to replace ITO in electronics devices [13,14]. However, these conductive polymers ' electrical efficiency is much lower than that of ITO. In addition, despite their flexibility, the mechanical properties of these conductive polymers are fragile thus hybridise those polymers with different conductive materials were used to overcome its drawback.

Silver nanowires (AgNW) were used as fixable transparent conductive electrodes in transparent conductor systems due to outstanding electrical conductivity and transmission properties [15]. Wang et al.14 demonstrated the advantages of AgNW as electrodes due to its excellent properties including electrical conductivity, high transparency results and great mechanical properties. Nevertheless, the AgNW deposition on the substrate has a weak van der Waals force which reduces the contact region between the AgNW and the substrate, result in a weak adhesion force [16]. Moreover, it is easy to separate AgNWs from the substrate by physical/mechanical distortion. Even so, the AgNW production today is unstable mainly due to oxidation and atmospheric deformation once exposed to light, moisture or gas,

which result in loss of electrical conductivity that considered as one of the main factors in electronic applications [17,18].

While the progress finding better alternatives are still under progress, large number of studies using alternative conductive materials, for instance graphene has been studied [19–23]. Graphene is a meriting contender to replace contemporary electronic applications. A group of scientists from Manchester University, UK, supervised by Andre Geim and Kostya Novoselov, discovered Graphene in 2004. [24]. The top-down approach of graphene synthesis is either performed by mechanical or chemical exfoliation for high yield of pristine graphene and graphene oxide. Pristine graphene (**Figure 1.2b**) possesses pristine properties introduced in the earlier literature as their synthesis process does not sacrifice high electrical and thermal conductivity ($2.5 \times 10^5 cm^2.V^{-1}s^{-1}$ and above 3000 $Wm^{-1}.K^{-1}$), optical transparency (~97 %), and superior mechanical strength Young's modulus of 1 TPa [24,25]. Graphene oxide (**Figure 1.2b**) is another important derivative and starting material for many applications having numerous oxygen functional groups (hydroxyl, carboxyl, ketone, epoxy) on its basal plane and edges [26]. Although these functional groups enable graphene oxide to be bonded with other materials by creating different covalent and non-valent bonds, the material has to sacrifice some pristine properties of graphene due to extensive chemical modification. Therefore, a further reduction process is introduced to synthesise reduced graphene oxide (**Figure 1.2c**) for the purpose of restoring the pristine graphene properties [27].

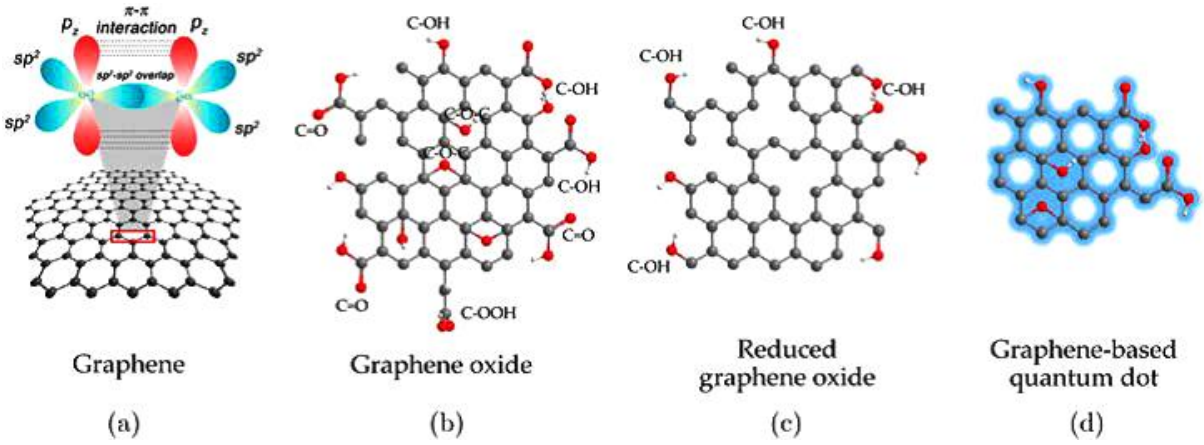

Figure 1.2 Forms of graphene-based materials, (a) pristine graphene with sp^2-hybridized carbon, chemically modified graphene (b) GO; (c) rGO and (d) graphene quantum dot [28].

1.2 Aims and Objectives

The aim of this Ph.D. program is to explore the application of graphene materials and their composites for developing new generation of conductive films technology for various electronic applications including transparent conductive films TCF, wearable devices, and supercapacitor device. Several types of materials including graphene oxide (GO), rGO and AgNW and their combinations were explored. In particular, by means of using physical strategies including cold plasma and microwave techniques, this research developed simple, ultrafast, scalable and environmentally friendly processes to fabricate high preforming conductive films. The following project aims and objectives were set to achieve these outcomes.

AIM 1: Development of new approach for making highly conductive films by reduction of GO by atmospheric plasma.

Objective 1: Identifying the limitations of main approaches used for reduction of GO and optimization of plasma process for ultrafast and scalable preparation of graphene film based on atmospheric pressure plasma jets (APPJs).

Objective 2: Introduce ultrafast and scalable process for reduction of graphene oxide (GO) based on atmospheric pressure plasma jets (APPJs).

***Objective 3*:** Fabrications of practical applications of prepared atmospheric plasma reduced graphene films such as supercapacitor device, transparent conductive (TCFs) and flexible electrode.

AIM 2: Development of a new concept to engineer graphene based multifunctionally graded surfaces with continuous graduated change of structural, chemical, wettability, charge, surface, energy, electrical and thermal conductivity.

Objective 1: Development and optimization of new method to engineer graphene surface gradients

Objective 2: Characterisation of multifunctional properties such chemistry, morphology thermoelectric properties and wettability

AIM 3: Development of graphene inks and their composites for high performing conductive film for a broad range of applications

Objective 1: Optimisation of graphene based composite ink for electronics applications and prepared highly conductive electrode on various substrates such as glass, polyethylene terephthalate (PET), textile and paper.

Objective 2: Exploring an easy way to increase the stability of AgNW electrodes and their performance to overcome the research gaps and limitations of materials used in transparent conductive films (TCFs) technology.

Objective 3: Fabrication of highly conductive and transparent ultra-thin nitrogen (N) doped graphene electrode from graphene inks by using a combination of microwave, ultrasonic nebulizer and thermal annealing.

1.3 Thesis outline

The thesis is organized by seven chapters to present the pervious aims and objectives with details described as follows:

Chapter 1

Introductory chapter provides an overall overview of the conductive coatings materials and backgrounds followed by short review on graphene derivatives, properties, and objectives of the Ph.D. program. Finally, the structural outline and contents of the individual chapter will be summarized corresponding to each objective.

Chapter 2

This chapter presents literature review and it is divided into three parts. First, literature review on graphene derivatives (graphene, graphene oxide and reduce graphene oxide) followed by discussion on intrinsic graphene properties. The second literature review is about

silver nanowire (AgNW) covering their synthesis methods, properties and their limitations. The third part provides background on plasma and recent progress on plasma-based reduction for graphene oxide methods.

Chapter 3

This chapter addresses the limitations and issue of main graphene reduction methods as well as the conventional plasma techniques for graphene reduction and present simple, fast cold plasma approach for scalable preparation of graphene conductive film on different substrates based on atmospheric pressure plasma jets (APPJs). This work was published in Carbon Carbon 127 (2018) 113-121.

Chapter 4

This chapter reports a new method to fabricate graphene base multifunctionally graded surfaces with continuous graduated change of structural, chemical, wettability, charge, surface, energy, electrical and thermal conductivity. The technique is easy, low - cost, scalable, applicable on different substrates (metals, plastic, textile, glass, curved, flexible) with the ability to produce large - scale multifunctional surface gradients, and managed to solve several fundamental and engineering matters that cannot be solved by homogeneous surfaces. The contents of Chapter 4 submitted to Advanced Material journal Feb 2019 DOI: 10.1002

Chapter 5

This chapter focuses on the investigation on the current limitations of conductive coatings materials. Furthermore, formulation and optimization of AgNW / pG ink using different pG and AgNW ratios to develop a range of coated substrate on various film including glass,

flexible poly(ethylene terephthalate), textile and paper. The purpose of proving that the pG layers offer a barrier shield against AgNW oxidation and have the extra benefit of improving the connections between wires and electrode stability. A sheet resistance of 18.23 Ω/sq and an optical transparency of 89% were obtained on the glass substrates. This work was published ACS Appl. Nano Mater. 2018, 1, 2249−2260

Chapter 6

This chapter presents new methods for the production of highly conductive and transparent ultrathin nitrogen (N) doped graphene electrode from graphene inks by combining microwave, ultrasonic nebulizer and thermal annealing. The resulting thin films proves to reduce the surface resistance in the range of 1.5×10^3 to 6.2×10^3 Ω/sq at transparency ranging from 68% to 82%, which offers encouraging eco-friendly, low-cost and scalable manufacture of high quality conductive N-doped graphene films. This work was published Chemical Engineering Journal 2018,338 (2018) 764–773

Chapter 7

Collects and summarizes the research that have been carried out and reported in this dissertation. The chapter also highlights some future direction on the conductive coating technology based on graphene.

1.4 References

1. Naghdi, S., Rhee, K., Hui, D., & Park, S. (2018). A Review of Conductive Metal Nanomaterials as Conductive, Transparent, and Flexible Coatings, Thin Films, and Conductive Fillers: Different Deposition Methods and Applications. Coatings, 8(8). doi:10.3390/coatings8080278
2. Kamyshny, A., & Magdassi, S. (2019). Conductive nanomaterials for 2D and 3D printed flexible electronics. Chemical Society Reviews. doi:10.1039/C8CS00738A
3. Abbel, R., Teunissen, P., Rubingh, E., Lammeren, T. v., Cauchois, R., Everaars, M.,Groen, P. (2014). Industrial-scale inkjet printed electronics manufacturing—production up-scaling from concept tools to a roll-to-roll pilot line. Translational Materials Research, 1(1), 015002. doi:10.1088/2053-1613/1/015002
4. Grau, G., Cen, J., Kang, H., Kitsomboonloha, R., Scheideler, W. J., & Subramanian, V. (2016). Gravure-printed electronics: recent progress in tooling development, understanding of printing physics, and realization of printed devices. Flexible and Printed Electronics, 1(2), 023002. doi:10.1088/2058-8585/1/2/023002
5. Layani, M., Kamyshny, A., & Magdassi, S. (2014). Transparent conductors composed of nanomaterials. Nanoscale, 6(11), 5581-5591. doi:10.1039/C4NR00102H
6. Grau, G., Cen, J., Kang, H., Kitsomboonloha, R., Scheideler, W. J., & Subramanian, V. (2016). Gravure-printed electronics: recent progress in tooling development, understanding of printing physics, and realization of printed

devices. Flexible and Printed Electronics, 1(2), 023002. doi:10.1088/2058-8585/1/2/023002

7. Subramanian, V., & Lee, T. (2012). Nanotechnology-based flexible electronics. Nanotechnology, 23(34), 340201-340201. doi:10.1088/0957-4484/23/34/340201

8. Bouden, S., Dahi, A., Hauquier, F., Randriamahazaka, H., & Ghilane, J. (2016). Multifunctional Indium Tin Oxide Electrode Generated by Unusual Surface Modification. Scientific Reports, 6, 36708. doi:10.1038/srep36708

9. Noor, N., & Parkin, I. P. (2013). Enhanced transparent-conducting fluorine-doped tin oxide films formed by Aerosol-Assisted Chemical Vapour Deposition. Journal of Materials Chemistry C, 1(5), 984-996. doi:10.1039/C2TC00400C

10. Wu, H., Kong, D., Ruan, Z., Hsu, P.-C., Wang, S., Yu, Z., . . . Cui, Y. (2013). A transparent electrode based on a metal nanotrough network. Nature Nanotechnology, 8, 421. doi:10.1038/nnano.2013.84

11. Zheng, Q., Li, Z., Yang, J., & Kim, J.-K. (2014). Graphene oxide-based transparent conductive films. Progress in Materials Science, 64, 200-247. Doi:10.1016/j.pmatsci.2014.03.004

12. Kaltenbrunner, M., White, M. S., Glowacki, E. D., Sekitani, T., Someya, T., Sariciftci, N. S., & Bauer, S. (2012). Ultrathin and lightweight organic solar cells with high flexibility. Nat Commun, 3, 770. doi:10.1038/ncomms1772

13. Yagci, Ö., Yesilkaya, S. S., Yüksel, S. A., Ongül, F., Varal, N. M., Kus, M., Icelli, O. (2016). Effect of boric acid doped PEDOT:PSS layer on the performance of P3HT:PCBM based organic solar cells. Synthetic Metals, 212, 12-18. doi:10.1016/j.synthmet.2015.11.010

14. Wang, B. Y., Yoo, T. H., Lim, J. W., Sang, B. I., Lim, D-S., Choi, W. K., ... Oh, Y. J. (2015). Enhanced light scattering and trapping effect of Ag nanowire mesh electrode for high efficient flexible organic solar cell. Small, 11(16), 1905-1911.doi:10.1002/smll.201402161

15. Kim, H.-J., Kang, K. H., & Kim, D.-E. (2013). Sliding and rolling frictional behavior of a single ZnO nanowire during manipulation with an AFM. Nanoscale, 5(13), 6081-6087. doi:10.1039/C3NR34029E

16. Gaynor, W., Burkhard, G. F., McGehee, M. D., & Peumans, P. (2011). Smooth Nanowire/Polymer Composite Transparent Electrodes. Advanced Materials, 23(26), 2905-2910. doi:10.1002/adma.201100566

17. Ahn, Y., Jeong, Y., & Lee, Y. (2012). Improved Thermal Oxidation Stability of Solution-Processable Silver Nanowire Transparent Electrode by Reduced Graphene Oxide. ACS Applied Materials & Interfaces, 4(12), 6410-6414. doi:10.1021/am301913w

18. Li, X., Zhu, Y., Cai, W., Borysiak, M., Han, B., Chen, D., . . . Ruoff, R. S. (2009). Transfer of Large-Area Graphene Films for High-Performance Transparent Conductive Electrodes. Nano Letters, 9(12), 4359-4363. doi:10.1021/nl902623y

19. Kim, H.-J., Seo, K.-J., & Kim, D.-E. (2016). Investigation of mechanical behavior of single- and multi-layer graphene by using molecular dynamics simulation. International Journal of Precision Engineering and Manufacturing, 17(12), 1693-1701. doi:10.1007/s12541-016-0196-4

20. Li, Z., Kandel, H. R., Dervishi, E., Saini, V., Xu, Y., Biris, A. R., . . . Biris, A. S. (2008). Comparative Study on Different Carbon Nanotube Materials in Terms of

Transparent Conductive Coatings. Langmuir, 24(6), 2655-2662. doi:10.1021/la701880h

21. Shin, Y. C., Novin, E., & Kim, H. (2015). Electrical and thermal conductivities of carbon fiber composites with high concentrations of carbon nanotubes. International Journal of Precision Engineering and Manufacturing, 16(3), 465-470. doi:10.1007/s12541-015-0063-8

22. Bae, K. M., Yang, H. D., Tufa, L. T., & Kang, T. J. (2015). Thermobattery based on CNT coated carbon textile and thermoelectric electrolyte. International Journal of Precision Engineering and Manufacturing, 16(7),1245-1250. doi:10.1007/s12541-015-0162-6

23. Novoselov, K. S., Geim, A. K., Morozov, S. V., Jiang, D., Zhang, Y., Dubonos, S. V., . . . Firsov, A. A. (2004). Electric Field Effect in Atomically Thin Carbon Films. Science, 306(5696), 666. doi:10.1126/science.1102896

24. Zhang, Y., Tan, Y.-W., Stormer, H. L., & Kim, P. (2005). Experimental observation of the quantum Hall effect and Berry's phase in graphene. Nature, 438, 201. doi:10.1038/nature04235

25. Novoselov, K. S., Fal′ko, V. I., Colombo, L., Gellert, P. R., Schwab, M. G., & Kim, K. (2012). A roadmap for graphene. Nature, 490, 192. doi:10.1038/nature11458

26. Compton, O. C., & Nguyen, S. T. (2010). Graphene Oxide, Highly Reduced Graphene Oxide, and Graphene: Versatile Building Blocks for Carbon-Based Materials. Small, 6(6), 711-723. doi:10.1002/smll.200901934

27. Pei, S., & Cheng, H.-M. (2012). The reduction of graphene oxide. Carbon, 50(9), 3210-3228. doi:10.1016/j.carbon.2011.11.010

28. Suvarnaphaet, P., & Pechprasarn, S. (2017). Graphene-Based Materials for Biosensors: A Review. Sensors (Basel, Switzerland), 17(10), 2161. doi:10.3390/s17102161.

Blank Page

Chapter 2

Literature review

2.1 Graphene materials

2.1.1 Graphene

Graphene is composed of 2-dimensional (2D) sheet of sp2-hybridized carbon atoms arranged in a hexagonal lattice. Allotropes of carbon are presented in **Figure 2.1** where the stack of many graphene layers, combined together by the Van der Waals force, results in 3D graphite, whereas the rolling of a single flake produces 1D carbon nanotubes and if the honeycomb layer is arranged to produce a spherical particle, they so called 0D fullerene [1]. Graphene has garnered much interest owing to its remarkable properties such as thermal, electrical and mechanical properties.

For the first time, one layer of the 2D atomic sheet can be separated where it is among the thinnest objects known [2]. The carbon-carbon (C-C) bond, the strongest bond in nature, locks these atoms covalently and gives them outstanding mechanical properties. Geim and Novoselov's studies, which demonstrate isolating single graphene flakes, confirmed the expectations of the theoretical studies in 2004, confusing the suggested that such 2D crystals are thermodynamically stable at infinitesimal temperatures only [2,3].

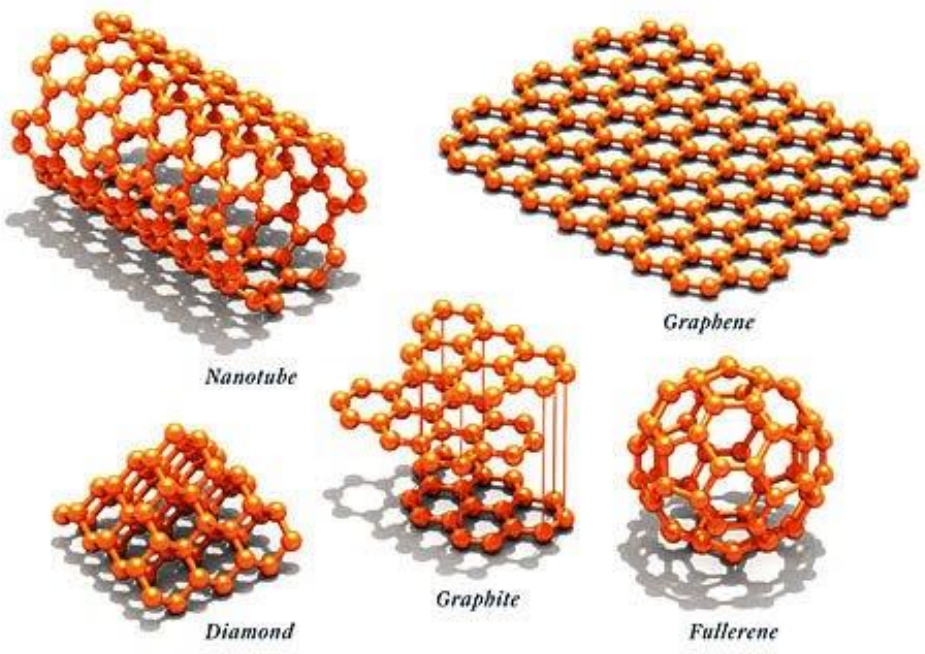

Figure 2.1: Allotropes of carbon [45].

One of the strongest identified materials distinguished by an outstanding high Young's module of ~ 1 TPa is one layer of graphene. Graphene is a 2D form (thin film), but also can be wrapped up into 0D (fullerenes), rolled into 1D (nanotubes) or stacked into 3D graphite forms, in which electronic properties are different due to their electronic band gap. In graphene scattering is low so that the Quantum Hall Effect (QHE) can be observed thus the novel band structure of graphene provides this old effect a new twist [4]. The difference of electronic band structure is because of a large difference between the in-plane C-C bond length (1.42 Å) as well as crystal structures and lattice parameters of two carbon allotropes. Electrons in graphene obey a linear dispersion relation [2].

2.1.2 Graphene synthesis

Since a single layer of graphene isolation was successfully confirmed, many studies devoted to develop new methods to obtain high quality pristine graphene because of its outstanding optical, thermal, structural, mechanical and electrical properties. Moreover, to achieve such remarkable characteristics, exfoliation of graphite to single-layer graphene is very essential. Graphene has a 2630 m^2/g precise theoretical surface area (SSA), which is more than the carbon black surface area. Graphene is highly packed because of the force of the van der Waals force. Consequently, graphene layers tend to restore and re-aggregate unless they are well isolated from one another. Preventing aggregation is therefore a crucial challenge in the synthesis of bulk graphene. Synthesis graphene can mainly be performed using chemical vapor deposition (CVD), mechanical exfoliation, epitaxial growth and chemical graphene oxide reduction [5-7].

Mechanical exfoliation use Scotch tape to separate the sheets of a piece of highly oriented pyrolytic graphite (HOPG) and transferring graphite layers to a SiO_2 substrate [8,9]. This method produces pristine graphene, but its low production limits this approach. Physical exfoliation is a technique that generates good- quality and unoxidized single layer graphene and is desirable where the graphene structure needs to be maintained [9]. In this method, solvent - graphene interactions balance the energy needed for exfoliation via surface energy matching of solvent and graphene. To exfoliate graphite in water to graphene surfactants such as sodium dodecylbenzene sulfonate and sodium cholate have been used. The aggregation of single layer graphene was avoided by high repulsive force between surfactant - coated graphene sheets [10-11]. It is possible to fabricate graphene sheet of intercalated graphite compounds (GICs), commonly known as expandable graphite. In order to stop graphite

agglomeration, GICs are formed by combining molecules between the graphite sheets or via the noncovalent bond of molecules onto the layers. The graphite is then expanded at a temperature of around 900 ° C. A study has reported the synthesis of great - quality single-layer graphene in organic solvents through continuous exfoliation - re - intercalation - expansion processes. The produced graphene shows highly electrical conductivity with a sheet resistance of 8 KΩ/square and a transparency more than 80% [12].

Chemical vapor deposition (CVD) is a substratum – technique that considered as a promising approach to produce high quality graphene by gas phase method, in which carbon is precipitation and growth onto transition metal substrates such as Cu or Ni at high temperature (i.e., 1000 °C). The solubility of the carbon on the substrate decreases when cooling and a thin film of carbon precipitates on the surface to create graphene layers. The thickness of the graphene layers is maintained by the cooling rate and the dissolved carbon concentration in the Ni substrate. Moreover, the film thickness is quite hard to control and the need for costly substrate is addition disadvantage of the CVD technique that restricts its implementation for large scale production [13-14]. It is interesting to note that Qu et al [15] reported a modified CVD method for the synthesis of nitrogen-doped graphene films using nitrogen-containing mixture gas as feed [15].

Epitaxial growth is also a substrate - based technique in which single layer graphene is grown on silicon carbide (SiC) by reduction of SiC substrate at high temperatures. High temperature treatment of SiC under vacuum result in silicon atoms being sublimated and graphene formed by the reorganization and graphitisation of carbon-enriched surface. As a result of the influence of interfacial effects in epitaxial graphene, several physical properties are different between epitaxial growth and mechanical exfoliation graphene [13-14]. This is due to the

influence of interfacial effects in epitaxial graphene, which are heavily dependent on both the silicon carbide substrate and many growth parameters.

2.1.3 Graphene oxide (GO)

Graphene oxide (GO) is a highly oxidized graphene derivative that has different functional groups carry oxygen including C=O, OH- and -COOH. Such functional groups are located on the graphene sheet edge and face plane, diagram shown in **Figure 2.2**, changing the sp^2 structure into a mixture of hybrid carbon sp^2 and sp^3. These sp^{3-} defects change the intrinsic pi-system conjugation and decrease mechanical properties, thermal and electrical conductivity. However, such functional groups make (GO) very promising material for variety of implementations, since it can be easily modified with multiple functional groups [16].

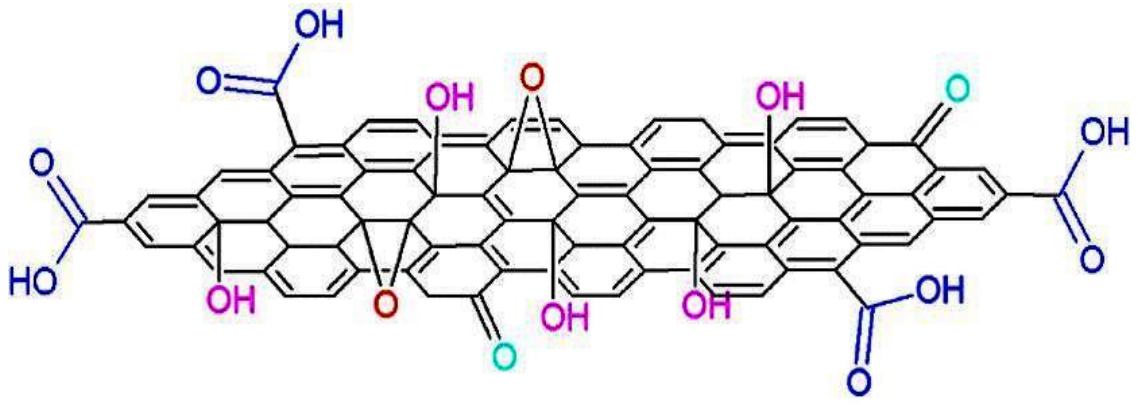

Figure 2.2. Diagram structure of (GO) [139].

2.1.4 GO synthesis

More than a century, Brodie reported oxidizing graphite method of highly oxidized graphite oxide with a C / O / H ratio of about 2.2/1/0.8 using mixture of $KClO_3$ and HNO_3 [17,18]. Staudenmaier modified the Brodie method, which replaced the oxidizing agent with a mixture of nitric acid and sulfuric acid [18]. Hummers and Offeman reported in 1958, a much less dangerous and so more efficient approach by using water free- mixture of sodium nitrate, potassium permanganate and concentrated sulfuric acid. This method is one of the most widely used today [19]. Tour and co - workers have developed lately the Hummers ' method by eliminating Sodium nitrate, increasing the amount of potassium permanganate, and reacting in a mixture 9:1 of sulfuric acid/phosphoric acid. The method has many advantages as it is easier procedure, higher yield, better efficiency, less flaws and no evolution of toxic gas while oxidation [20].

Commercial natural graphite sources are generally classified as flake graphite. This found naturally is purified to eliminate heteroatom contamination and contains many localized defects that can work as seed for the oxidation method. Nevertheless, the clarification of the accurate oxidation method still a continuous challenge given the complexity of flake graphite and its natural source defects [21].

2.15 Reduction of graphene oxide

GO's carbon structure can be restored by thermal reduction or by chemically reducing agent method. For this reason, earlier efforts engaged mostly with the use of hydrazine vapor [22]. However, the use of hydrazine needs care since it is very toxic and likely explosive. As a result, Many alternative approaches have been investigated. Sodium borohydride has been

shown to reduce graphene oxide effectively yet the method is slow, as it hydrolyzes slowly in water [23]. Many other reducing agents, including hydroquinone [24], vitamin C [25] and strongly alkaline solutions (KOH, NaOH) [25], are also used to reduce graphene oxide. Additionally more techniques are used to reduce graphene oxide by using hydrogen or oxygen plasma and by thermal annealing in high vacuum or inert atmospheric gas [26].

2.1.6 Intrinsic properties of graphene materials

Graphene is a 2D carbon allotrope with a honeycomb lattice where from all the rest graphitic allotropes can be obtained [27]. Graphene is the strongest material known, the thinnest, very flexible, transparent as well as electrically conductive [27,28]. All carbon atoms are sp^2 hybridized with σ bonds that are responsible for the stiffness of the lattice structure and a half-filled by π bonds that carry the current in graphene [29]. Each atom in graphene is naturally a surface atom and the π bonds responsible for electronic travel all around the carbon lattice. Thus the transport of a charge carrier in graphene is very sensitive to any changes in its immediate environment. Moreover, the physical properties of graphene can additionally be used to detect changes in the current when any molecules are adsorbed on the surface of graphene [30].

2.1.7 Mechanical properties

Any solid's mechanical properties rely on its inter - atomic bond strength. The strong C – C sp^2 bonds in graphene allow it to exceed any other material strength [27]. Highly anisotropic material is the bulk graphite material itself. The Young's modulus of graphite in - plane is 920 GPa and the Poisson ratio is 0.16 [31]. Experimentally and theoretically, the mechanical properties of both single layer and multilayer graphene were examined. Lee et al conducted

the first experimental research of elastic properties and graphene strength [32]. In this report, a graphene membrane was transferred on the array of trenches in SiO_2 and the mechanical readings were carried out by using on graphene the diamond-coated tip of the AFM . Exceptionally high Young's module of 1.0 TPa and the greatest tensile strength of 130 GPa were measured. A Young's modulus of 0.25 ± 0.15 TPa for a chemically reduced single layer graphene oxide using AFM reported by Gomez-Navarro et al [33].

2.1.8 Thermal properties

Bulk graphite delivers thermal conductivity of 1000 Wm^{-1} K^{-1}, which provides high graphene sheet thermal conductivity. Theoretically, graphene's intrinsic thermal conductivity reported to be isotropic, with a value of 2200 Wm^{-1} K^{-1} at 300 K, regardless of layer numbers [34]. Balandin et al studied the thermal conductivity in a suspended monolayer graphene using confocal micro-Raman spectroscopy [35]. The calculated thermal conductivity of the room temperature found up to 5300Wm^{-1} K^{-1}, which was obtained for a single layer graphene from the Raman G peak frequency reliance on the laser excitation power.

2.2 Silver nanowires (AgNWs)

Silver nanowires (AgNWs) are 1-dimensional silver nanostructures with usually 10–200 nm in width and 5–230 μm in length. Methods for AgNW's synthesis are obtained from those used in the production of semiconductor quantum wires and metallic alloys that have been found to have exceptional electrical and magnetic features [36]. Therefore, the conventional processes used to synthesize quantum dots and wires are also used to synthesis metallic wires including gold, silicone, selenium, gallium, aluminum and silver wires. In the early stages, AgNWs were synthesis mainly using electrochemical techniques, yet the AgNWs produced

by this method are not uniform and are obtained in low yield. As a result, in the past twenty years, the hard - template and soft - template techniques have been created. The polyol method is a notable example of the soft - template method, and broadly used by lots of researchers.

2.2.1 Synthesis of AgNWs by polyol process

Synthesis AgNW by using polyol methods have solved challenges in the preparation of AgNWs such as low yield and morphology disorder. The general idea of this method is the generation of noble metals (Ag, Au, Pd and Pt) by using ethylene glycol (EG) at 150 ° C to reduce noble metal salts and using polymer like polyvinylpyrrolidone (PVP) and to selectively adsorb onto the metals surfaces. Over the past decade, several types of polyol approach were reported. Another group of researchers have modified the polyol synthesis methods by using EG and glycerol as solvent and reducing agent. Glycerol has been found to have a significant reductant ability to change Ag^{+} to Ag comparative to EG [37,38].

The polyol method is a common technique for AgNWs preparation. This process depends on temperature - for oxidation EG and from (GA), that creates noble metal ion to be reduced to zerovalent. Such principles detail the mechanical aspect that the technique of polyol would be applied to synthesis AgNWs with fully- controlled diameters [39]. Skrabalak et al. observed that GA was procured when heating EG about 150 ° C air presences, which is the main reductant element for synthesis Ag nanostructure. **Figure 2.3 1** shows the format of reaction for EG reduction and GA formation [40]. Many parts that affect the kinetics of oxidation reaction have been examined for solution - phase synthesis of AgNWs [41-43].

Synthesis of the solution phase requires the soft templates using or caping agents that has an important part in AgNW synthesis. For the AgNWs preparation, various kinds of polymers stabilizer such as PVP, vitamin B2, sodium dodecylsulfonate (SDS), poly(vinyl alcohol) (PVA) and dextrin, poly(methyl vinyl ether) were used. The degree of polymerisation and the ratio of these stabilizing strongly affect the size and diameter of AgNW. PVP has been considered to an excellent polymer stabilizer in polyol method since it has a high degree of polymerization (3240) and is capable of supporting the growth of many nanostructures [44].

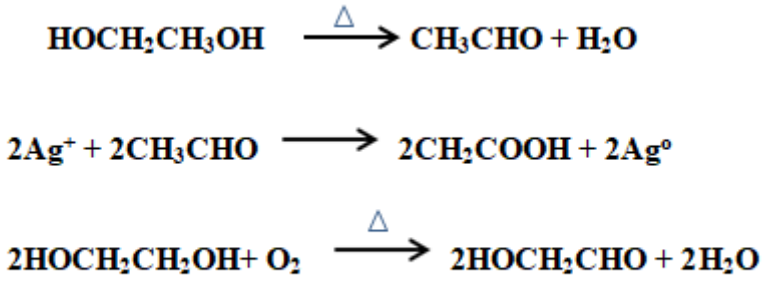

Figure 2.3. Catalytic oxidation of EG to GA and reduction of silver ions.

2.2.2 Properties and applications of AgNWs

Individual metal nanowires have very good electrical and thermal conductivity: silver is the most efficient electrical conductor, and gold, copper and even alloys such as Cu-Ni are also highly conductive. Moreover, electrical conductivity is still pretty high even for small nanowire diameters. It is lower in bulk metals for diameters about 45 nm for silver that approach the mean free path of electrons. Bid et al. was measure resistivity of AgNW film at room temperature and then calculated its electrical conductivity. [46]. The study shows in bulk material when the AgNW approaches the mean free path of electrons increases the

electron surface scattering, lead to increasing in AgNW electrical conductivity [46]. This increase, however, still reasonable for electrical conductivity performance, though it could reduce the stability is needed under high current density or temperature [47]. From an optical perspective, small thickness is advantageous for enhancing the transmittance and reducing the amount of light scattered by the AgNW [48]. Larger AgNW thickness increases the surface roughness, which mostly requires to be decreased for optoelectronic devices, particularly when it comes to very thin layers, like organic solar cells or OLEDs. Long AgNWs play an important key increasing the electrical conductivity at low concentration of AgNW. AgNW interconnections between each other have a great influence on the network's properties [49–51]. Moreover, the electrical conductivity in the AgNWs network can significantly decrease using different techniques, for example, thermal treatment [52, 53] chemical processing,[54] and laser sintering[55].

Mechanical property is one of AgNW ' features. Recently, a study done by Miller et al. shows that AgNW networks can remain stable up to 200 bending cycles of 15% strain and 75% tensile strain and with small decrease in electrical conductivity [56]. Moreover, due to AgNW unique properties, many studies and reports shows that it can be efficiently used into broad types of applications such as flexible organic light-emitting device (OLED) [57], touch screens [58], electromagnetic shielding [59], and antenna [60]. As previously mentioned, AgNWs have good flexibility and their electrical conductivity increases slightly when bending unlike ITO. Andrés et al. reported using high aspect ratio AgNW as an affordable option in comparison to ITO in organic solar cells (OSC), while they induce a slight reduction in the performance of energy conversion [61]. Another study, applying AgNWs as the top electrode in tandem OSCs, achieved energy conversion efficiency about 5.81 percent

[62]. The Fried et al. demonstrated capacitive touch modules using AgNW transparent conductive coatings, produced under actual production conditions with a high network ratio around 90 %, and high performance under different conditions such as temperature, humidity and energy [63]. Pei et al. showed good results on a healable capacitive touch screen where AgNWs are deposited in a thermally stable thin layer on a healable polymer film [64].

Yu et al. analysed the effect of silver material on the performance of AgNWs / PVA and AgNWs / epoxy coatings to efficiently shield radiofrequency (RF) and compared it with Silver nanoparticles AgNPs. Unlike AgNPs, silver nanowires were observed to be more effective at low material concentration, showing that high electrical conductivity can be obtained with less Ag ratio [65].

2.2.3 Stability limitations of AgNW and hybrid materials

AgNWs ' stability has been considered a potential limit for many electronic applications such as thermal, chemical and electrical stability. AgNW may have initial failure, for example, surface diffusion [66], electromigration methods and surface chemistry changes when presented to high temperatures showing **Figure 2.4** or current [67]. Environmental study such as high time, humidity, optical light and temperature proved to have critical effect on AgNWs [68,69]. Depending on the research groups, AgNW's environmental stability would be then quite different and can differ from several days to even years. For example, Mayousse et al. reported that the electrical conductivity of AgNW - based conductive film in the dark and air after 48 months had been negligibly degraded [68,69]. On the other hand, after only two weeks, Jiu et al. reported high degradation of AgNW in light and air conditions.

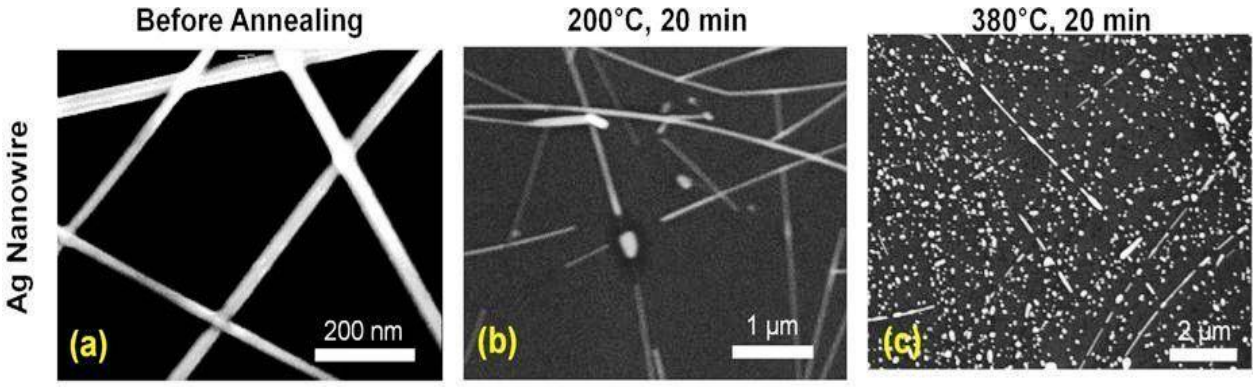

Figure 2.4. AgNWs after thermal annealing at different temperatures [140].

In addition, hybrid materials where combining AgNW with for instance graphene, conductive polymers, CNTs, or others conductive materials could improve the film properties. For example, a highly flexible and transparent conductive electrode was achieved by combining the mechanical properties of CNTs with the unique sheet resistance of AgNWs.[70] Another study shows the use of aluminum - doped zinc oxide atomic layer deposition technique on AgNWs resulting in a highly efficient transparent electrode used on Si - solar cells [71]. Other research has suggested hybrids between AgNW and other materials, such as graphene and conductive polymers such as PEDOT that open the door for multiple opportunities.

2.3 Plasma technologies for engineering graphene materials

Plasma refers to a state of matter that exists in the form of quasi-neutral gases made of neutral and charged particles (neutrons, ions, and electrons) exhibiting collective behavior [72]. This state of matter only exists under special circumstances and became known following the work of various scientists notably Irving Langmuir in the early decades of the 20th century. They stablished that by introducing neutral gases to stronger electromagnetic fields or heating

them at extremely high temperatures producing an plasma beam that was characterized by increased electrical conductivity in combination with long-range magnetic and electric fields [73].

During the decades that followed, extensive research was undertaken to bring to light the unique properties of plasma and its potential for use in various industrial applications [73]. The electric and magnetic fields generated using plasma have presented limitless opportunities that are currently revolutionizing several industrial applications. As well as explored to synthesis new materials, modify pre-formed materials, and remove toxic/ harmful objects.

2.3.1 Background

Plasma dates back to the mid-19th century evidenced by the work of Julius Plucker and later on his student Hoham Wilhelm through their examination of electrodeless discharges in Germany. William Crookes posited in 1879 that plasma accounts for 99% of the elements in space [74]. However, it was until 1928 that Irving Langmuir discovered the structure and formation of plasma. Continued research on the properties of plasma birthed thermal plasma technologies in the 1960s that were initially used in Bucharest by Eugene Badarau [73]. During the 90s, nanoscience received a major boost following the discovery by Iijima where plasma was used to process carbon nanotubes (CNTs). Prior to this discovery, CNTs had become the basic units of nanotechnology and nanoscience ushering in a new era of extensive research activities on plasma use in the production of nanomaterials [75].

Extensive research activities provided an opportunity for testing plasma-based applications in nanotechnology thereby yielding superior outcomes in reference to the resultant

nanomaterials' structure, complexity, and functionality [74]. Moreover, plasma use made it possible to undertake bottom-up and top-down nanofabrication ,[76] expand the varieties of nanoparticles [77-81], and revolutionize traditional industries such as medicine [82,83], agriculture [84], nutrition [85], space missions [86], and national security [74,87].

2.3.2 Plasma reduction for GO

Plasma techniques have been extensively applied in the production of microelectronic structures for many years. The main objectives for using plasma methods are surface cleaning, etching, and enhancement of material surface features such as hydrophilic properties, electrical conductivity and other. By the rise of nanomaterials, plasma techniques have been applied to produce and functionalize nanostructures, offering novel features in the production method such as economy and safety. Plasma systems are therefore commonly applied for nanomaterials production via the plasma - enhanced chemical vapor deposition (PECVD) technique as well as for the modification of surface features. Low radiofrequency temperature plasma having chemical active particles offers hopes for GO functionalization and reduction [88–92]. Plasma method is a process of functionalization and reduction of (GO) that is efficient, ecofriendly and comparatively cheap. GO plasma approach is of interest in the development different applications such as gas sensors [93, 94], optoelectronics devices [95], bio-sensors [96–98], transparent electrodes [99, 100]. Different techniques are applied to do plasma treatments that can be possibly classified in "low" and "remote" operations [101], as well as low and atmospheric pressures [102]. This helps identify the influence of plasma on GO properties. The commonly used treatments for GO treatment are ammonia, methane, nitrogen hydrogen, fluorine, and oxygen plasma. The treatment for each one of those plasmas has characteristics in relation to the ions chemical activity, stimulated

by ultraviolet radiation and electrons. Moreover, Lots of studies applied to plasma effects on carbon nanomaterials are combined with the investigation of graphene and CNTs properties. Even though plasma treatment results in an efficient reduction of GO and changes its properties, only a few studies have been done on this field. Next is a short review that takes into account the plasma influences of different gases on GO properties, considering the technique conditions.

2.3.3 O_2 plasma treatment

Oxygen plasma processing of GO can be applied to different surface films, to functionalize [93, 96, 107] or by oxidation to produce GO from graphene [108–112]. The O_2 plasma is highly chemical aggressive, normally resulting in major changes in graphene's structural and electrical conductivity features: even by using low power in a short time treatment, a high degree of defect is produced in the graphene structure [113]. Nevertheless, with mild plasma treatments, the ratio of defects production under O_2 plasma treatment can be dramatically reduced, using low power, increase the distance from the sample source, use of filters and grids [96,113–116]. The XPS results of low - pressure O_2 plasma performed on (rGO) shows an introduction of several oxygen-functional groups [22]. Alike outcomes were reported with O_2 plasma treatment of graphene where epoxy (C-O-C) and carboxyl (C-OH) functional groups have been introduced to the basal face and edges plan of graphene as well as reduction of sp2-hybridized carbon bonds [96,108,114].

A study of the influence of O_2 plasma on the conductivity of rGO showed that the electrical conductivity decreases when increasing the plasma power or/and treatment time. [116]. When using high power and long treatment periods, it becomes difficult to measure the electrical conductivity because it was lower than the instrument's limitation scale (< 0.001 $Sxcm^{-1}$).

Measurements of scanning electron microscopy (SEM) have shown that most rGOs are gone [116]. The scholar describe this via that the O_2 plasma damages sp^2 regions in rGO and add different oxygen groups to the rGO defect regions, resulting in the etching of rGO by converting it into amorphous carbon. However, following a gentle' treatment technique, the conductivity of oxidized graphene by O_2 plasma can be saved.

2.3.4 N_2 and NH_3 plasma treatment

Gasses such as N_2 [122, 123–125] and NH_3 [117–121] are applied in several works to treat GO by plasma. Kim et al. applied NH_3 plasma with a power of 10 Watt and a pressure of 100 mTorr for formation of nitrides in rGO [22]. In addition, following the treatment using NH_3 plasma, several O_2 groups including, O-H, C=O and COOH on GO films was dramatically removed and replaced by C-N bonds. In shorter than 10 mins, the percentages of nitrogen to carbon quantities (N / C) and oxygen to carbon densities (OF) was approximately 10 and 23 % [119].

Nitrogen constructs in the graphene layer pyrrole (pyrrolic - N), pyridine (pyridinic - N) and graphite (quaternary, graphic - N) configurations with carbon atoms [126, 127–129]. Nitrogen pyridine and pyrrole configurations produce a p - type conductivity, whereas graphitic N increases the concentration of electrons [126, 130]. Kim et al, explained that pyridine and pyrrole configurations of nitrogen are primarily added in graphene by NH_3 plasma treatment, And the N / C and O / C percentages depend on plasma treatment time. Another study [22] confirmed the same results, which shows the percentage of pyridinic - N (48 %) being more than Pyrrolic - N (29 %) and Graphitic - N (15 %). Simultaneously, N_2 plasma treatment can cause an increase in oxygen amount. Kim et al. [119] reported an improvement in the conductivity with longer NH_3 plasma treatment and at the same time

reduction in the optical transparency. The scholars explain the electrical conductivity increase from 100 S/m to 1666 S/m of rGO sheets by the influence of nitrogen doping and oxygen reduction. Moreover, Reduced transmission is because the restoring of electronic conjugation in rGO. The film's surface roughness turn to smoother until the treatment period hits 10 minutes and no additional changes after that [119].

2.3.5 Atmospheric pressure plasma jets (APPJs)

The widespread use of low-pressure plasma in industrial applications resulted from their potential advantages. These plasmas make it possible to specify the properties of nanomaterials in a predetermined fashion using a wide range of substrates. However, operationalizing this technology is expensive with the vacuum systems requiring continuous maintenance. Moreover, the size of the vacuum chambers limits the size of materials that can be processed using plasma jets. The above mentioned technicalities birthed the use of APPJs (**Figure 2.5** Schematic of APPJs system) despite the challenges associated with the latter which requires high voltages to sustain a glow under low pressures [129].

In recent decades, APPJ applications in bioengineering, food manufacturing and agriculture have brought great recognition [81, 131]. Additional intriguing employment of APPJs in the processing of materials such as metal synthesis from liquid methods [132,133], Surface purification and modification [134], Inactivation of sterilisation and microbes [135], Nanoparticles and nanocrystals synthesis [135,136], thin film deposition of metal oxides [137], and surface activation of graphite and carbon cloth [138].

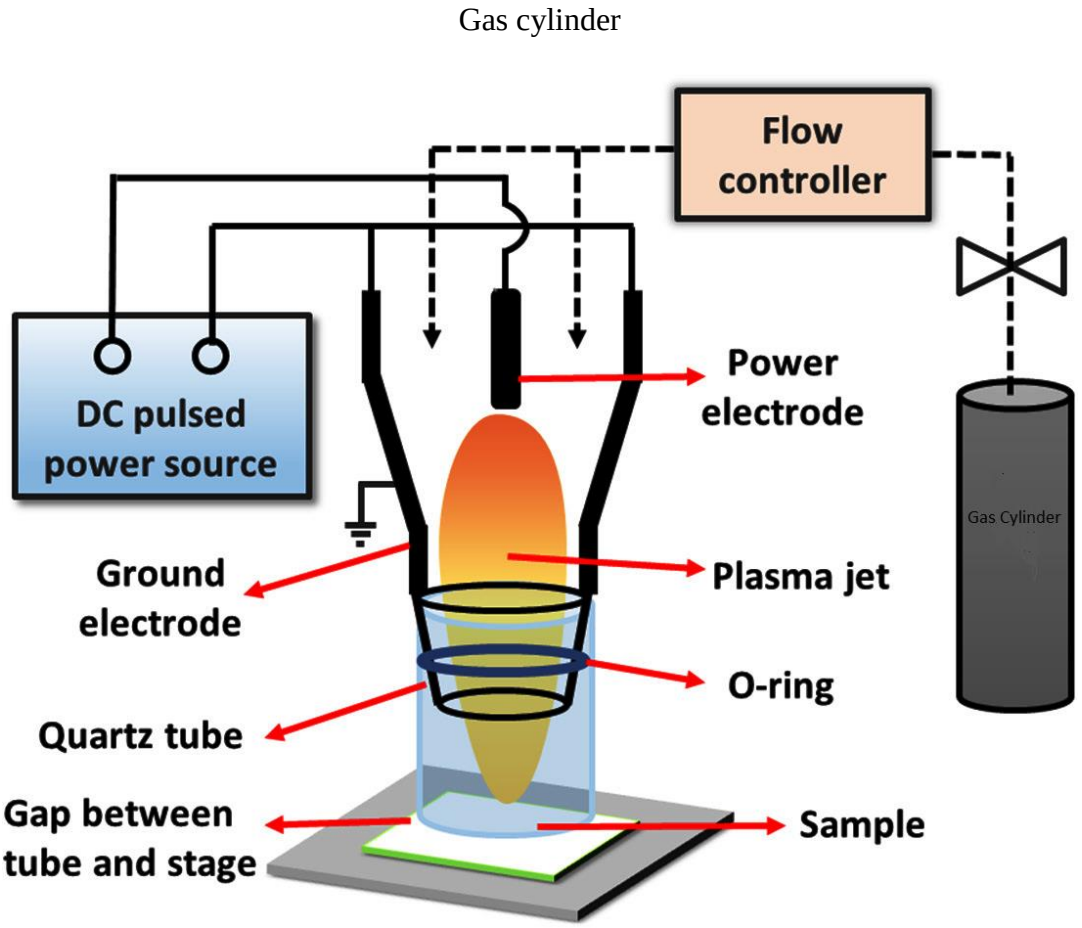

Figure 2.5. Schematic of APPJs system [131].

2.4 Gaps and motivation for this research work

The growth of graphene with exceptional chemical, thermal, electrical, mechanical and optical properties and the ability to make graphene films with various chemistries and surfaces make them an ideal choice for versatile applications. The reduction of GO to graphene by de-oxidation and removal of oxygen groups as well as recovery of carbon structures offers excellent electrical conductivity, chemical structure improvement and enhanced mechanical strength. For reduction graphene oxide (rGO) two main methods were

used, chemical and thermal process. The first method requires using strong chemical reduction with reduction agents that are very toxic and it takes a long time as well as the use of dispersing agents (surfactants) which add defects and affect the quality of rGO. On the other hand, thermal reduction of GO has been proven to remove oxygen effectively, but that high temperature, equipment-dependent and required limit range of substrates. Thus the electrical conductivity of rGO films produced by these techniques is low compared to pristine graphene. A new strategy of physical methods based on irradiation reduction such as microwave, plasma, UV and flask. Particularly, the plasma methods, for example, the reduction of GO by using NH_3, H_2, O_2 plasma, N_2 plasma and others. Such techniques are not only capable of reducing GO to rGO, but also of producing chemical functionalization or graphene surface doping, which is excellent for various applications . However, most of these plasma methods are costly and involved vacuum chambers, pumping systems, specific environments, and can use the only small sample area in batch mode that restricts its scalability and application for large samples and mass production of films and devices. In addition, the thermal reduction in the O_2 free and inert (Ar or NH_3) atmosphere using a high temperature that can efficiently reduce GO and afford improved electrical conductivity films. However, high temperature operation of this process limits the use range of temperature sensitive substrates such as polymers and plastics, textiles required for many applications (flexible and wearable electronics, heating etc.). It is therefore highly demanding for many applications to have scalable techniques that able to efficiently reduce GO films and produce either thin transparent or thick conductive graphene films at low temperatures, using environmentally friendly conditions through quick and simple direct treatment without damaging the underneath substrate.

Thre crucial limitation of AgNW electrodes is that they are oxidized easily, leading to a change in properties that lead to electrodes becoming erratic over time. Multiple techniques have been introduced to solve this problem, such optical sintering to weld the junction and combining other materials to form a stable network or coating layer on AgNWs to improve stability under ambient storage requirements. It has also been reported that AgNW film stability can be improved by combining AgNWs with different materials such as CNTs, graphite, conductive polymers, and metal nanowires. Adding such materials, however, can change surface roughness, optical transparency and the device contact point, which can significantly reduce the performance of transparent conductive electrodes (TCEs) in many applications. To address these limitations it is necessary to combine AgNW with significantly higher conductivity, lower defects and higher stability material compared to previously graphene used materials.

A wide range of surface - based chemical and structural gradients have been produced in recent years using polymers, self - assembled monolayers, porous materials, nanoparticles films and used to investigate fundamental difficulties like lateral sensory systems, protein adsorption, cell attachment, proliferation and differentiation. Nevertheless, at only a few tens of microns, these methods were able to generate surface gradients and were limited to only one or two properties such as chemistry and morphology. For numerous fundamental and practical applications, surface gradients at the macro scale with a combination of multiple properties are important but have not yet been achieved.

2.5 References

1. Katsnelson, M. I. (2007). Graphene: carbon in two dimensions. Materials Today, 10(1), 20-27. doi:https://doi.org/10.1016/S1369-7021(06)71788-6
2. Bunch, J. S., van der Zande, A. M., Verbridge, S. S., Frank, I. W., Tanenbaum, D. M., Parpia, J. M., McEuen, P. L. (2007). Electromechanical Resonators from Graphene Sheets. Science, 315(5811), 490-493. doi:10.1126/science.1136836.
3. Novoselov, K. S., Geim, A. K., Morozov, S. V., Jiang, D., Zhang, Y., Dubonos, S. V.Firsov, A. A. (2004). Electric Field Effect in Atomically Thin Carbon Films. Science, 306(5696), 666-669. doi:10.1126/science.1102896
4. Novoselov, K. S., Jiang, D., Schedin, F., Booth, T. J., Khotkevich, V. V., Morozov, S. V., & Geim, A. K. (2005). Two-dimensional atomic crystals. Proceedings of the National Academy of Sciences of the United States of America, 102(30), 10451-10453. doi:10.1073/pnas.0502848102.
5. Singh, V., Joung, D., Zhai, L., Das, S., Khondaker, S. I., & Seal, S. (2011). Graphene based materials: Past, present and future. Progress in Materials Science, 56(8), 1178-1271. https://doi.org/10.1016/j.pmatsci.2011.03.003
6. Hu, N., Wang, Y., Chai, J., Gao, R., Yang, Z., Kong, E. S.-W., & Zhang, Y. (2012). Gas sensor based on p-phenylenediamine reduced graphene oxide. Sensors and Actuators B: Chemical, 163(1), 107-114. doi:10.1016/j.snb.2012.01.0.
7. Stankovich, S., Dikin, D. A., Dommett, G. H. B., Kohlhaas, K. M., Zimney, E. J., Stach, E. A., . . . Ruoff, R. S. (2006). Graphene-based composite materials. Nature, 442, 282. doi:10.1038/nature04969
8. Hernandez, Y.; Nicolosi, V.; Lotya, M.; Blighe, F. M.; Sun, Z.; De, S.; McGovern, I. T.; Holland, B.; Byrne, M.; Gun'Ko, Y. K.; Boland, J. J.; Niraj, P.; Duesberg, G.;

Krishnamurthy, S.; Goodhue, R.; Hutchison, J.; Scardaci, V.; Ferrari, A. C.; Coleman, J. N., High-yield production of graphene by liquid-phase exfoliation of graphite, Nat Nano, 2008, 3, 563-568.

9. Novoselov, K. S., Geim, A. K., Morozov, S. V., Jiang, D., Zhang, Y., Dubonos, S. V., Firsov, A. A. (2004). Electric Field Effect in Atomically Thin Carbon Films. Science, 306(5696), 666-669. doi:10.1126/science.1102896

10. Green, A. A., & Hersam, M. C. (2009). Solution Phase Production of Graphene with Controlled Thickness via Density Differentiation. Nano Letters, 9(12), 4031-4036. doi:10.1021/nl902200b

11. Lotya, M., Hernandez, Y., King, P. J., Smith, R. J., Nicolosi, V., Karlsson, L. S., . . . Coleman, J. N. (2009). Liquid Phase Production of Graphene by Exfoliation of Graphite in Surfactant/Water Solutions. Journal of the American Chemical Society, 131(10), 3611-3620. doi:10.1021/ja807449u

12. Li, X., Zhang, G., Bai, X., Sun, X., Wang, X., Wang, E., & Dai, H. (2008). Highly conducting graphene sheets and Langmuir–Blodgett films. Nature Nanotechnology, 3, 538. doi:10.1038/nnano.2008.210.

13. Allen, M. J., Tung, V. C., & Kaner, R. B. (2010). Honeycomb Carbon: A Review of Graphene. Chemical Reviews, 110(1), 132-145. doi:10.1021/cr900070d

14. Zheng, Q., Li, Z., Yang, J., & Kim, J.-K. (2014). Graphene oxide-based transparent conductive films. Progress in Materials Science, 64, 200-247. doi:https://doi.org/10.1016/j.pmatsci.2014.03.004

15. Qu, L., Liu, Y., Baek, J.-B., & Dai, L. (2010). Nitrogen-Doped Graphene as Efficient Metal-Free Electrocatalyst for Oxygen Reduction in Fuel Cells. ACS Nano, 4(3), 1321-1326. doi:10.1021/nn901850u

16. Compton, O. C., Jain, B., Dikin, D. A., Abouimrane, A., Amine, K., & Nguyen, S. T. (2011). Chemically Active Reduced Graphene Oxide with Tunable C/O Ratios. ACS Nano, 5(6), 4380-4391. doi:10.1021/nn1030725

17. Brodie Benjamin, C. (1859). XIII. On the atomic weight of graphite. Philosophical Transactions of the Royal Society of London, 149, 249-259. doi:10.1098/rstl.1859.0013.

18. Young, R. J., Kinloch, I. A., Gong, L., & Novoselov, K. S. (2012). The mechanics of graphene nanocomposites: A review. Composites Science and Technology, 72(12), 1459-1476. doi:https://doi.org/10.1016/j.compscitech.2012.05.005.

19. Hummers, W. S., & Offeman, R. E. (1958). Preparation of Graphitic Oxide. Journal of the American Chemical Society, 80(6), 1339-1339. doi:10.1021/ja01539a017

20. Marcano, D. C., Kosynkin, D. V., Berlin, J. M., Sinitskii, A., Sun, Z., Slesarev, A., . . . Tour, J. M. (2010). Improved Synthesis of Graphene Oxide. ACS Nano, 4(8), 4806-4814. doi:10.1021/nn1006368

21. Dreyer, D. R., Park, S., Bielawski, C. W., & Ruoff, R. S. (2010). The chemistry of graphene oxide. Chemical Society Reviews, 39(1), 228-240. doi:10.1039/B917103G

22. Pei, S., & Cheng, H.-M. (2012). The reduction of graphene oxide. Carbon, 50(9), 3210-3228. doi:10.1016/j.carbon.2011.11.010

23. Shin, H.-J., Kim, K. K., Benayad, A., Yoon, S.-M., Park, H. K., Jung, I.-S., . . . Lee, Y. H. (2009). Efficient Reduction of Graphite Oxide by Sodium Borohydride and Its Effect on Electrical Conductance. Advanced Functional Materials, 19(12), 1987-1992. doi:10.1002/adfm.200900167

24. Wang, G., Yang, J., Park, J., Gou, X., Wang, B., Liu, H., & Yao, J. (2008). Facile Synthesis and Characterization of Graphene Nanosheets. The Journal of Physical Chemistry C, 112(22), 8192-8195. doi:10.1021/jp710931h

25. Fernández-Merino, M. J., Guardia, L., Paredes, J. I., Villar-Rodil, S., Solís-Fernández, P., Martínez-Alonso, A., & Tascón, J. M. D. (2010). Vitamin C Is an Ideal Substitute for Hydrazine in the Reduction of Graphene Oxide Suspensions. The Journal of Physical Chemistry C, 114(14), 6426-6432. doi:10.1021/jp100603h.

26. Fan, X., Peng, W., Li, Y., Li, X., Wang, S., Zhang, G., & Zhang, F. (2008). Deoxygenation of Exfoliated Graphite Oxide under Alkaline Conditions: A Green Route to Graphene Preparation. Advanced Materials, 20(23), 4490-4493. doi:10.1002/adma.200801306

27. Gómez-Navarro, C., Weitz, R. T., Bittner, A. M., Scolari, M., Mews, A., Burghard, M., & Kern, K. (2007). Electronic Transport Properties of Individual Chemically Reduced Graphene Oxide Sheets. Nano Letters, 7(11), 3499-3503. doi:10.1021/nl072090c

28. Geim, A. K., & Novoselov, K. S. (2007). The rise of graphene. Nature Materials, 6, 183. doi:10.1038/nmat1849

29. Lee, N. J., Yoo, J. W., Choi, Y. J., Kang, C. J., Jeon, D. Y., Kim, D. C., . . . Chung, H. J. (2009). The interlayer screening effect of graphene sheets investigated by Kelvin probe force microscopy. Applied Physics Letters, 95(22), 222107. doi:10.1063/1.3269597

30. Castro Neto, A. H., Guinea, F., Peres, N. M. R., Novoselov, K. S., & Geim, A. K. (2009). The electronic properties of graphene. Reviews of Modern Physics, 81(1), 109-162. doi:10.1103/RevModPhys.81.109

31. Liao, M., & Koide, Y. (2011). Carbon-Based Materials: Growth, Properties, MEMS/NEMS Technologies, and MEM/NEM Switches. Critical Reviews in Solid State and Materials Sciences, 36(2), 66-101. doi:10.1080/10408436.2011.572748

32. Li, P., You, Z., & Cui, T. (2012). Graphene cantilever beams for nano switches. Applied Physics Letters, 101(9), 093111. doi:10.1063/1.4738891

33. Lee, C., Wei, X., Kysar, J. W., & Hone, J. (2008). Measurement of the Elastic Properties and Intrinsic Strength of Monolayer Graphene. Science, 321(5887), 385-388. doi:10.1126/science.1157996

34. Gómez-Navarro, C., Burghard, M., & Kern, K. (2008). Elastic Properties of Chemically Derived Single Graphene Sheets. Nano Letters, 8(7), 2045-2049. doi:10.1021/nl801384y

35. Xie, G., Shen, Y., Wei, X., Yang, L., Xiao, H., Zhong, J., & Zhang, G. (2014). A bond-order theory on the phonon scattering by vacancies in two-dimensional materials. Scientific reports, 4, 5085. doi:10.1038/srep05085

36. Balandin, A. A., Ghosh, S., Bao, W., Calizo, I., Teweldebrhan, D., Miao, F., & Lau, C. N. (2008). Superior Thermal Conductivity of Single-Layer Graphene. Nano Letters, 8(3), 902-907. doi:10.1021/nl0731872

37. Prokes, S., & Wang, K. (1999). Novel Methods of Nanoscale Wire Formation. MRS Bulletin, 24(8), 13-19. doi:10.1557/S0883769400052842

38. Sun, Y., Mayers, B., Herricks, T., & Xia, Y. (2003). Polyol Synthesis of Uniform Silver Nanowires: A Plausible Growth Mechanism and the Supporting Evidence. Nano Letters, 3(7), 955-960. doi:10.1021/nl034312m

39. Yang, C., Gu, H., Lin, W., Yuen, M. M., Wong, C. P., Xiong, M., & Gao, B. (2011). Silver Nanowires: From Scalable Synthesis to Recyclable Foldable Electronics. Advanced Materials, 23(27), 3052-3056. doi:10.1002/adma.201100530

40. Sun, Y., & Xia, Y. (2002). Large-Scale Synthesis of Uniform Silver Nanowires Through a Soft, Self-Seeding, Polyol Process. Advanced Materials, 14(11), 833-837. doi:10.1002/1521-4095(20020605)14:11<833::Aid-adma833>3.0.Co;2-k

41. Zhang, D., Ryu, K., Liu, X., Polikarpov, E., Ly, J., Tompson, M. E., & Zhou, C. (2006). Transparent, Conductive, and Flexible Carbon Nanotube Films and Their Application in Organic Light-Emitting Diodes. Nano Letters, 6(9), 1880-1886. doi:10.1021/nl0608543

42. Wiley, B., Sun, Y., & Xia, Y. (2005). Polyol Synthesis of Silver Nanostructures: Control of Product Morphology with Fe(II) or Fe(III) Species. Langmuir, 21(18), 8077-8080. doi:10.1021/la050887i

43. Jin, R., Cao, Y., Mirkin, C. A., Kelly, K. L., Schatz, G. C., & Zheng, J. G. (2001). Photoinduced Conversion of Silver Nanospheres to Nanoprisms. Science, 294(5548), 1901-1903. doi:10.1126/science.1066541

44. Li, X., Wang, L., & Yan, G. (2011). Review: Recent research progress on preparation of silver nanowires by soft solution method and their applications. Crystal Research and Technology, 46(5), 427-438. doi:10.1002/crat.201100023

45. Sinitskii, A., & Tour, J. M. (2010). Graphene electronics, unzipped. IEEE Spectr., 47(11), 28-33. doi:10.1109/mspec.2010.5605889

46. Bid, A., Bora, A., & Raychaudhuri, A. K. (2006).Temperature dependence of the resistance of metallic nanowires of diameter $\ensuremath {\geqslant}15

\phantom{\rule{0.3em}{0ex}}\mathrm{nm}$: Applicability of Bloch-Gr\"uneisen theorem. Physical Review B, 74(3), 035426. doi:10.1103/PhysRevB.74.035426

47. Scardaci, V., Coull, R., Lyons, P. E., Rickard, D., & Coleman, J. N. (2011). Spray Deposition of Highly Transparent, Low-Resistance Networks of Silver Nanowires over Large Areas. Small, 7(18), 2621-2628. doi:10.1002/smll.201100647

48. Araki, T., Jiu, J., Nogi, M., Koga, H., Nagao, S., Sugahara, T., & Suganuma, K. (2014). Low haze transparent electrodes and highly conducting air dried films with ultra-long silver nanowires synthesized by one-step polyol method. Nano Research, 7(2), 236-245. doi:10.1007/s12274-013-0391-x

49. Nirmalraj, P. N., Bellew, A. T., Bell, A. P., Fairfield, J. A., McCarthy, E. K., O'Kelly, C., . . . Boland, J. J. (2012). Manipulating Connectivity and Electrical Conductivity in Metallic Nanowire Networks. Nano Letters, 12(11), 5966-5971. doi:10.1021/nl303416h

50. Bellew, A. T., Manning, H. G., Gomes da Rocha, C., Ferreira, M. S., & Boland, J. J. (2015). Resistance of Single Ag Nanowire Junctions and Their Role in the Conductivity of Nanowire Networks. ACS Nano, 9(11), 11422-11429. doi:10.1021/acsnano.5b05469

51. Nian, Q., Saei, M., Xu, Y., Sabyasachi, G., Deng, B., Chen, Y. P., & Cheng, G. J. (2015). Crystalline Nanojoining Silver Nanowire Percolated Networks on Flexible Substrate. ACS Nano, 9(10), 10018-10031. doi:10.1021/acsnano.5b03601

52. Lagrange, M., Langley, D. P., Giusti, G., Jiménez, C., Bréchet, Y., & Bellet, D. (2015). Optimization of silver nanowire-based transparent electrodes: effects of density, size and thermal annealing. Nanoscale, 7(41), 17410-17423. doi:10.1039/C5NR04084A

53. Coskun, S., Selen Ates, E., & Emrah Unalan, H. (2013). Optimization of silver nanowire networks for polymer light emitting diode electrodes. Nanotechnology, 24(12), 125202. doi:10.1088/0957-4484/24/12/125202.

54. Zhan, K., Su, R., Bai, S., Yu, Z., Cheng, N., Wang, C.,Zhao, X.-Z. (2016). One-pot stirring-free synthesis of silver nanowires with tunable lengths and diameters via a Fe3+ & Cl− co-mediated polyol method and their application as transparent conductive films. Nanoscale, 8(42), 18121-18133. doi:10.1039/C6NR04972A

55. Lee, J., Lee, P., Lee, H., Lee, D., Lee, S. S., & Ko, S. H. (2012). Very long Ag nanowire synthesis and its application in a highly transparent, conductive and flexible metal electrode touch panel. Nanoscale, 4(20), 6408-6414. doi:10.1039/C2NR31254A

56. Miller, M. S., O'Kane, J. C., Niec, A., Carmichael, R. S., & Carmichael, T. B. (2013). Silver Nanowire/Optical Adhesive Coatings as Transparent Electrodes for Flexible Electronics. ACS Applied Materials & Interfaces, 5(20), 10165-10172. doi:10.1021/am402847y

57. Lee, H., Lee, D., Ahn, Y., Lee, E.-W., Park, L. S., & Lee, Y. (2014). Highly efficient and low voltage silver nanowire-based OLEDs employing a n-type hole injection layer. Nanoscale, 6(15), 8565-8570. doi:10.1039/C4NR01768D.

58. Liang, J., Li, L., Tong, K., Ren, Z., Hu, W., Niu, X.,Pei, Q. (2014). Silver Nanowire Percolation Network Soldered with Graphene Oxide at Room Temperature and Its Application for Fully Stretchable Polymer Light-Emitting Diodes. ACS Nano, 8(2), 1590-1600. doi:10.1021/nn405887k

59. Yang, C., Gu, H., Lin, W., Yuen, M. M., Wong, C. P., Xiong, M., & Gao, B. (2011). Silver Nanowires: From Scalable Synthesis to Recyclable Foldable Electronics. Advanced Materials, 23(27), 3052-3056. doi:10.1002/adma.201100530

60. Komoda, N., Nogi, M., Suganuma, K., Kohno, K., Akiyama, Y., & Otsuka, K. (2012). Printed silver nanowire antennas with low signal loss at high-frequency radio. Nanoscale, 4(10), 3148-3153. doi:10.1039/C2NR30485F

61. Andrés, L.J., Menéndez, M.F., Gomez, D., Martínez, A.L., Bristow, N.D., Kettle, J.P., Menéndez, A.M., & Ruiz, B. (2015). Rapid synthesis of ultra-long silver nanowires for tailor-made transparent conductive electrodes: proof of concept in organic solar cells. Nanotechnology, 26 26, 265201 .

62. Guo, F., Li, N., Radmilović, V. V., Radmilović, V. R., Turbiez, M., Spiecker, E., . . . Brabec, C. J. (2015). Fully printed organic tandem solar cells using solution-processed silver nanowires and opaque silver as charge collecting electrodes. Energy & Environmental Science, 8(6), 1690-1697. doi:10.1039/C5EE00184

63. Fried, A., XiaoHui, Z., Abrahamson, J., Chao, W., Jiping, L., Monson, R., . . . Tseng-Lung, C. (2015, 27-30 July 2015). Latest advances in silver nanowire based touch module reliability. Paper presented at the 2015 IEEE 15th International Conference on Nanotechnology (IEEE-NANO).

64. Li, J., Liang, J., Li, L., Ren, F., Hu, W., Li, J. Pei, Q. (2014). Healable Capacitive Touch Screen Sensors Based on Transparent Composite Electrodes Comprising Silver Nanowires and a Furan/Maleimide Diels–Alder Cycloaddition Polymer. ACS Nano, 8(12), 12874-12882. doi:10.1021/nn506610p

65. Yu, Y.-H., Ma, C.-C. M., Teng, C.-C., Huang, Y.-L., Lee, S.-H., Wang, I., & Wei, M.-H. (2012). Electrical, morphological, and electromagnetic interference shielding properties of silver nanowires and nanoparticles conductive composites. Materials Chemistry and Physics, 136(2), 334-340. doi:https://doi.org/10.1016/j.matchemphys.2012.05.024

66. Khaligh, H. H., & Goldthorpe, I. A. (2013). Failure of silver nanowire transparent electrodes under current flow. Nanoscale Research Letters, 8(1), 235. doi:10.1186/1556-276x-8-235

67. Li, H., Biser, J. M., Perkins, J. T., Dutta, S., Vinci, R. P., & Chan, H. M. (2008). Thermal stability of Cu nanowires on a sapphire substrate. Journal of Applied Physics, 103(2), 024315. doi:10.1063/1.2837053

68. Bellet, D., Lagrange, M., Sannicolo, T., Aghazadehchors, S., Nguyen, V. H., Langley, D. P., Muñoz-Rojas, D., Jiménez, C., Bréchet, Y., … Nguyen, N. D. (2017). Transparent Electrodes Based on Silver Nanowire Networks: From Physical Considerations towards Device Integration. Materials (Basel, Switzerland), 10(6), 570. doi:10.3390/ma10060570

69. Jiu, J., Wang, J., Sugahara, T., Nagao, S., Nogi, M., Koga, H., . . . Uchida, H. (2015). The effect of light and humidity on the stability of silver nanowire transparent electrodes. RSC Advances, 5(35), 27657-27664. doi:10.1039/C5RA02722E.

70. Lee, P., Ham, J., Lee, J., Hong, S., Han, S., Suh, Y. D., . . . Ko, S. H. (2014). Highly Stretchable or Transparent Conductor Fabrication by a Hierarchical Multiscale Hybrid Nanocomposite. Advanced Functional Materials, 24(36), 5671-5678. doi:10.1002/adfm.201400972

71. Göbelt, M., Keding, R., Schmitt, S. W., Hoffmann, B., Jäckle, S., Latzel, M., . . . Christiansen, S. (2015). Encapsulation of silver nanowire networks by atomic layer deposition for indium-free transparent electrodes. Nano Energy, 16, 196-206. doi:https://doi.org/10.1016/j.nanoen.2015.06.027

72. Bonizzoni, G., & Vassallo, E. (2002). Plasma physics and technology; industrial applications. Vacuum, 64(3), 327-336. doi:https://doi.org/10.1016/S0042-207X(01)00341-4.

73. Ohls, K., & Bogdain, B. (2016). History of inductively coupled plasma atomic emission spectral analysis: from the beginning up to its coupling with mass spectrometry. Journal of Analytical Atomic Spectrometry, 31(1), 22-31. doi:10.1039/C5JA90043C

74. Nokhandani, A.M., Otaghsara, S.M., Abolfazli, M.K., Masoumeh, Karimi, Z., Adel, F., Babapour, H., & Atae, G. (2015). A Review of New Method of Cold Plasma in Cancer Treatment.

75. Meyyappan, M. (2011). Plasma nanotechnology: past, present and future. Journal of Physics D: Applied Physics, 44(17), 174002. doi:10.1088/0022-3727/44/17/174002

76. Vourdas, N., Kontziampasis, D., Kokkoris, G., Constantoudis, V., Goodyear, A., Tserepi, A.Gogolides, E. (2010). Plasma directed assembly and organization: bottom-up nanopatterning using top-down technology. Nanotechnology, 21(8), 085302. doi:10.1088/0957-4484/21/8/085302

77. Arabi, M., Ghaedi, M., Ostovan, A., Tashkhourian, J., & Asadallahzadeh, H. (2016). Synthesis and application of molecularly imprinted nanoparticles combined ultrasonic assisted for highly selective solid phase extraction trace amount of celecoxib from human plasma samples using design expert (DXB) software. Ultrasonics Sonochemistry, 33, 67-76. doi:https://doi.org/10.1016/j.ultsonch.2016.04.022

78. Balasubramanian, C., Godbole, V. P., Rohatgi, V. K., Das, A. K., & Bhoraskar, S. V. (2004). Synthesis of nanowires and nanoparticles of cubic aluminium nitride. Nanotechnology, 15(3), 370-373. doi:10.1088/0957-4484/15/3/024

79. Heon Lee, Sung Hoon Park, Seong-Gyu Seo, Sun-Jae Kim, Sang-Chai Kim, Young-Kwon Park and Sang-Chul Jung, "Preparation and Characterization of Copper Nanoparticles via the Liquid Phase Plasma Method", Current Nanoscience (2014) 10: 7. https://doi.org/10.2174/15734137096661311112217 41

80. Jiang, H., Manolache, S., Wong, A. C. L., & Denes, F. S. (2004). Plasma-enhanced deposition of silver nanoparticles onto polymer and metal surfaces for the generation of antimicrobial characteristics. Journal of Applied Polymer Science, 93(3), 1411-1422. doi:10.1002/app.20561.

81. Patel, J., Němcová, L., Maguire, P., Graham, W. G., & Mariotti, D. (2013). Synthesis of surfactant-free electrostatically stabilized gold nanoparticles by plasma-induced liquid chemistry. Nanotechnology, 24(24), 245604. doi:10.1088/0957-4484/24/24/245604

82. Wang, S., Huang, P., & Chen, X. (2016). Stimuli-Responsive Programmed Specific Targeting in Nanomedicine. ACS Nano, 10(3), 2991-2994. doi:10.1021/acsnano.6b00870

83. Chauhan, V. P., Popović, Z., Chen, O., Cui, J., Fukumura, D., Bawendi, M. G., & Jain, R. K. (2011). Fluorescent Nanorods and Nanospheres for Real-Time In Vivo Probing of Nanoparticle Shape-Dependent Tumor Penetration. Angewandte Chemie International Edition, 50(48), 11417-11420. doi:10.1002/anie.201104449.

84. Wang, P., Lombi, E., Zhao, F.-J., & Kopittke, P. M. (2016). Nanotechnology: A New Opportunity in Plant Sciences. Trends in Plant Science, 21(8), 699-712. doi:10.1016/j.tplants.2016.04.005.

85. Huang, Q., Yu, H., & Ru, Q. (2010). Bioavailability and Delivery of Nutraceuticals Using Nanotechnology. Journal of Food Science, 75(1), R50-R57. doi:10.1111/j.1750-3841.2009.01457.x

86. Krishen, K. (2008). New technology innovations with potential for space applications. Acta Astronautica, 63(1), 324-333. doi:https://doi.org/10.1016/j.actaastro.2007.12.047.

87. Ostrikov, K. (2011). Control of energy and matter at nanoscales: challenges and opportunities for plasma nanoscience in a sustainability age. Journal of Physics D: Applied Physics, 44(17), 174003. doi:10.1088/0022-3727/44/17/174003

88. Gao, W. (2015). Graphene oxide: Reduction recipes, spectroscopy, and applications. 10.1007/978-3-319-15500-5

89. Alam, S., Sharma, N., & Kumar, L. (2017). Synthesis of Graphene Oxide (GO) by Modified Hummers Method and Its Thermal Reduction to Obtain Reduced Graphene Oxide (rGO) *.

90. Chen, D., Feng, H., & Li, J. (2012). Graphene Oxide: Preparation, Functionalization, and Electrochemical Applications. Chemical Reviews, 112(11), 6027-6053. doi:10.1021/cr300115g

91. S. C. Ray (Ed.). (2015).Applications of Graphene and Graphene-Oxide Based Nanomaterials (pp. i-iii). Oxford: William Andrew Publishing.

92. Zhao, H., Fan, S., Chen, Y., Feng, Z., Zhang, H., Pang, W., . . . Zhang, M. (2017). Oxygen Plasma-Treated Graphene Oxide Surface Functionalization for Sensitivity Enhancement of Thin-Film Piezoelectric Acoustic Gas Sensors. ACS Applied Materials & Interfaces, 9(46), 40774-40781. doi:10.1021/acsami.7b09547

93. Muhammad Hafiz, S., Ritikos, R., Whitcher, T. J., Md. Razib, N., Bien, D. C. S., Chanlek, N., . . . Rahman, S. A. (2014). A practical carbon dioxide gas sensor using room-temperature hydrogen plasma reduced graphene oxide. Sensors and Actuators B: Chemical, 193, 692-700. doi:https://doi.org/10.1016/j.snb.2013.12.017

94. Yu, Y.-Y., Kang, B. H., Lee, Y. D., Lee, S. B., & Ju, B.-K. (2013). Effect of fluorine plasma treatment with chemically reduced graphene oxide thin films as hole transport layer in organic solar cells. Applied Surface Science, 287, 91-96. doi:https://doi.org/10.1016/j.apsusc.2013.09.078

95. Chae, M.-S., Kim, J., Jeong, D., Kim, Y., Roh, J. H., Lee, S. M., . . . Hwang, K. S. (2017). Enhancing surface functionality of reduced graphene oxide biosensors by oxygen plasma treatment for Alzheimer's disease diagnosis. Biosensors and Bioelectronics, 92, 610-617. doi:https://doi.org/10.1016/j.bios.2016.10.049

96. Wang, Y., Shao, Y., Matson, D. W., Li, J., & Lin, Y. (2010). Nitrogen-Doped Graphene and Its Application in Electrochemical Biosensing. ACS Nano, 4(4), 1790-1798. doi:10.1021/nn100315s

97. Ke, Z., Ma, Y., Zhu, Z., Zhao, H., Wang, Q., & Huang, Q. (2018). Non-thermal hydrogen plasma processing effectively increases the antibacterial activity of graphene oxide. Applied Physics Letters, 112(1), 013701. doi:10.1063/1.5012132

98. Lee, S. W., Mattevi, C., Chhowalla, M., & Sankaran, R. M. (2012). Plasma-Assisted Reduction of Graphene Oxide at Low Temperature and Atmospheric Pressure for Flexible Conductor Applications. The Journal of Physical Chemistry Letters, 3(6), 772-777. doi:10.1021/jz300080p

99. Huang, C., Wang, Y., Lu, T., & Li, Y. (2017). Flexible Transparent Electrode of Hybrid Ag-Nanowire / Reduced-Graphene-Oxide Thin Film on PET Substrate Prepared Using H 2 / Ar Low-Damage Plasma.

100. Walton, S. G., Hernández, S. C., Boris, D. R., Petrova, T. B., & Petrov, G. M. (2017). Electron beam generated plasmas for the processing of graphene. Journal of Physics D: Applied Physics, 50(35), 354001. doi:10.1088/1361-6463/aa7d12

101. Dey, A., Chroneos, A., Braithwaite, N. S. J., Gandhiraman, R. P., & Krishnamurthy, S. (2016). Plasma engineering of graphene. Applied Physics Reviews, 3(2), 021301. doi:10.1063/1.4947188

102. Seah, C.-M., Vigolo, B., Chai, S.-P., & Mohamed, A. R. (2016). Mechanisms of graphene fabrication through plasma-induced layer-by-layer thinning. Carbon, 105, 496-509. doi:10.1016/j.carbon.2016.04.072

103. Bianco, G. V., Sacchetti, A., Ingrosso, C., Giangregorio, M. M., Losurdo, M., Capezzuto, P., & Bruno, G. (2018). Engineering graphene properties by modulated plasma treatments. Carbon, 129, 869-877. doi:https://doi.org/10.1016/j.carbon.2017.11.015

104. Childres, I., Jauregui, L. A., Tian, J., & Chen, Y. P. (2011). Effect of oxygen plasma etching on graphene studied using Raman spectroscopy and electronic transport measurements. New Journal of Physics, 13(2), 025008. doi:10.1088/1367-2630/13/2/025008

105. Rao, F., Li, W., & Dong, L. (2011, 15-18 Aug. 2011). Layer engineering of graphene with oxygen plasma etching. Paper presented at the 2011 11th IEEE International Conference on Nanotechnology.

106. Kondratowicz, I., Nadolska, M., Şahin, S., Łapiński, M., Prześniak-Welenc, M., Sawczak, M., . . . Żelechowska, K. (2018). Tailoring properties of reduced graphene oxide by oxygen plasma treatment. Applied Surface Science, 440, 651-659. doi:https://doi.org/10.1016/j.apsusc.2018.01.168

107. Cheng, H.-E., Wang, Y.-Y., Wu, P.-C., & Huang, C.-H. (2016). Preparation of large-area graphene oxide sheets with a high density of carboxyl groups using O2/H2 low-damage plasma. Surface and Coatings Technology, 303, 170-175. doi:https://doi.org/10.1016/j.surfcoat.2016.03.028

108. Huang, C.-H., Su, C.-Y., Lai, C.-S., Li, Y.-C., & Samukawa, S. (2014). Ultra-low-damage radical treatment for the highly controllable oxidation of large-scale graphene sheets. Carbon, 73, 244-251. doi:https://doi.org/10.1016/j.carbon.2014.02.060

109. Ostovari, F., Abdi, Y., & Ghasemi, F. (2012). Controllable formation of graphene and graphene oxide sheets using photo-catalytic reduction and oxygen plasma treatment. Eur. Phys. J. Appl. Phys., 60(3), 30401.

110. Choi, K., Lim, J., Rani, J. R., Yoon, H. S., Oh, J., Hong, T., . . . Kim, J. H. (2013). Terahertz and optical study of monolayer graphene processed by plasma oxidation. Applied Physics Letters, 102(13), 131901. doi:10.1063/1.4795526

111. Lee BJ, Jeong GH. Plasma oxidation of thermally grown graphenes and their characterization. Vacuum. 2013;87:200e204. DOI: 10.1016/j.vacuum.2012.02.02

112. Felten, A., Eckmann, A., Pireaux, J. J., Krupke, R., & Casiraghi, C. (2013). Controlled modification of mono- and bilayer graphene in O_2, H_2 and CF_4 plasmas. Nanotechnology, 24(35), 355705. doi:10.1088/0957-4484/24/35/355705

113. Nolan, H., Kumar, N.A., Rezvani, M.E., Hallam, T., & Duesberg, G.S. (2013). Functionalisation of Graphene Surfaces with Downstream Plasma Treatments. Carbon, 2013;54:283-290. DOI: 10.1016/j.carbon.2012.11.04

114. Lim, W. S., Kim, Y. Y., Kim, H., Jang, S., Kwon, N., Park, B. J., . . . Yeom, G. Y. (2012). Atomic layer etching of graphene for full graphene device fabrication. Carbon, 50(2), 429-435. doi:https://doi.org/10.1016/j.carbon.2011.08.058

115. Santoso, I., Singh, R. S., Gogoi, P. K., Asmara, T. C., Wei, D., Chen, W., . . . Rusydi, A. (2014). Tunable optical absorption and interactions in graphene via oxygen plasma. Physical Review B, 89(7), 075134. doi:10.1103/PhysRevB.89.075134

116. Kim, J. H., Ko, E., Hwang, J., Pham, X.-H., Lee, J. H., Lee, S. H., . . . Seong, G. H. (2015). Large-Scale Plasma Patterning of Transparent Graphene Electrode on Flexible Substrates. Langmuir, 31(9), 2914-2921. doi:10.1021/la504443a

117. Kim, M. J., Jeong, Y., Sohn, S., Lee, S. Y., Kim, Y. J., Lee, K., . . . Jang, J.-H. (2013). Fast and low-temperature reduction of graphene oxide films using ammonia plasma. AIP Advances, 3(1), 012117. doi:10.1063/1.4789545

118. Kim, H. T., Kim, C.-d., & Park, C. (2014). Reduction and nitridation of graphene oxide (GO) films at room temperature using inductively coupled NH_3 plasma. Vacuum, 108, 35-38. doi:https://doi.org/10.1016/j.vacuum.2014.05.018 48. Kim MJ, Jeong Y, Sohn SH, Lee SY, Kim YJ, Lee K, Kahng YH, Jang JH. Fast and low temperature reduction of graphene oxide films using ammonia plasma. AIP Advances. 2013;3:012117. DOI: 10.1063/1.4789545

119. Lee, S.-Y., Kim, C., & Kim, H. T. (2015). Difference in chemical reactions in bulk plasma and sheath regions during surface modification of graphene oxide film using

capacitively coupled NH_3 plasma. Journal of Applied Physics, 118(10), 103303. doi:10.1063/1.4930044

120. Lavanya, J., Gomathi, N., & Neogi, S. (2014). Electrochemical performance of nitrogen and oxygen radio-frequency plasma induced functional groups on tri-layered reduced graphene oxide. Materials Research Express, 1(2), 025604. doi:10.1088/2053-1591/1/2/025604

121. Kumar, N. A., Nolan, H., McEvoy, N., Rezvani, E., Doyle, R. L., Lyons, M. E. G., & Duesberg, G. S. (2013). Plasma-assisted simultaneous reduction and nitrogen doping of graphene oxide nanosheets. Journal of Materials Chemistry A, 1(14), 4431-4435. doi:10.1039/C3TA10337D

122. Mohai, M., & Bertóti, I. (2016). Modification of graphene-oxide surface in nitrogen and argon glow discharge plasma. Surface and Interface Analysis, 48(7), 461-464. doi:10.1002/sia.5929

123. Neustroev, E. P., Burtseva, E. K., Soloviev, B. D., Prokopiev, A. R., Popov, V. I., & Timofeev, V. B. (2018). Modification of graphene oxide films by radiofrequency N_2 plasma. Nanotechnology, 29(14), 144002. doi:10.1088/1361-6528/aaabe3

124. Gokus, T., Nair, R. R., Bonetti, A., Böhmler, M., Lombardo, A., Novoselov, K. S., . . . Hartschuh, A. (2009). Making Graphene Luminescent by Oxygen Plasma Treatment. ACS Nano, 3(12), 3963-3968. doi:10.1021/nn9012753

125. Usachov, D., Vilkov, O., Grüneis, A., Haberer, D., Fedorov, A., Adamchuk, V. K., . . . Vyalikh, D. V. (2011). Nitrogen-Doped Graphene: Efficient Growth, Structure, and Electronic Properties. Nano Letters, 11(12), 5401-5407. doi:10.1021/nl2031037

126. Rybin, M., Pereyaslavtsev, A., Vasilieva, T., Myasnikov, V., Sokolov, I., Pavlova, A., . . . Obraztsova, E. (2016). Efficient nitrogen doping of graphene by plasma treatment. Carbon, 96, 196-202. doi:https://doi.org/10.1016/j.carbon.2015.09.056

127. Shao, Y., Zhang, S., Engelhard, M. H., Li, G., Shao, G., Wang, Y., . . . Lin, Y. (2010). Nitrogen-doped graphene and its electrochemical applications. Journal of Materials Chemistry, 20(35), 7491-7496. doi:10.1039/C0JM00782J

128. Tao, H., Yan, C., Robertson, A. W., Gao, Y., Ding, J., Zhang, Y., . . . Sun, Z. (2017). N-Doping of graphene oxide at low temperature for the oxygen reduction reaction. Chemical Communications, 53(5), 873-876. doi:10.1039/C6CC08776K

129. Schutze, A., Jeong, J. Y., Babayan, S. E., Jaeyoung, P., Selwyn, G. S., & Hicks, R. F. (1998). The atmospheric-pressure plasma jet: a review and comparison to other plasma sources. IEEE Transactions on Plasma Science, 26(6), 1685-1694. doi:10.1109/27.747887

130. Mariotti, D., Belmonte, T., Benedikt, J., Velusamy, T., Jain, G., & Švrček, V. (2016). Low-Temperature Atmospheric Pressure Plasma Processes for “Green” Third Generation Photovoltaics. Plasma Processes and Polymers, 13(1), 70-90. doi:10.1002/ppap.201500187

131. Surowsky, B., Schlüter, O., & Knorr, D. (2014). Interactions of Non-Thermal Atmospheric Pressure Plasma with Solid and Liquid Food Systems: A Review. Food Engineering Reviews, 7(2), 82-108.

132. Foest, R., Kindel, E., Ohl, A., Stieber, M., & Weltmann, K. D. (2005). Non-thermal atmospheric pressure discharges for surface modification. Plasma Physics and Controlled Fusion, 47(12B), B525-B536. doi:10.1088/0741-3335/47/12b/s38

133. Kelly-Wintenberg, K., Sherman, D. M., Tsai, P. P., Gadri, R. B., Karakaya, F., Zhiyu, C., . . . Montie, T. C. (2000). Air filter sterilization using a one atmosphere uniform glow discharge plasma (the volfilter). IEEE Transactions on Plasma Science, 28(1), 64-71. doi:10.1109/27.842866

134. Kramer, N. J., Aydil, E. S., & Kortshagen, U. R. (2015). Requirements for plasma synthesis of nanocrystals at atmospheric pressures. Journal of Physics D: Applied Physics, 48(3), 035205. doi:10.1088/0022-3727/48/3/035205

135. Barwe, B., Riedel, F., Cibulka, O. E., Pelant, I., & Benedikt, J. (2015). Silicon nanoparticle formation depending on the discharge conditions of an atmospheric radio-frequency driven microplasma with argon/silane/hydrogen gases. Journal of Physics D: Applied Physics, 48(31), 314001. doi:10.1088/0022-3727/48/31/314001

136. Bose, A. C., Shimizu, Y., Mariotti, D., Sasaki, T., Terashima, K., & Koshizaki, N. (2006). Flow rate effect on the structure and morphology of molybdenum oxide nanoparticles deposited by atmospheric-pressure microplasma processing. Nanotechnology, 17(24), 5976-5982. doi:10.1088/0957-4484/17/24/012

137. Wang, C., & Chen, J.-Z. (2015). Atmospheric-pressure-plasma-jet sintered nanoporous SnO_2. Ceramics International, 41(4), 5478-5483. doi:https://doi.org/10.1016/j.ceramint.2014.12.118

138. Jang, J., Park, D.-Y., Hong, K.-H., Song, S., Kim, K., Eo, Y.-J., . . . Chung, C.-H. (2018). Improvement of Contact Resistance Between Each Silver Nanowire and Thermal Stability of Silver Nanowire Transparent Electrodes by Electrodeposition. Nanoscience and Nanotechnology Letters, 10(4), 528-532. doi:10.1166/nnl.2018.2671

139. Singh, R. K., Kumar, R., & Singh, D. P. (2016). Graphene oxide: strategies for synthesis, reduction and frontier applications. RSC Advances, 6(69), 64993-65011. doi:10.1039/C6RA07626B

140. Hwang, B., An, Y., Lee, H., Lee, E., Becker, S., Kim, Y.-H., & Kim, H. (2017). Highly Flexible and Transparent Ag Nanowire Electrode Encapsulated with Ultra-Thin Al2O3: Thermal, Ambient, and Mechanical Stabilities. Scientific Reports, 7, 41336. doi:10.1038/srep41336

Blank Page

Chapter 3

Atmospheric plasma for engineering graphene films

Statement of Authorship

Title of Paper	Scanning atmospheric plasma for ultrafast reduction of graphene oxide and fabrication of highly conductive graphene films and patterns
Publication Status	☑ Published ☐ Accepted for Publication ☐ Submitted for Publication ☐ Unpublished and Unsubmitted work written in manuscript style
Publication Details	Carbon 127 (2018) 113-121

Principal Author

Name of Principal Author (Candidate)	
Contribution to the Paper	Under the supervison of Prof Dusan Losic developed ,designed and conducted the experiments , interpreted ,processed the data ,wrote manuscript draf and revised for submission
Overall percentage (%)	75%
Certification:	This paper reports on original research I conducted during the period of my Higher Degree by Research candidature and is not subject to any obligations or contractual agreements with a third party that would constrain its inclusion in this thesis. I am the primary author of this paper.
Signature	Date 05-03-2019

Co-Author Contributions

By signing the Statement of Authorship, each author certifies that:

I. the candidate's stated contribution to the publication is accurate (as detailed above);
II. permission is granted for the candidate to include the publication in the thesis; and
III. the sum of all co-author contributions is equal to 100% less the candidate's stated contribution.

Name of Co-Author	Tran Thanh Tung
Contribution to the Paper	CO-supervise and edited the manuscript and aided in developement of the exploerment
Signature	Date 5/3/2019

Name of Co-Author	Md J. Nine
Contribution to the Paper	edited the manuscript and analyse some data .
Signature	Date 05-03-2019

Please cut and paste additional co-author panels here as required.

Name of Co-Author	Mahmoud Moussa		
Contribution to the Paper	Help runing the electrochemical measurements and edited the manuscript ere		
Signature		Date	05/03/2019

Name of Co-Author	Shervin Kabiri		
Contribution to the Paper	Help running raman spectroscopy and edited the manuscript		
Signature		Date	05-03-2019

Name of Co-Author	Diana N.H. Tran		
Contribution to the Paper	Edited the manuscript		
Signature		Date	05/03/2019

Name of Co-Author	Dusan Losic		
Contribution to the Paper	Act as the primary supervisor ,aided in design and developement of the expierment and evaluation and edited the mansucript for submission .		
Signature		Date	

Carbon 127 (2018) 113–121

Contents lists available at ScienceDirect

Carbon

journal homepage: www.elsevier.com/locate/carbon

Scanning atmospheric plasma for ultrafast reduction of graphene oxide and fabrication of highly conductive graphene films and patterns

Faisal Alotaibi [a, b], Tran T. Tung [a, b], Md J. Nine [a, b], Shervin Kabiri [a, b], Mahmoud Moussa [a, b], Diana N.H. Tran [a, b], Dusan Losic [a, b, *]

[a] School of Chemical Engineering, The University of Adelaide, Adelaide, SA, 5005, Australia
[b] ARC Research Hub for Graphene Enabled Industry Transformation, The University of Adelaide, Adelaide, SA, 5005, Australia

ARTICLE INFO

Article history:
Received 6 August 2017
Received in revised form
7 October 2017
Accepted 23 October 2017
Available online 27 October 2017

Keywords:
Plasma
Air-plasma
Graphene film
Conductive film
Reduction of graphene oxide

ABSTRACT

A new method based on scanning atmospheric plasma for an ultrafast reduction of graphene oxide (GO) and preparation of highly conductive graphene films and patterns is presented. This simple method is shown to provide a direct and scalable fabrication of graphene films on flexible and shaped substrates with a variety of patterns for broad applications. An effective and ultrafast (~60 s) reduction of GO films into highly conductive graphene films at room temperature is demonstrated by this process that is impossible to achieve by conventional wet chemical and thermal reduction process. The software controlled x-y scanning unit allows fabrication of graphene films with variety of patterns on different substrates including glass, plastic, ceramics and metals with complex shapes required for flexible and wearable electronics and devices. Characterization results confirmed that a thin transparent graphene film can be produced with a surface sheets resistance of 22 kΩ/sq at the transparency of 88%, and a thick film (~25 μm) with a sheet resistance of 186 Ω/sq. A practical application of plasma fabricated graphene films was demonstrated for a supercapacitor devices able to deliver an outstanding volumetric capacitance of 536.55 F/cm^3 at a current density of 1 A/g.

1. Introduction

Graphene oxide (GO) produced by exfoliation of chemically oxidized graphite has been used as a precursor for synthesis of reduced GO or graphene in different forms (platelets, powders, films, fibers, and aerogels) for broad applications including environmental adsorbents, membranes, protective coatings, composite materials, electrodes for batteries, supercapacitors and sensing devices [1–4]. Due to chemical oxidation process of graphite, GO is decorated with abundant oxygen-containing functional groups (hydroxyl, epoxy, ketone and carboxyl groups) either on the basal plane or at the edges with a mixture of sp^2-and sp^3-hybridized carbon atoms that make GO electrically insulating and mechanically weak material [5–7]. The conversion of GO to graphene structure by de-oxidation and removal of these oxygen groups with the restoration of carbon structures provides establishing electrical conductivity, improving crystal structure and mechanical strength [7,8].

Two main approaches were used for reduction of GO to produce a reduced graphene oxide (rGO) or graphene based on wet chemical and thermal physical process. The first approach involves a strong chemical reduction using reducing agents such as hydrazine (N_2H_4), hydrofluoric acid (HF), hydroiodic acids (HI), sodium-ammonia solution [9], sodium borohydride ($NaBH_4$), and others that are usually highly toxic and the process requires very long time [7,9]. In addition, these methods need the use of dispersing agents (surfactant) that could introduce impurities and affect the performance of produced rGO for some applications. The electrical conductivity of rGO films prepared by these methods are also inferior compared with pristine graphene and additional further thermal annealing is still required. The second and more common approach is based on thermal reduction using high temperature under oxygen free and inert (H_2 or Ar) atmosphere that can reduce effectively and provide films with improved conductivity. However, high

* Corresponding author. ARC Research Hub for Graphene Enabled Industry Transformation, The University of Adelaide, Adelaide, SA, 5005, Australia.
E-mail address: dusan.losic@adelaide.edu.au (D. Losic).

https://doi.org/10.1016/j.carbon.2017.10.075
0008-6223/

Blank Page

Scanning atmospheric plasma for ultrafast reduction of graphene oxide and fabrication of highly conductive graphene films and patterns

3.1 Abstract

A new method based on scanning atmospheric jet plasma for an ultrafast reduction of graphene oxide (GO) and preparation of highly conductive graphene films and patterns is presented. This simple method is able to provide a direct and scalable preparation of a variety of graphene platforms on flexible and shaped substrates and patterns for broad applications. An effective and ultrafast (~ 60 s) reduction of GO films at near room temperature is demonstrated by converting them into highly conductive graphene films that seems impossible to achieve by conventional wet chemical and thermal reduction process. The scanning unit allows treating and patterning of a large area of GO films on different substrates including glass, plastic, ceramics and metals with complex shapes required for flexible and wearable electronics and devices. Characterization results confirmed that a thin transparent graphene film can be produced with a surface sheets resistance of 22 kΩ/sq at the transparency of 88 %, while a thick film (~25 μm) shows a sheet resistance as low as186 Ω/sq. A practical application of prepared graphene films was demonstrated with a supercapacitor device that is able to deliver a gravimetric capacitance of 134 F/g and an impressive volumetric capacitance of 536.55 F/cm^3 at a current density of 1 A/g.

3.2 Introduction

Graphene oxide (GO) produced by exfoliation of chemically oxidized graphite has been used as a basic source for synthesis of reduced GO or graphene in different forms (platelets, powders, films, fibers, and aerogels) for broad applications including environmental adsorbents, membranes, protective coatings, composite materials, electrodes for batteries and supercapacitors and sensing devices [1-4]. Due to chemical oxidation process of graphite, GO is decorated with abundant oxygen-containing functional groups (hydroxyl, epoxy, ketone and carboxyl groups) either on the basal plane or at the edges with a mixture of sp^2- and sp^3-hybridized carbon atoms that make GO electrically insulating and mechanically weak material [5-8]. The conversion of GO to graphene structure by de-oxidation and removal of these oxygen groups with the restoration of carbon structures provides establishing electrical conductivity, improving crystal structure and mechanical strength [7,8].

Two main approaches were used for reduction of GO to produce a reduced graphene oxide (rGO) product based on wet chemical and thermal physical process. The first approach involves a strong chemical reduction using reducing agents (e.g., N_2H_4, $NaBH_4$, HI, HF) that are highly toxic and the process is time consuming [7-9]. In addition, these methods usually require the use of dispersing agents (surfactant) that could introduce impurities and affect the quality of produced rGO. The electrical conductivity of rGO films prepared by these methods are also inferior and further thermal annealing is still required indicating their limited effectiveness. The second and more common approach is based on thermal reduction using high temperature under oxygen free (inert H_2 or Ar) atmosphere that can reduce effectively and provide films with improved the conductivity. However, high temperature operation of this process limits the use range of temperature sensitive substrates such as polymers and

plastics, textiles required for flexible and wearable electronics [10]. Therefore, to have scalable methods that can effectively reduce GO films and produce either thin or thick conductive graphene films in an atmospheric condition, at low temperature, using environmentally friendly conditions by fast and simple direct treatment without damaging the underlying substrate is a highly demanding for many applications.

To address these requirements and improve currently used methods for GO reduction several new strategies were explored including: green solution reduction process involving vitamin-C [11], non-aromatic amino acids [12], and dry methods using flash reduction, microwave irradiation [13], photocatalytic reduction [14], hydrothermal reduction, electrochemical reduction, laser and plasma induced reduction [15]. Among them plasma, created by electrical fields which leads to acceleration and heating of the electrons, has been recently introduced as one of a most promising method for ultrafast and scalable method for restoring graphene structure of rGO films. Several studies using plasma methods for GO reduction involving fluorine plasma [16], ammonia (NH_3) plasma [17], methane plasma [8], electron beam plasma in methane/argon mixture plasma [18], hydrogen plasma [19] and the others [20-24] have been reported. These methods are not only able to reduce GO into rGO, but also to perform chemical functionalization or doping of the graphene surface which is also desirable [8,24,25]. Nevertheless, most of these plasma techniques require high expensive and sophisticated vacuum chambers, pumping system, specific environment, and can use the only small size of samples in batch mode that limits their scalability and application for large samples and massive production of films and devices [26].

In this work to address these limitations of conventional plasma method we present a simple cold plasma approach based on atmospheric pressure plasma jets (APPJs), in which the

electrons in energy distribution are able to ionize gas-phase species and dissociate and excite the reactant gas through electro-impact collisions[27]. The atmospheric plasma provides not only high electron densities (> 10^{13} cm^{-3}) and high energetic electrons (> 20 eV), but also highly reactive gas species and radicals that react with the oxygen functional groups on GO films causing their ionization reduction and removal. This process happens over very short time (~1 min), being able to covert nonconductive thin and thick GO films into rGO films throughout all layers (not only the top surface). Moreover, by combining the plasma jet with software controlled scanning devices, we demonstrate for the first time that the application of our novel scanning plasma method for fast, scalable, controllable reduction of both thin and thick GO films on different substrates (glass, plastic and textile) with various shapes (circles, squares, lines, arrays, etc.) from micron to millimetre size patterns. The highly conductive films show promise for a broad range of applications including wearable electronics and energy storage devices.

3.3 Experimental

3.3.1 Materials:

Natural graphite rocks (Uley, Eyre Peninsula, South Australia) is supplied from a local mining site and milled into a fine powder using a bench top ring mill (Rocklabs). Potassium permanganate ($KMnO_4$, Sigma–Aldrich), 98 % sulphuric acid (H_2SO_4, Chem-Supply), phosphoric acid (H_3PO_4, Chem-Supply), 30% hydrogen peroxide (H_2O_2, Chem-Supply), 35 % hydrochloric acid (HCl, Chem-Supply) and ethanol (Chem-Supply) were used directly without further purification. High-purity milli-Q water (18.2 MΩ·cm at 25 °C, pH of 5.6).

3.3.1.1 Preparation of thin and thick GO films on different substrates

Glass substrates 2.4×2.4 cm were cleaned using piranha solution (3 sulfuric acid:1 hydrogen peroxide) for 20 minutes followed by cleaned in water for 10 minutes and then dried using low pressure air for 30 seconds. The GO dispersed into ethanol solution 0.5 mg/mL) and was then sprayed coating onto the glass substrate by a spray device (Neo For Iwata) with a diameter of 0.35mm nozzle. A flexible film was also prepared by spraying the GO dispersion onto a 5×5 cm polyethylene terephthalate (PET) substrate.

For the preparation of thick graphene films by APPJ method, GO aqueous dispersion (3 mg/mL) was casted on a glass petri dish (diameter of 50 mm), followed by low-temperature drying in a convection oven at 45 ^{o}C. A dried GO film with a thickness of 25 ± 0.5 μm peeled off from the petri dish was cut into the square shape of 20x20 mm and 50x50mm. These films were sandwiched between the two stainless steel dies with a round shape hole of 10 - 40 mm in diameter for exposing the GO sample during APPJ plasma treatment. For patterning samples, masks were needed during treatment of GO films. In parallel, GO films were also prepared for thermal annealing as a reference for the control experiment.

3.3.1.2 Atmospheric pressure plasma jet (APPJ) experiment setup for the reduction of GO films

Atmospheric plasma system (X4-800-USB from Diener Electronic GmbH + Co. KG, Germany)) which includes plasma jet device and plasma controller is combined with scanning engraving machine (software controlled) and a computer numerical control (CNC) box. The plasma device with a length of 210 mm and a nozzle diameter of 10 mm with X/Y/Z axis control can be moved over samples in both XY axis by a manual of software control. Air-plasma was operated at a high voltage power supply (300 W, 20 kHz) and a high

potential of ~10 kV was applied between anode and cathode for 1 min to generate an arc discharge of plasma. The three critical parameters to be considered for GO conversion by this process are the distances between plasma nozzle and GO films (different distances are tested and optimized to 20 mm for these experiments), scanning speed (optimized to ~ 10 mm/min), and exposure time towards plasma irradiation (explored 10, 30, 60, 90 and120 s). To compare with other methods control GO samples were thermally reduced under a temperature ranging from 150 - 250 °C in a convection oven.

3.3.2 Characterization of materials

Scanning electron microscope (SEM-FEI Quanta 450, Japan) was used to study the GO and rGO surface morphology, as well as to measure the film thickness. A high-resolution of Transmission Electron Microscope (TEM, Philips CM200, Japan) was used for imaging the exfoliated GO flakes at 200 kV. TEM sample was prepared by dispersing the GO and rGO-film in milli-Q water and ethanol, respectively with a mild sonication and then dropped onto TEM grids. Film XRD patterns were recorded by X-ray Diffraction (XRD, Rigaku-Miniflex 600, Japan) for GO, rGO pristine exfoliated graphene films at 40 kV and 15 mA in the range of 2θ = 3-70° with a scanning speed of 10°/min. Vibrational stretching mode of different oxygen functional groups in GO and rGO were studied by Fourier transform infrared spectroscopy (FTIR) (Nicolet 6700 Thermo Fisher, USA). Raman spectra were taken by using a HORIBA scientific instrument (LabRam HR800 Ev, Jobin Yvon, Horiba, France) for the GO and rGO surface coated on a microscope glass using a 50x objective and 532 nm laser (mpc 3000) as the excitation source. Thermogravimetric analysis (TGA) was carried out on a TGA Q5000 instrument with a heating rate of 5 °C min^{-1} under a nitrogen atmosphere. A

four-point-probe (Jandel, RM3000) was used for sheet resistance measurements which measured at an auto-range mode accelerating current from 50 to 10 μA.

3.3.3 Supercapacitor characterizations

The P-rGO films were cut into (1 cm x 1 cm) pieces, these two film pieces were sandwiched between two gold foils as the current collectors, and a piece of filter paper was used as a separator. All electrochemical measurements were carried out by using cyclic voltammetry (CV) and galvanostatic charge/discharge (CD) in a two-electrode cell configuration with 1.0 M H_2SO_4 as an electrolyte by a CHI 760E electrochemical workstation.

The gravimetric (C*wt*) and volumetric (C*vol*) capacitances were calculated from the charge/ discharge curves as follows:

$$Cwt = \frac{4I}{m(\frac{\Delta E}{\Delta t})} \qquad (1)$$

$$Cvol = \frac{4I}{V(\frac{\Delta E}{\Delta t})} \qquad (2)$$

where I, $(\Delta E/\Delta t)$, m and V are the applied constant current (A), the slope of the discharge curve, the total mass (g) and volume (cm^3) of the two electrodes, respectively

3.4 Results and discussion

The concept of developed method is presented in **Figure 3.1** showing the transforming of GO into rGO films by plasma beam irradiation and the real system with a CNC unit, which conducts the plasma jet scanning over a variety of GO films with and without substrates.

In the first experiment a series of GO films with different thickness were prepared by either spray coating (thin films) or casting (thick films) with a controllable mass of loaded GO from solution. These GO films were converted into rGO films by atmospheric plasma beam irradiation for 60 s by scanning process (**Figure 3.1a and b**). The visible yellowish GO film was immediately transformed into the dark colours indicating the de-oxygenation of GO and restoration of π-conjugation and producing rGO film (**Figure 3.1c**). To demonstrate the fabrication of a broad range of different flexible thick graphene films we prepared several types of samples of GO films coated on PET and glass substrates, using the scanning APPJ process for a treatment. **Figure 3.1d** shows a photo of typical flexible graphene thick film coated PET substrate that has a surface resistance of less than 1 kΩ/sq, and a photo of the its thin film with a surface resistance of few tens of kΩ/sq (transparency > 80%) is shown in **Figure 3.1e** after scanning APPJs treatment for a couple of mins. Several samples of graphene thick film with millimetre and micro size patterns on glass and PET were prepared by masking technique and controlled scanning treatment and typically showed in **Figure 3.1f and g** .

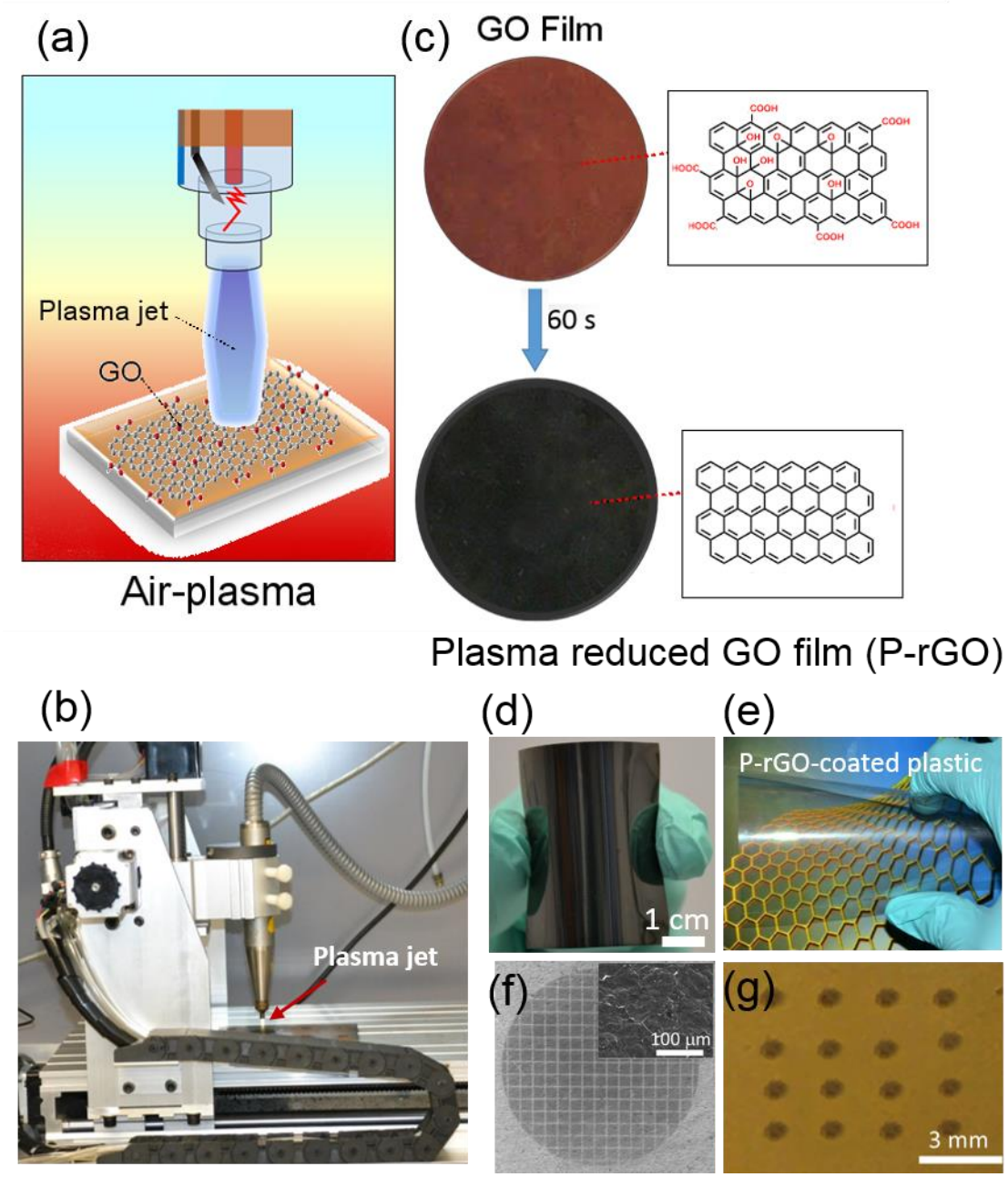

Figure 3.1. (a) Illustration of the atmospheric pressure plasma jet (APPJ) method showing plasma jet surface irradiation and reduction of GO films; (b) APPJs experiment setup for reduction of GO films, in which GO film sandwiched between stainless steel dies is exposed to the plasma beam; c) photo of circular film of GO – rGO conversion showing that a GO film (yellowish) is effectively reduced for < 1 min achieving highly conductive P-rGO film

(dark colour); photo of series examples of prepared graphene films and patterns including: (d) thick and (e) thin graphene film on the flexible substrate fabricated by scanning plasma treatment of GO coated PET film, f) square patterns of rGO after the plasma treatment, in which bright pitches are GO and dark colour represents P-rGO, g) graphene film with micro-patterns and array of graphene spots aligned over GO film matrix.

An optical image of an array of square patterns of rGO after the plasma treatment using TEM grid as a mask with the graphene feature length of single square units and pitches are 50 μm, is presented in **Figure 3.1f.** The surface of a typical square pattern contains overlapped and folded rGO sheets (inset). In the last example, an array of graphene circular spots in GO films was prepared by software controlled plasma scanning **(Figure 3.1g).** These array patterns can be used for micro reactors, cell studies and biosensing applications which are currently under explorations. These typical selected examples demonstrate the feasibility of the method for fabrication of a broad range of films with different shapes and patterns which are widely used in wearable and flexible device applications. These results showed simplicity and scalability of the method for batch and continuous fabrication of flexible graphene films for many application such as sensors, supercapacitors, electromagnetic interference shielding (EMI), antenna RFIDs, and protective coatings.

To demonstrate the capability of this method for fabrication of transparent thin graphene films, the influence of the film thickness on conductivity and transparency of graphene thin films on glass coated substrates was studied (**Figure 3.2**). It is clearly observed that an increasing of GO film thickness, the intensity of the colour is increasing from yellowish to yellow tones **(Figure 3.2a**) and bright to the dark shade which is due to increased thickness controlled by mass deposition of GO and its reduction. The sheet resistance and transmittance

of those non-conductive GO films were various values ranging from 14.4 to 10.2 MΩ and 92 % to 74 %, respectively based on the thickness dependence (**Figure 3.2b**). However, after less than 1 min of APPJs treatment, the optical transmittance of plasma reduced GO films with slightly dark colour was decreased ranging from 88 % (thinner) to 57 % (thicker film) showing the same thickness dependence observed by visual assessment. While their sheet resistances decreased more than two orders of magnitude compared with initial GO films showing a value in the range of 22 kΩ/sq (thinner) to 2 kΩ/sq (thicker film) (**Figure 3.2c**). This conductivity performance of the films is comparable with rGO films archived by traditional chemical or thermal reduction of GO films [29], or pristine graphene ink [30,31] Figure 2d shows the transparent film of GO-coated glass slide that converted into transparent conductive rGO film after plasma scanning (**Figure 3.2e**).

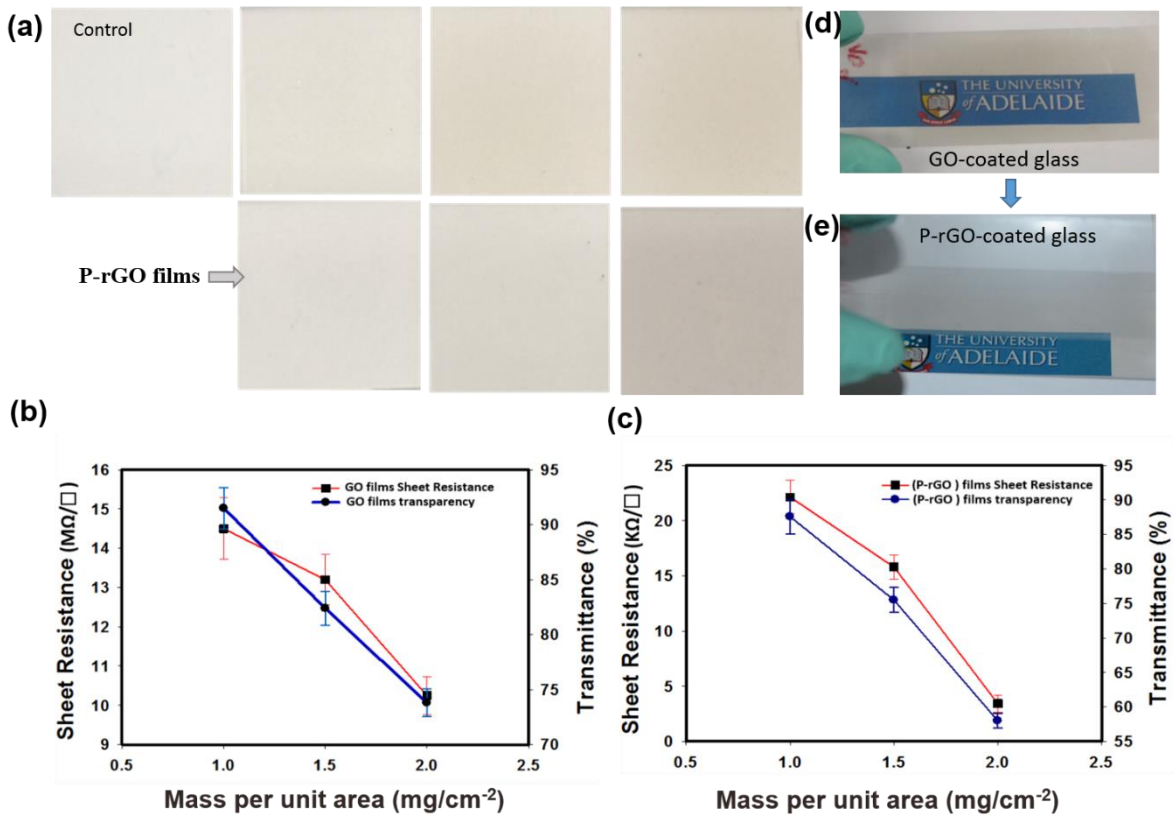

Figure 3.2. (a) Optical image of GO films produced by spray coating onto a glass substrate (top) and their reduced forms after APPJs treatment (P-rGO, bottom). (b) The sheet resistance and transmittance (at λ = 550 nm) versus amount of GO deposited onto substrate and (c) its performance (P-rGO film) after APPJs treatment. The typical optical image of GO-coated glass film (d) before and (e) after plasma treatment.

To confirm that the reduction of GO film to graphene film is performed across whole film structure not only on the top surface, a chromophore particle in aqueous dispersion behaviour was studied. A colloid system of GO (control) and P-rGO with the same concentrations (0.5 mg/mL) achieved by sonicating their powder in DI water for 20 min and then tested for dispersion stability and sedimentation effect **(Figure 3.3a)**.

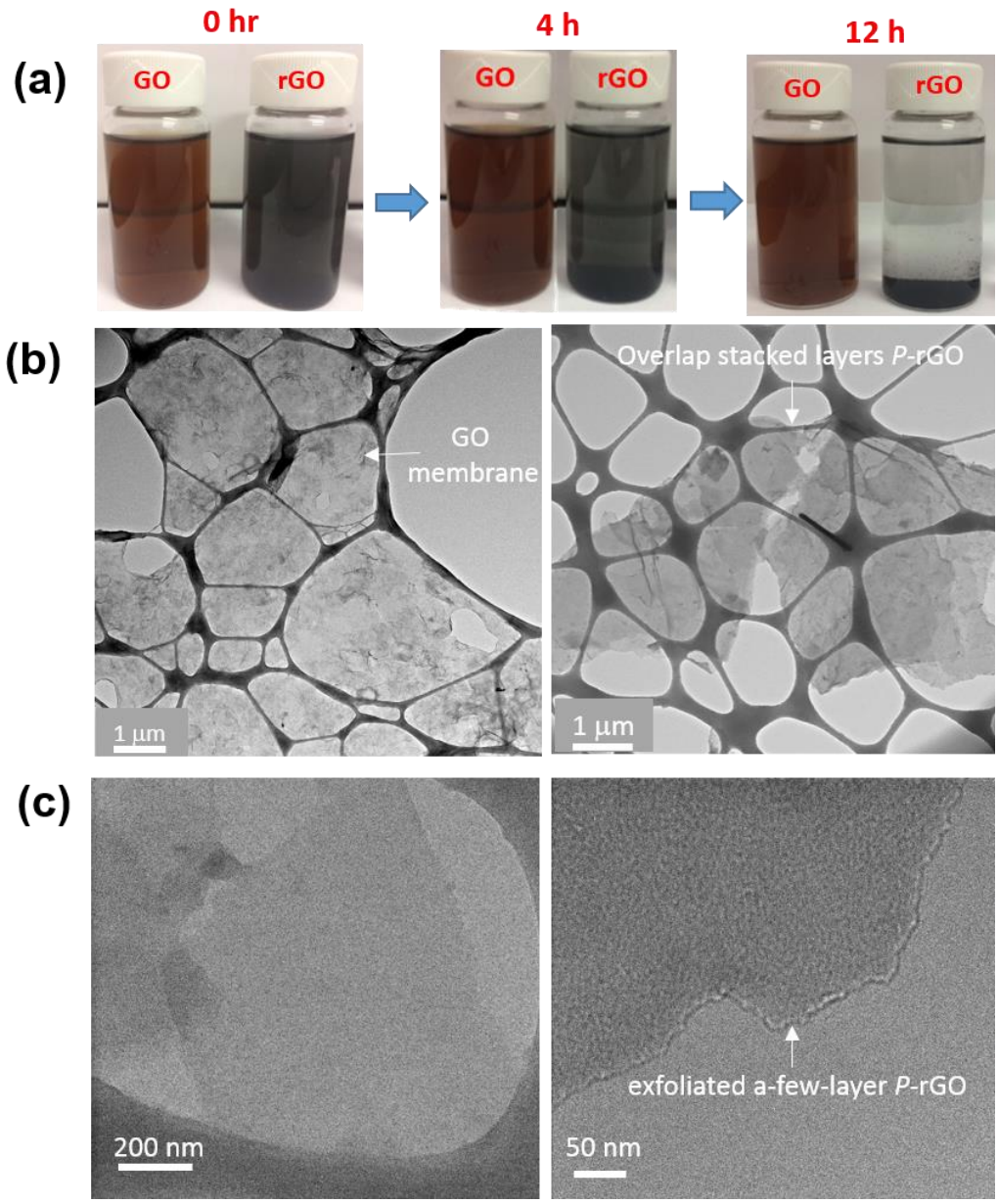

Figure 3.3. Effect of the GO reduction process on dispersion stability and structure of GO and plasma rGO particles taken from their films. (a) Photos showing dispersion and sedimentation of GO (control) and rGO (120 s plasma exposure) in aqueous solution for the different time. (b) TEM of GO particles obtained from dispersion sample after 8h of sedimentation, c) TEM of plasma treated rGO within 60 sec obtained from dispersion with low and high resolution images indicating flat and crystalline graphene structure.

This experiment shows that no treated GO dispersion was very stable with negligible change over 12 hours, as expected, due to hydrophilic and strong repulsion force between negatively charged GO sheets. Whereas, plasma treated P-rGO dispersion exhibits a temporary stability and starts settling down after about 4 h with a complete sedimentation after 12 h. This result indicates that GO film has been successfully reduced to graphene with removal of oxygen functional groups and significantly increased hydrophobicity of materials and that process is occurred in the bulk of the film not only on the top surface. The supernatant of both GO and P-rGO after 8h of sedimentation time was characterized by TEM imaging and presented in **Figure 3.3b and c.** A presentative TEM image of GO membrane contained a number of stacked layers over large scale (e.g., a continuous lateral size of at least ten μm) with winked, folded surface morphology. While a low magnification TEM image of the P-rGO film shows overlapping pices of rGO structures with reduced lateral size within several micrometres as shown in **Figure 3.3b**. The higher magnification TEM images of P-rGO (**Figure 3.3c**) indicate their flat structure with few-layer graphene sheets. This behaviour is unlikely to see in the chemical or thermal reduction of GO usually resulted in winked and folded rGO sheets. The reason for observing flatter and less wrinkled morphology can be explained by the plasma sheath (at the boudary between the plasma and the GO film) contained ionize species and excited reactant gases irradiation induced a different mechanism of a reduction process under the mechanical bombardment of plasma beam.

To further characterize structural changes after plasma treatment comparative SEM images from the top surface and cross-section of the non-treated area (GO) films before and after plasma treated area (P-rGO) are taken and presented in **Figure 3.4.** These images showed distinctive morphological differences between GO and plasma reduced GO. While the top of

GO film shows a micro rough surface with wrinkled GO sheets **(Figure 3.4a-b)**, plasma obtained rGO film is very smooth with fattened surface indicating the reducing of defects og reduced GO sheets (**Figure 3.4c**). This result is in agreement with the pervious report by Kim et al. showed the reduction of surface roughness of GO films with the exposure of NH_3-plasma (H. T. Kim et al., 2014).

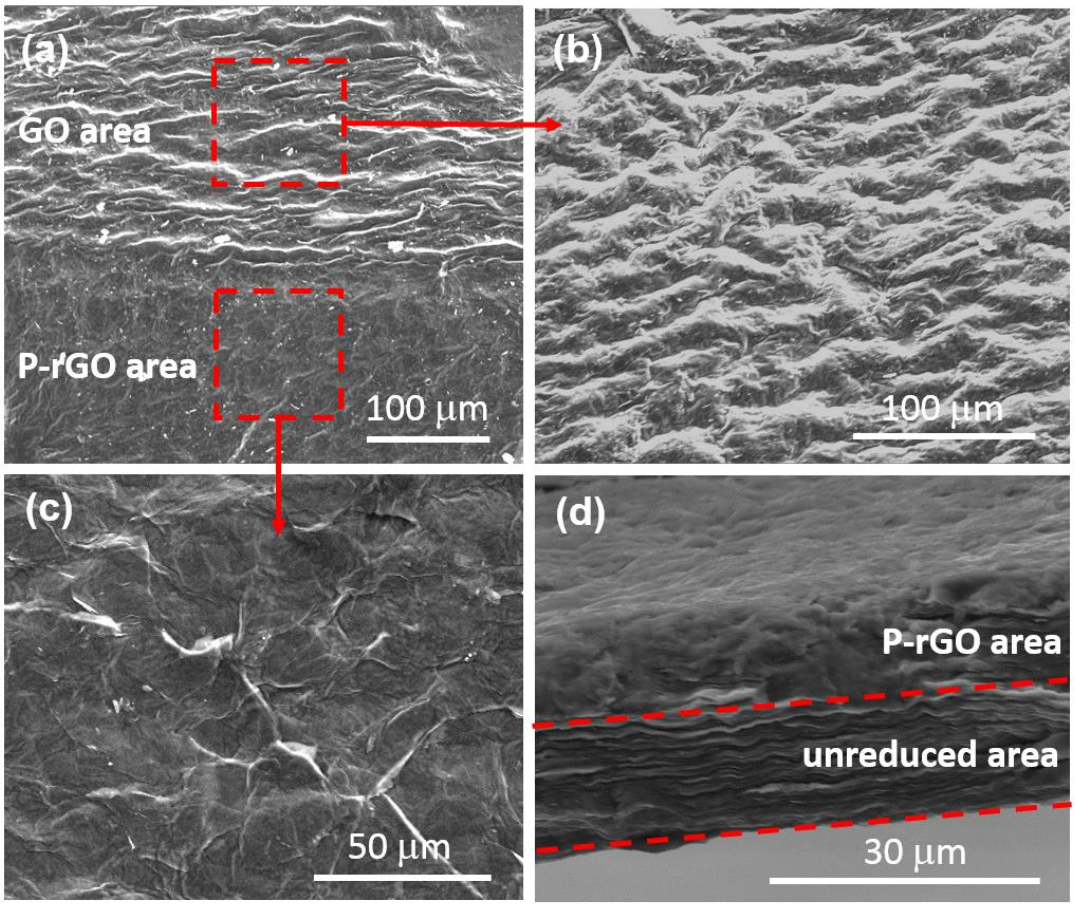

Figure 3.4. (a) Surface morphology of untreated GO film (masked) showing the wrinkled and rough area of non-reduced section (on the top) and plasma rGO film with treated area (on the bottom) showing a flat and reduced section, (b) magnified SEM image of untreated GO film shows wavy and wrinkled surface of GO, (c) higher resolution SEM image of plasma reduced area with interconnected linked rGO sheets and flat topography, (d) cross-sectional

SEM image of plasma treated GO film showing the top surface with reduced GO layer and less affected area at the bottom of cross-section (20 s exposure to plasma).

It is worth noting that this GO reduction process can be performed selectively on the top of the GO film by using masks, but also vertically across the GO layers by controlling exposure time and the distance between plasma jet and sample's surface. When shorter plasma exposure time is performed it was shown from the cross-sectional SEM imaging (**Figure 3.4d**) that only the top GO surface can be selectively converted to rGO without of changes of GO layers inside the film. With longer plasma expose time it was shown that the compactness of the layered rGO film increased, that confirms it is possible to achieve the dipper impact throughout the GO layers inside the film.

The characterization of chemical composition before and after removal of oxygen functional groups of the GO films by plasma process compared with thermal were studied using FTIR with results summarized in **Figure 3.5**. The typical characteristic FTIR peaks of GO-film are observed with the presence of O-H stretching vibrations at 3000-3500 cm^{-1} (broad), the vibration of C=O in carbonyl and carboxyl groups at 1730 cm^{-1}, and C-O (epoxy and alkoxy groups) stretching at 1225 cm^{-1} and 1050 cm^{-1}. The peaks at 1630 cm^{-1} and 1510 cm^{-1} are corresponding to the skeletal and in-plane C=C stretching vibrations of this 2D carbon allotrope [32]. However, the step-wise reduction by using the APPJs showed the gradual disappearance of the oxygen functional groups from the film which exhibits a saturate and complete reduction at 60 and 120 seconds of exposure time, respectively (**Figure 3.5a**). Results confirmed that after 120 s of plasma treatment entire GO is reduced into rGO with no detectable oxygen groups. To exclude the temperature effect of the plasma beam that can reach higher than 100 °C, we performed a control experiment by annealing GO film in a

convection oven at ~ 185 °C from 2 min to 20 min. This study of a temperature effect on the reduction of GO confirmed only minor changes on GO reductions for 120 s. It was found that a minimum 20 min of thermal reduction process is required to achieve the reduction degree of GO comparable with 10 s of exposure with air-plasma treatment (**Figure 3.5b**). This data providing unquestionable support that the effective removal of oxygen functional groups forms GO films under plasma beam irradiation is a different mechanism that excludes the major impact of a temperature.

The crystallinity change and thermal stability of P-rGO films were another parameters explored and summarized in **Figure 3.5c**. The XRD pattern showed a major 2θ peak of GO at 10.93^{o}, that corresponding to an interlayer distance of 0.81 nm. This expansion of d-spacing when compared with pristine graphene (PG) peak at 26.55° corresponding to a distance of 0.335 nm (**Figure 3.5c,** bottom) is attributed to different oxygen functional groups (hydroxyl, carboxyl, and epoxy) in GO plane and edge. The 2θ peak has been shifted to 2θ ~ 23^{o} with an interlayer space of 0.38 nm after plasma-induced reduction, indicating a major oxygen functional groups in GO has been removed to reduce the expansion and restore the hexagonal graphite structure [18]. The broader peak is observed compared with pristine graphene but stronger compared with thermally and chemically reduced GO showing stronger crystalline structure. The degree reduction of the GO-film and P-rGO-film was further analysed by evaluating their weight loss vs temperature in TGA curves. A different thermal stability of GO film and P-rGO films of 60 s and 120 s plasma treatment can be observed from **Figure 3.5d**. The GO film shows a sharp mass loss (57.68 %) in the range of temperature up to 250 °C due to the evaporation of trapped water molecules and unstable oxygen functional groups. Whereas, P-rGO films exhibit gradually degradation vs

temperature up to 450 °C with a mass loss of 28 % and 14 % for 60 and 120 s plasma treatment, respectively. This is attributed to the efficiency of reducing oxygen functional groups, in which longer exposure time gets a better reduction, and it seems to reach the complete reduction after 120 s treatment.

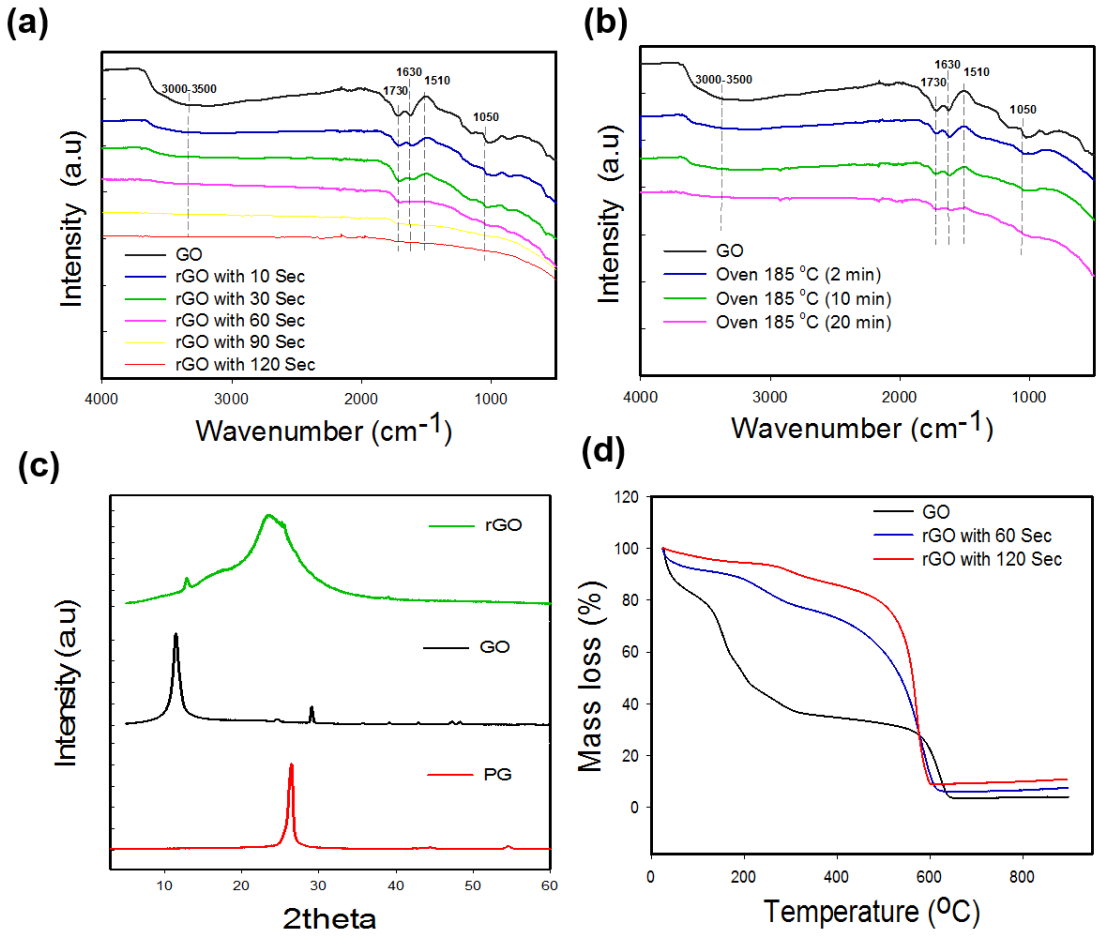

Figure 3.5. Chemical structure of different degree of reduction subjected to different exposure time to plasma. (a) FTIR spectra for GO and rGO with 10, 30, 60 and 120 s, (b) FTIR spectra for GO and thermally reduced-GO, (c) XRD patterns of P-rGO (120 s) in comparison with GO and exfoliated few-layer graphene, (d) TGA of GO and P-rGO after 60 s and 120 s plasma treatment, respectively.

Raman spectroscopy has been further used to study structural and chemical changes after APPJ reduction of GO films. **Figure 3.6a** shows Raman spectra of GO film and P-rGO films exposed to air-plasma for different exposure times. The Raman spectrum shows a typical D-band at 1345 cm^{-1} and G-band at 1590 cm^{-1} for GO film, which presents the defects or structural disorders (sp^3) and tangential vibration of carbon atoms (sp^2), respectively [25,32]. The Raman spectra of P-rGO films exhibit the same centered position of D-band and G-band, while increased G-band intensity versus exposure time. A comparison of the intensity ratio of D and G band (I_D/I_G) as a function of exposure time for GO and P-rGO was performed to study a degree of defects.

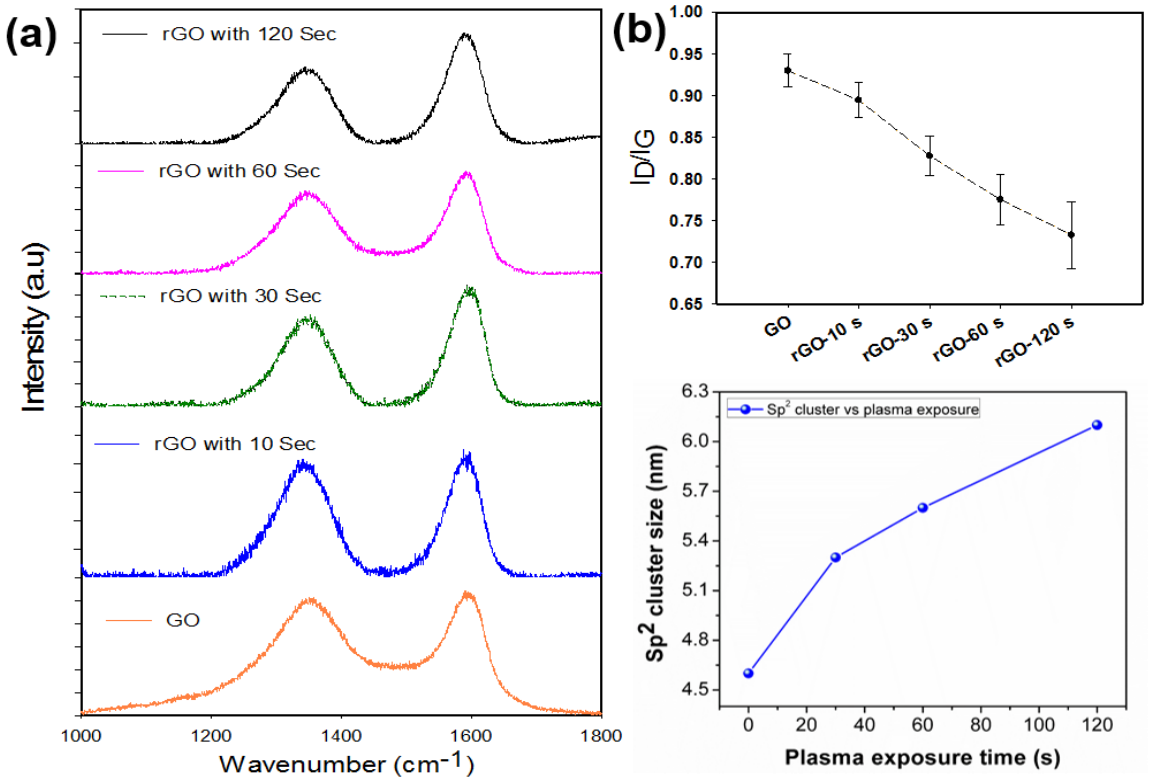

Figure 3.6. (a) Raman spectra for GO and P-rGO with 10, 30, 60 and 120 sec, (b) the difference in intensity ration between D and G band (I_D/I_G) versus exposure time and expanded sp^2 cluster size after plasma-induced reduction.

The **Figure 3.6b** showed significant decreases in the intensity ratio of I_D/I_G from 0.94 for the GO film (before treatment) to 0.72 for the P-rGO films (after 120 s treatment). The decrease of I_D/I_G means decrease of the defects and/or disorders of graphene films by (i) removal of impurities on the surface of GO (plasma cleaning), and (ii) no expanding sp^3 defective areas, but possibly healing or even repairing of lattice defects in graphene films during restore π-conjugated sp^2 network. This is in contrast with conventional process of chemical or thermal reduction, in which a decrease in the average size, but an increase in the number of sp^2 domain upon reduction leading to an increase of I_D/I_G. Based on the I_D/I_G ratio the sp^2 cluster size (La, nm) can be calculated from the equation developed by Tuinstra and Koenig [34]: $La = \frac{10^3}{227\,(\frac{I_D}{I_G})}$. By which the film before plasma treatment (GO) exhibited an average cluster size value of 4.6 nm, this value increased to 5.3, 5.6 and 6.1 nm corresponding to 30, 60 and 120 s explosure time of plasma irradiation. The cluster size is higher than conventional chemically reduced GO (~from 3.5 to 3 nm) and thermally reduced GO (~from 3.5 to 3.15 nm) and consistent with Ar/CH_4 plasma treated GO film as reported by M. Baraket et al [35].

Indeed, the plasma can be introduced more defects, functional groups and less crystalline for treatment of pristine exfoliated graphene, CVD graphene, pre-reduced graphene oxide [36,37]. However, it is also a different mechanism for treatment of GO films. The Raman data implies that the plasma treatment does not introduce additional defects into the reduced GO film as reported by Lee et al [10], whereas restoring the GO into high quality graphene film by defect repair as reported by Cheng et al [8] for methane plasma. The plasma treatment of GO also enables an expansion of the spatial distribution of sp^2 domains. These properties of reduced GO films cannot be expected by conventional reduction methods.

On the basic of the above results, we have proven that the oxygen functional groups are effectively removed from GO films by an irradiation of APPJs. To develop more evidence insight the restoration of π-conjugated network within the graphene sheets occurred by plasma-induced reduction, we performed series of sheet resistance measurement of P-rGO films on both of plasma treated side (top surface) and untreated side (bottom surface). As can be seen from the **Figure 3.7a**, the P-rGO film with a given thickness of 25 ± 0.5 μm shows a dramatically reduced in top-surface sheet resistances towards exposure time from 6.44 MΩ/sq for GO film to 4.35 kΩ/sq after reduction of 30 s, this is about 148 times lower. During this reduction duration, the difference in sheet resistance of the film-side exposure, between the top surface (exposed to the plasma) and the bottom surface, is considerable depending on "skin depth", and this effect is increasing with plasma exposure time. The sheet resistance of the P-rGO top film is reducing down to 186 Ω/sq after 60 s plasma treatment (reduced 34624 times), while the sheet resistances of the bottom surface dropped down to 680 Ω/sq. This indicated that a significant concentration of sp^2 clusters has been restored which leads to enhanced electrical transport, and the skin depth is expanded making enhanced electrical transport, that is close to the counter side. This data suggests that by this method is possible to make the films with conductivity gradients based on graphene films that will be reported in the following study. Further exposure time up to 120 s leading to decrease very gradually to the lowest sheet resistance of 160 Ω/sq and 560 Ω/sq for the top- and the bottom surface of the P-rGO, respectively (**Figure 3.7a, inset**). This reduction in sheet resistance, to our knowledge, is one of the lowest sheet resistances achieved among reduction of GO, and is better than those previously reported by other plasma-assisted reduction of GO, in which

surface resistance varies between (9.0 kΩ/sq to 1.62 MΩ/sq) [8,10,17,19] upon longer exposure time. A control experiment with thermal annealing of the GO-film has been performed at the ambient condition to monitor change in sheet resistance at the temperature of 185 °C. **Figure 3.7b** shows a gradually reduced in sheet resistance which dropped down from 6.42 to 2.15 MΩ/sq after 10 min thermal reduction which indicated a gentle reduction and very far from the low sheet resistances achieved by the plasma process. The controlled experiment by thermal annealing at 185 °C of GO films confirms again that temperature of plasma has a minor effect and reduction process is based on different mechanism. Figure 3.7c shows a rGO electrode fabricated scanning plasma treatment of GO coated PET film which indicated a resistance decreased from MΩ range (GO) to several kΩ (e.g., 8 kΩ measured by a multimeter with a distance of ~6 cm). A P-rGO coated fabric substrate as a conductive textile is displayed with a lighting LED, in which the plasma treatment created rGO sheet networks for conductive paths without any damage to the substrate surface (see SEM image). This data suggests that this APPJ technique can be used to prepare simple and ultrafast graphene coatings for wearable electronic devices.

In the final set of characterization experiments to further verify the different degrees of reduction of GO films versus plasma exposure time, a wettability study was performed by measuring static contact-angle (CA) of water on the surface of various P-rGO films. As revealed in **Figure 3.7d** (bottom), a CA of 45° is standing for the wettability of the hydrophilic GO film, in contrast, the P-rGO film shows an increase in CA to 55, 71, 88, 97 ° for a treatment duration of 10, 30, 60 and 120 s, respectively.

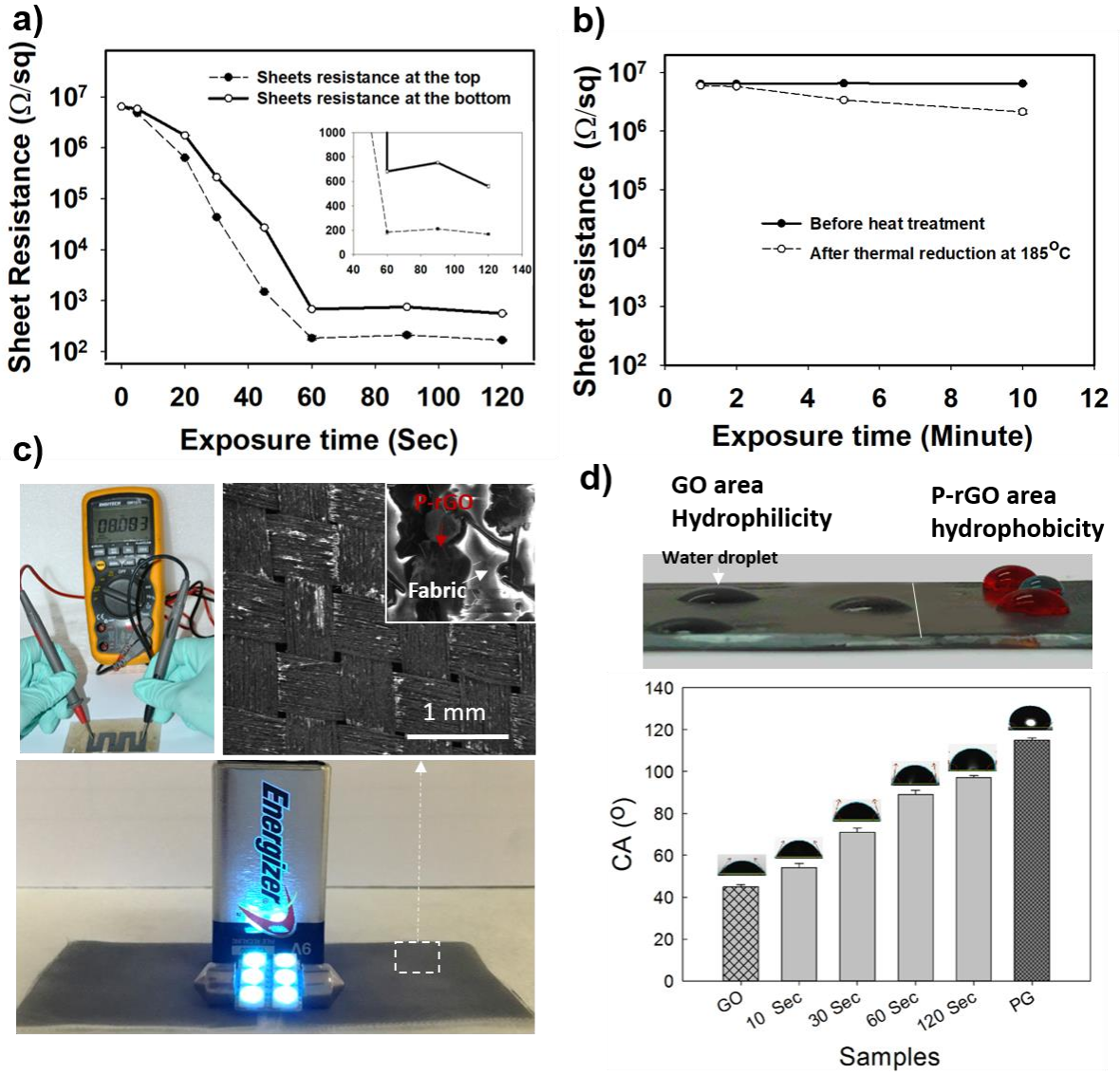

Figure 3.7. Effect of plasma-induced reduction on the sheet resistance of the GO films. (a) Sheet resistance varies of P-rGO films based on plasma exposure time (inset figure shows magnified the image of sheet resistance between the top- and the bottom surface of the P-rGO films. (b) Sheet resistance varies with an exposure time (in minutes) of thermal reduction in a convection oven at 185 °C showing a slight change of resistance in the range of mega-Ohm. (c) Graphene electrode achieved by plasma beam scanning on the GO coated PET film displaying a resistance decreased about two orders of magnitude from MΩ to kΩ range, and

P-rGO-coated fabric textile as conductive electrodes for a LED light. (d) Effect of plasma-induced reduction of GO films on the surface wettability in comparison to the pristine graphene. The GO film with a CA of ~ 45°, the change in CA measurements of P-rGO with different plasma exposure times: a CA of ~ 55° (10 s), ~71° (30 s), ~88° (60 s), and ~97° (120 s) that close to the super hydrophobicity of pristine graphene with a CA of ~115°. (d) An optical image of water droplets on GO (left) and P-rGO film (right, with dye) demonstrating hydrophilicity and hydrophobicity, respectively.

The change in CA resulted in hydrophobicity of P-rGO can be observed in **Figure 3.7d** (top), in which water droplets (with dye) showed very different wettability. This result suggested that an abrupt increase of CA after 60 s treatment indicating a significant reduction, also a saturated increment of CA was achieved after 120 s treatment, which is closed to the pristine graphene having different wettability ranging from 90 to 130 ° [38].

These successful results showing very high electrical conductivity and other desirable properties of prepared film raised the question about the mechanism for observed effective removal of oxygen functional groups from GO films by the APPJs treatment. The fact that the ionize gas-phase species, and dissociate and excite the reactant gas through electro-impact collisions that lead to bond-breaking, displacement of atoms in the surface region and charge accumulation [27], thus the influence of mechanical bombardment from highly energetic species in plasma irradiation is dependent on the graphene-based substrate and ion bombardment energy. In our cold plasma system, air as gas was used, which is a mixture of N_2, O_2, CO_2 and Ar and electron are not heated by external electrical fields. To make a glow discharge state of air-plasma by the applied power of 300 W that is able to ionize molecular O_2 in the air and form the plasma changed ions. When as-prepared GO film was irradiation

under plasmabeam, we propose these charged ions can bombard the GO with low kinetic energy though inelastic collisions causing oxygen-containing groups rupture from the GO surface as oxygen ions. These free moving ions can form covalent bonds with existing oxygen and form molecular O_2. This repetition promotes the removal oxygen functional species from the GO surface. On the other hand, the oxygen in the air could receive free electrons of plasmabeam, which convert oxygen into oxygen adsorbates (O^{2-} and O^{-}_2). These oxygen adsorbates transfers their free electrons to GO surface resulted in to enhance the doping level of the graphene film. In addition, a possible mechanism of reducing oxygen groups is that oxygen and nitrogen can react at relatively high temperatures, they undergo an endothermic reaction producing typically nitric oxide (NO) which is unstable and highly reactive [40]. The active gas NO further reacts with reactive species (COOH-, -CO-, OH-) on the GO surface to reduce surface functional groups and itself converts into nitrogen di-oxide (NO_2) following the equation given below; [40,41] .

$$2NO(g) + O_2(g) \underset{\Delta}{\rightarrow} 2NO_2\,(g)$$

$$2NO_2\,(g) \underset{\Delta}{\rightarrow} N_2\,O_4\,(g)$$

All of those mechanisms could convert GO films transferred from an insulator into a conductor by reduction of their sheet resistance. Although the exact healing and/or repairing defects mechanism for the reduction of GO films by air-plasma irradiation needs to be more elucidated, it is clear that the GO sheets are effectively reduced and decreased defects under plasma beam irradiation. The superior conductive rGO films could be achieved within a minute at low temperature, and without any alternation of bulk properties of graphene films that are not possible by existing reduction methods.

Finally, in order to demonstrate the practical application of plasma conversion of GO films into graphene these films were used as electrodes for assembly of a supercapacitor which performance was tested and presented selectively results (Figure 3.8). **Figure 3.8a** shows the cyclic voltammetry (CV) curves of the P-rGO electrodes at various scan rates, the curves are nearly rectangular, indicating an efficient double-layer formation and high performance when operated over a wide range of scan rates. A comparison of performance before (GO film) and after (P-rGO film) was performed as indicated in Figure 3.8b, in which GO shows a neglected capacitance response as compared to P-rGO electrode due to its low conductivity and high defects structure. The charge/discharge (CD) curves of the plasma rGO films are illustrated in **Figure 3.8c** showing the deviation from the linearity that is likely caused by a combination of electric double-layer capacitors (EDLC) from the graphene sheets and pseudo-capacitance from residual oxygen groups. **Figure 3.8d** displays the gravimetric (C*wt*) and volumetric (C*vol*) capacitances which were calculated from the charge/discharge curves of equation (1) and (2).

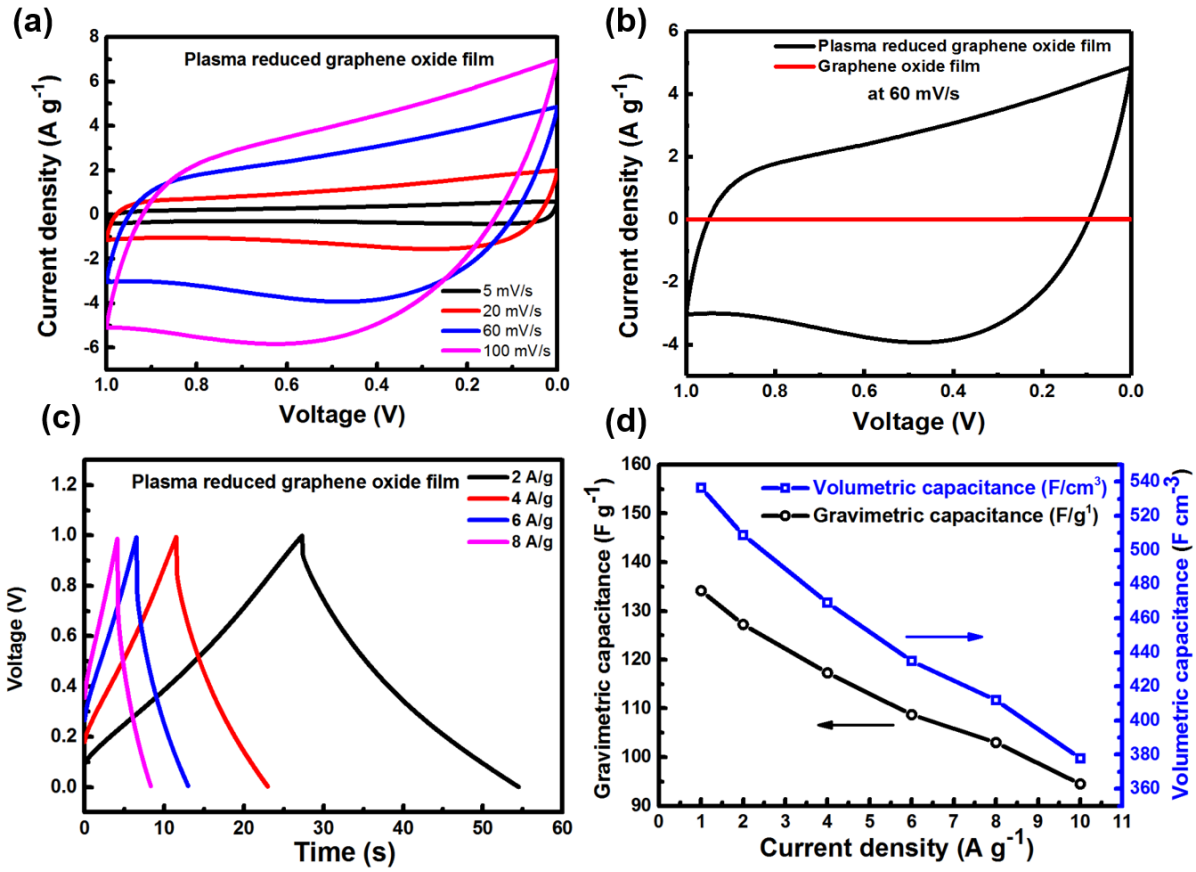

Figure 3.8. Electrochemical characterization of plasma rGO films: a) CV curves of the material at the scan rate between 1 and 100 mV s^{-1}; (b) A comparative capacitance response of GO and P-rGO film electrode; c) GCD curves of the material at various scan rates, (d) gravimetric capacitance and volumetric capacitances values versus scanning rate calculated from the charge/ discharge curves.

The P-rGO electrode shows a gravimetric capacitance (C*wt*) of 134 F/g and volumetric capacitance (C*vol*) of 536.55 F/cm^3 at a current density of 1 A/g. The gravimetric capacitance is lower in comparison with either APPJ or atmospheric-pressure glow discharge plasma treated GO for supercapacitor demonstrated in previous works [42,43]. The reason might be well-ordered and highly packed density in the present conductive films that resulted in superior conductive, unfortunately less ion-assessable surface area. However, the remarkable

value of volumetric capacitance of the present P-rGO electrode, that hasn't explored in that literature, is an advantage. This factor even more important than gravimetric capacitance for practical energy storage, where more energy can be stored in a limited space is critical for portable devices [44].

3.4 Conclusion

In summary, we present an efficient and rapid approach to reduce GO films by atmospheric plasma process combined with scanning capability that allows a simple, ultrafast and scalable preparation of highly conductive thin and thick graphene films on different type of substrates with various sizes, shapes and patterns. The method showed many advantages compared with existing GO reduction process being environmentally-friendly, low-cost, controllable, ultrafast, providing patterning capability and continuous processing mode without limitation for the substrates. The production of the present APPJ scanning treated graphene films enables low defects, superior conductivity and high performances. The reason for that are effective plasma beam afforded by both chemical reaction (charged oxygen ions) and mechanical bombardment led to the complete reduction of GO by efficient removal of oxygen functional groups within a minute, improvement of graphene structure and expanded sp^2 clusters size which are not possible with conventional reduction methods. The produced graphene films with a resistance of only 186 Ω/sq in a short reduction time of 60 s (or 160 Ω/sq for 2 min) without damage their structure is a pleasing performance compared with other methods. Practical applications of this process include promising transparent electrodes on both flexible and rigid substrates (typically with a sheet resistance of 22 kΩ/sq at the transparency of 88 %), and graphene film electrode for the supercapacitor is achieved a remarkable performance of Cvol of 536.55 F/cm^3 at a current density of 1 A/g. This

engineered graphene method will open new opportunities for multiple applications of conductive coatings, energy storages, flexible electronics, electromagnetic shielding antennas, RFID sensors and medical devices.

Acknowledgements

The authors acknowledge the support from Australian research Council under Linkage Scheme with the grant ARC Research Hub for Graphene Enabled Industry Transformation, IH 150100003 funding under Industrial Transformation Research.

3.5 Reference

1. Xu, Y., Shi, G., & Duan, X. (2015). Self-Assembled Three-Dimensional Graphene Macrostructures: Synthesis and Applications in Supercapacitors. Accounts of chemical research, 48(6), 1666. doi:10.1021/acs.accounts.5b001172.
2. Ogata, C., Kurogi, R., Hatakeyama, K., Taniguchi, T., Koinuma, M., & Matsumoto, Y. (2016). All-graphene oxide device with tunable supercapacitor and battery behaviour by the working voltage. Chem. Commun., 52(20), 3919-3922. doi:10.1039/c5cc09575a.
3. Tung, T. T., Yoo, J., Alotaibi, F. K., Nine, M. J., Karunagaran, R., Krebsz, M., . . . Losic, D. (2016). Graphene Oxide-Assisted Liquid Phase Exfoliation of Graphite into Graphene for Highly Conductive Film and Electromechanical Sensors. ACS Applied Materials & Interfaces, 8(25), 16521. doi:10.1021/acsami.6b04872

4. Nine, M. J., Cole, M. A., Tran, D. N. H., & Losic, D. (2015). Graphene: a multipurpose material for protective coatings. Journal of Materials Chemistry A, 3(24), 12580-12602. doi:10.1039/C5TA01010A

5. Dreyer, D. R., Park, S., Bielawski, C. W., & Ruoff, R. S. (2009). The chemistry of graphene oxide. Chemical Society Reviews, 39(1), 228-240. doi:10.1039/b917103g

6. Kian Ping, L., Qiaoliang, B., Goki, E., & Manish, C. (2010). Graphene oxide as a chemically tunable platform for optical applications. Nature Chemistry, 2(12), 1015. doi:10.1038/nchem.907

7. Pei, S., & Cheng, H.-M. (2012). The reduction of graphene oxide. Carbon, 50(9), 3210-3228. doi:10.1016/j.carbon.2011.11.010

8. Cheng, M., Yang, R., Zhang, L., Shi, Z., Yang, W., Wang, D., . . . Zhang, G. (2012). Restoration of graphene from graphene oxide by defect repair. Carbon, 50(7), 2581-2587. doi:10.1016/j.carbon.2012.02.016

9. Wang, Y., Shi, Z., & Yin, J. (2011). Facile synthesis of soluble graphene via a green reduction of graphene oxide in tea solution and its biocomposites. ACS Applied Materials & Interfaces, 3(4), 1127. doi:10.1021/am1012613

10. Lee, S. W., Mattevi, C., Chhowalla, M., & Sankaran, R. M. (2012). Plasma-Assisted Reduction of Graphene Oxide at Low Temperature and Atmospheric Pressure for Flexible Conductor Applications. The Journal of Physical Chemistry Letters, 3(6), 772. doi:10.1021/jz300080p

11. Fernández-Merino, M. J., Guardia, L., Paredes, J. I., Villar-Rodil, S., Solís-Fernández, P., Martínez-Alonso, A., & Tascón, J. M. D. (2010). Vitamin C Is an Ideal Substitute for Hydrazine in the Reduction of Graphene Oxide Suspensions. The Journal of Physical Chemistry C, 114(14), 6426-6432. doi:10.1021/jp100603h

12. Tran, D. N. H., Kabiri, S., & Losic, D. (2014). A green approach for the reduction of graphene oxide nanosheets using non-aromatic amino acids. Carbon, 76, 193-202. doi:10.1016/j.carbon.2014.04.067

13. Chen, W., Yan, L., & Bangal, P. R. (2010). Preparation of graphene by the rapid and mild thermal reduction of graphene oxide induced by microwaves. *Carbon, 48*(4), 1146-1152. doi:10.1016/j.carbon.2009.11.037

14. Gengler, R. Y. N., Badali, D. S., Zhang, D., Dimos, K., Spyrou, K., Gournis, D., & Miller, R. J. D. (2013). Revealing the ultrafast process behind the photoreduction of graphene oxide. *Nature Communications, 4*, urn:issn:2041-1723.

15. György, E., Pérez Del Pino, A., Logofatu, C., Cazan, C., & Duta, A. (2014). Simultaneous Laser-Induced Reduction and Nitrogen Doping of Graphene Oxide in Titanium Oxide/Graphene Oxide Composites. *Journal of the American Ceramic Society, 97*(9), 2718-2724. doi:10.1111/jace.13013

16. Yu, Y.-Y., Kang, B. H., Lee, Y. D., Lee, S. B., & Ju, B.-K. (2013). Effect of fluorine plasma treatment with chemically reduced graphene oxide thin films as hole transport layer in organic solar cells. *Applied Surface Science, 287*, 91-96. doi:10.1016/j.apsusc.2013.09.078

17. Kim, M. J., Jeong, Y., Sohn, S., Lee, S. Y., Kim, Y. J., Lee, K., . . . Jang, J.-H. (2013). Fast and low-temperature reduction of graphene oxide films using ammonia plasma. *AIP Advances, 3*(1). doi:10.1063/1.4789545

18. Baraket, M., Walton, S. G., Wei, Z., Lock, E. H., Robinson, J. T., & Sheehan, P. (2010). Reduction of graphene oxide by electron beam generated plasmas produced in methane/argon mixtures. *Carbon, 48*(12), 3382-3390. doi:10.1016/j.carbon.2010.05.031

19. Li, T., Patel, T., Banerjee, I., Pearce-Hill, R., Gallop, J., Hao, L., & Ray, A. K. (2015). Plasma treated graphene oxide films: structural and electrical studies.(Report). *26*(7), 4810.

20. Jaganathan, S., Yung-Fang, L., Kodepelly Sanjeeva, R., & Masahiro, Y. (2014). Submerged Liquid Plasma for the Synchronized Reduction and Functionalization of Graphene Oxide. *Scientific Reports, 4*(6). doi:10.1038/srep04395

21. Bodik, M., Zahoranova, A., Micusik, M., Bugarova, N., Spitalsky, Z., Omastova, M., . . . Siffalovic, P. (2017). Fast low-temperature plasma reduction of monolayer graphene oxide at atmospheric pressure. *Nanotechnology, 28*(14), 145601. doi:10.1088/1361-6528/aa60ef

22. Bo, Z., Qian, J., Han, Z. J., Duan, L., Qiu, K., Ostrikov, K., . . . Cen, K. (2015). Note: Rapid reduction of graphene oxide paper by glow discharge plasma. *Review of Scientific Instruments, 86*(5). doi:10.1063/1.4919732

23. Jaganathan, S., Yung-Fang, L., Kodepelly Sanjeeva, R., & Masahiro, Y. (2014). Submerged Liquid Plasma for the Synchronized Reduction and Functionalization of Graphene Oxide. *Scientific Reports, 4*(6). doi:10.1038/srep04395

24. Li, S., Wang, Z., Jiang, H., Zhang, L., Ren, J., Zheng, M., . . . Sun, L. (2016). Plasma-induced highly efficient synthesis of boron doped reduced graphene oxide for supercapacitors. Chem. Commun., 52(73), 10988-10991. doi:10.1039/c6cc04052g

25. Kim, H. T., Kim, C.-D., & Park, C. (2014). Reduction and nitridation of graphene oxide (GO) films at room temperature using inductively coupled NH_3 plasma. *Vacuum, 108*, 35-38. doi:10.1016/j.vacuum.2014.05.018

26. Dey, A., Chroneos, A., Braithwaite, N. S. J., Gandhiraman, R. P., & Krishnamurthy, S. (2016). Plasma engineering of graphene. *Applied Physics Reviews, 3*(2). doi:10.1063/1.4947188

27. Profijt, H. B., Potts, S. E., van de Sanden, M. C. M., & Kessels, W. M. M. (2011). Plasma-Assisted Atomic Layer Deposition: Basics, Opportunities, and Challenges. *Journal of Vacuum Science & Technology A: Vacuum, Surfaces, and Films, 29*(5). doi:10.1116/1.3609974

28. Zheng, Q., Li, Z., Yang, J., & Kim, J.-K. (2014). Graphene oxide-based transparent conductive films. *Progress in Materials Science, 64*, 200-247. doi:10.1016/j.pmatsci.2014.03.004

29. Wassei, J. K., & Kaner, R. B. (2010). Graphene, a promising transparent conductor. *Materials Today, 13*(3), 52-59. doi:10.1016/S1369-7021(10)70034-1

30. Torrisi, F., Hasan, T., Wu, W., Sun, Z., Lombardo, A., Kulmala, T. S., . . . Ferrari, A. C. (2012). Inkjet-printed graphene electronics. *ACS nano, 6*(4), 2992. doi:10.1021/nn2044609

31. Gao, Y., Shi, W., Wang, W., Leng, Y., & Zhao, Y. (2014). Inkjet Printing Patterns of Highly Conductive Pristine Graphene on Flexible Substrates. *Industrial & Engineering Chemistry Research, 53*(43), 16777-16784. doi:10.1021/ie502675z

32. Nine, M. J., Cole, M. A., Johnson, L., Tran, D. N. H., & Losic, D. (2015). Robust Superhydrophobic Graphene-Based Composite Coatings with Self-Cleaning and Corrosion Barrier Properties. *ACS applied materials & interfaces, 7*(51), 28482. doi:10.1021/acsami.5b09611

33. In Kyu, M., Junghyun, L., Rodney, S. R., & Hyoyoung, L. (2010). Reduced graphene oxide by chemical graphitization. *Nature Communications, 1*(6), 73. doi:10.1038/ncomms1067

34. Tuinstra, F., & Koenig, J. L. (1970). Raman Spectrum of Graphite. The Journal of Chemical Physics, 53(3), 1126-1130. doi:10.1063/1.1674108

35. Baraket, M., Walton, S. G., Wei, Z., Lock, E. H., Robinson, J. T., & Sheehan, P. (2010). Reduction of graphene oxide by electron beam generated plasmas produced in methane/argon mixtures. Carbon, 48(12), 3382-3390. doi:10.1016/j.carbon.2010.05.03136.

36. Ardavan, Z., Gwan-Hyoung, L., Sung Joo, A., Sunwoo, L., Nithin, M., Mauricio, T., . . . Nikhil, K. (2014). Effect of defects on the intrinsic strength and stiffness of graphene. Nature Communications, 5(1). doi:10.1038/ncomms4186

37. Nourbakhsh, A., Cantoro, M., Vosch, T., Pourtois, G., Clemente, F., van der Veen, M. H., . . . Sels, B. F. (2010). Bandgap opening in oxygen plasma-treated graphene. *Nanotechnology, 21*(43), 435203. doi:10.1088/0957-4484/21/43/435203

38. Hong, S.-J., Li, Y.-F., Hsiao, M.-J., Sheng, Y.-J., & Tsao, H.-K. (2012). Anomalous wetting on a superhydrophobic graphite surface. *Applied Physics Letters, 100*(12). doi:10.1063/1.3697831

39. Javad, R., Xi, M., Hemtej, G., Abhay, V. T., Fazel, Y., Yunfeng, S., . . . Nikhil, A. K. (2012). Wetting transparency of graphene. *Nature Materials, 11*(3), 217. doi:10.1038/nmat3228

40. Yang, F., Troncy, E., Francceur, M., Vinet, B., Vinay, P., Czaika, G., & Blaise, G. (1997). Effects of reducing reagents and temperature on conversion of nitrite and

nitrate to nitric oxide and detection of NO by chemiluminescence.(Automation and Analytical Techniques). *Clinical Chemistry, 43*(4), 657.

41. Moshage, H., Kok, B., Huizenga, J. R., & Jansen, P. L. (1995). Nitrite and nitrate determinations in plasma: a critical evaluation. *Clinical Chemistry, 41*(6 Pt 1), 892.

42. Bo, Z., Zhu, W., Tu, X., Yang, Y., Mao, S., He, Y., . . . Cen, K. (2014). Instantaneous Reduction of Graphene Oxide Paper for Supercapacitor Electrodes with Unimpeded Liquid Permeation. The Journal of Physical Chemistry C, 118(25), 13493-13502. doi:10.1021/jp5037734

43. Kuok, F.-H., Liao, C.-Y., Wan, T.-H., Yeh, P.-W., Cheng, I. C., & Chen, J.-Z. (2017). Atmospheric pressure plasma jet processed reduced graphene oxides for supercapacitor application. Journal of Alloys and Compounds, 692, 558-562. doi:10.1016/j.jallcom.2016.09.056

44. Gogotsi, Y., & Simon, P. (2011). True Performance Metrics in Electrochemical Energy Storage. *Science*, *334*(6058), 917-918. doi:10.1126/science.1213003

Blank Page

Chapter 4

Graphene based Multifunctionally Graded Surfaces

(MFGS)

Statement of Authorship

Title of Paper	Graphene based Multifunctionally Graded Surfaces (MFGS)
Publication Status	☐ Published ☐ Accepted for Publication ☑ Submitted for Publication ☐ Unpublished and Unsubmitted work written in manuscript style
Publication Details	Advanced Materials DOI: 10.1002 .Feb 2019

Principal Author

Name of Principal Author (Candidate)	Faisal ALotaibi
Contribution to the Paper	Under the supervison of Prof Dusan Losic developed ,designed and conducted the experiments , interpreted ,processed the data ,wrote manuscript draf and revised for submission
Overall percentage (%)	80%
Certification:	This paper reports on original research I conducted during the period of my Higher Degree by Research candidature and is not subject to any obligations or contractual agreements with a third party that would constrain its inclusion in this thesis. I am the primary author of this paper.
Signature	Date 5-3-2019

Co-Author Contributions

By signing the Statement of Authorship, each author certifies that:

i. the candidate's stated contribution to the publication is accurate (as detailed above);

ii. permission is granted for the candidate in include the publication in the thesis; and

iii. the sum of all co-author contributions is equal to 100% less the candidate's stated contribution.

Name of Co-Author	Tran T. Tung
Contribution to the Paper	CO-supervise aided in developement of the expierment ,edited the manuscript
Signature	Date 5/03/2019

Name of Co-Author	Md J. Nine
Contribution to the Paper	Edited the manuscript help analyse some data .
Signature	Date 05-03-2019

Please cut and paste additional co-author panels here as required.

Name of Co-Author	Dusan Losic		
Contribution to the Paper	Act as the primary supervisor ,aided in design and developement of the expierment and evaluation and edited the mansucript for submission .		
Signature		Date	8/05/2019

Advanced Materials

Graphene based Multifunctionally Graded Surfaces (MFGS)

--Manuscript Draft--

Manuscript Number:	
Full Title:	Graphene based Multifunctionally Graded Surfaces (MFGS)
Article Type:	Communication
Section/Category:	
Keywords:	multifunctionally graded surfaces, surface gradients, multifunctional surfaces, graphene films, atmospheric plasma
Corresponding Author:	Dusan Losic, PhD The University of Adelaide Adelaide, SA AUSTRALIA
Additional Information:	
Question	**Response**
Please submit a plain text version of your cover letter here.	Dr. Peter Gregory Editor-in-Chief of Advanced Materials WILEY-VCH Verlag GmbH & Co. KGaA, Weinheim Adelaide,6th January 2019 69451 Weinheim, Germany Dear Dr. Gregory, Please find enclosed our manuscript entitled "Graphene based Multifunctionally Graded Surfaces (MFGS)" by Faisal Alotaibi, Tran T. Tung, Md J. Nine, Dusan Losic submitted for consideration as a Communications Article in Advanced Materials. The concept of gradient materials and surfaces with continuous changes of their structural, chemical, physical, and other properties are developed in nature through millions of years of evolution to create astonishing materials and interfaces with unique properties, not possible with homogenous compositions. The bioinspired concept called "Functionally Graded Materials" has been developed and implemented to address many engineering and industrial problems. However, graded surfaces and interfaces that have an equal scientific and technological importance haven't share the same progress, being limited to micron scale and single function based gradients (such as chemical and structural). In this study, inspired by the success of functionally graded materials we introduced a new concept focused on surface or interfacial gradients with multiple properties we termed as "Multifunctionally Graded Surfaces" (MFGS). We demonstrated this concept to engineer unique multifunctional surfaces using graphene, resulting in continuous gradient changes of multiple functions including structural, chemical, charge, surface tension, surface energy, electrical and thermal conductivity at a large scale (>70 mm). We believe these new multifunctionally graded surfaces based on their low cost and scalable fabrication are an important progress in materials science and engineering of a new generation of bioinspired materials and systems for solving many fundamental and practical problems. Therefore, we do not have any doubt that the presented results will be of profound and immediate interest to the broad and interdisciplinary audience of Advanced Materials. All the authors confirm that this work has not been published previously and it is not under consideration for publication elsewhere. Furthermore, the publication of this work is approved by all authors and by the responsible authorities where the work was carried out.

	Sincerely yours, Prof. Dusan Losic
Do you or any of your co-authors have a conflict of interest to declare?	No. The authors declare no conflict of interest.
Corresponding Author Secondary Information:	
Corresponding Author's Institution:	The University of Adelaide
Corresponding Author's Secondary Institution:	
First Author:	Faisal Alotaibi
First Author Secondary Information:	
Order of Authors:	Faisal Alotaibi
	Tung Tran
	Nine Md Julker
	Dusan Losic, PhD
Order of Authors Secondary Information:	
Abstract:	Functionally graded materials and surface gradients are ubiquitous in nature, observed where gradual changes of molecular, chemical, structural, physical, and other properties are created to achieve complex and unique biological functions. Surface gradients based on this bioinspired concept have been explored using different materials, but have typically been limited to nano or micron scale and single function only. Graphene based materials that have outstanding multifunctional properties are introduced here to address these limitations and generate new types of gradients we termed multifunctionally graded surfaces (MFGS). A new method to engineer these surfaces with continuous graduated change of multiple functions including structural, chemical, wettability, charge, surface energy, electrical and thermal conductivity at a large scale (>70 mm) is presented. The fabrication is based on conversion of graphene oxide (GO) films by non-uniform exposure of atmospheric pressure plasma beam (APPs) to gradually remove GO oxygen functional groups across the surface, thus to create reduced graphene oxide (rGO). The method is simple, low-cost, scalable, applicable on different surfaces (metals, plastic, textile, glass, curved, flexible) with the ability to create multifunctional surface gradients at a large scale, and used for solving many fundamental and engineering problems that cannot be addressed with the homogeneous surfaces.

Blank Page

Chapter 4: Graphene based multifunctionally graded surfaces (MFGS)

4.1 Introduction

Functionally graded materials and surface gradients are ubiquitous in nature, observed where gradual changes of molecular, chemical, structural, physical, and other properties are created to achieve complex and unique biological functions. Surface gradients based on this bioinspired concept have been explored using different materials, but have typically been limited to nano or micron scale and single function only. Graphene based materials that have outstanding multifunctional properties are introduced here to address these limitations and generate new types of gradients we termed multifunctionally graded surfaces (MFGS). A new method to engineer these surfaces with continuous graduated change of multiple functions including structural, chemical, wettability, charge, surface energy, electrical and thermal conductivity at a large scale (>70 mm) is presented. The fabrication is based on conversion of graphene oxide (GO) films by non-uniform exposure of atmospheric pressure plasma beam (APPs) to gradually remove GO oxygen functional groups across the surface, thus to create reduced graphene oxide (rGO). The method is simple, low-cost, scalable, applicable on different surfaces (metals, plastic, textile, glass, curved, flexible) with the ability to create multifunctional surface gradients at a large scale, and used for solving many fundamental and engineering problems that cannot be addressed with the homogenous surfaces.

The concept of gradient materials and surfaces where structural, chemical, physical, and other properties are continuously changing are developed in nature through millions of years of evolution to create astonishing materials and interface designs with unique properties to achieve complex biological functions not possible with homogenous composition. The translation of this bioinspired concept into real applications to address many fundamental and engineering problems has been a tremendously active research field in the last few decades [1]. Functionally graded materials (FGM) as a new type of composite materials with two (or more) different components with continuous variation of their spatial composition profile including chemistry, size, shape, orientation, phase etc. have been introduced and successfully implemented to solve challenging engineering problems in the aerospace industry, defense, construction and medicine [2]. In addition to these graded bulk materials, surface gradients involving morphological, chemical, charge, surface energy, wettability and elasticity have also been deeply explored as an emerging platform for investigating cell-surface interactions and cellular response to surfaces including adhesion, function, proliferation, migration and differentiation [3-5]. These studies have been largely inspired by the pioneering by work of Chaudhury and Whiteside in the early 90s using self-assembled monolayers with chemical gradients generated by edge functional groups where wettability changes were used to move sessile water droplets uphill [6-7]. A broad range of surface-bound chemical and structural gradients using polymers, self-assembled monolayers, porous materials, nanoparticles films have been generated in recent decades and applied for the study of fundamental problems such as lateral sensory systems, protein adsorption, cell attachment, proliferation and differentiation [3, 4, 5,7, 8]. However, most of these approaches have been able to generate surface gradients at only several tens of microns and were limited to only single or two properties such as chemistry and morphology. Surface gradients at the macro

scale with a combination of multiple properties are important for many fundamental and practical applications, but have not been achieved yet.

4.2 Experimental section

Sample preparation: Natural graphite (Uley, Eyre Peninsula, South Australia) was used to prepare GO was synthesized using a modified Hammer's method as reported previously [25]. The GO dispersed into ethanol solution 0.5 mg/mL was sprayed onto cleaned glass slides (25x75 mm) by a spray device (Neo For Iwata). Atmospheric plasma system (X4-800-USB, Diener Electronic GmbH. Co. KG, Germany) with plasma jet device, plasma controller combined with software-controlled scanning platform was used to make GO-rGO gradient films using two modes of operations (Supporting info, Figure 4S1).

4.3 Characterization:

Scanning electron microscope (SEM-FEI Quanta 450, Japan) was used to characterize the GO-rGO gradient surface morphology. A benchtop 3D optical profiler (Bruker ContourGT-K1) was used for imaging surface profile and to quantify surface roughness. A high-resolution of Transmission Electron Microscope (TEM, Philips CM200, Japan) was used for imaging the GO-rGO samples at 200 kV. XRD patterns were recorded by X-ray Diffraction (XRD, Rigaku-Miniflex 600, Japan) at 40 kV and 15 mA in the range of 2θ = 3-70° with a scanning speed of 10°/min. Fourier transform infrared spectroscopy (FTIR) (Nicolet 6700 Thermo Fisher) was used for FTIR measurements. Raman spectroscopy was taken using a HORIBA scientific instrument (LabRam HR800 Ev, Jobin Yvon, Horiba, France) with a 50x objective and 532 nm laser (mpc 3000) as the excitation source. Thermogravimetric analysis (TGA) was carried out on a TGA Q5000 instrument with a heating rate of 5 °C min^{-1} under a

nitrogen atmosphere. A four-point-probe (Jandel, RM3000) was used for sheet resistance measurements which measured at an auto-range mode accelerating current from 50 to 10 μA. The infra read (IR) camera (FLIR E60) features a high resolution 320 × 240 thermal imaging sensor, 60 Hz full-window resolution. Ohmic or resistive heating by electric current of GO0RGO samples was performed with a power supply and current of 25 mA cm^{-1} of was applied for 90 second to generate heat followed by 70 seconds of cooling. The IR thermal imaging camera was used for continuous monitoring of the surface temperature and thermal images for the film surface during the heating period and cooling period when current was switched off. In order visually verify the heat transmission and conduction property, the gradient samples were placed on the hot plate at 80 °C and the changes of the film surface temperature was monitored by infrared camera for 30 sec. All thermal imaging data acquisition was processed using provided software Research IR supplied by FLIR.

4.4 Result and discussion

As graphene material has outstanding and tunable chemical, thermal, electrical, mechanical and optical properties, as well as the ability to create graphene films with various chemistries on different surfaces, it is an ideal solution for designing of multifunctional surface gradients, something not achievable with other materials [9-12]. Many methods for chemical modification of graphene derivatives such as graphene oxide (GO) and pristine graphene have been explored in recent years employing different approaches such as chemical, thermal reduction, plasma, microwave and laser treatment, but with limited studies for designing graphene surface gradients and their applications [13-15]. A few theoretical investigations have been reported to understand the electrical, optical, sensing and interfacial properties of

non-uniform surfaces of different types of graphene, but these have lacked practical realization and applications [16].

Inspired with the idea of functionally graded materials considering 3-dimensional (3-d) structures, in this work we introduce a new concept focused on surface or interfacial gradients with multiple properties, which we termed as multifunctionally graded surfaces (MFGS). A graded surface with multifunctional features is a widespread concept found in many biological systems in nature (diatoms, plant leaves, insects, skin) providing many advantages and unique properties, not achievable with homogeneous surfaces. The aim of this bioinspired approach is to generate a new type of surface gradients using specifically engineered graphene films to achieve continuous graduated change at a large scale (cm) of a range of properties such as chemical, charge, structural, wettability, optical, thermal and electrical conductivity **(Figure 4.1).** The concept is demonstrated by conversion of surface chemistry of GO with oxygen functionalities (carboxyl, phenolic, hydroxyl, epoxy, lactonic) into reduced GO using atmospheric pressure plasma (APP) with specific conditions able to provide continuous and asymmetrical plasma exposure.

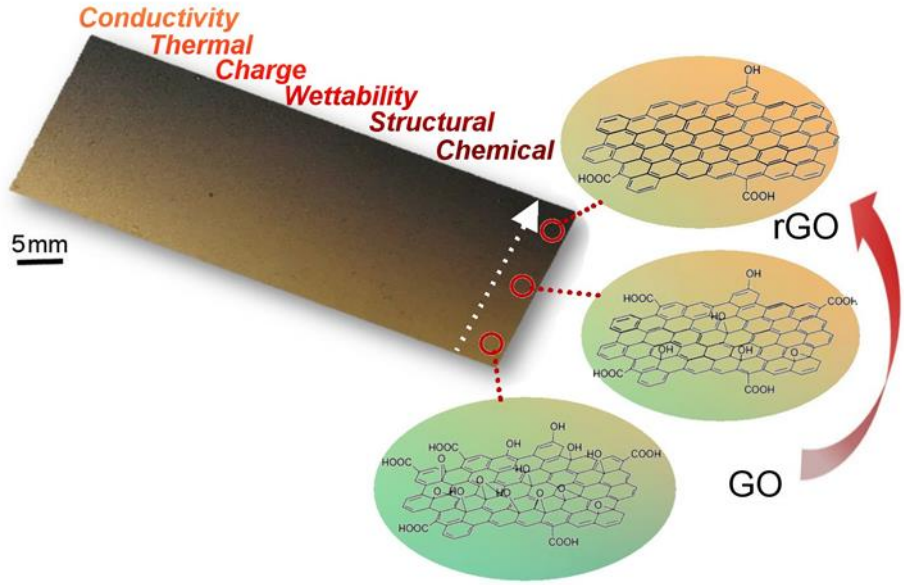

Figure 4.1: Schematic of Multifunctionally Graded Surfaces (MFGS) created with graphene oxide (GO)/reduced graphene oxide (rGO) films with gradual change of multiple properties including structural, chemical, charge, surface tension, electrical and thermal conductivity.

Photos of two plasma fabrication set-ups and several examples of fabricated Graphene Oxide to reduced Graphene Oxide (GO-rGO) gradient films on glass slides with different lengths, from 20 mm to 70 mm and 1d and 2d directions are presented in **Figure 4.2 and Figure 4S1.** A gradual color change on the surface of fabricated samples from golden light (GO side) to dark brown (rGO side) indicates a visible change of the surface chemistry from GO to rGO that corresponds to a level of reduction of oxygen functionality of GO and conversion to rGO by the plasma beam. A typical example of fabricated GO-rGO gradient films on glass slides (25 x 75 mm) with gradients formed in one direction (y) with length of 20-25 mm and width (x) of 75 mm is shown in **Figure 4.2 b.** These gradients are created by inclination of the

sample by 45° with constant distance to the scanning plasma beam (**Figure 4.2a**), thus providing asymmetrical plasma beam exposure with the highest intensity on the top of the sample and the lowest intensity at the bottom part. This condition creates the highest density of oxygen groups (carboxyl, phenolic, hydroxyl, epoxy, lactone) on the bottom end (GO surface, lowest plasma intensity), and this is gradually decreasing due to stronger exposure to the plasma beam causing their removal and conversion into rGO towards the top end of the sample. This angle method is limited to making gradients shorter than <25 mm. In order to make gradients with longer lengths (>70 mm) we propose another scanning method where the plasma beam is at a perpendicular position (90°) and with a constant distance to the sample surface. This method creates gradients by changing the speed of the plasma beam or by moving the stage holding the sample (**Figure 4.2c**). With this method, intensity of the plasma beam can be controlled over a longer distance and in both (x,y) directions (**Figure 4.2 c and d)**. This method could also be combined with masking techniques to create gradients with different dimensions, geometries and patterns. The method is very simple, fast (few minutes), low cost, and flexible to be applied for flat, solid, curved and flexible surfaces, and a broad range of materials (metals, plastics, glass, Si wafers, ceramics, textile, wood etc.)[17].

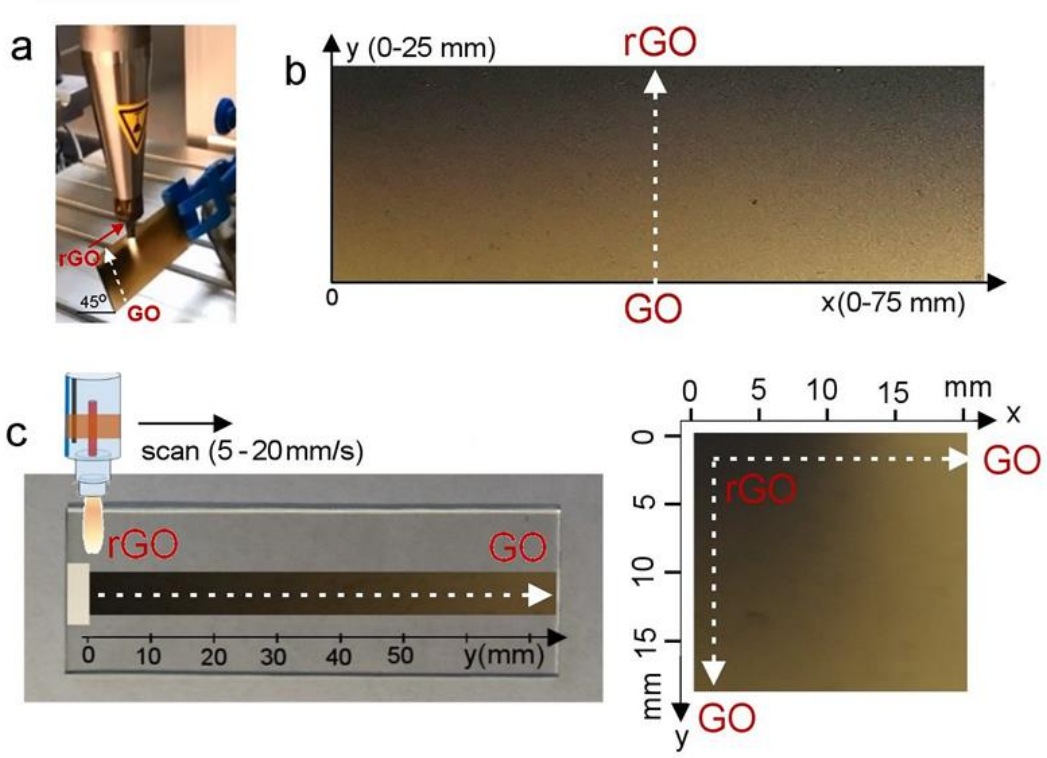

Figure 4.2: a) Fabrication set-up to generate asymmetrical atmospheric plasma beam for preparation of GO-rGO multifunctional graded surfaces (MFGS) with gradient length of 10-25 mm, b) Typical GO-rGO gradients fabricated on glass slide with gradient length of 25 mm (Y) and width 75 mm (x), c) Fabrication set-up to make very large GO-rGO gradients (>7 mm) by varying the speed of the plasma beam or by moving the stage holding the sample, d) Typical GO-rGO gradient fabricated on glass slide with 2-d gradients (length of 15 mm).

Morphological changes on the surface of fabricated GO-rGO gradients characterized at 3 representative spots (the 0 mm, central 10 mm and 20 mm) are confirmed at micron scale by optical, profilometric measurements, and SEM imaging, and then at nano scale by TEM imaging (**Figure 4.3)**. The optical images (**Figures 4.3a, 4.3b and 4.3c)** show that the grain size on GO surface was slightly expanded upon plasma irradiation, and shows more folds and wrinkles at the microscale with increased surface roughness. This observation is confirmed

by corresponding surface topography profiles showing slightly increasing surface roughness at central parts (10 mm, with mild GO reduction), and even higher roughness at the top part with entire GO reduction (20mm). The corresponding SEM images **(Figures 4.3 d, 4.3e and 4.3f)** from these spots confirm similar structural changes showing increased roughness caused by more wrinkled structures of graphene sheets due to higher exposure of plasma beam during GO to rGO conversion. These graduated morphological changes can be explained as results of changes of electron densities of the plasma beam. The plasma beam creates differences in oxygen reduction and mechanical bombardment, and leads to the reduction of GO sheets, transforming crystallinity, and expansion of rGO sheets in the film. [17]. TEM images of graphene structures taken at different spots of the gradient (**Figures 4.3g, 4.3h and 4.3i)** revealed structural changes of the graphene surface at nanoscale. The surface of initial GO film **(Figure 4.3g)** is composed of continuously stacked and overlapped layers of GO sheets with few layers thickness and irregular size of 1-2 microns size. The TEM image of plasma reduced rGO structures taken at 10 mm and 20 mm distance along the gradient (**Figure 4.3h and 4.3i)** showed the reduction of their lateral size and improved crystallinity caused by higher reduction level under the mechanical bombardment of the plasma beam.

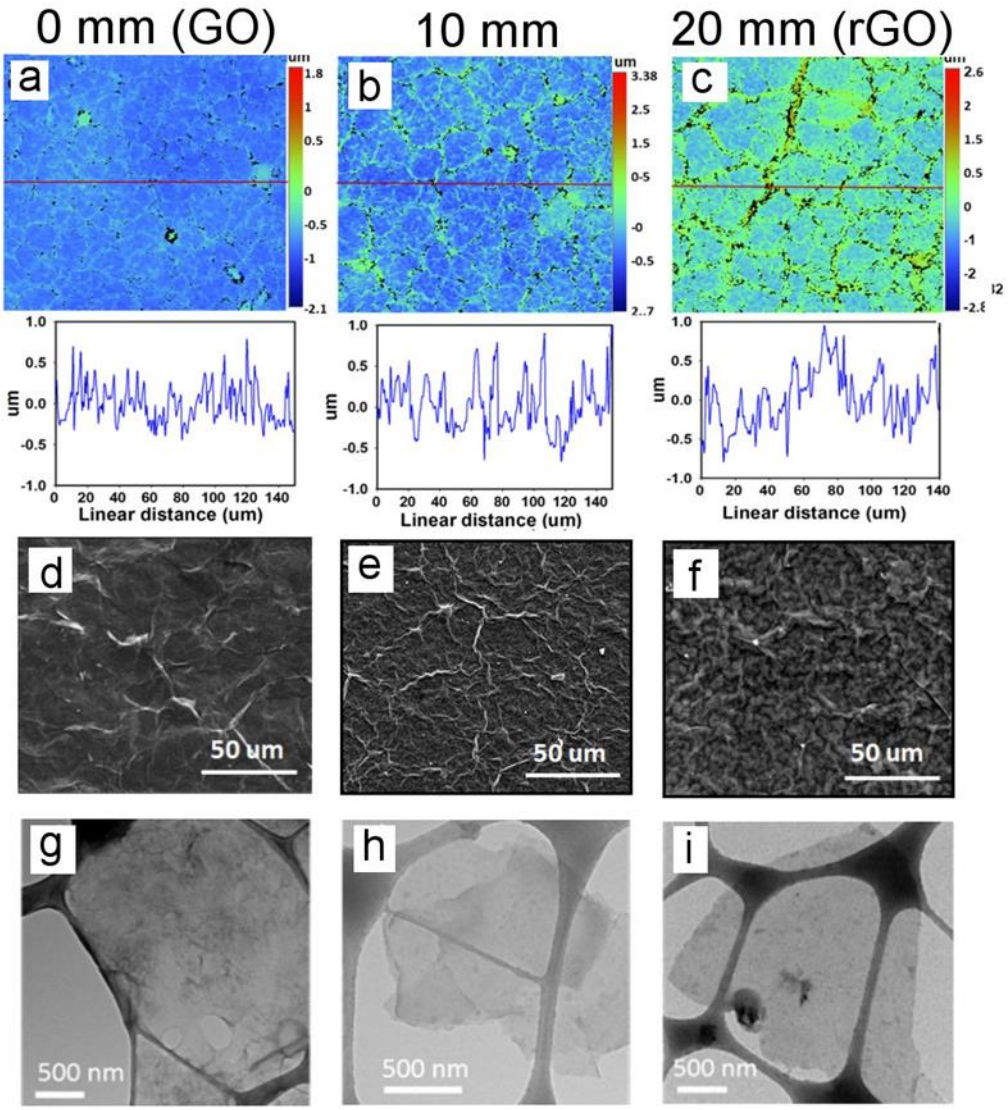

Figure 4.3: Characterization of structural and morphological changes of fabricated GO-rGO multifunctional graded surfaces taken at different positions (0 mm, 10 mm and 20 mm) along the gradient showing: a-c) Optical images with corresponding surface profile, d-f) SEM images and g-i) TEM images.

To confirm the formation of chemical gradients of fabricated GO-rGO films, characterization results using FTIR, Raman, X-ray diffraction and TGA performed at different distances along the gradient (0 mm, 5 mm, 10 mm, 15 mm and 20 mm) are summarized in **Figure 4.4.** The FTIR graph **(Figure 4.4a)** at initial spot (0 mm) exposed to the lowest intensity of plasma reveals typical signature of GO with oxygen groups showing peaks at 3000−3500 cm^{-1} (broad) and 1410 cm^{-1} (narrow) indicating O−H stretching vibrations, at 1730 cm^{-1} for C=O (carbonyl and carboxyl groups) stretching vibrations, and at 1225 and 1050 cm^{-1} for C−O (epoxy and alkoxy groups) stretching peaks. The skeletal and in-plane C=C stretching vibrations of this 2D carbon allotrope are observed at 1630 and 1510 cm^{-1} [18]. FTIR graphs taken at gradient spots with higher plasma exposure (5 mm, 10 mm, 15 mm and 20 mm) show decreases of these peaks, indicating gradual decrease of the density of oxygen functional groups across the gradient surface, with their eventual removal at the end (20 mm) showing a typical signature of rGO.

The changes of carbon surface chemistry at different distances along the gradient characterized by Raman spectroscopy are presented in **Figure 4.4b.** The Raman spectrum from GO spots (0 nm) shows a typical D-band at 1345 cm^{-1} confirming the defects or structural disorders (sp^3), and G-band at 1590 cm^{-1} tangential vibration of carbon atoms (sp^2), respectively [19] . The intensity ratio of D and G band I_D/I_G as a function of distance from GO-rich region to rGO region showed a gradual decrease from 1.3 (GO) to 1.04, 0.87 and 0.80 for the rGO films at gradient distances from 5 mm, 10 mm and 20 mm, respectively. This decrease of I_D/I_G is explained as a result of the healing of lattice defects in GO film during restoration of conjugated sp^2 network caused by plasma and in agreement with previous study for GO to rGO reduction using different methods [20].

To prove gradual change of crystallinity of fabricated GO-rGO gradients, XRD characterizations results performed at 3 gradient positions (0 mm, 10 mm and 20 mm) are shown in **Figure 4.4c**. The XRD pattern taken at 0 mm shows a characteristic sharp 2θ peak of GO at 10.93^{o} that corresponds to an interlayer distance of 0.81 nm. In addition to this peak after plasma-induced reduction at the distance of 10 mm a new broader 2θ peak has been observed at ~ 23^{o}, with an interlayer space of 0.38 nm indicating partial reduction of oxygen group. An XRD peak at ~ 23^{o} at position of 20 mm indicates a typical rGO structure confirming that major oxygen functional groups in GO have been removed and the hexagonal graphite structure has been fully restored. These XRD graphs at 3 different gradient positions with characteristic 2θ peaks of GO (0 mm), GO and rGO (10 mm), and rGO (20 mm) evidently confirms lateral changes of crystallinity across the gradient surface. The final experiment performed by TGA characterization summarized in **Figure 4.4d** confirms the difference in mass loss profile at different distances across GO-rGO gradients. This is a result of the loss of moisture, oxygen functional groups and carbon structure degradation, and shows typical TGA graphs that correspond to GO, mixed GO-rGO, and rGO. These combined characterization results confirmed that chemical gradients are successfully created with continuous and graduated changes with decreasing density of oxygen functional groups and increasing sp^2 hybridization along the gradient surface (0-25 mm).

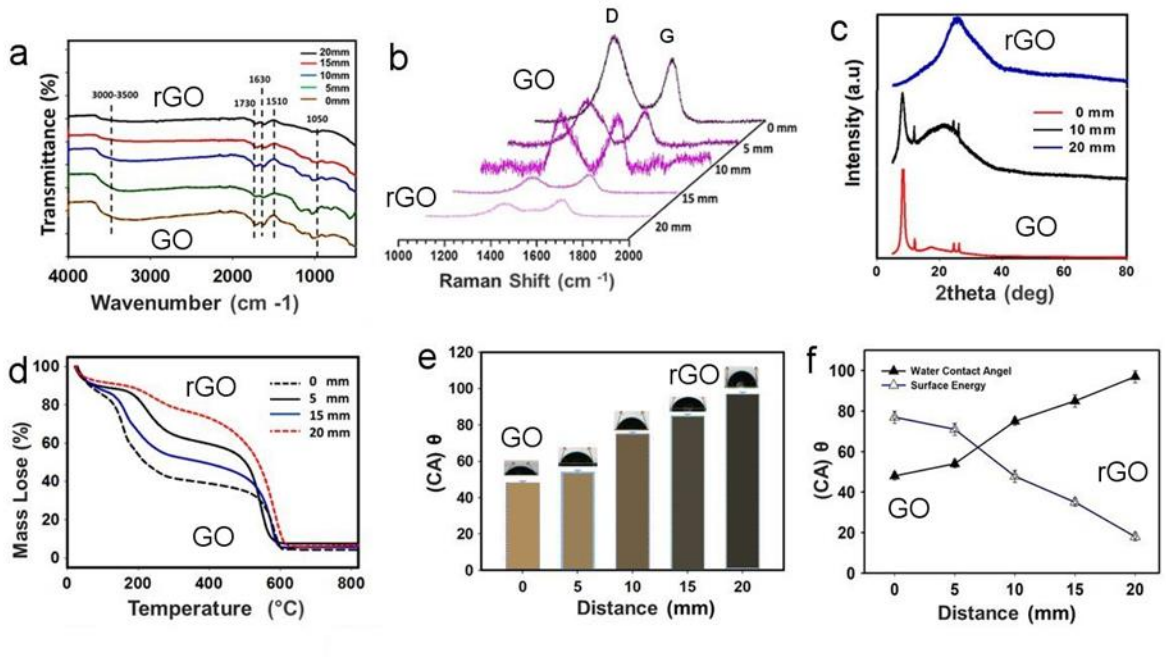

Figure 4. Characterization of chemical and interfacial properties of GO-rGO multifunctionally graded surfaces taken at different positions (0 mm, 5mm, 10 mm 15 mm and 20 mm) along the gradient showing a) FTIR spectra. b) Raman spectra, c) X-ray diffraction patterns (3 spots), d) TGA graphs (3 spots), e) water contact angle and f) surface energy.

The surface tension or wettability results of the water contact angle (CA) taken at different spots of the GO-rGO gradients are presented in **Figures 4.4e** and **Figure 42S**. A linear increase of CA from hydrophilic surface with CA ~45° at 0 mm related to GO, to slightly hydrophobic surface with CA 98.6° at 20 mm indicates an incremental reduction of hydrophilic oxygen functional groups and an increasing sp^2 hydrophobic surface that corresponds to intensity of the plasma exposure across the GO surface. **Figure 4.4f** shows the calculated surface energy for the different positions along the gradient indicating an opposite trend, in which the surface energy decreasing from 79.8 mJ/m^2 at 0 nm (GO) to the lowest

value of 18 mJ/m^2 at at 20 mm (rGO), which corresponds to conversion of GO to rGO across the sample. Changes in the surface charge across the GO-rGO film was measured by zeta potential charge across the gradient showing incremental changes from -45.5 V (0 mm), to -32.4 V (10 mm), and -10.7 mV (20 nm). These changes of wettability, surface energy and surface charge are important multifunctionality features showing the uniqueness of GO-rGO interface. Their potential applications are enormous including fog/water harvesting, micro-droplet transportation, tribology, self-cleaning, tissue engineering, controlled cellular growth, and are waiting to be explored.

The electrical conductivity gradients of GO-rGO films were demonstrated by changes of the sheet resistance measured stepwise across the gradient surface (0 mm to 25 mm) with results presented in **Figure 4.5a and Figure 4S3.** The significant changes were observed from 1.1x10^6 Ω/sq from GO spot (0 mm) to rGO spot (25 mm) 1.2x10^3 Ω/sq. **Figure 4.5b** shows typical current-voltage (I-V) curves obtained at different positions of the gradient film (0 mm, 10 mm and 20 mm). These I-V curves indicate that the graphene film exhibits semiconducting behavior as the current is non-linear when the bias voltage is large than 0.1 V. This observation also suggests that at the same applied voltage at position of 20 mm has the highest current, followed position of 10 mm and 0 mm, which is consistent with surface resistance measurements. The electrical conductivity from rGO spot for practical application is demonstrated by a simple experiment in **Figure 4S3** with led diode. It is well known that graphene has outstanding electrical properties based on its unique sp^2 and zero bandgap. In comparison, GO has significantly reduced conductivity due to disruption of the carrier transport by oxygen functional groups with sp^3 bonding and subsequent surface defects. These electrical conductivity gradients will open opportunities for broad engineering

applications such as electrophoretic, electro-separations, electrowetting, asymmetric electrodes, energy storage and harvesting, microfluidics, sensing, piezoelectric actuators, wearable electronics, robotics, transportation, thermal management, etc. [21].

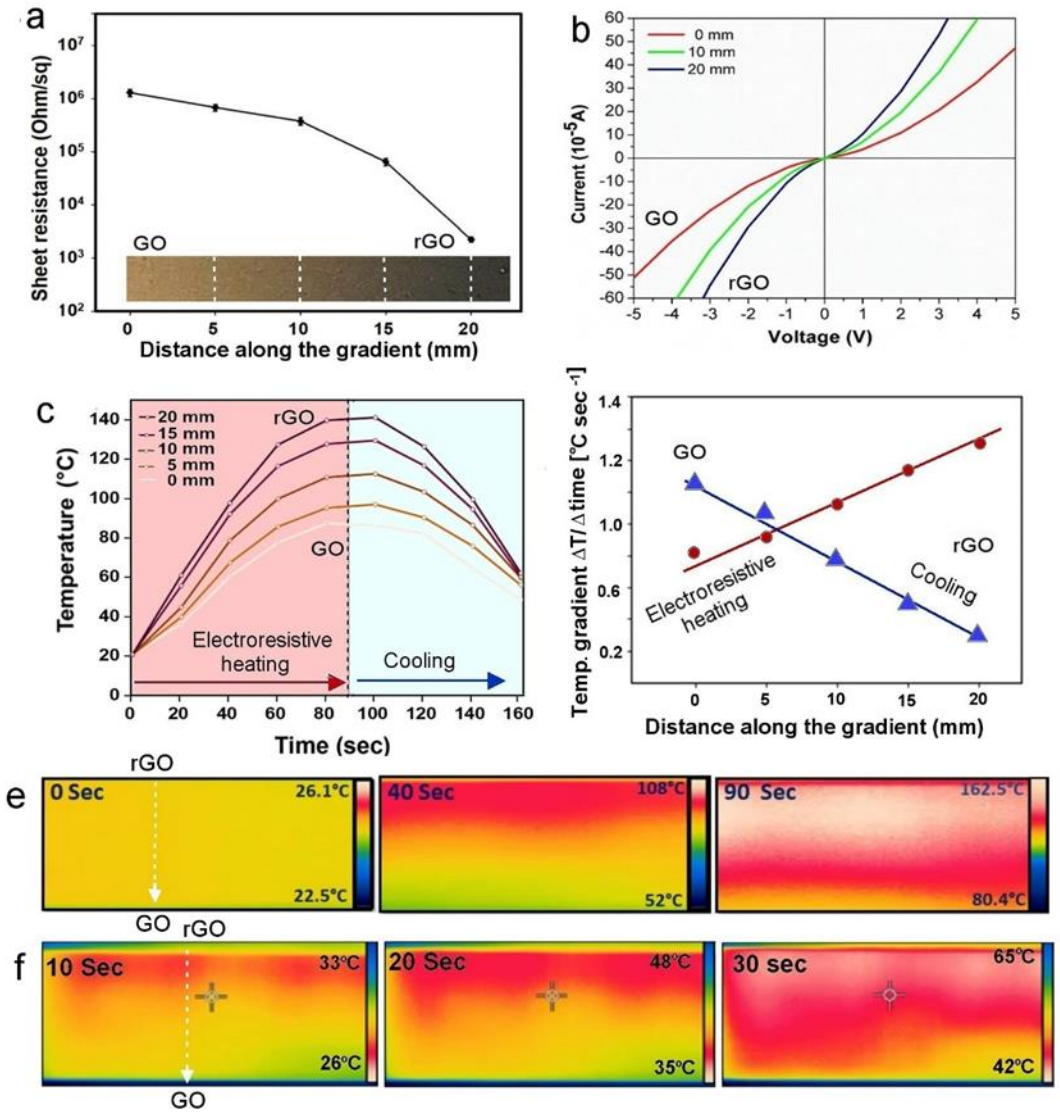

Figure 4.5. (a) Characterization of electrical, thermoelectrical and thermal conductivity of GO-rGO multifunctional graded surfaces (25 mm x 75 mm) taken at different positions along the gradient showing: a) sheet resistance measurements vs distance across the gradient, (b) I-V curve showing conductivity versus the gradient distance (0 mm, 10 mm and 20 mm), c)

surface temperature as a function of time at different gradient positions generated by electro resistive heating (90 sec with 25 mA cm^{-1}) followed by cooling-down (70 sec, power off), d) temperature gradients during heating and cooling at different gradient positions, e) Selected thermal camera images taken during electrical heating showing visual changes of surface temperature across the gradient, and f) Thermal camera images with visual changes of surface temperature across the gradients after exposed to hot plate at 80°C for 30 sec.

Finally, thermal conductivity gradients of fabricated GO-rGO films were demonstrated by performing Ohm resistive heating and heat conduction (transfer) experiments. **Figure 4.5c** presents a series of graphs of generated temperature by Ohm resistive heating during 90 sec following by cooling period of 70 sec at different positions of the gradient (0-20 mm). The GO region (0-5 mm) showed the lowest temperature increase which means the lowest thermoelectric conductivity compared the rGO region (20-25 mm) with the highest slope and the highest thermal conductivity. The linear increase of generated temperature across the GO-rGO surface was observed during both electrical heating and cooling stage showing similar slopes (°C/sec) across the gradient indicating their gradual thermoelectric properties **(Figure 4.5d).** Thermal images from infrared camera (**Figure 4.5e and Figure 4S3**) taken after 40 sec of this experiment showed visual changes of temperatures across the gradient surface (0-25 mm) from the lowest temperature of 52 °C at GO spot (0mm) to the highest temperature of 108°C at rGO spot (25 mm).

In order to verify the gradient change of the heat conduction and transfer properties the infrared camera is used to visually capture the temperature images generated from the GO-rGO substrates after exposure by heating from a hot plate at 80 °C. **Figure 4.5f** confirmed a

gradient change of the surface temperature from GO to rGO region where the GO region showed the lowest temperature, and the rGO region showed the highest temperature, and is in agreement with the previous experiment. The phonons are the main heat carrier in graphene and observed thermal and thermoelectric properties on GO-rGO can be explained by influence of their chemistry and defects [22]. The presence of oxygen groups on graphene surface is proven to suppress the density of state of the phonon in C-C bonds, and significantly reduce heat propagation [23]. Chou et al showed that the Seebeck coefficient is used for measurement of heat transport, and found that it is changing from 60 μV/°C for rGO to 10 μV/°C for GO, due to chemical reduction [24].

4.5 Conclusion

In summary, we have introduced and demonstrated the concept of multifunctionally graded surfaces (MFGS) using GO-rGO films with a gradient change of multiple properties including surface morphology, chemistry, wettability, surface charge, surface energy, electrical, thermoelectrical and thermal conductivity. The fabrication method is based on treatment of graphene oxide (GO) films by non-uniform exposure of atmospheric pressure plasma beam to gradually remove GO oxygen functional groups across the surface to form rGO. It was demonstrated that these gradients can be fabricated in both dimensions with controllable lengths from micron (<1 mm) to cm scale (>70 mm) which is one of the longest gradients reported in literature. The method is simple, very fast (1-2 minutes), low cost, environmentally friendly, and flexible to be applied for a broad range of substrates (flat, curved or flexible) and materials (metals, glass, ceramics, Si wafers, plastics, textile, wood etc.). The proposed concept provides many advantages compared with previously reported surface gradients that are limited to micron scale and single functions. The concept can be

used for broad applications and solving many challenging fundamental, medical, engineering and industrial problems not possible with uniform surfaces.

Acknowledgements

The authors acknowledge the support from Australian research Council under Linkage Scheme with the grant ARC Research Hub for Graphene Enabled Industry Transformation, IH 150100003 funding under Industrial Transformation Research.

4.6 References

1. Velasco-Hogan, A., Xu, J., & Meyers, M. A. (2018). Additive Manufacturing as a Method to Design and Optimize Bioinspired Structures. Advanced materials (Deerfield Beach, Fla.), 30(52), e1800940. doi:10.1002/adma.201800940; b) Koch, K., Bhushan, B., & Barthlott, W. (2009). Multifunctional surface structures of plants: An inspiration for biomimetics. Progress in Materials Science, 54(2), 137-178. doi:10.1016/j.pmatsci.2008.07.003 C) Xia, F., & Jiang, L. (2008). Bio-Inspired, Smart, Multiscale Interfacial Materials. Advanced Materials, 20(15), 2842-2858. doi:10.1002/adma.200800836

2. a) M. Niino, T. Hirai, R. Watanabe, J. Jpn. Soc. Compos. Mater. 1987, 13, 257; b) Stavros, T., Victor, B., & Guy, M. G. (2013). Structural Interfaces and Attachments in Biology (2013 ed. Vol. 9781461433170). New York, NY: New York, NY: Springer New York.; c) Mahamood, R. M. a. (2017). Functionally Graded Materials: Springer International Publishing : Imprint: Springer.; d) B. Kieback, B., Neubrand, A., & Riedel, H. (2003). Processing techniques for functionally graded materials. Materials Science & Engineering A, 362(1-2), 81-106. doi:10.1016/S0921-5093(03)00578-1

3. a) Ballav, N., Shaporenko, A., Terfort, A., & Zharnikov, M. (2007). A Flexible Approach to the Fabrication of Chemical Gradients. Advanced Materials, 19(7), 998-1000. doi:10.1002/adma.200602168. b) Love, J. C., Estroff, L. A., Kriebel, J. K., Nuzzo, R. G., & Whitesides, G. M. (2005). Self-assembled monolayers of thiolates on metals as a form of nanotechnology. Chemical reviews, 105(4), 1103. doi:10.1021/cr0300789; c) Yang, J., Rose, F. R. A. J., Gadegaard, N., & Alexander, M. R. (2009). A High-Throughput Assay of Cell-Surface Interactions using Topographical and Chemical Gradients. Advanced Materials, 21(3), 300-304. doi:10.1002/adma.200801942

4. a) Chen, C. S., Mrksich, M., Huang, S., Whitesides, G. M., & Ingber, D. E. (1997). Geometric Control of Cell Life and Death. Science, 276(5317), 1425-1428. doi:10.1126/science.276.5317.1425 ; b) Caliari, S. R., Weisgerber, D. W., Grier, W. K., Mahmassani, Z., Boppart, M. D., & Harley, B. A. C. (2015). Collagen Scaffolds Incorporating Coincident Gradations of Instructive Structural and Biochemical Cues for Osteotendinous Junction Engineering. Advanced Healthcare Materials, 4(6), 831-837. doi:10.1002/adhm.201400809 c) Li Jeon, N., Baskaran, H., Dertinger, S. K. W., Whitesides, G. M., Van De Water, L., & Toner, M. (2002). Neutrophil chemotaxis in linear and complex gradients of interleukin-8 formed in a microfabricated device. Nature Biotechnology, 20(8), 826. ; d) Segev-Bar, M., Konvalina, G., & Haick, H. (2015). High-Resolution Unpixelated Smart Patches with Antiparallel Thickness Gradients of Nanoparticles. Advanced Materials, 27(10), 1779-1784. doi:10.1002/adma.201405224

5. a) Yu, X., Wang, Z., Jiang, Y., & Zhang, X. (2006). Surface gradient material: from superhydrophobicity to superhydrophilicity. Langmuir : the ACS journal of surfaces

and colloids, 22(10), 4483. doi:10.1021/la053133c; b) Kunzler, T. P., Drobek, T., Schuler, M., & Spencer, N. D. (2007). Systematic study of osteoblast and fibroblast response to roughness by means of surface-morphology gradients. Biomaterials, 28(13), 2175-2182. doi:10.1016/j.biomaterials.2007.01.019; c) Zelzer, M., Majani, R., Bradley, J. W., Rose, F. R. A. J., Davies, M. C., & Alexander, M. R. (2008). Investigation of cell-surface interactions using chemical gradients formed from plasma polymers. Biomaterials, 29(2), 172.

6. Chaudhury, M. K., & Whitesides, G. M. (1992). How to make water run uphill. Science, 256(5063), 1539. doi:10.1126/science.256.5063.1539

7. a) J. Genzer, J., & Bhat, R. R. (2008). Surface-Bound Soft Matter Gradients. Langmuir, 24(6), 2294-2317. doi:10.1021/la7033164; b) Morgenthaler, S., Zink, C., & Spencer, N. D. (2008). Surface-chemical and -morphological gradients. Soft Matter, 4(3), 419-434. doi:10.1039/B715466F; c) Genzer, J. (2012). Soft matter gradient surfaces methods and applications. Hoboken, N.J.: Wiley.

8. a) Efimenko, K., & Genzer, J. (2001). How to Prepare Tunable Planar Molecular Chemical Gradients. Advanced Materials, 13(20), 1560-1563. doi:10.1002/1521-4095(200110)13:20<1560::AID-ADMA1560>3.0.CO ; b) Barry, J. J. A., Howard, D., Shakesheff, K. M., Howdle, S. M., & Alexander, M. R. (2006). Using a Core–Sheath Distribution of Surface Chemistry through 3D Tissue Engineering Scaffolds to Control Cell Ingress. Advanced Materials, 18(11), 1406-1410. doi:10.1002/adma.200502719; c) Engler, A. J., Sen, S., Sweeney, H. L., & Discher, D. E. (2006). Matrix Elasticity Directs Stem Cell Lineage Specification. Cell, 126(4), 677-689. doi:https://doi.org/10.1016/j.cell.2006.06.044

9. Schedin, F., Geim, A. K., Morozov, S. V., Hill, E. W., Blake, P., Katsnelson, M. I., & Novoselov, K. S. (2007). Detection of individual gas molecules adsorbed on graphene. Nature Materials, 6(9), 652. doi:10.1038/nmat1967

10. Kuilla, T., Bhadra, S., Yao, D., Kim, N. H., Bose, S., & Lee, J. H. (2010). Recent advances in graphene based polymer composites. Progress in Polymer Science, 35(11), 1350-1375. doi:https://doi.org/10.1016/j.progpolymsci.2010.07.005

11. Hernández, S. C., Bennett, C. J. C., Junkermeier, C. E., Tsoi, S. D., Bezares, F. J., Stine, R., . . . Walton, S. G. (2013). Chemical Gradients on Graphene To Drive Droplet Motion. ACS nano, 7(6), 4746-4755. doi:10.1021/nn304267b

12. Parviz, D., Das, S., Ahmed, H. S. T., Irin, F., Bhattacharia, S., & Green, M. J. (2012). Dispersions of Non-Covalently Functionalized Graphene with Minimal Stabilizer. ACS nano, 6(10), 8857-8867. doi:10.1021/nn302784m

13. Dey, A., Chroneos, A., Braithwaite, N. S. J., Gandhiraman, R. P., & Krishnamurthy, S. (2016). Plasma engineering of graphene. Applied Physics Reviews, 3(2). doi:10.1063/1.4947188

14. Liu, Q., & Xu, B. (2015). Actuating Water Droplets on Graphene via Surface Wettability Gradients. Langmuir, 31(33), 9070-9075. doi:10.1021/acs.langmuir.5b02335

15. Siyan, D., Weifeng, S., Shile, F., Shiping, Z., Yan, X., Dan, L., . . . Yongmei, Z. (2017). Controlled droplet transport to target on a high adhesion surface with multi-gradients. Scientific Reports, 7(1). doi:10.1038/srep45687

16. a) Sun, G., Pan, Y., Zhan, Z., Zheng, L., Lu, J., Pang, J. H. L., . . . Huang, W. (2011). Reliable and Large Curvature Actuation from Gradient-Structured Graphene Oxide. The Journal of Physical Chemistry C, 115(48), 23741-23744. doi:10.1021/jp207986m

b)Anno, Y., Imakita, Y., Takei, K., Akita, S., & Arie, T. (2017). Enhancement of graphene thermoelectric performance through defect engineering. 2D Materials, 4(2), 025019. doi:10.1088/2053-1583/aa57fc ; c) Xin, X., Fei, Z., Ma, T., Chen, L., Chen, M.-L., Xu, C., . . . Ren, W. (2017). Circular Graphene Platelets with Grain Size and Orientation Gradients Grown by Chemical Vapor Deposition. Advanced Materials, 29(16), 1605451. doi:10.1002/adma.20160545

17. Alotaibi, F., Tung, T. T., Nine, M. J., Kabiri, S., Moussa, M., Tran, D. N. H., & Losic, D. (2018). Scanning atmospheric plasma for ultrafast reduction of graphene oxide and fabrication of highly conductive graphene films and patterns. Carbon, 127, 113-121. doi:https://doi.org/10.1016/j.carbon.2017.10.075

18. Moon, I. K., Lee, J., Ruoff, R. S., & Lee, H. (2010). Reduced graphene oxide by chemical graphitization. Nature Communications, 1, 73. doi:10.1038/ncomms1067

19. a) Tuinstra, F., & Koenig, J. L. (1970). Raman Spectrum of Graphite. The Journal of Chemical Physics, 53(3), 1126-1130. doi:10.1063/1.1674108 b) Ferrari, A. C. (2007). Raman spectroscopy of graphene and graphite: Disorder, electron–phonon coupling, doping and nonadiabatic effects. Solid State Communications, 143(1), 47-57. doi:https://doi.org/10.1016/j.ssc.2007.03.052

20. Eigler, S., Dotzer, C., & Hirsch, A. (2012). Visualization of defect densities in reduced graphene oxide. Carbon, 50(10), 3666-3673. doi:https://doi.org/10.1016/j.carbon.2012.03.039

21. Zuo, L., Zhang, S., Li, H., & Chen, H. (2015). Toward Highly Efficient Large-Area ITO-Free Organic Solar Cells with a Conductance-Gradient Transparent Electrode. Advanced Materials, 27(43), 6983-6989. doi:10.1002/adma.201502827

22. Xu, Y., Li, Z., & Duan, W. (2014). Thermal and Thermoelectric Properties of Graphene. Small, 10(11), 2182-2199. doi:10.1002/smll.201303701

23. Bark, H., Ko, M., Lee, M., Lee, W., Hong, B., & Lee, H. (2018). Thermoelectric Properties of Thermally Reduced Graphene Oxide Observed by Tuning the Energy States. ACS Sustainable Chemistry & Engineering, 6(6), 7468-7474. doi:10.1021/acssuschemeng.8b00094

24. Choi, J., Tu, N. D. K., Lee, S.-S., Lee, H., Kim, J. S., & Kim, H. (2014). Controlled oxidation level of reduced graphene oxides and its effect on thermoelectric properties. Macromolecular Research, 22(10), 1104-1108. doi:10.1007/s13233-014-2160-4

4.7 Supporting Information

Graphene based multifunctionally graded surfaces (MFGS)

Experimental Section

Materials: Natural graphite was supplied from Uley, Eyre Peninsula, South Australia. Potassium permanganate ($KMnO_4$, Sigma–Aldrich), 98 % sulphuric acid (H_2SO_4, Chem-Supply), phosphoric acid (H_3PO_4, Chem-Supply), 30% hydrogen peroxide (H_2O_2, Chem-Supply), 35 % hydrochloric acid (HCl, Chem-Supply) and ethanol (Chem-Supply) were used directly without further purification. High-purity milli-Q water (18.2 MΩ·cm at 25 °C, pH of 5.6).

Sample preparations: Natural graphite rocks (Uley, Eyre Peninsula, South Australia) supplied from a local mining site and milled into a fine powder using a bench top ring mill (Rocklabs) to make graphene oxide (GO). GO was synthesized using a modified Hammer's method as reported previously. [29, 30]. Glass slides (25nn x 75 mm) were cleaned using piranha solution (3 sulfuric acid:1 hydrogen peroxide) for 20 minutes followed by rinse with water for 10 minutes before drying at ambient condition. The GO dispersed into ethanol solution 0.5 mg/mL) and was then sprayed onto the glass substrates by a spray device (Neo For Iwata) with a diameter of 0.35mm nozzle.

Atmospheric plasma system (X4-800-USB from Diener Electronic GmbH + Co. KG, Germany) which includes plasma jet device and plasma controller is combined with scanning platform (software controlled) and a computer numerical control (CNC) box. The plasma device with a length of 210 mm and a nozzle diameter of 10 mm with X/Y/Z axis control can be moved over samples in both XY axis by a manual of software control. Air-plasma was

operated at a high voltage power supply (300 W, 20 kHz) and a high potential of ~10 kV was applied between anode and cathode for less than 1 minute to generate an arc discharge of plasma. To make film with GO-rGO gradients (20-25 mm lengths and 75 mm width), GO coated glass samples were placed at an angle of 45° to the plasma jets before scanning in order to get asymmetrical intensity of plasma stream across the surface. The critical parameter here to achieve controllable gradients with continuous change across surface is to adjust the distances between plasma nozzle and GO films. Different distances were initially tested to achieve optimized gradients with 25 mm length with constant horizontal scanning speed cc ~ 15 mm/min). With this method the length of the gradient is limited by the length of asymmetrical plasma beam but their width is unrestricted and depends of the size of sample (in our case limited by the 75 mm size of glass slide). To make longer gradients (>7 mm) GO samples were placed horizontally on scanning stage and treated by plasma beam (at 90°) by different speed of the stage movement to achieve a gradual plasma exposure across the whole length of substrate (75 mm). Alternatively, the same results can be achieved by gradual moving of the plasma jet by software.

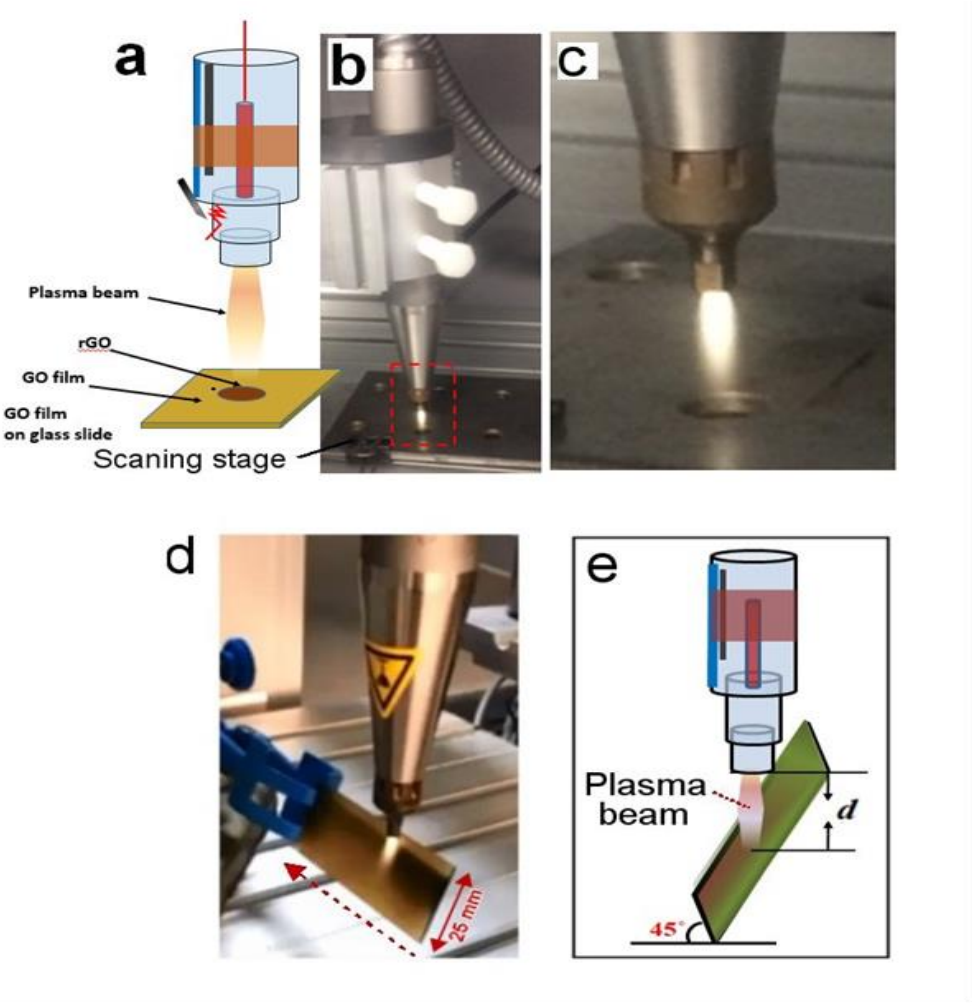

Figure 4S1. Fabrication set-up with plasma system used for preparation GO-rGO gradients showing plasma jet and the system for preparation shorter gradients where plasma jet is scanned with constant distance over the sample with 45 °.

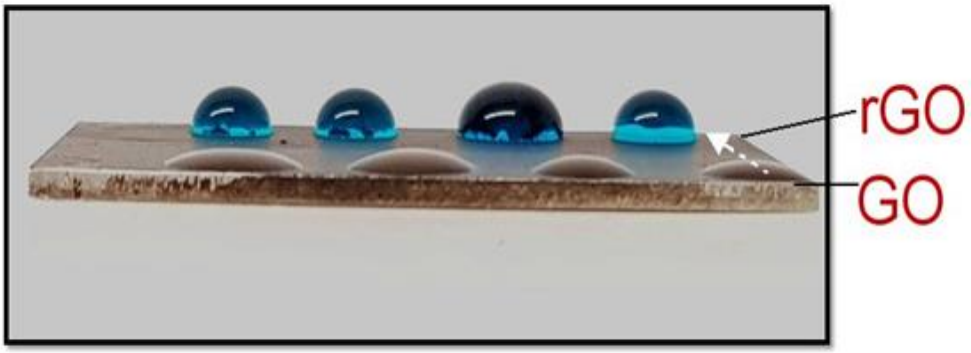

Figure 4S2. Photos of water droplets on GO-rGO gradients fabricated on glass slide.

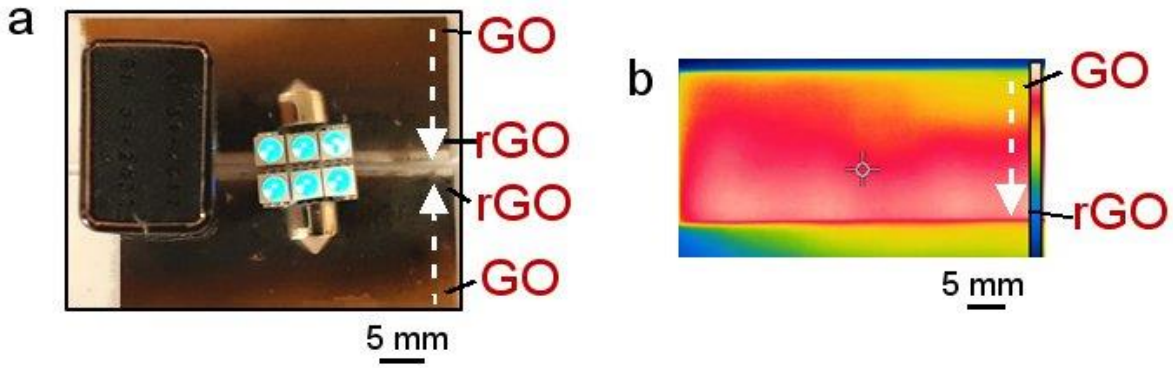

Figure 4S3. a) Photo showing of high conductivity of rGO section in gradient and b) photo of thermal gradients showing different thermal conduction after heating samples at hot plate.

Blank Page

Chapter 5

Silver nanowires with pristine graphene oxidation barriers for stable and high performance transparent conductive films

Statement of Authorship

Title of Paper	Silver Nanowires with Pristine Graphene Oxidation Barriers for Stable and High Performance Transparent Conductive Films
Publication Status	☑ Published ☐ Accepted for Publication ☐ Submitted for Publication ☐ Unpublished and Unsubmitted w ork w ritten in manuscript style
Publication Details	ACS Appl. Nano Mater. 2018, 1, 2249−2260

Principal Author

Name of Principal Author (Candidate)	Faisal Alotaibi		
Contribution to the Paper	Under the supervison of Prof Dusan Losic developed ,designed and conducted the experitments , interpreted ,processed the data ,wrote manuscript draft ,edited and revised for submission .		
Overall percentage (%)	80%		
Certification:	This paper reports on original research I conducted during the period of my Higher Degree by Research candidature and is not subject to any obligations or contractual agreements with a third party that would constrain its inclusion in this thesis. I am the primary author of this paper.		
Signature		Date	05 - 03 - 2019

Co-Author Contributions

By signing the Statement of Authorship, each author certifies that:

i. the candidate's stated contribution to the publication is accurate (as detailed above);
ii. permission is granted for the candidate in include the publication in the thesis; and
iii. the sum of all co-author contributions is equal to 100% less the candidate's stated contribution.

Name of Co-Author	Tran Thanh Tung		
Contribution to the Paper	CO-supervise aided in developement of the expierment , edited the manuscript		
Signature		Date	05/3/2019

Name of Co-Author	Md Julker Nine		
Contribution to the Paper	Runging the TA Instruments ,edited the manuscript		
Signature		Date	05-03-2019

Please cut and paste additional co-author panels here as required.

Name of Co-Author	Campbell J. Coghlan,		
Contribution to the Paper	Edited the manuscript .		
Signature		Date	

Name of Co-Author	Dusan Losic		
Contribution to the Paper	Act as the primary supervisor ,aided in design and developement of the expierment and evaluation and edited the mansucript for submission		
Signature		Date	8/05/2019

ACS APPLIED NANO MATERIALS
Cite This: ACS Appl. Nano Mater. 2018, 1, 2249−2260
Article
www.acsanm.org

Silver Nanowires with Pristine Graphene Oxidation Barriers for Stable and High Performance Transparent Conductive Films

Faisal Alotaibi,[†,‡] Tran Thanh Tung,[†,‡] Md Julker Nine,[†,‡] Campbell J. Coghlan,[†,‡] and Dusan Losic*[,†,‡]

[†]School of Chemical Engineering and [‡]ARC Research Hub for Graphene Enabled Industry Transformation, The University of Adelaide, Adelaide, SA 5005, Australia

Supporting Information

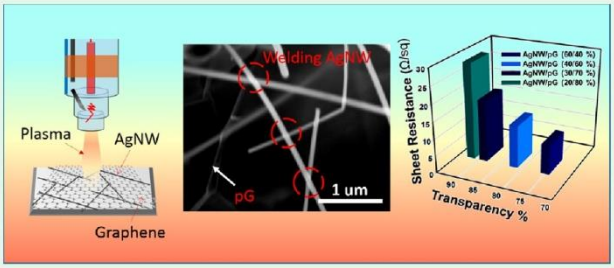

ABSTRACT: One-dimensional (1D) silver nanowires (AgNWs) have emerged as a leading candidate for the development of next-generation optoelectronic and wearable electronic devices. However, a key limitation of AgNW electrodes is that they are readily oxidized, resulting in a shift in properties leading to devices becoming erratic over time. To address this problem, we report a facile method to improve both the stability and performance of AgNW films. The AgNWs were combined with pristine graphene (pG) using an optimal (30/70 wt %) with the goals to prove that the pG sheets can provide a barrier shielding to protect against AgNW oxidation and have the additional benefit of improving the connections between wires and stability of the films. The fabrication of these films was demonstrated on wide range of substrates including glass, plastic, textile, and paper. A surface resistance of 18.23 Ω/sq and an optical transparency of 89% were obtained on the glass substrates, 50 Ω/sq and 88% transparency for poly(ethylene terephthalate) (PET), and 0.35 Ω/sq resistance on the textile substrate. Atmospheric pressure plasma jets (APPJ) treatment was further used to enhance the performance of the film (i.e., glass), resulting in a significant reduction of 30.6% in sheet resistance (15.20 Ω/sq) and an improvement of transparency to 91%. The stability of AgNW/pG film under environmental conditions and higher temperatures was significantly improved, showing only a minor increase in the sheet resistance after 30 days and at temperature increases up to 300 °C when compared with control (AgNW film) which shows a sharp increase after 8−10 days and is thermally stable until 150 °C as a result of Ag oxidation.

KEYWORDS: *silver nanowires, pristine graphene, silver nanowire films, conductive films, graphene films, transparent electrodes*

INTRODUCTION

Development of new nanomaterials and their specific properties are critically important for the development of low-cost, multifunctional, and easy-to-use optoelectronic devices. Transparent conductive films (TCFs) are essential components in devices including organic light-emitting diodes (OLEDs),[1] liquid crystal displays (LCDs),[2] touch screen panels (TSPs),[3] sensors,[4] flexible loudspeakers,[5] and organic solar cells (OSCs).[6] Indium tin oxide (ITO),[7] and fluorine tin oxide (FTO)[8] are two commonly commercialized TCFs materials owing to their excellent conductivity ($R < 30$ Ω/sq) and high transmittance (>90%).[9,10] However, the increasing cost of indium and other rare earth elements materials along with the brittleness and inability of ITO to be etched, patterned, or processed at high temperatures has limited its TCF applications. FTO materials suffer from low transparency in the near-infrared region and current leakage caused by its structural defects.[4]

To address these limitations and replace ITO/FTO materials, a broad range of nanomaterials including metal nanotroughs,[9] metal nanorods and nanowire networks,[10,11] carbon nanotube (CNT), and graphene films and their composites have been explored.[4,12] These materials provide comparable or improved electrical conductivity, transparency, and mechanical strength when compared to both ITO and FTO materials.[13] Silver nanowire (AgNW) has emerged as a leading alternative to ITO/FTO due to its high electrical conductivity (6.3×10^7 S/m) and high optical transmittance

Received: February 23, 2018
Accepted: April 30, 2018
Published: April 30, 2018

DOI: 10.1021/acsanm.8b00255
ACS Appl. Nano Mater. 2018, 1, 2249−2260

Blank Page

Chapter 5:

Silver nanowires with pristine graphene oxidation barriers for stable and high performance transparent conductive films

5.1 Abstract

One-dimensional (1D) silver nanowires (AgNWs) have emerged as a leading candidate for the development of next-generation optoelectronic and wearable electronic devices. However, a key limitation of AgNW electrodes is that they are readily oxidized, resulting a shift in properties leading to devices becoming erratic over time. To address this problem, we report a facile method to improve both the stability and performance of AgNW films. The AgNWs were combined with pristine graphene (pG) using an optimal (30/70 wt.%) with the goals to prove that the pG sheets can provide a barrier shielding to protect against AgNW oxidation and have the additional benefit of improving the connections between wires and stability of the films. The fabrication of these films was demonstrated on wide range of substrates including glass, plastic, textile and paper. A surface resistance of 18.23 Ω/sq and an optical transparency of 89 % was obtained on the glass substrates, 50 Ω/sq and 88% transparency for polyethylene terephthalate (PET), and 0.35 Ω/sq resistance on the textile substrate. Atmospheric pressure plasma jets (APPJ) treatment was further used to enhance the performance of the film (i.e. glass) resulting in a significant reduction of 30.6% in sheet resistance (15.20 Ω/sq) and an improvement of transparency to 91%. The stability of AgNW/pG film under environmental conditions and higher temperatures was significantly improved showing only a minor increase in the sheet resistance after 30 days and at

temperature increases up to 300 °C when compared with control (AgNW film) which shows a sharp increase after 8-10 days and is thermally stable until 150 °C as result of Ag oxidation.

Keywords. Silver nanowires, pristine graphene, silver nanowire films, conductive films, graphene films, transparent electrodes

5.2 Introduction

Development of new nanomaterials and their specific properties are critically important for the development of low-cost, multifunctional and easy-to-use optoelectronic devices. Transparent conductive films (TCFs) are essential components in devices including organic light-emitting diodes (OLEDs)[1], liquid crystal displays (LCDs)[2], touch screen panels (TSPs)[3], sensors[4], flexible loudspeakers [5], and organic solar cells (OSCs) [6]. Indium tin oxide (ITO) [7], and fluorine tin oxide (FTO) [8], are two commonly commercialized TCFs materials owing to their excellent conductivity ($R < 30$ Ω/square) and high transmittance (>90%) [9,10]. However, the increasing cost of indium and other rare earth elements materials along with the brittleness and inability of ITO to be etched, patterned or processed at high temperatures has limited its TCF applications. FTO materials suffer from low transparency in the near-infrared region and current leakage caused by its structural defects [4].

To address these limitations and replace ITO/FTO materials a broad range of nanomaterials including metal nanotroughs[9], metal nanorods and nanowire networks [10,11], carbon nanotube (CNT), graphene films and their composites have been explored [4,12]. These materials provide comparable or improved electrical conductivity, transparency and mechanical strength when compared to both ITO and FTO materials [13]. Silver nanowire

(AgNW) has emerged as a leading alternative to ITO/FTO due to its high electrical conductivity (6.3×10^7 S/m) and high optical transmittance (80 – 90%) [11-13].Nevertheless, current generation AgNW films suffer from instability due to oxidation and atmospheric corrosion when exposed to natural light, humidity and gas (i.e hydrogen sulfide), resulting in a loss in conductivity that limited their use in practical applications [15,16]. The oxidation of AgNWs at the wire junctions, caused by exposure to moisture and air, results in the formation of silver oxides, i.e., AgO, Ag_2O or Ag_2S, which leads to sharp increases in resistance of electrical–conductivity [15,16]. To overcome this problem, multiple methods have been proposed including sintering in reducing environment, room and/or low temperature welding processing, plasmonic welding, optical sintering to weld the junction and combining other materials to form a stable network, or coating layer on AgNWs to improve stability under ambient storage conditions. It has been reported that the stability of AgNW film can be improved by combining AgNWs with other materials such as carbon nanotubes, graphite, conductive polymers (i.e. PEDOT) and metal nanowires [12, 17-20]. However, the addition of other materials can affect surface roughness, optical transparency and the contact point of the devices that can dramatically reduce the overall performance of TCEs in different applications.

Graphene and its outstanding electrical and thermal conductivity along with high temperature stability, impermeability, chemical inertness, optical transparency and barrier properties makes it particularly attractive for the versatile applications in transparent electrodes of optoelectronic devices [21-24]. Graphene is also recognized as a promising material for many other engineering applications [25-27]. It has previously been shown to address the limitations of AgNWs and improve performances of AgNW-based composite films. For

example chemical vapor deposition (CVD) growth graphene and graphene oxide (GO) have been used to wrap AgNWs and the composite material provided a sheet resistance (Rs) of 22 Ω/sq at the optical transparency (T) of 88% [28], and an Rs of 14 Ω/sq at a T of 88% [29], respectively. CVD graphene has also been shown to improve the optical sintering efficiency under xenon flash lamp treatment allowing for the formation of high yield stacked graphene/AgNWs which has a Rs of 18.5 Ω/sq at the transmittance of 87% [30]. The performances of these hybrid materials are comparable and in some cases superior to the ITO-based TCEs and making them ideal to supplant them in practical applications for the development of a new generation of high performance TCEs. However, the methods based on CVD graphene growth are expensive for production and establishing facilities and have limited scalability. In comparison, the use of GO and its reduced form (rGO) is reported, but with limits to considreably improve the film conductivity and stability. The possible solution to overcome these limitations is to use the combination of AgNW with pristine graphene (pG) which has significantly better conductivity, lower defects and higher stability compared to previously used graphene materials. The pG material produced from natural graphite by low cost and scalable processes could significantly reduce the cost and production scalability of these hybrid films. Surprisingly this option is not yet explored that requires new research to determine the performance of the hybrid films in terms of “conductive transparent film”, adhesion and especially stability with respect to environment and high temperature.

In this scenario this paper presents several new approaches toward the development of hybrid AgNW/pG films with high conductivity, transparency and stability for a broad range of applications including flexible and wearable electronic devices. The rationale of our approach is to combine the high conductivity and barrier properties of pG sheets with the superior

conductivity of AgNWs to achieve the synergistic effect of 1D-2D inorganic-organic hybrid obtained by atmospheric pressure plasma jets (APPJs) treatment for considerable improving conductivity and stability of the films while maintaining transparency. A demonstration of a proposed concept for fabrication of high performing the AgNW/pG flexible transparent films is shown in **Figure 5.1**. In this concept, firstly we formulated and optimized AgNW/pG ink using different ratio of pG and AgNWs and prepared series of coated films on four different substrates including glass, flexible polyethylene terephthalate (PET), textile and paper. Subsequently, a fast APPJ treatment (Figure 5.1a) on the prepared AgNW/pG thin films was carried out to improve connection between AgNWs and the resulting film showed a significant improvement in performance due to the reduced sheet resistance and increased optical transparency (Figure 5.1b). This resolves the most challenging aspect of making transparent conductive electrodes/films. The series of prepared films were characterized to confirm their structures, composition and evaluate their conductivity, transparency and stability compared with bench mark films required for commercial applications.

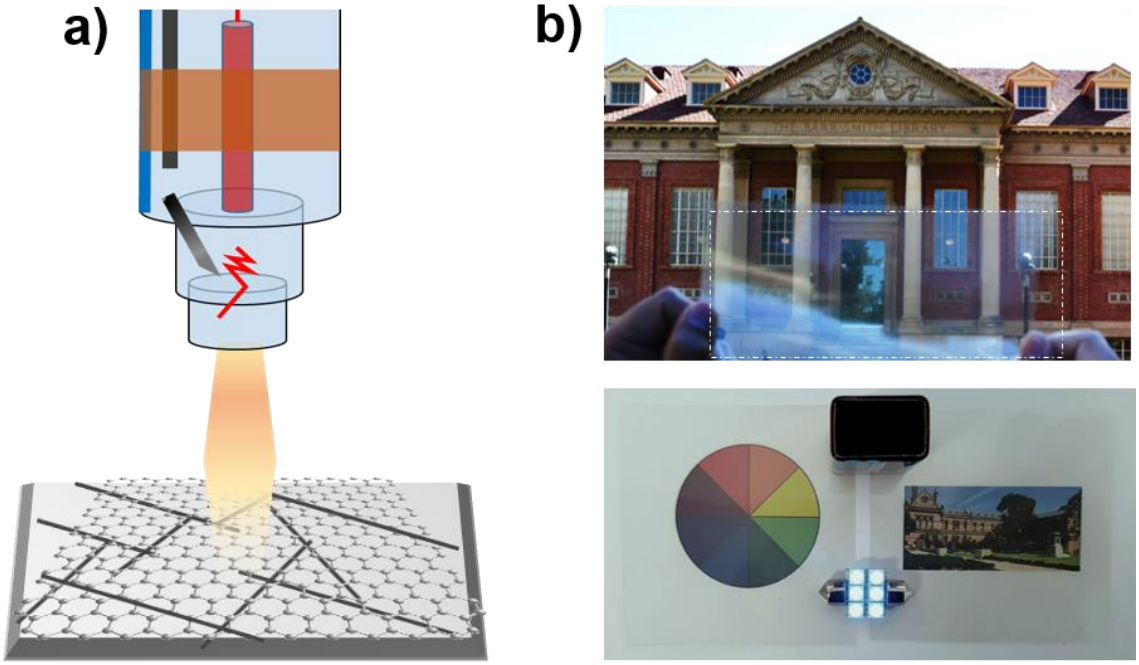

Figure 5.1. Schematic presentation of (a) the plasma enhancement of AgNW/graphene composite thin film that provides welding AgNWs at their junctions; (b) a demonstration of the flexible transparent electrode of AgNW/pG hybrid for lighting LED.

5.3 Experimental section

5.3.1 Materials and chemicals

Graphite flakes with a purity of 99.9% was supplied from Valence industry, Unley, South Australia. Silver nitrate ($AgNO_3$), polyvinylpyrrolidone (PVP, MW~ 55,000), tetraproplylammonium bromide (TBAB) and ethylene glycol (EG), sodium chloride (NaCl) , isopropyl alcohol (≥ 99.7%,) were purchased from Chem-Supply Pty Ltd.

5.3.2 Preparation of silver nanowire (AgNWs) and pristine graphene (pG)

A modified polyol synthesis method was used to prepare AgNWs though the reduction of $AgNO_3$ (precursor) by EG as a solvent reduction in the presence of PVP as stabilizer and capping agent, TBAC as an ionic additive as described previously [31,32]. Briefly, PVP (2.0 g), TBAB (45 mg) and a mediated agent of NaCl dissolved in EG (100 mL) in a 250 mL three-necked flask, and then heated up to 100 °C. A precursor of the $AgNO_3$ solution was made by dissolving $AgNO_3$ (2.2 g) in EG (60 mL) by gentle stirring for 10 min before being added dropwise into the mixture. The mixture was heated to 145 °C, maintained for 30 min then cooled to room temperature. The AgNWs after washing with ethanol to remove residual

PVP, solvent EG and unreacted agents were collected and re-dispersed into ethanol solution at a concentration of 0.7 mg ml^{-1}.

Pristine graphene was prepared by mechanical high shear exfoliation of expanded graphite as previously described [33]. Briefly, expanded graphite (1 g) was sonicated for 30 min in a solvent mixture of water and acetone (500 mL) without using any surfactant or stabilizer, followed by high shear mixing at very high shear speed for at least 1 h. The graphene exfoliation was collected and dried in a convection oven (70 °C).

5.3.3 Preparation of silver nanowire and pristine graphene ink (AgNW/pGs)

Conductive ink AgNW/pGs was prepared by dispersing graphene in isopropyl alcohol and mixing with the AgNWs solution in different weight percentage ratios (60:40, 40:60, 30:70, 20:80) followed by bath sonicated for 30 min.

5.3.4 Preparation of silver nanowire and pristine graphene composite films (AgNW/pG) on glass, PET and textile substrates

Glass substrates (2.5 × 2.5 cm) were cleaned using piranha solution (H_2SO_4:H_2O_2 of 3:1)) for 20 min followed by cleaning with DI water for 10 min and then dried using compressed air for 20 s. The AgNW/pG ink (30:70 wt.%) was then spray coated onto a glass substrate using a spray device (Neo For Iwata) with 0.35 mm nozzle onto heated substrate (80 °C) to ensure the evaporation of isopropyl alcohol. The spraying distance and spraying pressure of the nozzle was 12 cm, and 220 mbar, respectively. Atmospheric pressure plasma jets (APPJs) was preformed using the system which was explained in detail in our previous work [34]. The

APPJ operated at a high voltage power supply (300 W, 20 kHz) and a high potential of ~10 kV was applied between anode and cathode for 1 min to generate an arc discharge of plasma. The distances between plasma nozzle and AgNW/pG films was optimized at 20 mm, and the exposure time towards plasma irradiation was surveyed with 0, 3, 6, 9, 12 and15 s.

For preparation of flexible films, the AgNW/pG ink was applied to A4 size poly (ethylene terephthalate) (PET) substrates by a manually controlled wire-wound rod (Meyer rod) and dry at 60 °C for 5 min.

To prepare conductive fabrics, the AgNW/pG ink was applied to a 100 mm × 100 mm HYTEX® 1000 fiberglass textile substrates by spray coating with (Neo For Iwata) 0.35mm nozzle and dried in oven at 60 °C for 5 min to guarantee a fast evaporation of Isopropyl alcohol or ethanol.

5.4 Characterization

The morphology of the prepared films was characterized by a scanning electron microscope (SEM) at an accelerating voltage of 10 kV. Transmission electron microscopy (TEM) analysis was carried out by using a TEM (Tecnai G2 Spirit) operated at 120kV. The sheet resistance of AgNW TCFs was measured by using a standard four-point probe method (Jandel RM3000 Test Unit, USA). Optical transmittance spectra were obtained on a UV−vis−NIR spectrometer**.** X-ray diffraction (XRD) patterns were recorded using a Rigaku-Miniflex 600, X-ray diffractometer (Japan) using Cu-Kα radiation. Raman spectra were taken using a HORIBA scientific instrument (LabRam HR800 Ev, Jobin Yvon, Horiba, France) for the graphene species. Vibrational stretching mode of different oxygen functional groups in AgNWs and AgNW/pG were studied by Fourier transform infrared spectroscopy (FTIR)

(Nicolet 6700 Thermo Fisher, USA). Thermogravimetric analysis was accomplished by a TA instruments (Q-500, Tokyo, Japan) in the N_2 atmosphere.

5.5 Results and discussion

5.5.1 The structural and composition characterization of AgNW/pG thin films

The structural characteristics and morphology of AgNWs and pG used for inks formulations and the films preparation are shown in **Figure 5.2**. SEM images of AgNWs (**Figure 5.2a and b**) show well-defined nanowires structures with long and thin AgNWs. The size and length of nanowires structure were optimized by modifying the synthetic parameters to achieve their optimal length of 30 - 50 µm and diameter of 30-50 nm. These dimensions are critical for obtaining superior optical and electrical properties in combination with the size of graphene sheets. The structure of dispersed pG sheets were confirmed by SEM imaging in **Figure 5.2 c and d** showing a quite larger size ranging from 10 to 30 µm with 3 to 15 layers confirmed by TEM and AFM measurements (see Supporting Information, S1) as well as Raman characterization. The chemical structure of the pG was also analyzed which indicated a low concentration of oxygen of 4.48 (At.%) and an O:C ratio of 0.041, which is similar to the 0.047 ratio of expanded graphite precursor.

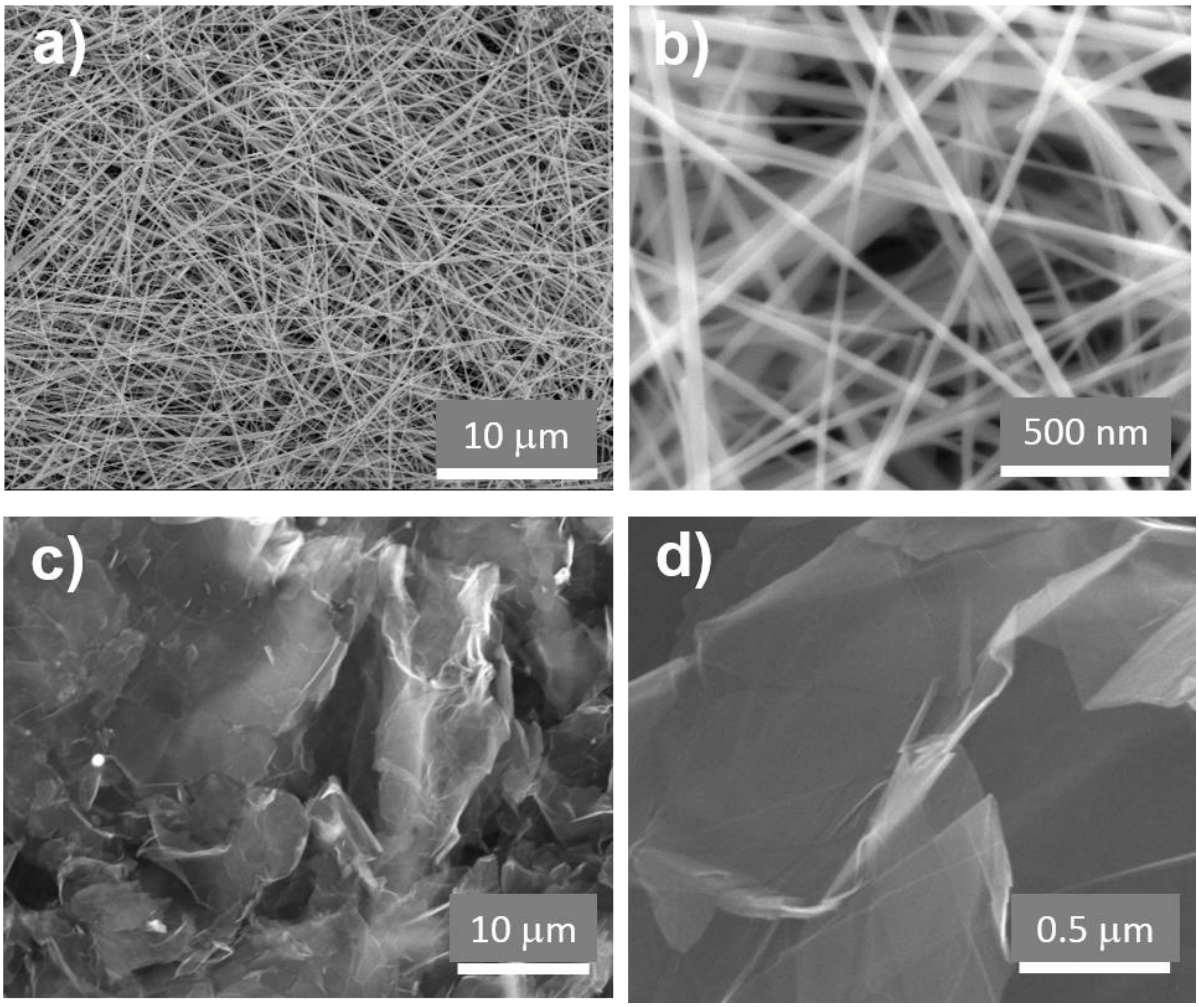

Figure 5.2. Morphology of two initial materials in powder form: AgNWs and pG used for inks formulation and preparation of conductive transparent films. (a-b) SEM images of AgNWs with optimized shapes and sizes providing better optical and electrical properties, and (c-d) SEM images of shear exfoliated pG sheets with few layers.

The SEM images of prepared AgNW/pG films are presented in **Figure 5.3**. The images confirmed that graphene sheets are incorporated into a AgNWs network showing multilayered film structures which can be seen in **Figure 5.3** (a and b). TEM images (**Figure 5.3c and d**) revealed the interconnections between AgNWs (30 – 50 nm) and graphene. The AgNWs are interconnected in two ways: direct crossed-wire junctions at lateral level and

through graphene with wires vertically in next layer. This multilayer structures of film composed with 1D (AgNW) and 2D (pG) structure is critical to minimizes the high-resistance junctions in AgNW networks observed in previous work which are dominant, and determines the other properties (e.g., optical and mechanical) of the hybrid films [35,36]. The resistance in the NW network is related to the length, density and diameter of nanowires and can be described by following equation:

$$R_S \sim (D - N_C)^{\alpha} L_S^{\beta}$$

Where D is the density of the NW, L is the average NW length, α is a parameter related to spatial arrangement, and β is a parameter related to junction resistance and intrinsic conductivity of the material.

It is important to state that the dimensions (length and diameter) of prepared AgNWs used in this work were optimized to ensure minimal resistance. A network with longer NW with a small diameter but higher density shows lower resistance due to its percolative nature.

The addition of superhydrophobic pG with a contact angle (CA) value of 143 ± 2° into hydrophilic AgNWs (**Figure 5.3e**) resulted in a significant change to the wettability of the AgNWs by increasing the contact angle up to 129 ± 2° in the AgNW/pG (**Figure 5.3f**) enhancing its moisture repellent properties.

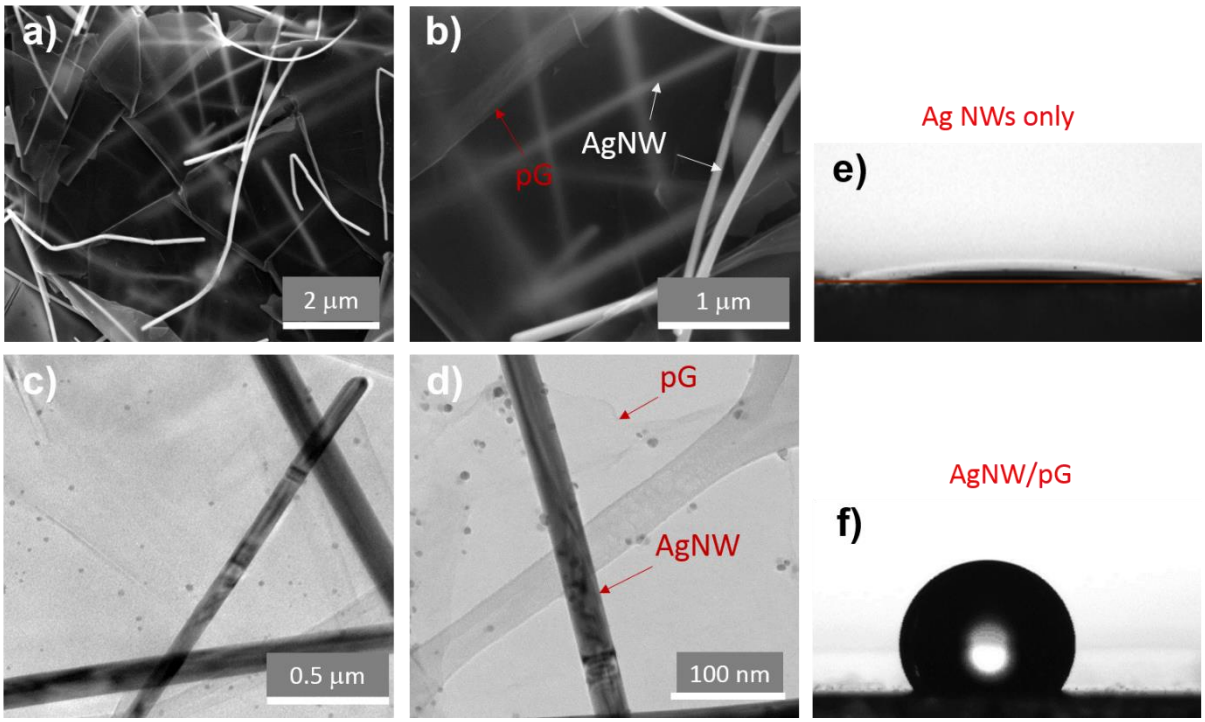

Figure 5.3. (a-b) SEM images of the AgNW/pG hybrid film showing graphene sheets intercalated AgNWs resulted in interconnected AgNW networks on both sides of graphene surface; (c-d) The TEM images show AgNWs with thin diameter ranging from 30 to 50 nm are randomly aligned over graphene surface which determines electrical, optical and mechanical properties of the hybrid films; and (e-f) water contact angle (CA) of AgNW and AgNW/pG films confirmed their hydrophilic and hydrophobic interfacial properties, respectively.

The XRD pattern of prepared pG is presented in **Figure 5.4 a** showing a major peak of 2θ position at 26.5° (C(002)) which is typical of high quality graphene material. The C(002) peak has well-defined shape in the AgNW/pG film but is less crystalline when contrasted against metallic silver which displayed 2θ at 38°, 44°, 64° and 77° corresponding to the

planes of (111), (200) and (311) of face-centered cubic Ag. This result confirms the formation of the composite material of AgNWs and graphene.[37] The Raman spectrum of pG presented in **Figure 5.4b**, shows three typical graphene bands: D-band (1350 cm^{-1}), G-band (1580 cm^{-1}) and 2D-band (2688 cm^{-1}) [38,39]. While the positions of D and G peaks are shifted slightly towards the right 8 cm^{-1} and 3 cm^{-1}, respectively, these peaks are less symmetric, have higher intensity and display an increase of the full-width-at-half-maximum (FWHM) in the hybrid AgNW/pG material [40,41]. This behavior suggests that not only that there is additional disorders and defects caused by the AgNWs incorporated graphene sheets, but also that there is a charge doping effect between the two materials in the film. In addition, the 2D peak in the hybrid material has shifted considerably (15 cm^{-1}), and a narrow FWHM and reduction in its intensity were observed, which is due to the increasing electron-hole scattering, in which the AgNWs cause surface-enhanced Raman scattering (SERS) activity in the hybrid materials [42].

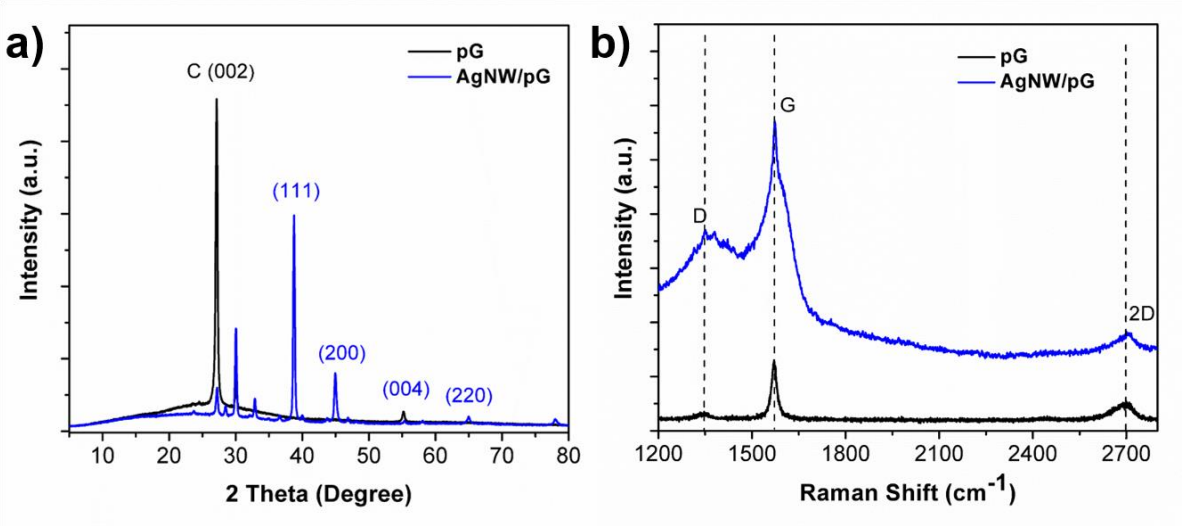

Figure 5.4. (a) XRD patterns of pG and AgNW/pG film showing the 2θ position at 26.5 corresponds to (002) honeycomb network, whereas 2θ position of 38° (111), 44° (200), 64° (220), 77° (311) correspond to metallic AgNWs network. (b) Raman spectrum of pG showing typical signature of graphene and AgNW/pG hybrid film indicates high disorder level of pG sheets due to AgNWs sitting on both surfaces of the graphene sheet.

5.5.2 The sheet resistance and transparency of AgNW/pG thin films

Solution processing using inks is typically seen to be the most effective method for scaling up production of transparent conductive films using graphene composites because of its low-cost fabrication method. To prepare inks with well-dispersed conductive fillers it is critical to overcome the van der Waals interactions between pG sheets and AgNWs using different dispersants and solvents. Usually, for dispersion of materials a surfactant is used to reduce the surface tension before coating, as the viscosity of the material is maintained which prevents contact line recession and de-wetting. However, there is a typically negative effect of their additions on the conductivity and/or a shift in the properties of the conductive material due to

their insulating nature. In our approach, a small residual amount of PVP can be detected on the surface of the AgNWs after washing (purifying) forming a thin layer of ~ 0.62- 0.68 nm (see Supporting Information, S2). This layer acts as surfactant in the hybrid inks, where the AgNWs and graphene sheets are stabilized in a colloid system. The AgNW and graphene ratio has been investigated for transparent electrode performance, which is a trade-off between surface resistance and optical transparency of the films. For fabrication of the transparent conductive films, the as-formulated AgNW/pG inks with differing ratios were coated onto (2.4 x 2.4 cm) glass and A4 size PET substrates by spray coating and bar coating, respectively.

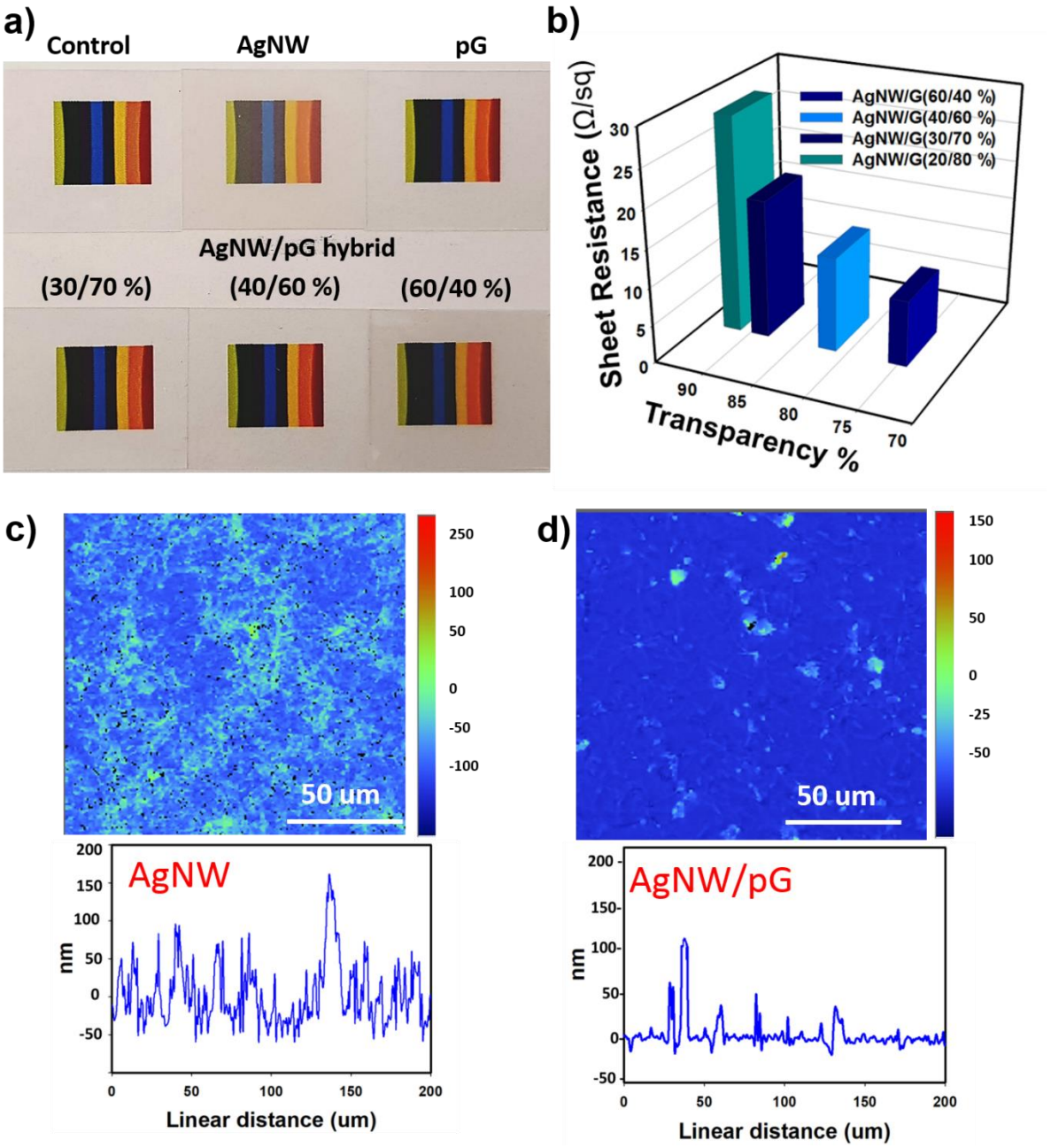

Figure 5.5. (a) Optical images of glass (control), AgNW and pG only film (top) and the composite AgNW/pG films (bottom) prepared spray coating onto glass substrates, using different AgNW/pG ratio; (b) the influence of AgNW/pG ratio on the sheet resistance and transparency. Comparative topography images and surface profile of (c) AgNW film and (d) AgNW/pG film showing the pG-reduced roughness surface.

The influence of AgNW/pG ratios on the performance (sheet resistance and transparency) of the prepared conductive films on glass substrates is presented in **Figures 5.5.** Optical images of prepared samples by spray coating on glass (**Figure 5.5a**) showed a comparative visual appearance of thin films, in which the reference samples of both pG and AgNW films were also prepared using the same volume of ink for coating. It can be observed the visual appearance was controlled by the AgNW/pG ratio, and the optical transparency of the film is likely determined by the silver nanowires content due to their lower aspect ratio resulted in lower electrical percolation thresholds (compared to the pG). Results in **Figure 5.5b** show that increasing the AgNW concentration in AgNW/pG films (or ink formulations) resulted in a decrease in sheet resistance (Rs) and transparency (T). The highest T value of 95% and Rs of 26 Ω/sq was achieved for the 20/80 wt% ratio, while the lowest Rs = 6 Ω/sq at T = 75% for the 60/40 wt.% ratio. These results can be explained by the fact that the abundance of AgNWs forming overlapping networks and the reduction in surface smoothness arising from unwanted agglomeration negatively impacting transparency. This can be observed in the optical images and their profile, while the AgNW film (**Figure 5.5c**) showed an inhomogeneous and rough surface the AgNW/pG (30/70 wt.%) showed less roughness at the nanoscale level (**Figure 5.5d**).

To demonstrate the scalability for the generation of flexible transparent electrodes at large scale, thin AgNW/pG films were fabricated by coating onto a A4 sized PET substrate. **Figure 5.6 a and b** show the prepared flexible electrode and the light being produced from the LED confirming their electrical conductivity. The flexible films exhibit a similar trend observed on glass substrates on influence of AgNW/pG ratio on their Rs and T (**Figure 5.6 c and d).** The Rs values were in the range of 20 to 60 Ω/sq and T ranging from 73 to 92% based on the

variation of AgNW/pG ratio from 20/80 to 60/40 wt.%. The produced AgNW/pG film on PET (30/70 wt.%) with an Rs of 50 Ω/sq at T = 88% again showed the best performances that for flexible electrodes with applications in optoelectronic devices.[36,39]

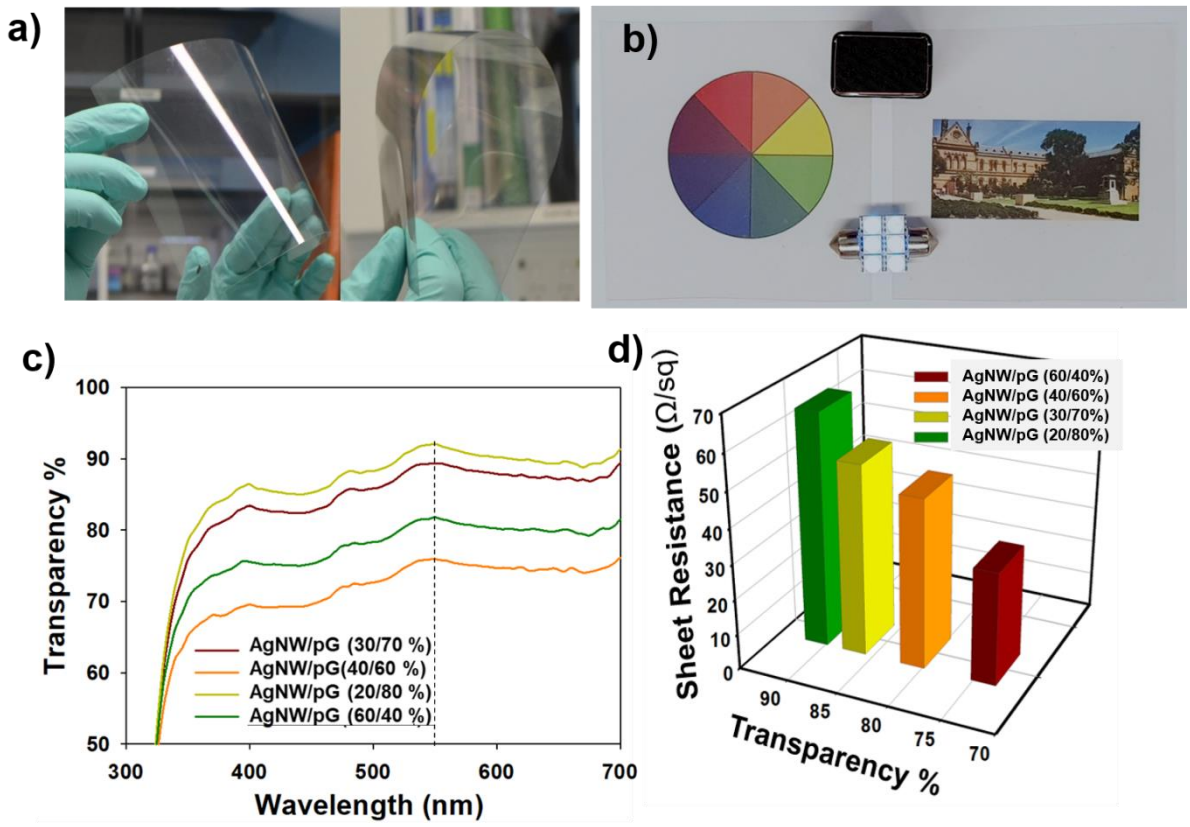

Figure 5.6. (a-b) Optical images of flexible and transparent conductive AgNWs/pG films manufactured by a draw-bar coating hybrid inks onto PET substrate showing electrical conductivity with LED light. (c-d) The influence of AgNW/pG ratio on the sheet resistance and transparency.

Analysis of the results shown above determined that the optimal ink formulation was AgNW/pG (30/70 wt.%) as it provided great performance based on the best trade-off between the resistance and transparency in the films. The high performance of present transparent electrodes on both rigid and flexible substrates is achieved principally by the synergistic

effect between AgNWs and pG, where 1D conducive AgNWs are assembled onto large interconnected networks and 2D conductive graphene is intercalated between them.

In order to evaluate the coatings performances of the optimized AgNW/pG (30/70 wt.%) on different substrates, the ink formulation was spray coated on selected non-conductive substrates including textile, elastomer PDMS and cellulosic filter paper and their conductivity results were summarized in **Figure 5.7**. SEM images from the top surface of these AgNW/pG films on of the textile (**Figure 5.7 a and b**), PDMS (**Figure c and d**) and filter paper (**Figure 5.7 e and f**) show rough surfaces of AgNW/pG composites contained both AgNWs and pG formed conductive pathways on the insulative substrates. Results show that increasing the number of coating layers decreases the sheet resistance of the films allowing for the tuning of resistance in the range of several Ω to few tens of Ω (data not shown). For example, the conductive textile (**Figure 5.7g**) with multilayer coatings showed a resistance of 1-3 Ω for conducting a LED, while conductive paper (**Figure 5.7h**) with the same thickness displayed a resistance of 35 Ω (measured by a multimeter for across a distance of ~15 cm). These data suggests that by developing the AgNW/pG inks it is possible to make highly conductive films on the broad range of materials including different type of textiles (fabric), plastics and cellulosic materials (paper). This opens up new possibilities for designing, low-cost and scalable production of flexible, stretchable and wearable electronics on these materials that is completive to other commercial conductive inks which are more expensive and have larger environmental footprint including toxicity.

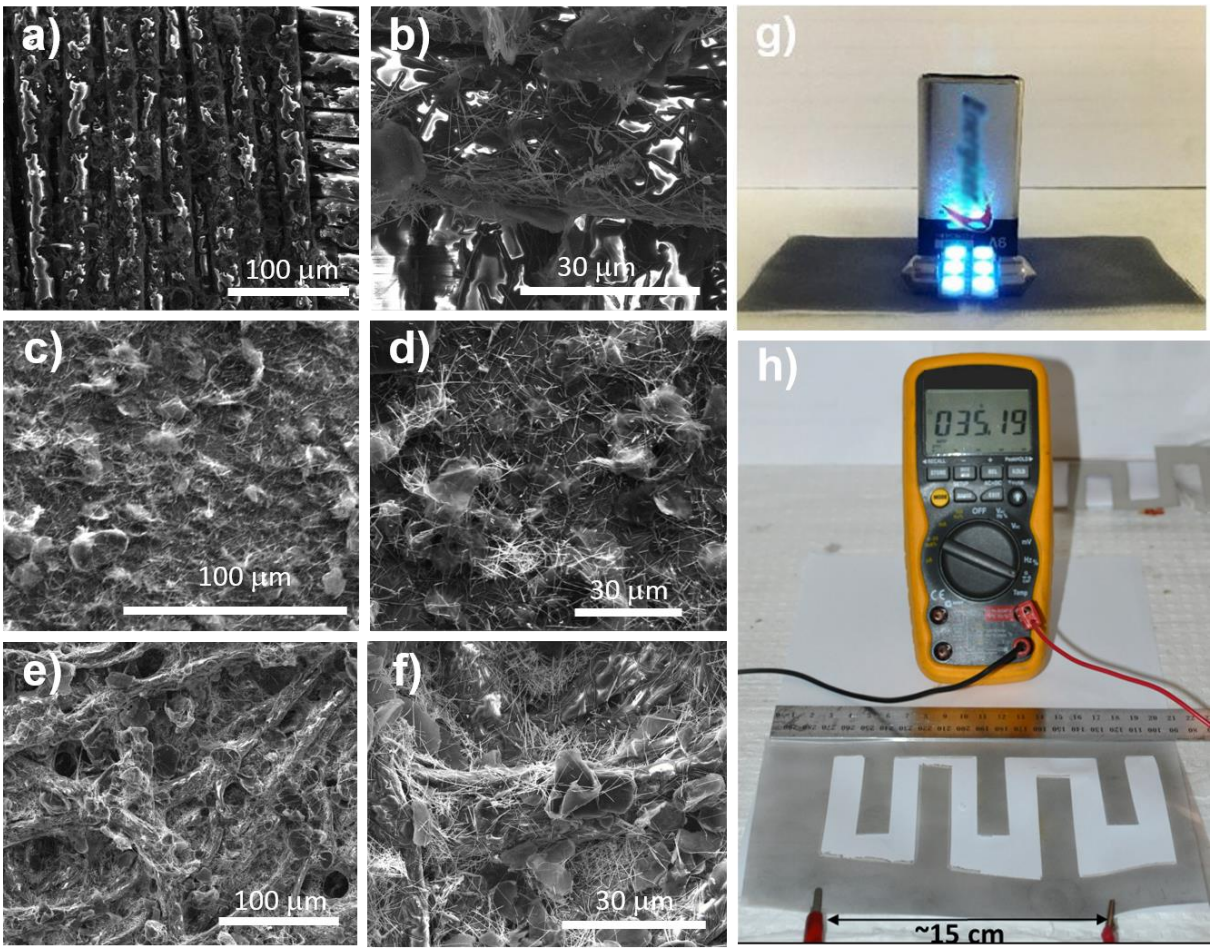

Figure 5.7. SEM images of the top surface of prepared AgNW/pG films by spray coatings on different substrates including (a and b) textile (inset image showing textile structure has bar scale is 0.5 mm), (c and d) elastomer PDMS and (e and f) paper showing interconnected networks of AgNWs and pG structures. (g) A demonstration of conductivity AgNW/pG coated textile with LED. (h) A conductive AgNW/pG networks coated paper showed a resistance of ~35 Ω when measured across a distance of ~15 cm by a two-probe multi-meter.

5.5.3 The characterization of the film stability under environmental and high temperature conditions

The low stability of AgNWs under ambient conditions and decay of their conductivity under harsh environmental conditions is the most critical limitation and has prevented their broader use in practical applications. The oxygen and thermal stability of the prepared films compared with control samples were tested in a series of aging and annealing experiments by monitoring Rs change at ambient condition (25 °C with a RH of 54%) for up to 60 days and with temperatures ranging between 25 to 350 °C. The results presented in **Figure 5.8a** show that the resistance of AgNW films exhibited a sharp increase after 8-10 days under ambient condition resulting from oxidation and corrosion caused by oxygen and moisture. In contrast, the AgNW/pG film showed a slow increase in resistance up to 30 days which then plateaus up until day 60. The comparative FTIR spectra during this aging process were obtained and presented in **Figure 5.8b** to monitor these changes and the formation of oxygen-containing groups on the AgNWs surface. The presence of these functional groups were seen to increase significantly after exposure to ambient atmosphere for 15 days compared with graphene protected AgNWs. The slight change in resistance occurs from the permeation of oxygen and H_2O through a network of AgNWs in defects or cracks at a much slower rate than the AgNWs without graphene.[43] These results indicate that graphene acts as a barrier to protect AgNWs from both oxygen and moisture, due to its gas barrier and superhydrophobic properties (CA~143.8°) enhancing its moisture repellence. The comparative SEM images of oxidized AgNWs and graphene protected AgNWs after 20 days exposed to environmental conditions are shown in the **Figure 5.8 c and d.** These images confirmed a visible

degradation and structural changes of AgNWs as results of oxidation and corrosion which is not observed on the AgNW/pG films.

The temperature stability and performance of AgNW films at high temperature is another critical parameter that was explored in this study. Both AgNW and AgNW/pG films showed no changes in Rs at a temperature up to 120 °C (**Figure 5.8e**). However, the Rs of the AgNW films was found to intensely increase with a temperature exceeding 150 °C, whereas the AgNW/pG films showed a slight increase up to 300 °C. The low thermal stability of AgNW films was explained as a result of increased level of oxidation at the wire junctions and followed by corrosion or fusion.[30] A significant increase of annealing stability of the AgNW/pG films is caused by the superior thermal conductivity of pristine graphene, which can readily distribute heat energy and at same time prevent Ag from oxidation. After 350 °C, the resistance of AgNW/pG film increases sharply, which is due to thermal degradation and oxidization AgNWs and/or oxidized graphene in atmosphere.

It is worthy to mention that different substrates for coating with the hybrid material could impact on stability behavior. The properties including wetting ability (hydrophilic/hydrophobic), mechanical properties (flexible/rigid, roughness), physicochemical properties (surface chemistry, moisture, thermal stable) of the substrates, are more or less affect the stability of the conductive films in different tests conditions.

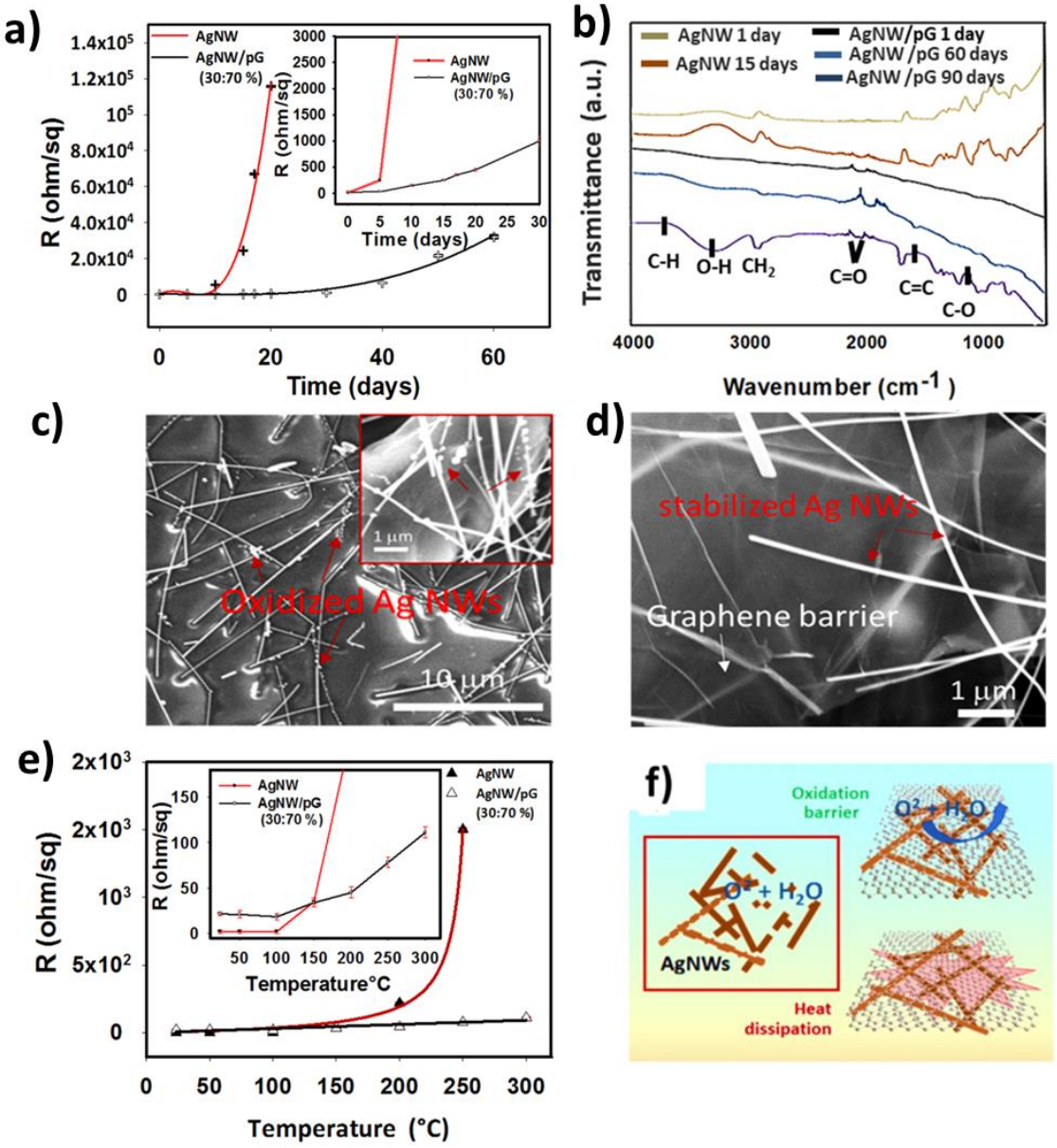

Figure 5.8. A comparative environmental and thermal stability of AgNW and AgNW/pG films at the ambient conditions and annealing process. (a) The change of the sheet resistance during aging at the ambient conditions during 60 days showing a big difference between AgNWs, with sharply increase resistance after 8 days, compared with the AgNW/pG films that are stable up to 30 days and gradually change resistance up to 60 days of testing. (b) FTIR spectra monitored from these films during aging time showing oxidation process on

AgNWs; (c-d) SEM images of AgNW and AgNW/pG films showing oxidized and degraded AgNWs which are, in contrast, stable and unchanged in AgNW/pG films; (e) the changes of the sheet resistance of both films during annealing at temperatures ranging from 30 to 300 °C, showing a significant difference between AgNWs with sharply increase resistance after 150 °C compared with AgNW/pG films that are stable up to 300 °C due to the graphene (f) acting as an oxidation barrier and dissipating heat.

The mechanism of the AgNWs oxidation process and the role graphene plays as oxidation barrier and heat dissipation is schematically shown in **Figure 5.8f**. As stated previously, untreated AgNWs are hydrophilic and susceptible to degradation under ambient conditions resulting in oxidation and corrosion. In contrast, graphene has planar geometry, inert surface chemistry, is hydrophobic and has a high thermal conductivity which has been reported to act as a excellent physical barrier to protect metals from oxidation and corrosion. When graphene is added to AgNWs for coating the platelets are oriented in a perpendicular fashion to the path of diffusion, referred to as the tortuous path model for high aspect ratio materials. Thus, penetrant molecules have an increased or longer mean-free path around the platelets. On the other hand, the remarkable thermal conductivity for heat dissipation under high temperature avoided local heating or ‘hot-spot’, and improved the thermal stability. These results are in agreement with previous studies done by Liang et al. [28], Yang et al. [20] and Ahn et al.[44] that reported these graphene properties.

5.5.4 Plasma enhanced performance of AgNW/pG thin films

To further enhance the performance of AgNW/pG thin films on glass substrates, ultrafast treatment using atmospheric pressure plasma jets (APPJs) was performed to improve the connectivity between AgNWs and graphene to increase the electrical conductivity and the stability. The APPJs concept for modification and improving conductivity of GO converted into rGO was successfully demonstrated in our previous work [34]. Two experimental procedures were investigated: firstly, plasma was used on AgNW/pG films, with different ratios, coated on glass substrates for 6 s; and secondly the time of plasma treatment was varied (0-10 s) using the optimized AgNW/pG (30/70 wt.%) film. The sheet resistance of the AgNW/pG films with different AgNW/pG ratios upon exposure to a 6 s to plasma beam is presented in **Figure 5.9a**. The sheet resistance level reduction of 18, 24, 28 and 31.2 % was observed for the sample 20/80 wt.%, 30/70 wt.%, 40/60 wt.% and 60/40%, respectively. The films with higher AgNW percentages show increased the reduction of resistance, since more junctions that could be welded by plasma are present in such films. **Figure 5.9b** shows the performance (the sheet resistance vs transparency) of the AgNW/pG film (30/70 wt.%) for different plasma treatment times, ranging from 0 to 10 s. As expected the sheet resistance of the films decreased by ~ 15 % from 19.86 Ω/sq (before) to 17.33 Ω/sq after a 3 s plasma treatment, while the optical transparency increased slightly from 89.8 to 90.5%. The sheet resistance decreased significantly ~ 30.6 %, from 19.86 to 15.20 Ω/sq along with an increase transmittance from 89.5 to 91 %, after a 6s exposure of samples. The reduction in resistance coupled with the increase in transparency can be attributed to the improved connections between the uncapped AgNWs formed by cleaning a layer of capping PVP *via* plasma beam. This layer could be removed under high energetic electrons (> 20 eV) and reactive gas species (O^{2-} and O^{-}_{2}, NOx) of plasma treatment, which facilitates welding of AgNWs or

plasma sintering. The images presented in **Figure 5.9 c-e** indicate that AgNWs are being welded at the junctions caused by heating effects at high contacted resistance. This mechanism is similar to optical sintering of bare AgNWs at junctions after 10-120 s by means of a tungsten–halogen lamp reported in previous work with similar impact on improved conductivity of AgNW/pG films.[45] In addition, in contrast to graphene oxide (abundant oxygen groups), which is reduced under plasma irradiation resulted in darker films. The pG (>95% C) is not reduced, thus resulting in a lighter film when treated, allowed higher optical transparency meanwhile lower resistance. This new finding is critical and cannot be achieved by other techniques.

It is important to state that the charged ions bombarded the hybrid materials with low kinetic energy though inelastic collisions causing AgNW cold welding, and the graphene sheet, in this context, acts to protect the AgNWs from high energetic electrons and reactive gas species cause etching of AgNWs (negative impact) from plasma treatment. This can be clearly observed when using longer exposure (> 6s) of plasma which resulted in a poor conductivity. For instance, typically after a 9s of plasma treatment, the resistance is increased to 44 Ω/sq at a higher transmittance of 92.4 % (**Figure 5.9e**). Plasma treatment of more than 10 s caused disorder of the graphene basal plane, subsequently the graphene sheets were oxidized by reactive gas species under the hash conditions. For instance, after 12-15 s of plasma treatment the resistance of AgNW/pG films is increased beyond 1 kΩ/sq which confirm our hypothesis of shielding effect of graphene barriers on AgNWs that is broken during longer exposure time. These results indicate the importance to optimize plasma irradiation condition (time, distance, and energy) depends on plasma equipment, which can be achieved in controllable way. The mechanism based on the results obtained by SEM images of AgNWs connections

before and after 3-6 s of irradiation is proposed and presented in **Figure 5.9f.** The scheme is showing three stages of this process including an initial crossing stage, welding stage that provide optimal performance and fusing/disruption stage with the "overdose" plasma treatment. The last and unwanted condition reflects the degradation of the films, where AgNWs are fusing that disrupts the conductive pathways and should be prevented by optimization of the plasma process. The Raman spectra of AgNW/pG films versus plasma treatment time were investigated and are shown in the Supporting Information, while there is no change in the position of Raman peaks, the G peak is sharper after 3-6 s of plasma treatment which suggests a higher crystallinity of the graphene plane. However, longer duration plasma treatment of 9 and 12 s result in a lower G band, higher D band, and removal of the 2D band (see Supporting Information 5S3). This indicates that the "overdose" plasma treatment causes disorder of the graphene basal plane, which is then oxidized graphene sheets. It is worthy to mention that the pG only film displayed almost no change in resistance after 10 s treatment, but similarly its resistance increased significantly after 15 s due to the lack of adhesion resulted in damage of the film.

Finally, the mechanical adhesion of the prepared films of AgNWs and AgNW/pG before and after plasma treatment were tested by using a scotch tape method (see Supporting Information 5S4). The AgNWs film clearly showed the imprint of film after pressing and peeling off from the glass substrate. The hybrid AgNW/pG film exhibits better adhesive property, but it is still possible to peel off the conductive layer. Interestingly, the hybrid film after plasma treatment (6s) significantly improved adhesion on substrate. The mechanism of the plasma sintering of bare AgNWs at junctions allowed for a strong scaffold and high pack of the hybrid films. Additionally, the AgNWs sandwiched/intercalated graphene sheets

avoids sliding between them. These factors resulted in the better mechanical properties of the hybrid films attached on substrate.

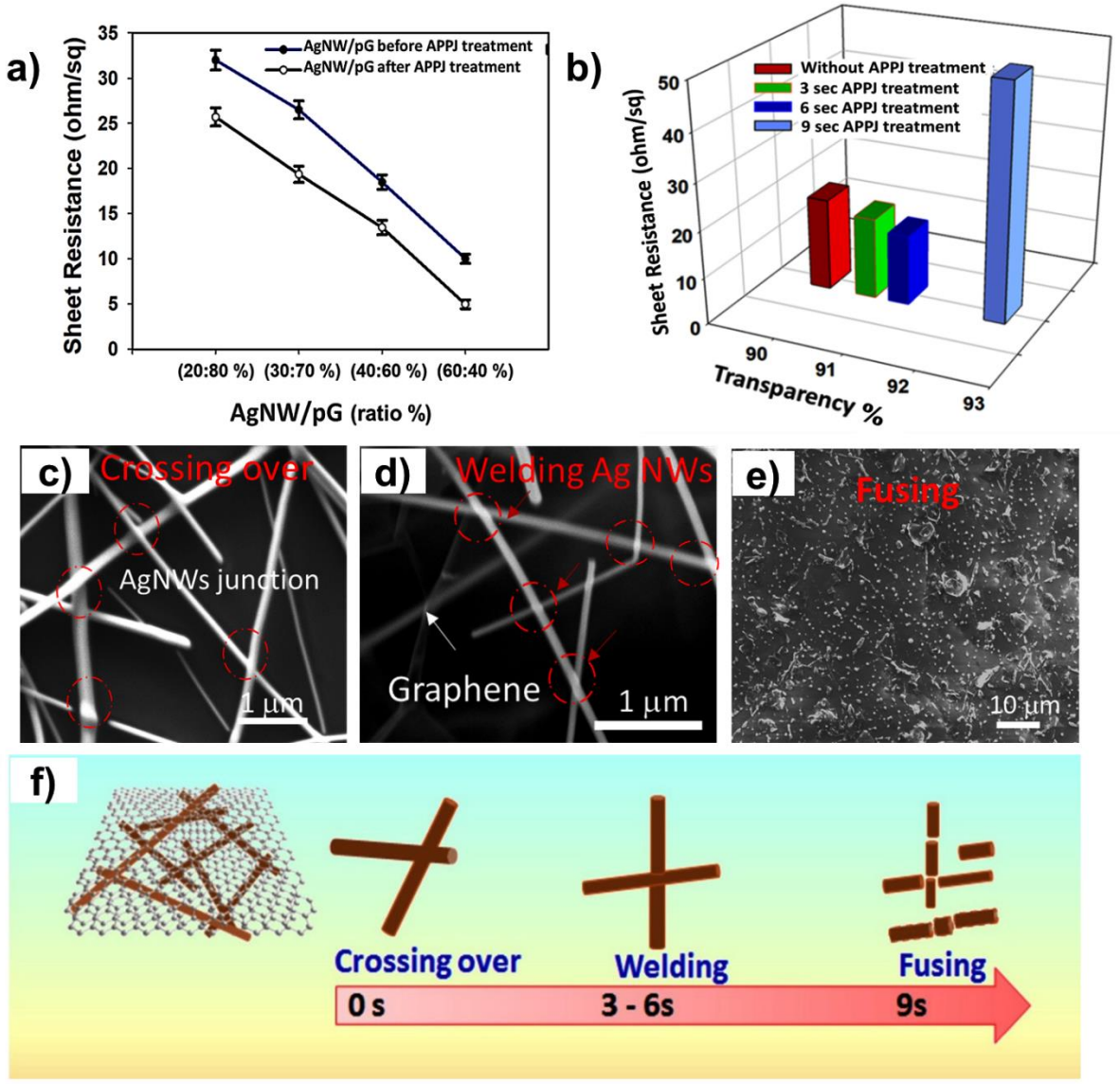

Figure 5.9. (a) The influence of short atmospheric pressure jet plasma (APPJs) treatment of AgNW/pG prepared by different AgNW/pG ratio on their sheet resistance showing a significant decrease in resistance after plasma irradiation (compared with not treated film); (b) Optimizing the film performance (the sheet resistance and transparency) of AgNW/pG

content (30/70 wt.%) using different exposure time of APPJ treatment showing 6 sec as optimal conditions. (c-d) SEM imaging of plasma treated the AgNW/pG films showing that AgNWs at junctions are transferred from crossing to welding that explains the reduction of their resistance. (e) SEM images of AgNW/pG treated over longer plasma process (>9 sec) showed degradation and fusing of AgNWs. (f) The proposed mechanism of the plasma irradiation of the AgNW/pG film where AgNWs at junctions were welded during short process or fused or defragmented during longer duration plasma treatment.

In general the use of APPJ provides enhanced performance of AgNW/pG thin film achieved due to the graphene layering and wrapping which facilitate AgNW sintering at junctions and offers protection from plasma etching. This is also enhanced the mechanical adhesion between the conductive film and substrate. This impressive results and improvements of transparency and conductivity along with enhanced stability of AgNW/pG films can have an enormously impact and extend their commercial applications.[45-48]

5.6 Conclusion

In summary, several new approaches toward the development of highly transparent and conductive films on both flexible and rigid substrates based on combination of AgNWs and pristine graphene were explored and presented. Optimal results on conductive ink formulation composed of AgNWs (30-50 μm long, and 30-50 nm diameters) and pristine few-layer graphene sheets showed the best results at the 30/70 wt.% ratio of AgNW to pG. The prepared AgNWs film on glass substrate shows a surface resistance of 18.23 Ω/sq at an optical transparency of 89 %, which are acceptable for many optoelectronic applications. The application of developed inks was also successfully demonstrated on broad range of non-conductive substrates including textile, PDMS and paper showing excellent conductivity for

application in wearable electronics. The stability characterization under environmental conditions of the AgNW/pG film showed significantly improved durability with minor increase in resistance up to 30 days compared with the control AgNW film which showed a sharp increase after 8-10 days as result of Ag oxidation and corrosion. The AgNW/pG film showed outstanding thermal stability after annealing at 300 °C, while control film displayed a significant increase in resistance at 150 °C. The mechanism of graphene barrier oxidation is revealed proposing graphene sheets acting as a physical barrier to protect the AgNW surface from oxygen and moisture and also providing the heat dissipation. The performance of AgNW/pG films was further improved by a short APPJs treatment (e.g. 6s) to significantly reduce the sheet resistance (~30.6%), enhancement of the transparency (1.2 %), and increase the mechanical adhesive property. The presented results are among the best performing AgNW/graphene films reported to date and is a key step for their conventional and emerging applications.

Supporting Information Available: AFM and TEM image of pristine graphene exfoliated from expanded graphite confirming few-layer graphene sheets (**Figure 5S1**); TEM image of AgNWs after washing (**Figure 5S2**); Raman spectrum of materials after plasma treatment (**Figure 5S3**); Adhesive property of conductive thin film on glass substrates before and after plasma treatment conductive film on glass substrates (**Figure 5S4**).

Acknowledgements

The authors acknowledge the support from Australian research Council under Linkage Scheme with the grant ARC Research Hub for Graphene Enabled Industry Transformation, IH 150100003 funding under Industrial Transformation Research.

5.7 Reference

1. Chen, S., Deng, L., Xie, J., Peng, L., Xie, L., Fan, Q., & Huang, W. (2010). Recent Developments in Top-Emitting Organic Light-Emitting Diodes. Advanced Materials, 22(46), 5227-5239. doi:10.1002/adma.201001167
2. Fu, W., Liu, L., Jiang, K., Li, Q., & Fan, S. (2010). Super-aligned carbon nanotube films as aligning layers and transparent electrodes for liquid crystal displays. *Carbon, 48*(7), 1876-1879. doi:10.1016/j.carbon.2010.01.026
3. Madaria, A. R., Kumar, A., & Zhou, C. (2011). Large scale, highly conductive and patterned transparent films of silver nanowires on arbitrary substrates and their application in touch screens. Nanotechnology, 22(24), 245201. doi:10.1088/0957-4484/22/24/245201
4. Zheng, Q., Li, Z., Yang, J., & Kim, J.-K. (2014). Graphene oxide-based transparent conductive films. *Progress in Materials Science, 64*, 200-247. doi:10.1016/j.pmatsci.2014.03.004
5. Xu, S., Man, B., Jiang, S., Liu, M., Yang, C., Chen, C., & Zhang, C. (2014). Graphenesilver nanowire hybrid films as electrodes for transparent and flexible loudspeakers. *CrystEngComm, 16*(17), 3532-3539. doi:10.1039/c3ce42656d
6. Granqvist, C. G. (2007). Transparent conductors as solar energy materials: A panoramic review. Solar Energy Materials and Solar Cells, 91(17), 1529-1598. doi:10.1016/j.solmat.2007.04.031
7. Wang, X., Zhi, L., & Müllen, K. (2008). Transparent, conductive graphene electrodes for dye-sensitized solar cells. *Nano letters, 8*(1), 323. doi:10.1021/nl072838r
8. Chen, Z., Li, W., Li, R., Zhang, Y., Xu, G., & Cheng, H. (2013). Fabrication of highly transparent and conductive indium-tin oxide thin films with a high figure of merit via

solution processing. *Langmuir : the ACS journal of surfaces and colloids, 29*(45), 13836. doi:10.1021/la4033282

9. Noor, N., & Parkin, I. P. (2013). Enhanced transparent-conducting fluorine-doped tin oxide films formed by Aerosol-Assisted Chemical Vapour Deposition. *J. Mater. Chem. C, 1*(5), 984-996. doi:10.1039/c2tc00400c

10. Hui, W., Desheng, K., Zhichao, R., Po-Chun, H., Shuang, W., Zongfu, Y., . . . Yi, C. (2013). A transparent electrode based on a metal nanotrough network. *Nature Nanotechnology, 8*(6), 421. doi:10.1038/nnano.2013.84

11. Hu, L., Wu, H., & Cui, Y. (2011). Metal nanogrids, nanowires, and nanofibers for transparent electrodes. *MRS Bulletin, 36*(10), 760-765. doi:10.1557/mrs.2011.234

12. Hecht, D. S., Hu, L., & Irvin, G. (2011). Emerging Transparent Electrodes Based on Thin Films of Carbon Nanotubes, Graphene, and Metallic Nanostructures. In (Vol. 23, pp. 1482-1513). Weinheim.

13. Azulai, D., Belenkova, T., Gilon, H., Barkay, Z., & Markovich, G. (2009). Transparent metal nanowire thin films prepared in mesostructured templates. *Nano letters, 9*(12), 4246. doi:10.1021/nl902458j

14. Wu, Z., Chen, Z., Du, X., Logan, J. M., Sippel, J., Nikolou, M., . . . Rinzler, A. G. (2004). Transparent, conductive carbon nanotube films. *Science (New York, N.Y.), 305*(5688), 1273. doi:10.1126/science.1101243

15. Jiu, J., Wang, J., Sugahara, T., Nagao, S., Nogi, M., Koga, H., . . . Uchida, H. (2015). The effect of light and humidity on the stability of silver nanowire transparent electrodes. *RSC Adv., 5*(35), 27657-27664. doi:10.1039/c5ra02722

16. Elechiguerra, J. L., Larios-Lopez, L., Liu, C., Garcia-Gutierrez, D., Camacho-Bragado, A., & Yacaman, M. J. (2005). Corrosion at the Nanoscale: The Case of

Silver Nanowires and Nanoparticles. *Chemistry of Materials, 17*(24), 6042-6052. doi:10.1021/cm051532n

17. Tung, T. T., Kim, T. Y., Shim, J. P., Yang, W. S., Kim, H., & Suh, K. S. (2011). Poly(ionic liquid)-stabilized graphene sheets and their hybrid with poly(3,4-ethylenedioxythiophene). *Organic Electronics, 12*(12), 2215-2224. doi:10.1016/j.orgel.2011.09.012

18. Tung, T. T., Pham-Huu, C., Janowska, I., Kim, T., Castro, M., & Feller, J. F. (2015). Hybrid Films of Graphene and Carbon Nanotubes for High Performance Chemical and Temperature Sensing Applications. *Small, 11*(28), 3485-3493. doi:10.1002/smll.201403693

19. Yang, S. B., Choi, H., Lee, D. S., Choi, C. G., Choi, S. Y., & Kim, I. D. (2015). Improved Optical Sintering Efficiency at the Contacts of Silver Nanowires Encapsulated by a Graphene Layer. *Small, 11*(11), 1293-1300. doi:10.1002/smll.201402474

20. Tokuno, T., Nogi, M., Jiu, J., & Suganuma, K. (2012). Hybrid transparent electrodes of silver nanowires and carbon nanotubes: a low-temperature solution process. *Nanoscale Research Letters, 7*(1), 1-7. doi:10.1186/1556-276X-7-281

21. Xu, Q., Song, T., Cui, W., Liu, Y., Xu, W., Lee, S.-T., & Sun, B. (2015). Solution-processed highly conductive PEDOT:PSS/AgNW/GO transparent film for efficient organic-Si hybrid solar cells. *ACS applied materials & interfaces, 7*(5), 3272. doi:10.1021/am508006q

22. Bao, Q., & Loh, K. P. (2012). Graphene photonics, plasmonics, and broadband optoelectronic devices. *ACS nano, 6*(5), 3677. doi:10.1021/nn300989g

23. Wu, C., Kim, T. W., Li, F., & Guo, T. (2016). Wearable Electricity Generators Fabricated Utilizing Transparent Electronic Textiles Based on Polyester/Ag Nanowires/Graphene Core-Shell Nanocomposites. *ACS nano*, *10*(7), 6449. doi:10.1021/acsnano.5b08137

24. Lee, H., Kim, M., Kim, I., & Lee, H. (2016). Flexible and Stretchable Optoelectronic Devices using Silver Nanowires and Graphene. *Advanced Materials*, *28*(22), 4541-4548. doi:10.1002/adma.201505559

25. Nine, M. J., Cole, M. A., Johnson, L., Tran, D. N. H., & Losic, D. (2015). Robust Superhydrophobic Graphene-Based Composite Coatings with Self-Cleaning and Corrosion Barrier Properties. ACS applied materials & interfaces, 7(51), 28482. doi:10.1021/acsami.5b09611

26. Nine, M. J., Cole, M. A., Tran, D. N. H., & Losic, D. (2015). Graphene: a multipurpose material for protective coatings. *Journal of Materials Chemistry A*, *3*(24), 12580-12602. doi:10.1039/C5TA01010A

27. Tung, T. T., Yoo, J., Alotaibi, F. K., Nine, M. J., Karunagaran, R., Krebsz, M., . . . Losic, D. (2016). Graphene Oxide-Assisted Liquid Phase Exfoliation of Graphite into Graphene for Highly Conductive Film and Electromechanical Sensors. ACS applied materials & interfaces, 8(25), 16521. doi:10.1021/acsami.6b04872

28. Liang, J., Li, L., Tong, K., Ren, Z., Hu, W., Niu, X., . . . Pei, Q. (2014). Silver nanowire percolation network soldered with graphene oxide at room temperature and its application for fully stretchable polymer light-emitting diodes. *ACS nano*, *8*(2), 1590. doi:10.1021/nn405887k

29. Yang, S. B., Choi, H., Lee, D. S., Choi, C. G., Choi, S. Y., & Kim, I. D. (2015). Improved Optical Sintering Efficiency at the Contacts of Silver Nanowires

Encapsulated by a Graphene Layer. *Small, 11*(11), 1293-1300. doi:10.1002/smll.201402474

30. Chen, R., Das, S. R., Jeong, C., Khan, M. R., Janes, D. B., & Alam, M. A. (2013). Co-Percolating Graphene-Wrapped Silver Nanowire Network for High Performance, Highly Stable, Transparent Conducting Electrodes. *Advanced Functional Materials, 23*(41), 5150. doi:10.1002/adfm.201300124

31. Coskun, S., Aksoy, B., & Unalan, H. E. (2011). Polyol Synthesis of Silver Nanowires: An Extensive Parametric Study. *Crystal Growth & Design, 11*(11), 4963-4969. doi:10.1021/cg200874g

32. Kim, T., Kim, Y. W., Lee, H. S., Kim, H., Yang, W. S., & Suh, K. S. (2013). Uniformly Interconnected Silver-Nanowire Networks for Transparent Film Heaters. *Advanced Functional Materials, 23*(10), 1250-1255. doi:10.1002/adfm.201202013

33. Keith, R. P., Eswaraiah, V., Claudia, B., Ronan, J. S., Umar, K., Arlene, O. n., . . . Jonathan, N. C. (2014). Scalable production of large quantities of defect-free few-layer graphene by shear exfoliation in liquids. *Nature Materials, 13*(6), 624. doi:10.1038/nmat3944

34. Alotaibi, F., Tung, T. T., Nine, M. J., Kabiri, S., Moussa, M., Tran, D. N. H., & Losic, D. (2018). Scanning atmospheric plasma for ultrafast reduction of graphene oxide and fabrication of highly conductive graphene films and patterns. *Carbon, 127*, 113-121. doi:10.1016/j.carbon.2017.10.075

35. Xu, L. Y., Yang, G. Y., Jing, H. Y., Wei, J., & Han, Y. D. (2014). Ag–graphene hybrid conductive ink for writing electronics. *Nanotechnology, 25*(5), 055201. doi:10.1088/0957-4484/25/5/055201

36. Lee, H., Kim, I., Kim, M., & Lee, H. (2016). Moving beyond flexible to stretchable conductive electrodes using metal nanowires and graphenes. *Nanoscale, 8*(4), 1789-1822. doi:10.1039/c5nr06851g

37. Bari, B., Lee, J., Jang, T., Won, P., Ko, S. H., Alamgir, K., . . . Guo, L. J. (2016). Simple hydrothermal synthesis of very-long and thin silver nanowires and their application in high quality transparent electrodes. *Journal of Materials Chemistry A, 4*(29), 11365-11371. doi:10.1039/C6TA03308C

38. Tung, T. T., Chen, S. J., Fumeaux, C., & Losic, D. (2016). Scalable realization of conductive graphene films for high-efficiency microwave antennas. *J. Mater. Chem. C, 4*(45), 10620-10624. doi:10.1039/c6tc03583c

39. Lee, M.-S., Lee, K., Kim, S.-Y., Lee, H., Park, J., Choi, K.-H., . . . Park, J.-U. (2013). High-performance, transparent, and stretchable electrodes using graphene-metal nanowire hybrid structures. *Nano letters, 13*(6), 2814. doi:10.1021/nl401070p

40. Qianqian, D., Ying, S., Maodu, C., Hui, L., Xianzhong, Y., Yingqi, Q., . . . Mengtao, S. (2016). Ultrafast Dynamics of Plasmon-Exciton Interaction of Ag Nanowire-Graphene Hybrids for Surface Catalytic Reactions. *Scientific Reports, 6*(1). doi:10.1038/srep32724

41. Tae Hoon, S., Seula, L., Kyung Hyun, M., Chandramohan, S., Ah Hyun, P., Gun Hee, L., . . . Myung Jong, K. (2016). The role of graphene formed on silver nanowire transparent conductive electrode in ultra-violet light emitting diodes. *Scientific Reports, 6*(1). doi:10.1038/srep29464

42. Aroca, R. F., Goulet, P. J. G., Dos Santos, D. S., Alvarez-Puebla, R. A., & Oliveira, O. N. (2005). Silver nanowire layer-by-layer films as substrates for surface-enhanced Raman scattering. *Analytical chemistry, 77*(2), 378. doi:10.1021/ac048806v

43. Shi, L., Wang, R., Zhai, H., Liu, Y., Gao, L., & Sun, J. (2015). A long-term oxidation barrier for copper nanowires: graphene says yes. *Phys. Chem. Chem. Phys., 17*(6), 4231-4236. doi:10.1039/c4cp05187d

44. Ahn, Y., Jeong, Y., & Lee, Y. (2012). Improved thermal oxidation stability of solution-processable silver nanowire transparent electrode by reduced graphene oxide. *ACS applied materials & interfaces, 4*(12), 6410. doi:10.1021/am301913w

45. Erik, C. G., Wenshan, C., Judy, J. C., Fakhruddin, M., Stephen, T. C., Christoforo, M. G., . . . Mark, L. B. (2012). Self-limited plasmonic welding of silver nanowire junctions. *Nature Materials, 11*(3), 241. doi:10.1038/nmat3238

46. Bellew, A. T., Manning, H. G., Gomes Da Rocha, C., Ferreira, M. S., & Boland, J. J. (2015). Resistance of Single Ag Nanowire Junctions and Their Role in the Conductivity of Nanowire Networks. *ACS nano, 9*(11), 11422. doi:10.1021/acsnano.5b05469

47. Tung, T. T., Nine, M. J., Krebsz, M., Pasinszki, T., Coghlan, C. J., Tran, D. N. H., & Losic, D. (2017). Recent Advances in Sensing Applications of Graphene Assemblies and Their Composites. *Advanced Functional Materials, 27*(46), n/a-n/a. doi:10.1002/adfm.201702891

48. Dong, H., Wu, Z., Jiang, Y., Liu, W., Li, X., Jiao, B., . . . Hou, X. (2016). A Flexible and Thin Graphene/Silver Nanowires/Polymer Hybrid Transparent Electrode for Optoelectronic Devices. *ACS applied materials & interfaces, 8*(45), 31212. doi:10.1021/acsami.6b09056

5.8 Supporting Information

Silver Nanowires with Pristine Graphene Oxidation Barriers for Stable and High Performance Transparent Conductive Films

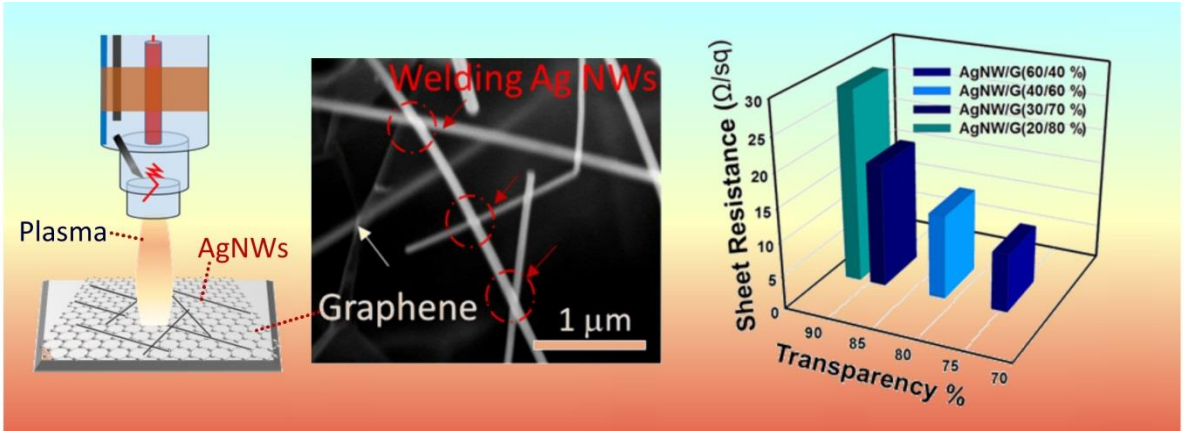

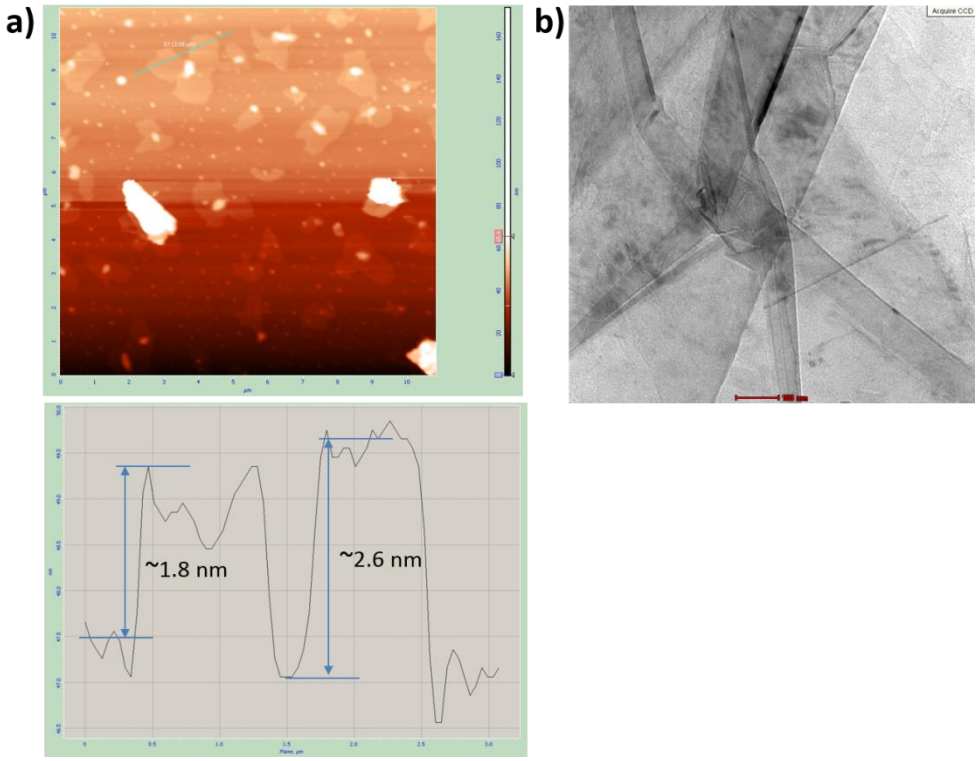

Figure 5S1. (a) AFM and (b) TEM image of pristine graphene exfoliated from expanded graphite confirming few-layer graphene sheets.

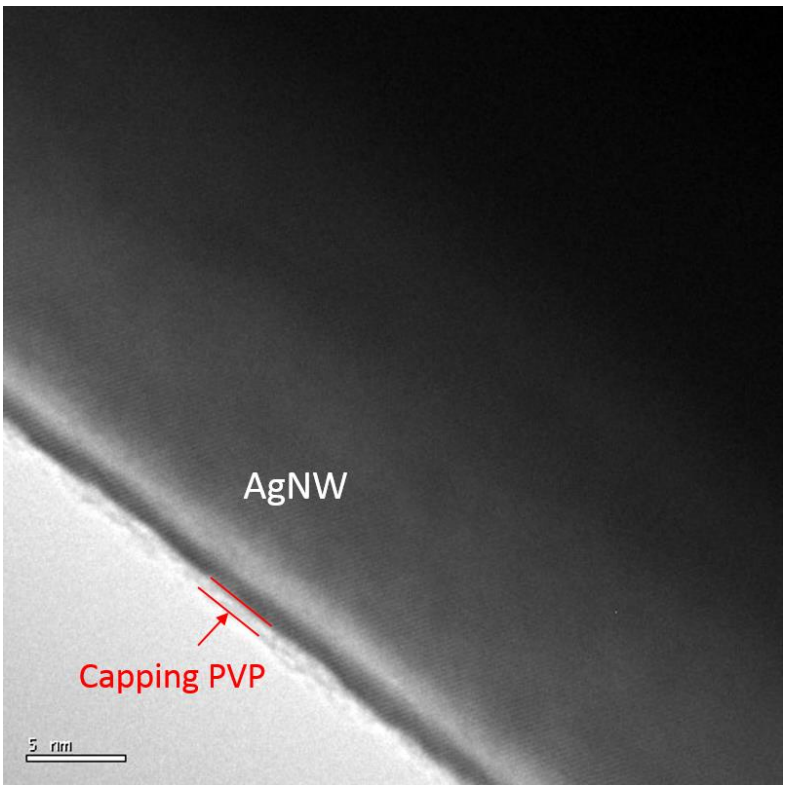

Figure 5S2. TEM image of AgNW showing a very thin layer (~0.6-0.8 nm) of capping agent residual after washing.

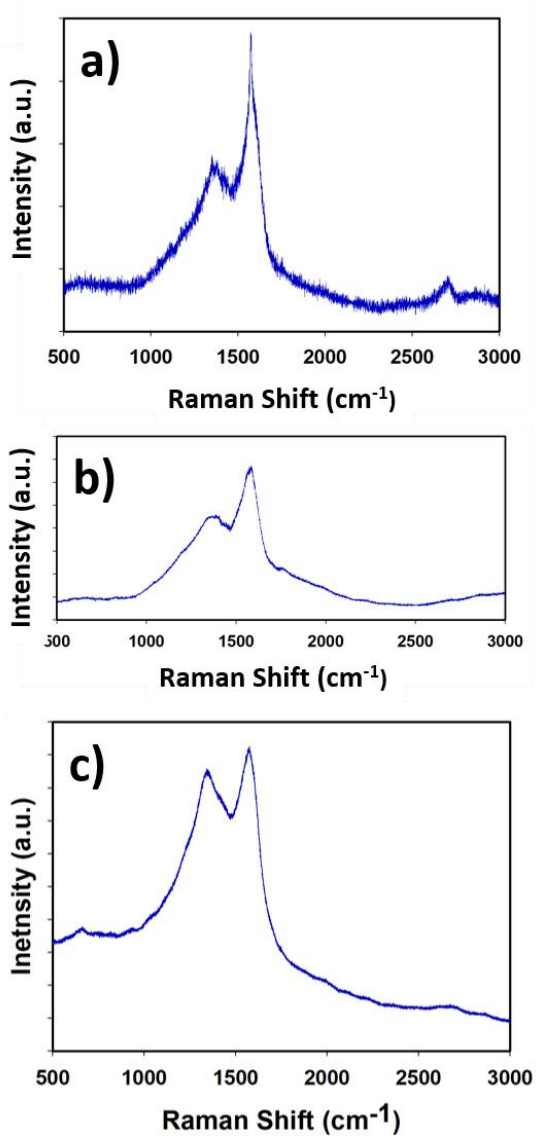

Figure 5S3. Raman spectrum of (a) AgNW/pG after 3-6 s, (b) 9 s and (c) 12 s of plasma treatment (APPJs) showing an optimizing plasma irradiation time (3-6s), "overdose" treatment resulted in fusing AgNWs and then oxidized pG.

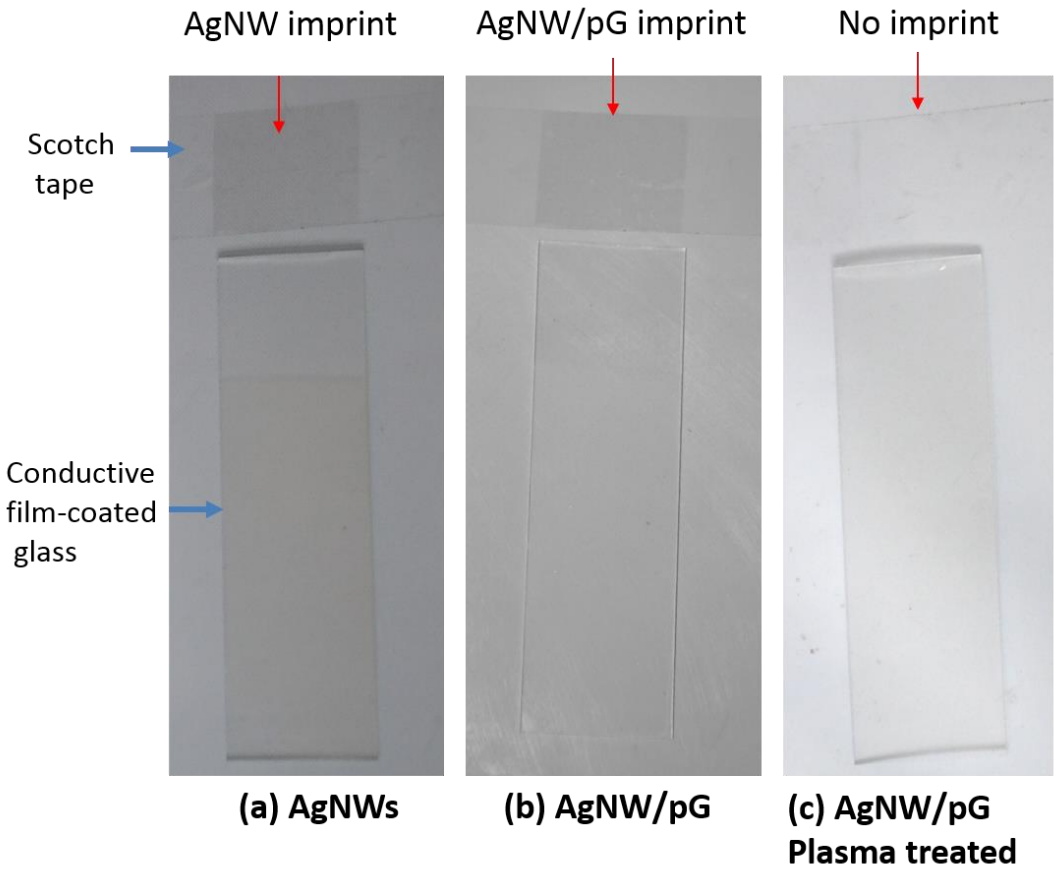

Figure 5S4. Adhesive property of (a) AgNW alone, (b) AgNW/pG and (c) plasma treated AgNW/pG conductive film on glass substrates, in which the conductive layer of AgNWs and AgNW/pG can be peeled off and imprint on tape after testing, while plasma-induced welding AgNWS at junctions allows scaffold the adhesion property of the hybrid film.

Blank Page

Chapter 6

Engineering of highly conductive and ultra-thin nitrogen-doped graphene films by combined methods of microwave irradiation, ultrasonic spraying and thermal annealing

Statement of Authorship

Title of Paper	Engineering of highly conductive and ultra-thin nitrogen-doped graphene films by combined methods of microwave irradiation, ultrasonic spraying and thermal annealing
Publication Status	☑ Published ☐ Accepted for Publication ☐ Submitted for Publication ☐ Unpublished and Unsubmitted w ork w ritten in manuscript style
Publication Details	Chemical Engineering Journal 338 (2018) 764–773

Principal Author

Name of Principal Author (Candidate)	Faisal ALotaibi
Contribution to the Paper	Under the supervison of Prof Dusan Losic conducted some of experitments , interpreted , processed some data edite manuscript for submission .
Overall percentage (%)	35%
Certification:	This paper reports on original research I conducted during the period of my Higher Degree by Research candidature and is not subject to any obligations or contractual agreements with a third party that would constrain its inclusion in this thesis. I am the primary author of this paper.
Signature	Date 05-03-2019

Co-Author Contributions

By signing the Statement of Authorship, each author certifies that:

i. the candidate's stated contribution to the publication is accurate (as detailed above);

ii. permission is granted for the candidate in include the publication in the thesis; and

iii. the sum of all co-author contributions is equal to 100% less the candidate's stated contribution.

Name of Co-Author	Tran Thanh Tung
Contribution to the Paper	Developed ,designed and conducted the experitments , interpreted ,processed the data ,wrote manuscript draft ,edited and revised for submission
Signature	Date 12-03-2019

Name of Co-Author	Md J. Nine
Contribution to the Paper	Edite manuscrip and analyse some data
Signature	Date 12-03-2019

Please cut and paste additional co-author panels here as required.

Name of Co-Author	Rifat Silvaa		
Contribution to the Paper	Anaylse some data and edited the mansucript		
Signature		Date	10-03-2019

Name of Co-Author	Diana N.H. Trana		
Contribution to the Paper	Edit the mansucript for submmission		
Signature		Date	10-3-2019

Name of Co-Author	Izabela Janowska		
Contribution to the Paper	Anaylse some data		
Signature		Date	

Name of Co-Author	Dusan Losica		
Contribution to the Paper	Act as primery supervisour ,aiding in desing the expierments and evaluation and edited the mansucript		
Signature		Date	12/03/2019

Chemical Engineering Journal 338 (2018) 764–773

Contents lists available at ScienceDirect

Chemical Engineering Journal

journal homepage: www.elsevier.com/locate/cej

Engineering of highly conductive and ultra-thin nitrogen-doped graphene films by combined methods of microwave irradiation, ultrasonic spraying and thermal annealing

Tran Thanh Tung[a,b], Faisal Alotaibi[a,b], Md J. Nine[a,b], Rifat Silva[a,b], Diana N.H. Tran[a,b], Izabela Janowska[c], Dusan Losic[a,b,*]

[a] School of Chemical Engineering, The University of Adelaide, Adelaide, SA 5005, Australia
[b] ARC Research Hub for Graphene Enabled Industry Transformation, The University of Adelaide, North Terrace, Adelaide, SA 5005, Australia
[c] Institut de Chimie et Procédés pour l'Énergie, l'Environnement et la Santé (ICPEES), CNRS UMR 7515-University of Strasbourg, 25 rue Becquerel, 67087 Strasbourg, France

HIGHLIGHTS

- N-doped graphene films were fabricated by combined method.
- Graphene oxide mixed poly(ionic liquids) treated by microwave irradiation was used as an ink.
- High conductivity and high transparency was achieved.
- The film conductivity and level of doping can be controlled by annealing.
- Method is simple, scalable and applicable for broad applications.

ARTICLE INFO

Keywords:
Graphene thin films
N-doped graphene
Graphene inks
Graphene coatings
Ultrasonic spaying

ABSTRACT

We report a new method for the fabrication of highly conductive and transparent ultrathin nitrogen (N) doped graphene films from graphene inks by combining a microwave treatment, ultrasonic nebulizer coating and thermal annealing. The starting graphene oxide (GO) solution was mixed with poly(ionic liquids) (PIL) and treated with microwave (Mw) irradiation to prepare Mw-rGO@PIL inks, which is a gentle reduction of PIL-attached reduced graphene oxide (rGO). In this non-contacting heating method, the PIL was used to not only mediate microwave irradiation and prevent disorder of the graphitic structure, but also repair the lattice defects and introduce nitrogen into the graphitic structure. The ultra-thin graphene films were prepared using the nebulizer for controlling the aerosol droplet distribution of the Mw-rGO@PIL inks coated onto quartz or glass substrates. The prepared films displayed a surface resistance of ~1.45×10^7 Ω/sq at a transparency of ~87%. A further thermal treatment was conducted to improve the conductivity of the prepared films by annealing at a high temperature (900 °C), which allowed complete reduction of oxygen containing groups, enhanced graphitization, and reordering of the basal graphene plane and N-doping of the carbon lattice (pyrolytic PIL). The resulting thin films significantly reduced the surface resistance in the range of 1.5×10^3 to 6.2×10^3 Ω/sq at a transparency ranging from 68 to 82%, respectively. The presented method involving *in situ* N-doping offers a promising environmentally-friendly, low-cost and scalable manufacture of high-quality conductive N-doped graphene films.

1. Introduction

Graphene films have excellent electrical, mechanical, chemical and optical properties and been explored to design new materials and devices for a broad range of applications including flexible electronics, flexible screens, antennas, chemical sensors, biosensors, energy storage, solar cells, transparent conducting electrodes, and protective coatings [1–6]. Depending on the properties requirements (e.g. conductivity, thickness, transparency and mechanical properties) these films can be fabricated in the form of single layers, thin transparent or thick

* Corresponding author at: School of Chemical Engineering, The University of Adelaide, Adelaide, SA 5005, Australia.
E-mail address: dusan.losic@adelaide.edu.au (D. Losic).

https://doi.org/10.1016/j.cej.2018.01.085
Received 21 October 2017; Received in revised form 8 January 2018; Accepted 16 January 2018
Available online 04 February 2018
1385-8947/

Blank Page

Engineering of highly conductive and ultra-thin nitrogen-doped graphene films by combined methods of microwave irradiation, ultrasonic spraying and thermal annealing

6.1 Abstract:

We report a new method for the fabrication of highly conductive and transparent ultrathin nitrogen (N) doped graphene films from graphene inks by combining microwave treatment, ultrasonic nebulizer coating and thermal annealing. The starting graphene oxide (GO) solution was mixed with poly(ionic liquids) (PIL) and treated with microwave (Mw) irradiation to prepare Mw-rGO@PIL inks, which is a gentle reduction of PIL-attached reduced graphene oxide. In this non-contacting heating method, the PIL was used to not only mediate microwave irradiation and prevent disorder of the graphitic structure, but also repair the lattice defects and introduce nitrogen into the graphitic structure. The ultra-thin graphene films were prepared using the nebulizer for controlling the aerosol droplet distribution of the Mw-rGO@PIL inks coated onto quartz or glass substrates. The prepared films displayed a surface resistance of ~1.45×10^7 Ω/sq at a transparency of ~87%. A further thermal treatment was conducted to improve the conductivity of the prepared films by annealing at a high temperature (900 °C), which allowed complete reduction of oxygen containing groups, enhanced graphitization, and reordering of the basal graphene plane and N-doping of the carbon lattice (pyrolytic PIL). The resulting thin films significantly reduced the surface resistance in the range of 1.5×10^3 to 6.2×10^3 Ω/sq at transparency ranging from 68 to 82%, respectively. The presented method involving *in situ* N-doping offers a promising

environmentally-friendly, low-cost and scalable manufacture of high-quality conductive N-doped graphene films.

6.2 Introduction

Graphene films have excellent electrical, mechanical, chemical and optical properties and been explored to design new materials and devices for a broad range of applications including flexible electronics, flexible screens, antennas, chemical sensors, biosensors, energy storage, solar cells, transparent conducting electrodes, and protective coatings [1-6]. Depending on the properties requirements (e.g. conductivity, thickness, transparency and mechanical properties) these films can be fabricated in the form of single layers, thin transparent or thick graphene films using various deposition and coating techniques including chemical vapour deposition (CVD), sputtering, solution spraying, drop casting, dip coating, spin coating, and printing [5-7]. Among them, a solution-processed fabrication based on the dispersion of exfoliated graphene in a certain solvent with or without surfactants, called graphene inks, is the most desirable method for rapid manufacturing of low-cost thin and thick graphene films [8-10]. For example, Li et al. reported transparent films grown through Langmuir-Blodgett (LB) assembly achieved sheet resistance (Rs) of 8 kΩ/sq at corresponding optical transmittances (T) of ~ 83 % [11]. De et al. have demonstrated graphene-based films with Rs of $10^3 - 10^6$ Ω/sq at transmittance values ranging from 35 to 90% [12]. A Rs of 9900 Ω/sq at T of 93.7 for rGO film reduced by sodium borohydride ($NaBH_4$) and doped by gold trichloride ($AuCl_3$) [13], and a film with Rs of 3110 Ω/sq at T of 90% for edge-selective functionalization of graphite with thermal reduction [14]. However, graphene inks used for the thin films preparations have a number of limitations due to the various printing rheological requirements (density, surface tension, viscosity) and the use of additional

ingredients and binders that have an impact on the electrical conductivity and surface properties [15,16].

Another approach to prepare graphene thin films is to use graphene oxide (GO) as pre-coatings as it has better adhesion and binding properties to common substrates (glass, plastic, textile, Si wafer, etc). Unfortunately, GO contains abundant oxygen functional groups on its basal plane and edges that create structural defects and result in large energy band gaps in the electron density states, and consequently lowers the film's conductivity. In order to restore the structural and electronic properties of GO, conventional chemical routes with reducing agents were generally used. However, they are restricted from toxicity or negative environmental impact, and lack of complete removal of oxygen groups from the structure [17,18]. To address this problem, a new reduction method of GO based on microwave treatment has been recently introduced [19,23]. The advantage of electromagnetic radiation is that the energy is directly converted into heat that is distributed uniformly, which enables rapid heating of reactant without interaction with the surrounding [20,24]. Thus, the irradiation method has been demonstrated as less destructive, economical, ultrafast and eco-friendly for the controllable reduction of GO (rGO) [20,25-28]. Nevertheless, the development of these methods has not been translated for practical applications of transparent conductive graphene films since the reduction efficiency is still low, and there are limitations of producing reproducible rGO films under an ambient condition (burn) or even protective environment [26-28].

Recently, spray pyrolysis has been introduced, in which the mist of aqueous suspension of GO from ultrasonic nebulizer was transported in a tube furnace at high temperature by the N_2 gas carrier [29-31]. During the process, droplets containing GO sheets accumulated at the

surface shrink as solvents evaporate when they pass through the furnace that result in the collapse of the rGO sheet to form a crumpled ball structure. This coating layer with 3D texture or crumpled topographies allow high surface area electrodes for battery and supercapacitor applications [30,32,33]. However, this method is not applicable for the fabrication of transparent thin graphene films since they provide negative affect to optical transparency and high contacting resistance between the crumpled graphene balls. Therefore further improvements and the development of new methods that are simple, scalable and provide highly conductive and transparent graphene films specially for nitrogen (N)-doped graphene films is still open and needs to be solved.

In this work, considering these limitations and disadvantages we present a simple and scalable route to fabricate transparent and highly conductive N-doped graphene films from GO by combining microwave irradiation, ultrasonic spray coating and thermal annealing. This concept is schematically presented in Figure 6.1 showing a three-step process. In the first step, a microwave treatment of GO combined with poly(ionic liquids) (PIL is proposed to prepare a special graphene ink (referred to as Mw-rGO@PIL) in order to achieve several tasks. The use of PILs is to not only improve structural integrity and repair the lattice defects upon a short microwave-induced GO reduction, but also will provide an N source for N-doping the carbon lattice. In the second step, the Mw-rGO@PIL is used as a well-dispersed ink for fabricating uniform and pinhole-free rGO thin films by employing a nebulizer spraying technique. During this process, the PIL modified-rGO dispersion was delivered through the atomizer nozzle by N_2 gas where it is nebulized into small uniform droplets with a narrow distribution of aerosol particles. Finally, these films were subjected to further thermal annealing at a high temperature of 900 °C under a protective environment (referred to

as a-Mw-rGO), in order to complete reduction of oxygen containing groups along with enhanced graphitic levels and N doping graphene process. This step is proposed to provide the greater conductivity of the transparent conductive films. Therefore this combined method provides several technical advantages that include: scalable, eco-friendly, flexible and low-cost fabrication process. The fabrication of N-doped graphene films with enhanced physicochemical properties (without using any gas sources and toxic N-containing organic precursors) is highly homogenous, pinhole-free and well-adhered on the substrates, which is not well-manufactured by conventional methods (e.g., spray, dip, bar, spin coating and drop casting), and thus the concept presents valuable contribution in this field. The comparative characterization of prepared starting material (GO), inks (Mw-rGO@PIL) and N-doped graphene films (a-Mw-rGO) during the different stages of the fabrication process were performed by SEM, HRTEM, UV-Vis, FTIR, XPS and Raman to confirm their properties and suitability of this method for the fabrication of high-performance N-doped graphene films.

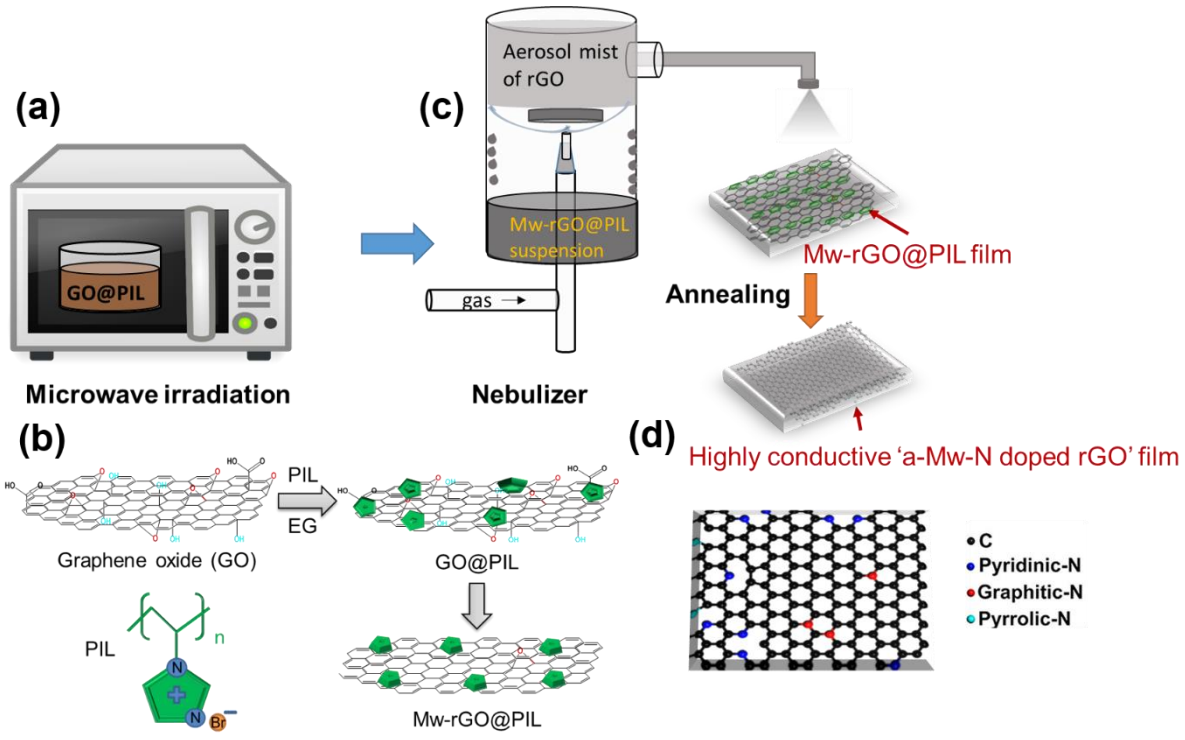

Figure. 6.1. Schematic diagram of the fabrication approach of highly conductive N-doped graphene thin films that combines 3 steps. In the first step (a - b), the GO modified with PILs was heated under microwave irradiation to make well-dispersed Mw-rGO@PIL inks. In the second step (c), the ink was used for the preparation of thin films by an aerosol mist coating using a nebulizer. In the final step, these coated films weere thermally annealed to achieve highly conductive and transparent N-doped graphene thin films.

6.3 Experimental section

6.3.1 Preparation of graphene inks by reduction of PIL-adsorbed GO and microwave irradiation treatment

GO were synthesised by the modified Hummer's method from graphite powder, and poly(1-vinyl-3-ethylimidazolium bromide) based poly(ion liquids) was prepared as reported in previous literature [21,34]. GO suspension (1 mg/mL) was prepared by dispersing the GO powder (200 mg) in ethylene glycol (200 mL) under mild sonication, and then mixed with PIL (200 mg). A ceramic cup was used to transfer the suspension that was placed in a domestic microwave oven (Panasonic) and treated at 1000 W for 1 - 2 min. After cooling down, the reaction, in which GO@PIL converted to rGO@PIL by reducing the oxygen groups under microwave irradiation heating formed chromophore aggregation by π-stacking of the graphene material and settled down at the bottom of the container. By washing several times with water and ethanol, the Mw-rGO@PIL is re-dispersed in ethanol and isopropanol (mild sonication) to prepare graphene ink suspension with typically a concentration of 0.5 mg/mL.

6.3.2 Fabrication of graphene films and thermal annealing treatment

The prepared Mw-rGO@PIL ink dispersion was used for manufacturing thin graphene films by using a nebulizer spray technique. The ultrasonic nozzle (Sonazer 241PG) with a frequency of 2.4 mHz (produced by a piezoelectric transducer) was used. An atomized spray

produced from the ultrasonic nozzle is used to produce a pinhole-free and uniform coating by controlling the aerosol droplet distribution [28]. The ink was deposited onto quartz substrates (2.4x2.4 cm) then placed on a hot-plate at 100 °C with an 8 cm distance between the nozzle and substrate. The generated rGO@PIL aerosols were transported perpendicularly to the substrate by the N_2 gas carrier with a spray rate of 0.3 mL/min. The whole deposition time for completing a thin film is about 45 min, and the thin film thickness can be controlled by adjusting the volume of the graphene ink. We have prepared three dozen film samples for optimizing resistance and transparency, and found a good reproducibility of the coatings. In parallel to the thin films preparation by this method, we were also prepared films by manual sprayed layer-by-layer coatings with the same condition and inks for comparison. The rGO@PIL thick films were prepared by a vacuum filter method for making free-standing films for characterization.

For thermal annealing treatment, both of the as-prepared graphene thin films (deposited on quartz) and thick film (free-standing film) were placed in a tube furnace, heated up to 900 °C with a ramp of 10 °C/min, and maintained (30 min) at the final temperature for pyrolysis of PIL under inert gas. Afterwards, the furnace was slowly cooled down to room temperature. These graphene films were subjected for a comparative characterization.

6.3.3 Characterization of prepared materials and films

Scanning electron microscopy (SEM) images of prepared materials and films were recorded using a Quanta 450 instrument operated at an acceleration voltage of 15 kV and an emission current of 10 mA. Transmission electron microscopy (TEM) was conducted on a Philips CM 200 microscope operated at 200 kV. The IR spectrum was measured using a Fourier Transform Infrared (FT-IR) spectrometer (Nicolet 6700 FTIR). X-ray photoelectron

spectroscopy (XPS) measurements were performed with ESCA2000 (VG Microtech) system using a monochromatizedaluminum Kα anode. The Raman mapping spectra were recorded using a DXR^{TM}xi Raman Imaging Microscope. Spectra were recorded over the range of 500 - 4000 cm^{-1} with an excitation wavelength of 532 nm. The surface resistance was obtained using a CMT series JANDEL four-point probe at room temperature in which a current of 10 μA was applied. The optical transmittance was carried out by using a UV-vis (Shimadzu UV-1601, Japan) with the wavelength ranging from 200 to 800 nm.

6.4 Result and discussion

The properties of the prepared conductive and transparent films with a term of "conductivity of transparency" were studied by measuring the sheet resistance and optical transparency at a wavelength of 550 nm (UV-vis). The thickness of the prepared films is finely tuned by varying the ink concentration and coating time. Figure 6.2a shows a photo of the quartz substrates (control), GO and Mw-rGO@PIL thin film (top), and post-annealing a-Mw-rGO film (bottom) indicating the colour alternation dependent on the treatment process. The optical transparency of these films is displayed in Figure 6.2b. A reduction of resistance along with optical transparency and tuning transparent-conductive properties of GO, Mw-rGO@PIL and a typical a-Mw-rGO thin film, respectively, is demonstrated in Figure 6.2c.

The GO film (control) has a sheet resistance of $6.8x10^{10}$ Ω/sq with 89.3% transparency, while the Mw-rGO@PIL film exhibits a reduced resistance of ~$1.5x10^{7}$ Ω/sq at a transmittance of 87%. The conductivity and transparency of the a-Mw-rGO films varied based on a trade-off between the resistance and transmittance in which, typically, a resistance of $6.2x10^{3}$ Ω/sq obtained with a ~82% transparency, and lower resistance of ~$3.8x10^{3}$ Ω/sq and $1.5x10^{3}$ Ω/sq could be reached at which the transparency would be as low as ~76% and 68%, respectively.

The performances of these transparent conductive films are well comparable with other graphene thin films prepared by the Langmuir–Blodgett method and annealed under H_2 gas reduction (Rs ~ 8 kΩ, T ~ 80%) [11], photochemically reduced GO (Rs ~ 1.6 kΩ, T ~ 70%) [36], thermally reduced GO (Rs ~ 3.2 kΩ, T ~ 65%) [(Yin et al., 2010)], supersonic kinetic sprayed rGO and annealed at 400-500 °C (Rs ~ 19 kΩ, T ~ 73.3%) [38], and other literature [1,6].

A benchmarking performance of the prepared films in this work and literature reports has been plotted in Figure 6.2d. In fact, the conductivity and transparency of electrodes are requested depending on the specific applications, and the perfomance of the fabricated thin films can meet the requirements of touch screen, OLED, e-readers, and sensors [27], but still need further improvement for the optoelectronic devices such as photovoltaic and solar cells applications [1,10]. The following comparative characterization of materials and prepared films at different states will be discussed in detail to better understand and confirm their high performance.

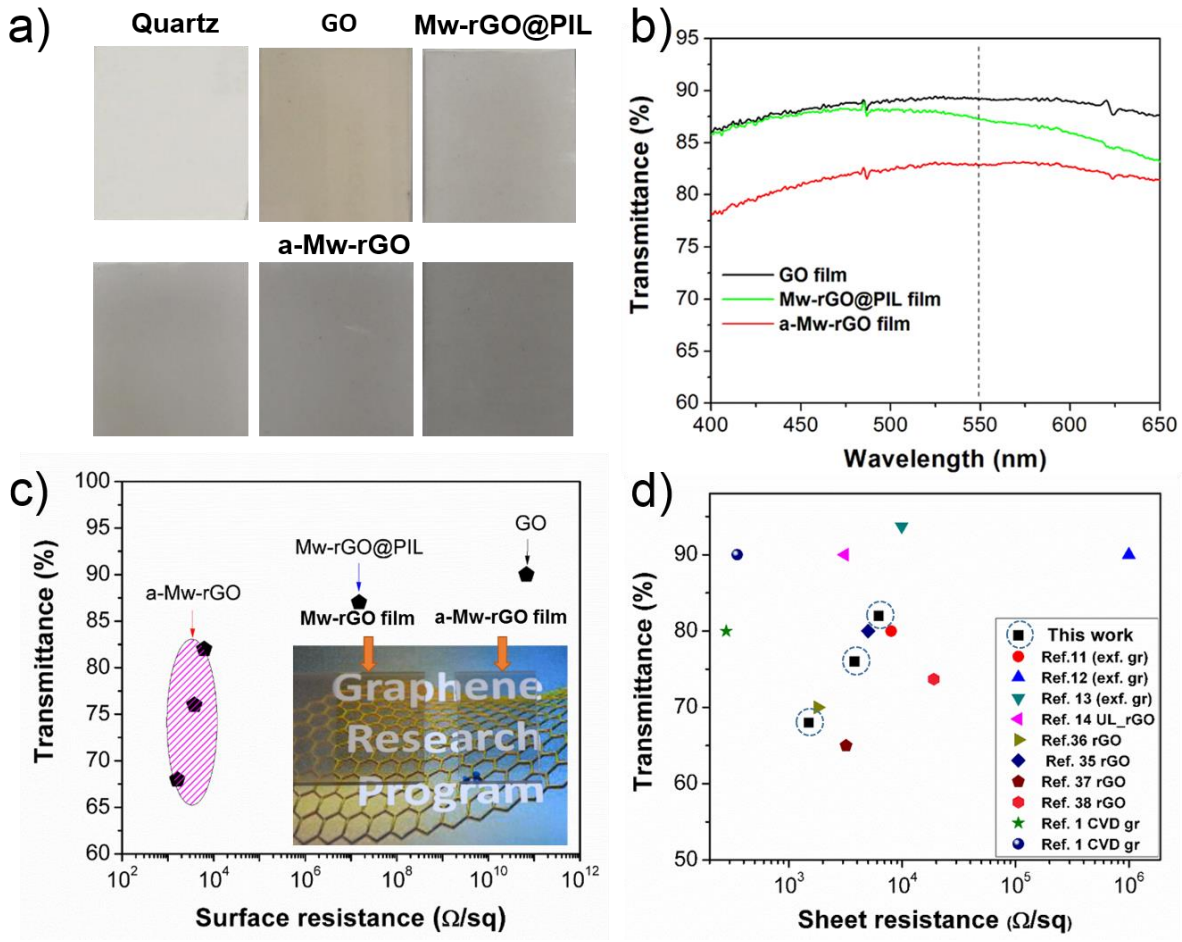

Figure 6.2. (a) Optical images of the quartz substrate, GO and Mw-rGO@PIL thin film (top), and a-Mw-rGO thin film (bottom), (b) light transmittance spectra of samples where the transmittance values were measured at wavelength of 550 nm, (c) transparent conductive films performance of graphene-based thin films manufactured by the nebulizer coating technique, and a digital image of the microwave irradiation and thermal annealed graphene film (inset), and (d) a comparative performance of the prepared N-doped graphene thin films presented in this work and graphene films in previous reports. Data plotted are based on optical transmittance vs. sheet resistance.

The fabrication of the graphene thin films from graphene inks is usually based on wet-coating processes such as bar coating, spin coating, drop casting, and spray coating which are simple,

low cost and scalable. However, these coating methods have some disadvantages to achieve highly reproducible and uniform films caused by self-aggregation, and inhomogeneous distribution of graphene layers over substrates after the solvents have dried in the process. To address these limitations, here we highlight the use of an ultrasonic spray coating technique using a nebulizer in comparison with the conventional manual spray coating. The N-doped graphene films using Mw-rGO@PIL ink were prepared by both methods to compare their surface morphology (roughness) and homogeneity. Comparative results displaying the optical images, profile of film topography and SEM images of the prepared films are shown in Figure 6.3.

Both 2D and 3D optical images of the manually sprayed coating sample (Figure. 6.3a and b) showed an inhomogeneous and rough graphene film at the microscale. In contrast, the optical images of the nebulized coating confirmed better homogeneity and fine graphene particles with less folds and wrinkles at the microscale (Figure. 6.3c and d). This observation is well confirmed by the topography profile of their surfaces (Figure. 6.3e) showing that the profile height of the spray coating in both X (top) and Y axis (bottom) is considerably higher than that of the ultrasonic coating by the nebulizer. Typically, in the X profile the measured arithmetic mean of profile roughness (Ra), root-mean square of profile roughness (Rq), and total height roughness (Rt) are 0.03, 0.06, and 0.36 μm, respectively. These values have notably decreased for the nebulized coating with Ra = 0.01 μm, Rq = 0.02 μm, and Rt = 0.13 μm. The SEM images of these films show in Figure. 6.3f and g for the spray and nebulize coatings, respectively, confirm again the folding structure and wrinkle of graphene along with the higher roughness surface for the spray technique. The inhomogeneity and roughness of the film are critical parameters influencing the conductivity and transparency properties of

the graphene films. These results obviously confirm advantages of the nebulizer coating technique to achieve thin and homogenous graphene films that explains reasons for their better performances.

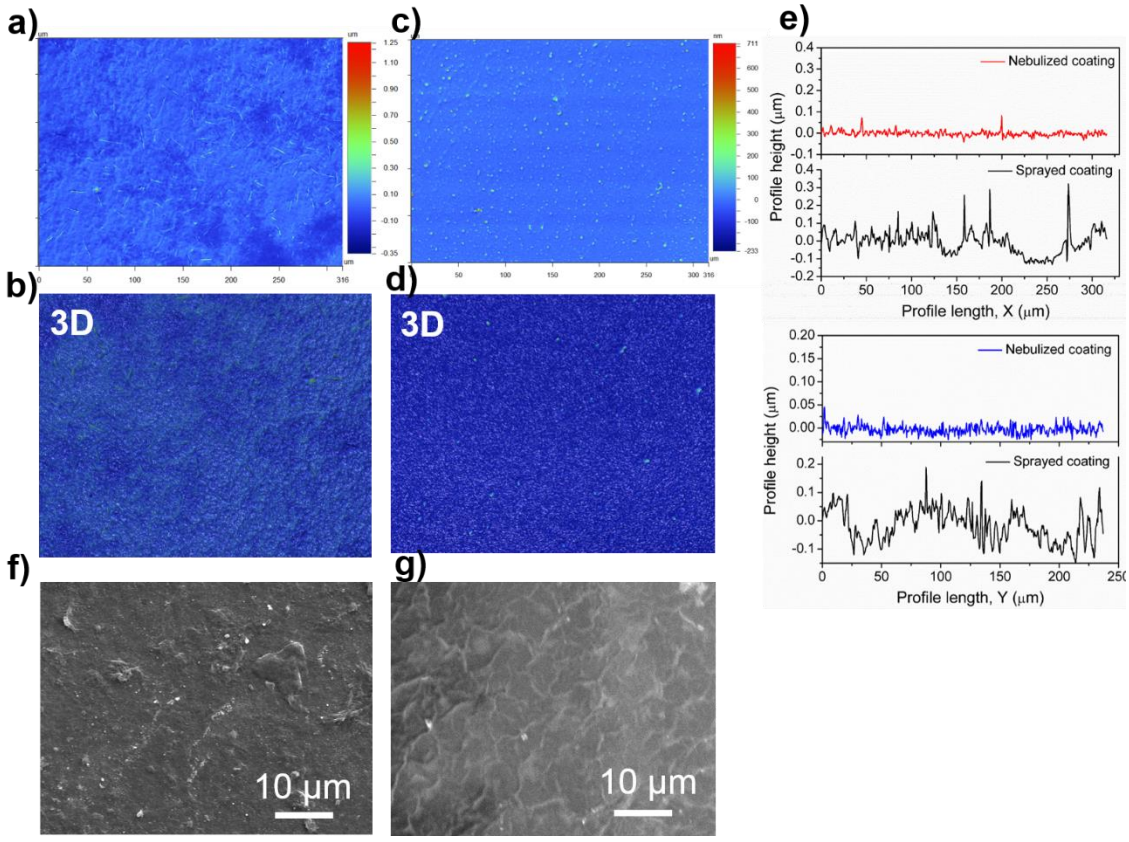

Figure. 6.3. Comparative images of graphene films prepared by coating of Mw-rGO@PIL inks on glass substrates by using (a and b) conventional spray coating and (c and d) ultrasonic nebulizer coating, (e) comparative surface profile parameter on X (top) and Y (bottom) axis of spray and nebulize coating. Comparative SEM images of (f) spray and (g) nebulize coating.

To examine how the microwave-induced reduction and further annealing effect to the recovery of the π-conjugated structure resulted in tuning the electrical properties of Mw-rGO@PIL and a-Mw-rGO films. The sheet resistance of these thick films (free-standing) was

measured by four-point probe method which is presented in Figure 6.4a**.** Results show that the sheet resistance of GO films decreased substantially by the Mw-induced reduction and additional thermal annealing process. The resistance of GO film is 1.24×10^6 Ω/sq that was reduced more than two orders of magnitude to 1.17×10^4 Ω/sq for the Mw-rGO@PIL film (Figure. 6.4b, SEM image). A significantly reduced sheet resistance to a value of ~ 5 Ω/sq after further annealing is achieved in the a-Mw-rGO film contained highly purified few-layer graphene sheets (Figure. 6.4c). This data indicates a mild reduction of GO by microwave irradiation and a high degree of de-oxygenation and graphitization of the rGO structure. This observation is confirmed with XPS elemental analysis (Figure. 6.4d), which revealed the C/O ratio increased from 1.3 of GO to 4.1 of Mw-rGO@PIL, and increased up to 14.8 for a-Mw-rGO sample. In addition, the hybrid inclusion of N into the graphene structure was monitored with N content decreasing from 3.3 At.% (before) to 0.98 At.% after thermal annealing, where the N atoms doped the carbon lattice in various N bonding configurations (Figure. 6.4e).

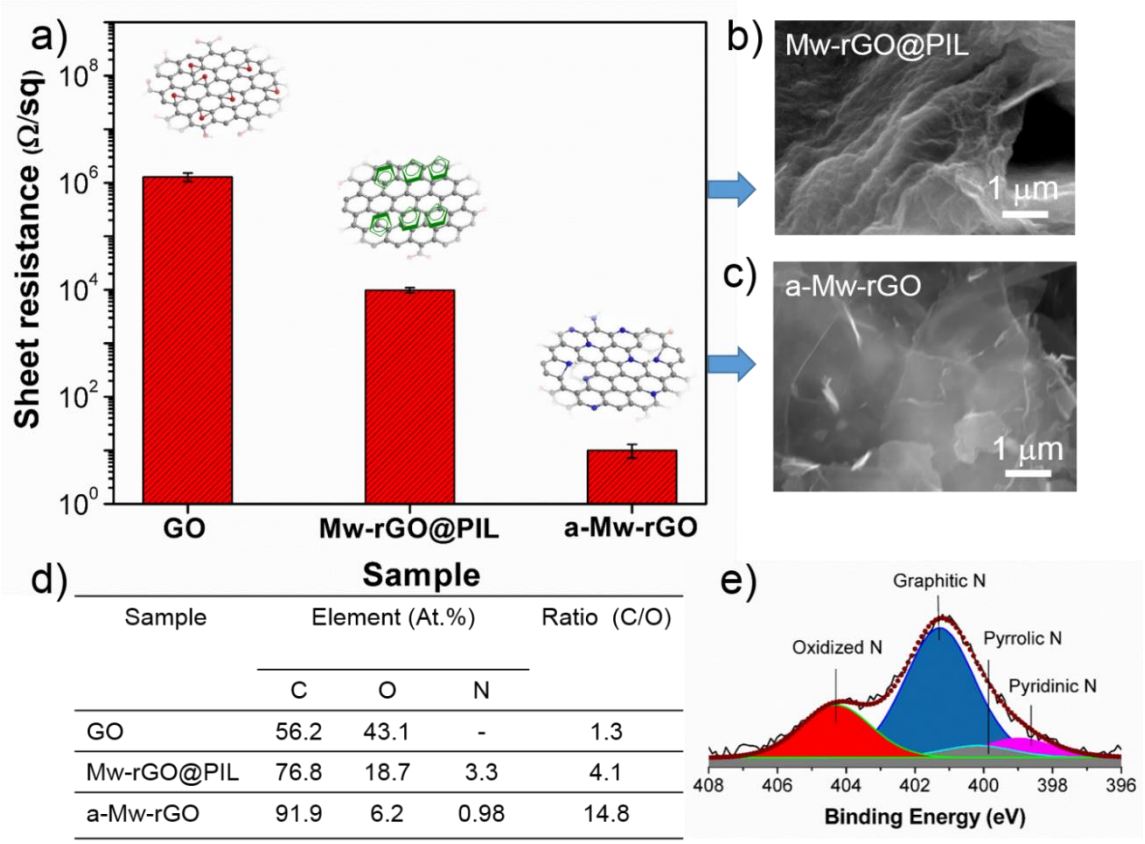

Sample	Element (At.%)			Ratio (C/O)
	C	O	N	
GO	56.2	43.1	-	1.3
Mw-rGO@PIL	76.8	18.7	3.3	4.1
a-Mw-rGO	91.9	6.2	0.98	14.8

Figure 6.4. (a) Sheet resistance of GO free-standing film compared with the Mw-rGO@PIL film obtained after microwave treatment and further thermal annealing (a-Mw-rGO), (b-c) corresponding SEM images of the films. (d) Elemental composition of the the films from XPS analysis with a C/O ratio which increased moderately after the microwave irradiation and sharply after the annealing process. (e) The N1s XPS spectra for N-doped graphene confirming different types of nitrogen atoms integrated into the graphitic structure of the a-Mw-rGO sample.

A quaternary refers to N atoms substituted for C atoms in the hexagonal ring (sp^2 hybridized) is a major bonding configuration, which was reported to contribute to the enhancing conductivity [28,39]. It is worthy to mention that the N content can be varied by changing the ratio of GO and PIL, and the pyrolysis temperature (the higher temperature the lower N

content), while the C-N bonding configuration can be tuned by changing the annealing temperature and normalizing time. Therefore, we optimized the annealing temperature to obtain the quaternary form as the dominant compared to other forms. The highly conductive N-doped graphene film with low resistance was achieved by our method that is comparable with the completed reduction of rGO films by the thermal method [40-44].

The microstructure of the GO film (control) and the films prepared by microwave irradiation inks was investigated by TEM and presented in Figure. 6.5. Figure. 6.5a shows a typical image of GO with coexisting sp^2 carbon domains and sp^3 defects in the structure. In the HR-TEM image (Figure. 6.5b), it can be easily visualized that the hole-like structure of beneath defects with the size of 1 to 3 nm (white phase) are randomly distributed over the sp^2 matrix domain (dark phase). It should also be taken into account that these defects can be attributed to the high-energy (hundreds keV) electron beam that may generate these undesired defects or structural changes during TEM measurement [45]. It is worthy to mention that, the GO sheet is unstable under electro-beam irradiation therefore hole-like defects can be expanding after a few seconds and damage the interior of the graphene lattice. In contrast, the Mw-rGO@PIL sample shows a continuous graphene lattice by restoring and expanding the sp^2 carbon lattice while removing oxygenated groups (Figure. 6.5c). This rGO sheet is also stable under electron-beam irradiation thus avoiding the additional undesired defects. Besides, during microwave irradiation by introducing temperature for the reduction of oxygen containing groups, self-repairing can occur on the graphene sheets based on the carbon ad-atoms from the existing carbon rich area (sp^2 domain) were quickly reoccupy the vacancy defects (Figure. 6.5c, inset). This mechanism is consistent with the self-repairing of graphene

defects by plasma or high-temperature treatment [41,46]. The other consideration is that PIL acts as patches that can cover the hole-like defects of rGO due to its similar aromatic rings.

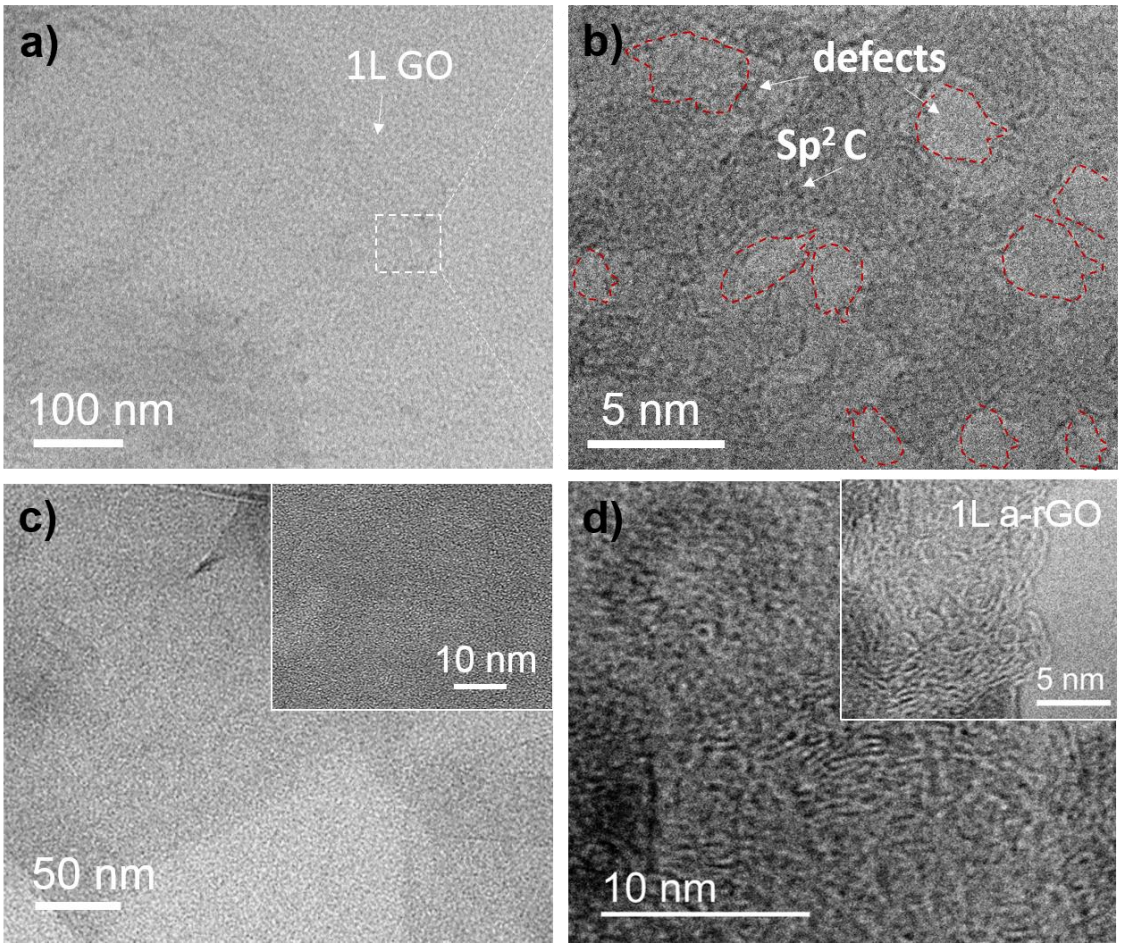

Figure. 6.5. (a) TEM and (b) HR-TEM images of GO (control) with different magnification which present both sp^2 carbon and sp^3 defects area, (c) TEM image of microwave-induced reduction of GO (Mw-rGO@PIL), (d) high magnification image (HR-TEM) of annealing sample (a-Mw-rGO) showing high level of graphitization and N-doped graphene lattice.

Figure. 6.5d displays the HR-TEM image after further annealing of Mw-rGO@PIL at 900 °C (a-Mw-rGO) showing high crystallinity indicative of the higher graphitization level. It is believed that at this high temperature the rest of the oxygenated groups have been completely

reduced, and the structure changes through the rearrangement of the π-electron networks in the basal plane [27], as well as a further increase in the number of sp^2 domains. The dark phase presented on the carbon lattice might be assigned to the carbonized N-containing compounds.

The comparative structures of the control sample (GO) and graphene films prepared by coating Mw-rGO@PIL inks before after the annealing was further investigated by Raman characterization and displayed in Figure. 6.6 The Raman spectrum shows a typical D-band at 1350 cm^{-1} (sp^3-hybridized carbons, defects) and G-band at 1592 cm^{-1} (sp^2-hybridized carbon atoms, tangential vibration) for GO, in which the intensity ratio of D and G band (I_D/I_G) is calculated with a value of 1.08 suggesting a high defects level. However, the Mw-rGO@PIL graphene film shows an increased G band over D-band indicating a recovery of the sp^2 carbon domains, and the I_D/I_G is decreased to 0.79 confirming a lower defect level after removing the partly oxygen functional groups. The Raman spectroscopy imaging was taken by scanning on the sample's surface (Figure. 6.6, right side) showing that the carbon area (red colour) in the Mw-rGO@PIL had expanded as compared to GO sample. It is worthy to mention that during the conventional reductions, the rGO sheet is believed to undergo structural changes through the rearrangement of the π-electron networks in the basal plane [27]. The increase in the number of sp^2 domains as well as the disorders and defects density are also increased, that is reflected by an increased intensity of the D-band and G-band (I_D/I_G) in the Raman spectrum. In contrast, the Mw-rGO@PIL shows a decrease in I_D/I_G, the reasons can be interpreted as (i) a rapid microwave irradiation allows fast and non-contacting heating avoiding the disordered structure, but allows a highly ordered structure [(Voiry et al., 2016)], and (ii) retards expansion of sp^3 defective areas, and possibly repairing the lattice defects in

the graphene structure [41]. These results are consistent with the morphology observed by TEM and as discussed above (Figure. 6.5c).

Further annealing of the Mw-rGO@PIL film under pyrolysis of N-containing compound (PIL) produces a significantly higher graphitic level, as the carbon area (red color) presented in the Raman spectroscopy imaging (a-Mw-rGO) increased and narrowed the D band. The I_D/I_G shows only little change from 0.79 to 0.81 that is related to the distorted graphitic structure under high temperature and N-doping carbon lattice. The thick G peak (FWHM) together with the higher I_D/I_G indicates a disorder in the plane rather than at the edges, so the thinner G peak after the annealing confirms perfectly the higher crystallinity of the plane. Interestingly, the 2D band at 2690 cm^{-1}, the second order of the D band, is clearly observed indicating a restoring of the structural integrity of graphene by reordering of the basal plane, in which pre-treatment of microwave irradiation allowed reorganization of the carbon bonds as reported by Voiry et al. [26]. It should be mentioned that the intense 2D band is normally absence or shouldered in the conventional reduction of GO by either the chemical or thermal methods.

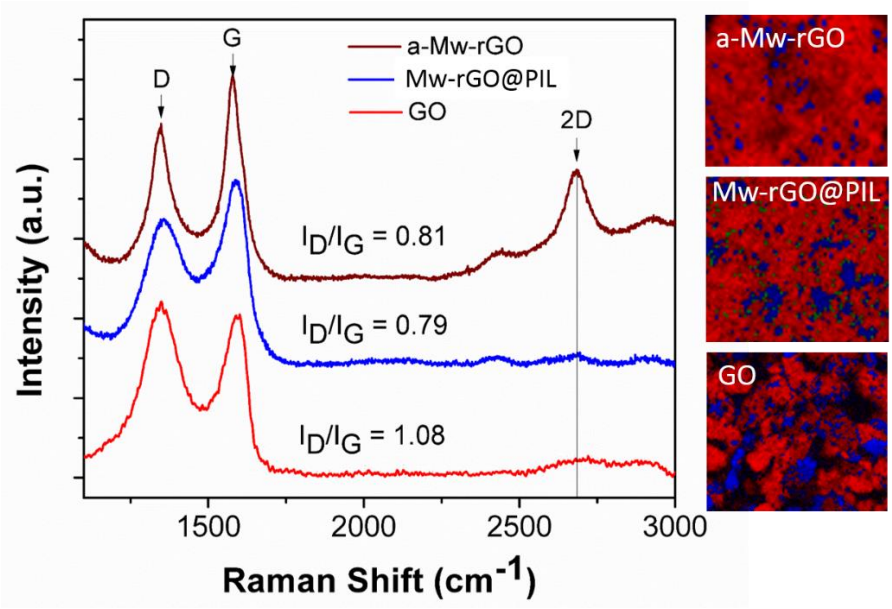

Figure. 6.6. Raman spectra of GO (red, control) and Mw-rGO@PIL (blue) films before and after annealing (a-Mw-rGO (brown) for comparison which shows defect and graphitic levels of samples. The spectra recorded on the red area in the corresponding optical images obtained by Raman spectroscopy imaging.

Chemical structure analysis of the materials before and after microwave treatment was characterized in order to evaluate how effective the oxygenated group decomposed from GO surfaces. The UV-vis spectra in Figure. 6.7a displays aromatic C=C plasmon peak red shifted from 230 nm (GO) to 260 nm (Mw-rGO@PIL), and the dispersing state of samples (inset). The characteristics of GO and chemical functional groups bound to the rGO surface after the microwave-induced reduction have been determined by chemical structure analysis of FTIR spectra. These oxygen functional groups were notably decreased from the initiated state after the microwave treatment, while peaks shifted and added peaks due to the adsorption of PIL (Figure. 6.7b)

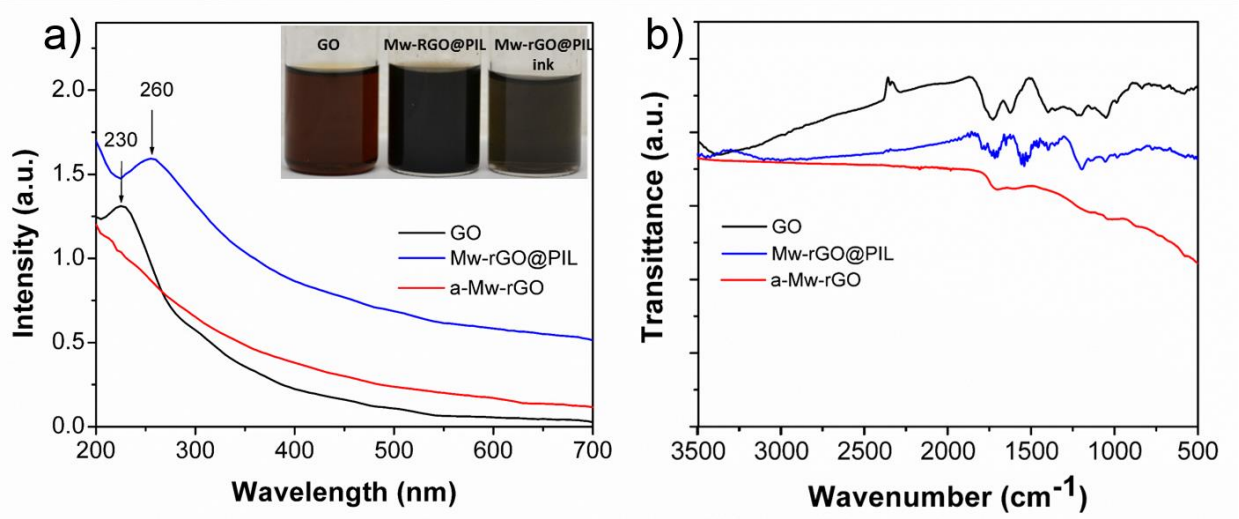

Figure. 6.7. a) UV-vis spectra show the π-π* transition of aromatic C=C plasmon peak of GO was red shifted after microwave irradiation (Mw-rGO@PIL), b) a compared FTIR spectra of GO and Mw-rGO@PIL sample showing functional groups originated GO were decreased, shifted and an added peak was found indicating PIL adsorbed onto rGO surface.

Finally, the comparative XPS characterization of GO (control) and the prepared graphene films by the ultrasonic nebulized process using Mw-rGO@PIL inks before and after annealing are presented in Figure 6.8**.** XPS graphs indicate that the atomic % (At.%) carbon increased from 56.2 for GO to 76.8 and 91.9 for Mw-rGO@PIL and a-Mw-rGO, respectively. While the oxygen concertation decreased orderly from 43.1 for GO to 20.6 and 6.2 by microwave reduction and post-annealing, respectively.

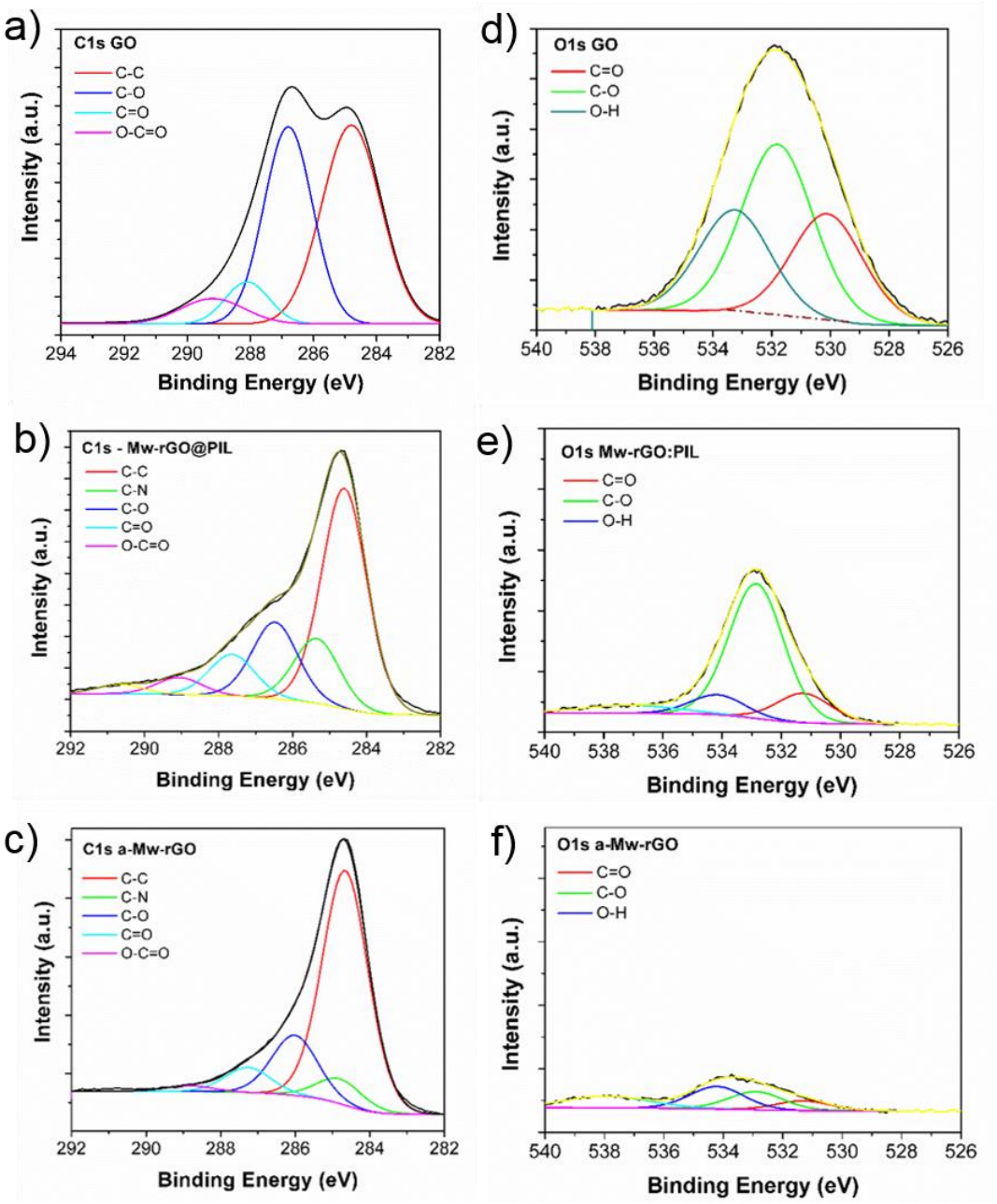

Figure 6.8. XPS spectra of C1s and O1s for (a and d) GO, (b and e) Mw-rGO, (c and f) annealing Mw-rGO showing a significant increase of the carbon species, while strong reduction of the oxygen functional groups after each state of microwave irradiation and annealing.

Figure. 8a shows the C1s XPS spectrum of GO which is deconvoluted into four peaks corresponding to carbon atoms in different functional groups: the C-C in aromatic rings, the oxygenated C in C-O, C=O, and O-C=O. The oxygenated groups in GO steadily decreased, while the C-C bonds increased in the Mw-rGO@PIL sample (Figure. 6.8b). However, the existing oxygenated groups was notable indicating a mild reduction. Post-treatment of Mw-rGO@PIL under high temperature (a-Mw-rGO) confirmed that the oxygenated functional groups have been removed effectively from the graphene material, meanwhile recovering the C-C bonds (Figure. 6.8c). The O1s spectra are also in line with C1s, where the oxygen bonding structure is moderately reduced when GO (Figure. 6.8d) undergoes the microwave irradiation (Figure. 6.8e) and substantially decreases after thermal annealing (Figure. 6.8f).

6.5 Conclusion

We have demonstrated a new and reliable method for the fabrication of highly conductive and transparent N-doped graphene films by combining microwave irradiation, a nebulizer spray technique and thermal annealing. The graphene ink was developed based on GO modified with PILs and treated by fast microwave irradiation. By this process, the PILs assembled on rGO structures was achieved providing good inks dispersion required for ultrathin films fabrication and N course for doping graphene. The ultrasonic nebulizer spraying method of prepared ink allows considerable better uniformity of the graphene films and consistency compared to the conventional spraying technique. Characterizations using HRTEM, Raman, XPS and FTIR provided all required information to confirm the reduction process, the structural changes (after each treatment) and elucidate their influence on the conductivity performance of the films. The properties of the prepared N-doped graphene films after thermal annealing showed low surface resistivity ranging from $1.5x10^3$ to $6.2x10^3$

Ω/sq at the corresponding transparency of 68 to 82%, where the thick film (~20 μm) showed a value ~ 5 Ω/sq. These performances were achieved due to pre-microwave treated PIL-modified GO ink that provides a mild reduction of oxygenated groups on GO, preventing disordering of the graphitic structure and repaired the lattice defects that are critical for the highly ordered structure under post-annealing. The thermal annealing process resulted in a complete de-oxygenation, increased graphitization level, and allowed the N-doped graphene with quaternary forms which significantly improved the conductive property. The presented concept provides several advantages for the production of high performing N-doped graphene films that includes good uniformity of the film, controllable doping, conductivity, transparency and thickness. These properties are important for many practical applications such as electrodes for energy storage and productions, solar cells, sensors, flexible electronics, EMI shielding, radio frequency (RF) tags, microwave antennas, and protective coatings.

Acknowledgements

The authors acknowledge the support from Australian research Council under Linkage Scheme with the grant ARC Research Hub for Graphene Enabled Industry Transformation, IH 150100003 funding under Industrial Transformation Research.

6.6 Reference

1. Wassei, J. K., & Kaner, R. B. (2010). Graphene, a promising transparent conductor. *Materials Today, 13*(3), 52-59. doi:10.1016/S1369-7021(10)70034-1
2. Rinaldo, R., Alberto, V., Stefano, P., & Bruno, S. (2014). The role of graphene for electrochemical energy storage. *Nature Materials, 14*(3). doi:10.1038/nmat4170

3. Tung, T. T., Chen, S. J., Fumeaux, C., & Losic, D. (2016). Scalable realization of conductive graphene films for high-efficiency microwave antennas. *J. Mater. Chem. C, 4*(45), 10620-10624. doi:10.1039/c6tc03583c

4. Tung, T. T., Nine, M. J., Krebsz, M., Pasinszki, T., Coghlan, C. J., Tran, D. N. H., & Losic, D. (2017). Recent Advances in Sensing Applications of Graphene Assemblies and Their Composites. *Advanced Functional Materials, 27*(46), n/a-n/a. doi:10.1002/adfm.201702891

5. Nine, M. J., Cole, M. A., Tran, D. N. H., & Losic, D. (2015). Graphene: a multipurpose material for protective coatings. *Journal of Materials Chemistry A, 3*(24), 12580-12602. doi:10.1039/C5TA01010A

6. Morales-Masis, M., De Wolf, S., Woods-Robinson, R., Ager, J. W., & Ballif, C. (2017). Transparent Electrodes for Efficient Optoelectronics.

7. Pirzado, A. A., Jouane, Y., Le Normand, F., Akilimali, R., Papaefthimiou, V., Ghimbeu, C. M., & Janowska, I. (2014). Electrical Transport in "Few-Layer Graphene" Film Prepared by the Hot-Spray Technique: The Effect of Thermal Treatment. The Journal of Physical Chemistry C, 118(2), 873-880. doi:10.1021/jp4103433

8. Jaber-Ansari, L., & Hersam, M. C. (2012). Solution-processed graphene materials and composites. *MRS Bulletin, 37*(12), 1167-1175. doi:10.1557/mrs.2012.182

9. Wang, S., Ang, P. K., Wang, Z., Tang, A. L. L., Thong, J. T. L., & Loh, K. P. (2010). High mobility, printable, and solution-processed graphene electronics. *Nano letters, 10*(1), 92. doi:10.1021/nl9028736

10. Bonaccorso, F., Sun, Z., Hasan, T., & Ferrari, A. C. (2010). Graphene photonics and optoelectronics. *Nature Photonics, 4*(9), 611. doi:10.1038/nphoton.2010.186

11. Xiaolin, L., Guangyu, Z., Xuedong, B., Xiaoming, S., Xinran, W., Enge, W., & Hongjie, D. (2008). Highly conducting graphene sheets and Langmuir–Blodgett films. *Nature Nanotechnology, 3*(9), 538. doi:10.1038/nnano.2008.210

12. De, S., King, P. J., Lotya, M., O' Neill, A., Doherty, E. M., Hernandez, Y., . . . Coleman, J. N. (2010). Flexible, Transparent, Conducting Films of Randomly Stacked Graphene from Surfactant-Stabilized, Oxide-Free Graphene Dispersions. *Small, 6*(3), 458-464. doi:10.1002/smll.200901162

13. Shin, H. J., Kim, K. K., Benayad, A., Yoon, S. M., Park, H. K., Jung, I. S., . . . Lee, Y. H. (2009). Efficient Reduction of Graphite Oxide by Sodium Borohydride and Its Effect on Electrical Conductance. *Advanced Functional Materials, 19*(12), 1987-1992. doi:10.1002/adfm.200900167

14. Bae, S.-Y., Jeon, I.-Y., Yang, J., Park, N., Shin, H. S., Park, S., . . . Baek, J.-B. (2011). Large-area graphene films by simple solution casting of edge-selectively functionalized graphite. *ACS nano, 5*(6), 4974. doi:10.1021/nn201072m

15. Yang, W., & Wang, C. (2016). Graphene and the related conductive inks for flexible electronics. *J. Mater. Chem. C, 4*(30), 7193-7207. doi:10.1039/c6tc01625a

16. Patent Application Titled "Enhanced Conductivity, Adhesion and Environmental Stability of Printed Graphene Inks with Nitrocellulose" Published Online (USPTO 20180010001). (2018). *Chemicals & Chemistry*, 4201.

17. Pei, S., & Cheng, H.-M. (2012). The reduction of graphene oxide. *Carbon, 50*(9), 3210-3228. doi:10.1016/j.carbon.2011.11.010

18. Bo, Z., Qian, J., Han, Z. J., Duan, L., Qiu, K., Ostrikov, K., . . . Cen, K. (2015). Note: Rapid reduction of graphene oxide paper by glow discharge plasma. *Review of Scientific Instruments, 86*(5). doi:10.1063/1.4919732

19. Zhu, Y., Murali, S., Stoller, M. D., Velamakanni, A., Piner, R. D., & Ruoff, R. S. (2010). Microwave assisted exfoliation and reduction of graphite oxide for ultracapacitors. *Carbon, 48*(7), 2118-2122. doi:10.1016/j.carbon.2010.02.001

20. Schwenke, A. M., Hoeppener, S., & Schubert, U. S. (2015). Synthesis and Modification of Carbon Nanomaterials utilizing Microwave Heating. *Advanced Materials, 27*(28), 4113-4141. doi:10.1002/adma.201500472

21. Kim, T., Chang Kang, H., Thanh Tung, T., Don Lee, J., Kim, H., Seok Yang, W., . . . Suh, K. S. (2012). Ionic liquid-assisted microwave reduction of graphite oxide for supercapacitors. *RSC Adv., 2*(23), 8808-8812. doi:10.1039/c2ra21400h

22. Wong, C. H. A., Sofer, Z., Klímová, K., & Pumera, M. (2016). Microwave Exfoliation of Graphite Oxides in HS Plasma for the Synthesis of Sulfur-Doped Graphenes as Oxygen Reduction Catalysts. *ACS applied materials & interfaces, 8*(46), 31849. doi:10.1021/acsami.6b10199

23. Economopoulos, S. P., Rotas, G., Miyata, Y., Shinohara, H., & Tagmatarchis, N. (2010). Exfoliation and chemical modification using microwave irradiation affording highly functionalized graphene. *ACS nano, 4*(12), 7499. doi:10.1021/nn101735e

24. Janowska, I., Chizari, K., Ersen, O., Zafeiratos, S., Soubane, D., Costa, V., . . . Pham-Huu, C. (2010). Microwave synthesis of large few-layer graphene sheets in aqueous solution of ammonia. *Nano Research, 3*(2), 126-137. doi:10.1007/s12274-010-1017-1

25. Khai, T. V., Kwak, D. S., Kwon, Y. J., Cho, H. Y., Huan, T. N., Chung, H., . . . Kim, H. W. (2013). Direct production of highly conductive graphene with a low oxygen content by a microwave-assisted solvothermal method. *Direct production of highly conductive graphene with a low oxygen content by a microwave-assisted solvothermal method, 232*, 346-355.

26. Voiry, D., Yang, J., Kupferberg, J., Fullon, R., Lee, C., Jeong, H. Y., . . . Chhowalla, M. (2016). High-quality graphene via microwave reduction of solution-exfoliated graphene oxide. *Science (New York, N.Y.), 353*(6306), 1413. doi:10.1126/science.aah3398

27. Arthur, D., Silvy, R. P., Wallis, P., Tan, Y., Rocha, J.-D. R., Resasco, D., . . . Hurley, W. (2012). Carbon nanomaterial commercialization: Lessons for graphene from carbon nanotubes. *MRS Bulletin, 37*(12), 1297-1306. doi:10.1557/mrs.2012.276

28. Van Khai, T., Na, H. G., Kwak, D. S., Kwon, Y. J., Ham, H., Shim, K. B., & Kim, H. W. (2012). Significant enhancement of blue emission and electrical conductivity of N-doped graphene. *Journal of Materials Chemistry, 22*(34), 17992. doi:10.1039/c2jm33194b

29. Bang, J. H., & Suslick, K. S. (2010). Applications of Ultrasound to the Synthesis of Nanostructured Materials. *Advanced Materials, 22*(10), 1039-1059. doi:10.1002/adma.200904093

30. Luo, J., Jang, H. D., Sun, T., Xiao, L., He, Z., Katsoulidis, A. P., . . . Huang, J. (2011). Compression and aggregation-resistant particles of crumpled soft sheets. *ACS nano, 5*(11), 8943. doi:10.1021/nn203115u

31. Chen, Y., Guo, F., Jachak, A., Kim, S.-P., Datta, D., Liu, J., . . . Hurt, R. H. (2012). Aerosol synthesis of cargo-filled graphene nanosacks. *Nano letters, 12*(4), 1996. doi:10.1021/nl2045952

32. Luo, J., Zhao, X., Wu, J., Jang, H. D., Kung, H. H., & Huang, J. (2012). Crumpled Graphene-Encapsulated Si Nanoparticles for Lithium Ion Battery Anodes. *The journal of physical chemistry letters, 3*(13), 1824. doi:10.1021/jz3006892

33. Deng, S., & Berry, V. (2016). Wrinkled, rippled and crumpled graphene: an overview of formation mechanism, electronic properties, and applications. *Materials Today, 19*(4), 197-212. doi:10.1016/j.mattod.2015.10.002

34. Tung, T. T., Kim, T. Y., Shim, J. P., Yang, W. S., Kim, H., & Suh, K. S. (2011). Poly(ionic liquid)-stabilized graphene sheets and their hybrid with poly(3,4-ethylenedioxythiophene). *Organic Electronics, 12*(12), 2215-2224. doi:10.1016/j.orgel.2011.09.012

35. Tung, T. T., Castro, M., Kim, T. Y., Suh, K. S., & Feller, J.-F. (2012). Graphene quantum resistive sensing skin for the detection of alteration biomarkers. *Journal of Materials Chemistry, 22*(40), 21754. doi:10.1039/c2jm34806c

36. Petridis, C., Konios, D., Stylianakis, M. M., Kakavelakis, G., Sygletou, M., Savva, K., . . . Kymakis, E. (2016). Solution processed reduced graphene oxide electrodes for organic photovoltaics. *Nanoscale Horiz., 1*(5), 375-382. doi:10.1039/c5nh00089k

37. Yin, Z., Sun, S., Salim, T., Wu, S., Huang, X., He, Q., . . . Zhang, H. (2010). Organic photovoltaic devices using highly flexible reduced graphene oxide films as transparent electrodes. *ACS nano, 4*(9), 5263. doi:10.1021/nn1015874

38. Kim, D. Y., Sinha-Ray, S., Park, J. J., Lee, J. G., Cha, Y. H., Bae, S. H., . . . Yoon, S. S. (2014). Self-Healing Reduced Graphene Oxide Films by Supersonic Kinetic Spraying. Advanced Functional Materials, 24(31), 4986-4995. doi:10.1002/adfm.201400732

39. Wang, H., Maiyalagan, T., & Wang, X. (2012). Review on Recent Progress in Nitrogen-Doped Graphene: Synthesis, Characterization, and Its Potential Applications. ACS Catalysis, 2(5), 781-794. doi:10.1021/cs200652y

40. López, V., Sundaram, R. S., Gómez-Navarro, C., Olea, D., Burghard, M., Gómez-Herrero, J., . . . Kern, K. (2009). Chemical Vapor Deposition Repair of Graphene Oxide: A Route to Highly-Conductive Graphene Monolayers. *Advanced Materials, 21*(46), 4683-4686. doi:10.1002/adma.200901582

41. Cheng, M., Yang, R., Zhang, L., Shi, Z., Yang, W., Wang, D., . . . Zhang, G. (2012). Restoration of graphene from graphene oxide by defect repair. Carbon, 50(7), 2581-2587. doi:10.1016/j.carbon.2012.02.016.

42. Eda, G., Fanchini, G., & Chhowalla, M. (2008). Large-area ultrathin films of reduced graphene oxide as a transparent and flexible electronic material. *Nature Nanotechnology, 3*(5), 270. doi:10.1038/nnano.2008.83

43. Su, C.-Y., Xu, Y., Zhang, W., Zhao, J., Liu, A., Tang, X., . . . Li, L.-J. (2010). Highly efficient restoration of graphitic structure in graphene oxide using alcohol vapors. *ACS nano, 4*(9), 5285. doi:10.1021/nn101691m

44. Renteria, J. D., Ramirez, S., Malekpour, H., Alonso, B., Centeno, A., Zurutuza, A., . . . Balandin, A. A. (2015). Strongly Anisotropic Thermal Conductivity of Free-Standing Reduced Graphene Oxide Films Annealed at High Temperature. *Advanced Functional Materials, 25*(29), 4664-4672. doi:10.1002/adfm.201501429

45. Yuan, W., Chen, J., & Shi, G. (2014). Nanoporous graphene materials. *Materials Today, 17*(2), 77-85. doi:10.1016/j.mattod.2014.01.021

46. Rozada, R., Paredes, J., Villar-Rodil, S., Martínez-Alonso, A., & Tascón, J. (2013). Towards full repair of defects in reduced graphene oxide films by two-step graphitization. *Nano Research, 6*(3), 216-233. doi:10.1007/s12274-013-0298-6

Blank Page

Chapter 7

Conclusions and recommendations for future works

7.1 Conclusion

This dissertation advances engineering of multi-functional conductive thin films using graphene materials and their composites. Furthermore, it raises the current knowledge of graphene based conductive coatings by demonstrating real-life applicability of graphene thin films for electrodes and optoelectronic applications.

Chapter 2: This chapter presents literature review and research gaps in the field related to this thesis. The background and fundamental properties of graphene derivatives that are suitable for diverse applications were studied. From the study, it is evident that graphene exhibits superior mechanical, electrical, electro-chemical and optical properties, thus have become a suitable material conductive coatings. Moreover, fundamental properties and synthesis methods of silver nanowire were discussed as well as the drawback for this technology. In addition, the background and application of plasma were highlighted and presented those plasma methods that are mainly applied to reduce and functionalization GO by using different gases. The following conclusions can be drawn

- Graphene is a carbon sheet of one atom and is produced by mainly four common methods chemical vapor deposition (CVD), mechanical exfoliation, epitaxial growth and chemical graphene oxide reduction. Because of graphene outstanding properties, many applications of graphene in different manufacturing have been reported.
- Silver nanowire as electrodes and poly synthesis method were reviewed. AgNW's electrical, mechanical, optical properties are excellent compare to ITO and other current materials used. However, besides being cheaper and mechanically more flexible, there is a concern related to the use of silver nanowire in different applications such as high surface roughness and weak adhesion of AgNWs.

- Plasma techniques have been applied to produce and functionalize nanostructures, offering novel features in the production method such as economy and safety. Plasma method is a process of functionalization and reduction of (GO) that is efficient, ecofriendly and comparatively cheap to other used methods. Furthermore, oxygen plasma treatment results in a rapid etching of the GO sheets, followed by a significant amount of defects. Treatment in nitrogen plasma does not result in aggressive etching however special measurement should be taken to avoid formation of defects.

Chapter 3: An effective and fast method to atmospheric plasma process reduction of GO films in combination with scanning ability has been reported.

- This technique offered a simple and scalable production of highly conductive graphene films on different substrates with various thickness, sizes, shapes and patterns. Compared to the existing GO reduction method, this technique provides many benefits such as eco-friendly, low - cost, controllable, ultrafast, providing patterning capability and continuous processing mode without limiting substrates size and shape, and providing low - defect graphene films and high conductivity.
- The plasma beam affords a novel combination of chemical reaction and mechanical bombardment resulting in complete GO reduction by efficiently removing functional groups of oxygen within a minute. It was dictated that the marked improvement in graphene structure and clusters size of sp^2 is not achievable with current methods used of GO reduction. The produced graphene films with sheet resistance of 186 ohm/sq in a short reduction time of one minute (or 160 Ω /sq for 120 seconds) without damage their structure is a pleasing performance compared with other methods.

- Many effective applications of the given process were demonstrated, such as the fabrication of conductive thin and thick transparent graphene films on flexible substrates, different micro patterns and supercapacitor graphene film electrodes. Excellent performance of supercapacitor showing very high volumetric capacitance (Cvol) of 536.55 F/cm^3 at a current density of 1A/g is demonstrated.

Chapter 4: In this chapter, a concept of multifunctionally graded surfaces (MFGS) using GO-rGO films with a gradient change of multiple properties including surface morphology, chemistry, wettability, surface charge, surface energy, electrical, thermoelectrical and thermal conductivity has been introduced and demonstrated.

- The fabrication method gradually removed GO oxygen functional groups across the surface to form rGO. These gradients can be fabricated in both dimensions with controllable lengths from micron (<1 mm) to cm scale (>70 mm) which is one of the longest gradients reported in literature.
- The method is simple, very fast (1-2 minutes), low cost, environmentally friendly, and flexible to be applied for a broad range of substrates (flat, curved or flexible) and materials (metals, glass, ceramics, Si wafers, plastics, textile, wood etc.).
- The proposed concept provided many advantages compared with previously reported surface gradients that are limited to micron scale and single functions. The concept can be used for broad applications and solving many challenging fundamental, medical, engineering and industrial problems not possible with uniform surfaces.

Chapter 5: This chapter discussed and introduced several new methods to the development of highly transparent and conductive electrode on both flexible and hard substrates based on the combination of AgNWs and pristine graphene.

- The optimal results on conductive ink formulation composed of AgNWs (30−50 μm long and 30−50 nm diameters) and pristine few-layer graphene sheets showed the best results at the 30/70 wt % ratio of AgNW to pG. The prepared AgNWs film on glass substrate shows a sheet resistance of 18.23 Ω/sq at an optical transparency of 89%, which are acceptable for many optoelectronic applications.
- The application of optimal inks was also successfully proved on broad range of nonconductive substrates including textile, and paper showing excellent conductivity for application in wearable electronics.
- The stability characterization under environmental conditions of the AgNW/pG film showed significantly improved durability with minor increase in resistance up to 30 days compared with the control AgNW film which showed asharp increase after 8−10 days as result of Ag oxidation and corrosion. Moreover, the mechanism of graphene barrier oxidation is revealed proposing graphene sheets acting as a physical barrier to protect the AgNW surface from oxygen and moisture and also providing the heat dissipation. The AgNW/pG film showed outstanding thermal stability after annealing at 300 °C, while control film displayed a significant increase in resistance at 150 °C.
- The performance of AgNW/pG films was further improved by a short APPJs treatment (e.g., 6 s) to significantly reduce the sheet resistance (∼30.6%), enhancement of the transparency (1.2%), and increase of the mechanical adhesive property.

Chapter 6: This chapter has demonstrated a new and reliable method for the fabrication of highly conductive and transparent N-doped graphene films by combining microwave irradiation, a nebulizer spray technique and thermal annealing.

- The graphene ink was developed based on GO modified with PILs and treated by fast microwave irradiation. The PILs assembled on rGO structures was achieved providing good inks dispersion required for ultrathin films fabrication and N course for doping graphene.
- The ultrasonic nebulizer spraying method of prepared ink provided considerable better uniformity of the graphene films and consistency compared to the conventional spraying technique.
- The properties of the prepared N-doped graphene films after thermal annealing showed low surface resistivity ranging from 1.5×10^3 to 6.2×10^3 Ω/sq at the corresponding transparency of 68 to 82%, where the thick film (~20 μm) showed a value ~5 Ω/sq. These performances were achieved due to pre-microwave treated PIL-modified GO ink that provides a mild reduction of oxygenated groups on GO, preventing disordering of the graphitic structure and repaired the lattice defects that are critical for the highly ordered structure under post-annealing.
- The thermal annealing process resulted in a complete de-oxygenation, increased graphitization level, and allowed the N-doped graphene with quaternary forms which significantly improved the conductive property.

7.2 Future work and recommendations

As demonstrated from the presented research output included in this thesis, engineering of multi-functional conductive thin films using graphene materials and their composites have enormous potential for multifunctional applications in the field of conductive coatings. The outstanding electrical and mechanical properties of graphene provide unprecedented scope for progress in the pursuit of advanced and new generation of conductive coating technologies. Following research topics are proposed to explore in future.

- Overall, the results of atmospheric plasma treatments APPJ on GO properties are not fully understood, comparing the number of studies dedicated to other plasma based graphene treatment. Further investigations should be performed to examine the influence of a plasma of a mixture of various gasses on GO structure and properties to enhance the qualities of graphene oxide functionalization mechanisms in different plasma and films.
- The ability to control the uniform AgNWs parameters during synthesis is still a challenge for future use of AgNWs as electrode materials.
- Since AgNW studies are comparatively new, there is a need for further work on AgNW stability providing more alternative techniques to increase its environmental stability.
- More improvements could be made to extend gradient properties such as attaching magnetic nanoparticle MNP to fabricate magnetic graphene gradients. This can have possible applications in electronics including supercapacitors, advanced anode materials for lithium - ion batteries, magnetically targeted delivery of drugs,

photothermal therapy and magnetic resonance imaging as well as to overcome the MNP drawbacks and taking advantage of both materials properties.